

THE EFFECTS OF DETUNING UPON
THE VIBRATION OF BLADED DISCS

by

D.J. Ewins

A dissertation submitted to the
University of Cambridge for the
degree of Doctor of Philosophy

Trinity College
Cambridge

November, 1966

Summary

An investigation is made into the effects of detuning upon the vibrations of a bladed disc. A theoretical analysis is developed in terms of receptances from which natural frequencies and modal shapes may be determined. An alternative approximate analysis is proposed which enables extremely efficient computation of estimates of these natural frequencies.

By examining the equations of motion of the system, it is possible to predict two distinct types of vibration mode. An extensive programme of computation is made for the case of uniform five bladed discs using both methods of solution, and the results confirm the existence of these two types of mode. Also, the precise effects of detuning by the introduction of small differences between the blades are established, and it is found that certain forms of detuning cause a natural frequency splitting effect in specific modes of vibration.

Consideration of a simplified analytical model leads to the conclusion that, for certain modes, detuning always causes one or more blades to experience a higher stress level than is attained in a perfectly tuned system. However, it is also found that the other modes suffer their highest stress levels in a tuned system, and that for these modes, detuning can be favourable.

Detuning effects are observed and measured experimentally on a simple physical model. Good agreement is achieved between measured and computed data for five bladed discs in every case that is examined. Many of the results obtained in this investigation apply to bladed discs in general, and they agree qualitatively with other published work.

PREFACE

This thesis describes work which was carried out by the author in Cambridge between December 1963 and September 1966, and acknowledgement is made to Professor Sir John Baker who made available the facilities of the University Engineering Laboratories during that period.

The author wishes to express his sincere thanks to Dr. R.W. Gregory, whose willing guidance as supervisor has been invaluable to the progress of the research. His assistance in the preparation of the thesis has been particularly appreciated.

The work was sponsored by a joint contract with Bristol Siddeley Engines Ltd. and Rolls Royce Ltd., and the many discussions and exchanges of ideas resulting from this association were invaluable aids to an understanding of the practical aspects of the problem.

The research incorporated an extensive programme of digital computation which was carried out partly on **EDSAC II**, but mostly on Titan, successive computers of the Cambridge University Mathematical Laboratory, and **Dr. M.V. Wilkes** is thanked for the provision of the computing service.

Grateful acknowledgement is made to the Science Research Council (formerly D.S.I.R.) for the financial support of a Research Studentship throughout the course of the three years.

Apart from the advice and help given freely by members of the department and both sponsoring firms, which is gratefully acknowledged, and except where stated otherwise, the work reported in this thesis is the original work of the author. It has not been submitted, either in whole or in part, to any other university.

D.J. Ewins

CONTENTS

	<u>Page</u>
Preface	
1 INTRODUCTION TO THE RESEARCH	
1.1 The nature of the problem	1
1.2 A summary of previously published work	3
1.3 The scope of the present research	6
2 A GENERAL ANALYSIS OF THE UNDAMPED VIBRATION OF A BLADED DISC	
2.1 Introduction	8
2.2 Receptances of blades and discs	10
2.3 A receptance analysis of undamped free vibration	11
2.4 An analysis of undamped forced vibration	13
2.5 The normal modes of vibration of blades and discs	14
2.6 Equations of motion for a bladed disc in matrix form	16
2.7 Solution of the equations of motion by matrix manipulation	19
3 SOME PROPERTIES OF UNIFORM VIBRATING BLADES AND DISCS	
3.1 Introduction	21
3.2 Flexural vibrations of a free free beam	22
3.3 End receptances of a free free beam in closed form	25
3.4 End receptances in a series form - an approximation	28
3.5 Flexural vibrations of a freely supported circular disc	30
3.6 Edge receptances of a free disc in closed form	35
3.7 Edge receptances in a series form	39
3.8 Point receptances	42
4 A NUMERICAL STUDY OF A UNIFORM BLADED DISC	
4.0 Summary	45
4.1 Application of the receptance method of solution to a uniform model of a bladed disc	45
4.2 Properties of the receptance determinant	47
4.3 Natural frequency solutions using the receptance method	50
4.4 Calculation of modal shapes	52
4.5 Application of the matrix method of solution to a uniform model	55
4.6 Eigenvalue estimates of natural frequency	59
4.7 Eigenvector estimates of modal shape	61
4.8 Vibration characteristics of bladed discs	64

	<u>Page</u>	
5	DETUNING A FIVE BLADED DISC - (I) NATURAL FREQUENCIES	
5.1	Introduction	66
5.2	A systematic analysis of detuning	68
5.3	Calculations made using the receptance method	73
6	DETUNING A FIVE BLADED DISC - (II) MODAL SHAPES AND VIBRATION LEVELS	
6.1	Introduction	76
6.2	Single modes	77
6.3	Double modes	80
6.4	A simplified double mode	84
7	THE DESIGN AND DEVELOPMENT OF THE EXPERIMENTAL EQUIPMENT	
7.1	Requirements of an experimental model	89
7.2	The design of a model	90
7.3	Suspension and damping tests	93
7.4	Instrumentation and other equipment	95
7.5	Development of receptance measuring technique	97
7.6	Calibration of the damping assembly	100
8	EXPERIMENTAL PROGRAMME, PROCEDURE AND RESULTS	
8.1	Objectives of the experimental investigation	101
8.2	Experimental procedure	102
8.3	Experiments on tuned systems	104
8.4	Detuned systems - I. Natural frequencies	106
8.5	Detuned systems - II. Damped response	109
8.6	Summary of the experimental results	114
9	CONCLUSIONS	
9.0	General conclusion	116
9.1	Vibrations of tuned bladed discs	116
9.2	The effects of detuning	117
9.3	Application of the results to other systems	118
9.4	Limitations and extension of the work	119

	<u>Page</u>
APPENDICES	
1 Notation	121
2 Inertia coefficients for normal modes of a disc	124
3 Derivation of closed form disc receptance expressions	126
4 Equations of motion of a bladed disc	131
5 A mechanism of natural frequency splitting	136
6 Piezoelectric transducers	140
7 Computed data for the experimental model	144
8 References and bibliography	146

CHAPTER 1

INTRODUCTION TO THE RESEARCH

1.1 The nature of the problem

Vibration has always presented a major problem in the development of turbomachinery by imposing excessive stress levels on various components, causing them to fail. In the introductory lecture of a conference* held recently in Cambridge, Dr. D.M. Smith** surveyed current vibration **problems** in turbomachinery and in many cases traced their **development** from the early days of steam turbines. He found it **convenient** to divide such problems into two **types** - one involving motion of the whole machine, such as might be brought about by **flexural vibrations** of a rotor shaft, and the other concerned with the vibrations of individual components. **The** great majority of problems of this second type are associated with vibrations of the blades and discs, and it is with these that the present study is concerned.

It is possible in many cases to treat the blades as cantilevers, either vibrating individually or grouped together in a ring or cascade in which case they are mechanically coupled by a rigid disc or **annulus**. Such is the case in many axial flow **compressors**, **where** any coupling between one blade and another is **either through** rigid body motion of the disc, or of an aerodynamic nature. Omission of any coupling effects which might arise from the flexibility of the disc, simplifies considerably analysis of **the** motion, and consequently, **aerodynamic** effects may be considered in greater detail than would otherwise be **possible**.

* Applied **Mechanics** Group Convention (**I.Mech.E.**) Cambridge, 1966.

** References may be found in alphabetical order of authors in Appendix 2.

However, there are cases in which this simplification is invalid because of strong coupling between blades due to the flexibility of the disc to which they are attached. In the earlier days of steam turbines, a number of failures occurred which were clearly caused by participation of the disc in the vibrations. Experimental investigations which were made at the time confirmed the importance of this type of vibration, and demanded reconsideration of the basis upon which design calculations were made. Thereafter, discs tended to become stiffer, although vibration problems of this nature are currently reappearing in gas turbines. An analysis of the mechanical vibrations of a bladed disc may only be made in general terms, while techniques for numerical application of theory to practical systems have not yet been perfected.

There are several methods which might be employed to eliminate or reduce the harmful effects of vibration. Foremost of these is the development of design techniques, numerical methods *etc. sc* that the vibratory properties of bladed discs may be accurately predicted, as also may the sources of excitation. With this information it should be possible to reduce the incidence of resonant conditions. In the absence of accurate estimates of resonant frequencies, an obvious remedy is the provision of sources of damping so that the acuteness of resonance may be eased. Many attempts have been made to devise such a solution, but none has yet been perfected. A third possible method might be either to 'detune' the system, for example by introducing small differences between a set of blades, or, alternatively and at the other extreme, to tune the blades until they are as nearly as possible identical. Put rather crudely, the argument in *favour* of detuning is that the severity of resonance would be reduced by avoiding having a large number of identical natural frequencies. The supporters of tuning put the contrary view that differences between blades would inflict higher stresses on *some* blades (and lower upon others), thereby worsening the situation, The research which forms

the subject of this thesis relates to the effects and possible benefits of detuning.

1.2 A summary of previously published work

Although there is a large amount of published material on vibration in turbomachinery, very little discussion is to be found on the current topic of detuning. Thus it is necessary to survey the literature for more general studies of blade and disc vibration, and it is found that these fall into two categories. Those in the first are the more numerous and are concerned with the cantilever vibration of blades, either alone or connected by a rigid disc or casing; the other group includes those cases in which blade coupling through a flexible disc is admitted.

Since the introduction of axial flow compressors, considerable efforts have been made to determine the vibration characteristics of cantilevered blades. Shannon (1945) produced a comprehensive review of experimental and numerical techniques for determining these characteristics, but the approximate methods then used for calculations have since been found inadequate. An extensive computational and experimental programme of research into more accurate methods is being made by Carnegie, and a number of results have already been published (1959, 1964, 1966). Other workers have also proposed alternative methods for computing the natural frequencies of complex, twisted blades, but although such work is essential to practical application of the analyses described in this thesis, it is not relevant to the problem of detuning. Aerodynamic aspects of blade vibration have also been examined by Whitehead (1957, 1966) and others, but such studies generally relate to systems with simplified vibratory properties, This approach may be usefully applied to more complex vibratory systems (in which the aerodynamic effects are usually ignored) as it serves to define the likely forms of excitation.

Of particular interest to the present work are two assessments of the effects of detuning on a set of blades which are connected by a disc or casing. Whitehead (1964, 1966) has shown that detuning always has a favourable effect on self excited vibration (flutter), but is detrimental to forced vibration resulting from external excitation in that it causes an increase in the maximum stress. A recent unpublished report by Stratford (1966) considers the effect of detuning on blades which are attached to, and vibrating in the plane of, a rigid disc. Coupling between the blades in this case is the result of small torsional oscillations of the disc as a rigid body. The analysis indicates that a specific form of detuning in which there is a sinusoidal variation of blade natural frequency around the disc, together with unfavourable conditions of excitation, can give rise to large increases in stress levels in comparison with those obtained in a perfectly tuned system. Neither of the studies just mentioned considers in detail the coupling between the blades which results from flexibility of the disc.

An investigation into the effects of detuning on the vibration of circular discs is reported in two papers by Tobias and Arnold (1957) and Tobias (1957). Both papers present a linear theory describing the effect of imperfections in a disc on its **flexural** vibrations, and it is found that for each combination of n nodal diameters and s nodal circles, the disc possesses two individual modes of vibration which have close natural frequencies. The first paper goes on to study the consequences of this property on the vibration of an imperfect disc when it is rotating, and examines in detail the 'standing wave' phenomenon which is experienced in turbines. The results of this study, together with an extensive experimental programme, indicate that the inclusion of imperfections can greatly reduce the severity of the vibrations associated with standing waves. In the second paper, Tobias extends the theory to consider vibration at larger amplitudes. In this case, the equations of motion become non-linear, and their solution

explains certain experimental observations reported in the first paper.

In 1955 Armstrong presented an analysis of the vibration properties of a stationary bladed disc using mechanical receptances, Prior to this, methods for determining natural frequencies were essentially approximate, and estimates were sometimes in error by as much as **20%**. There had also been a number of papers describing experimental observations of vibration of the bladed disc as a single composite component, but these reports are only of passing interest to the present work and reference may be made to Armstrong's thesis for a more detailed discussion.

Armstrong's method of solution assumes that modal shapes of the bladed disc have a number of nodal diameters and circles in the same way as does a disc without any blades. It is possible on this basis to derive a frequency equation in terms of the receptances of the disc and the blades. One limitation of this method is the assumption that all the blades are identical, and as such it cannot be directly applied to study detuned systems. Armstrong's analytical work was supplemented by experiments on a system with 80 nominally identical blades, and also by a series of tests on the same system under various detuned conditions, When the system was detuned, several modes of vibration were found to 'split' into pairs of modes with almost identical modal shapes and very close natural frequencies, but no simple pattern of behaviour can be detected. The conclusion drawn by Armstrong from a number of response measurements was that detuning was always unfavourable in that it resulted in a greater incidence of high stress levels than was found in the tuned system.

Since 1955, this method has been developed to enable its application to practical **systems**, as described by Armstrong, Christie and Hague (1966). However, no other work on bladed discs has been published, and the effects of detuning which were observed 'en passant' by Armstrong, remain largely unaccounted for.

1.3 The scope of the present research

The closing paragraphs of the previous section clearly suggest a topic for further work, since the precise effects of detuning on a bladed disc are largely unknown. The present research is intended to contribute to a better understanding of bladed disc vibrations, and in particular to examine in detail the mechanism and consequences of detuning.

In order to achieve this object, it is necessary first to devise quicker and more convenient methods than exist at present for calculating natural frequencies and modal shapes, and then make a detailed study of discs with non-identical blades. This is a truly formidable undertaking for 'real' discs of non constant thickness carrying twisted and non-uniform blades. The complexity of such 'real' systems entails extra expenditure of thought and time which, in themselves, reduce both the quantity of numerical data which can be assembled by way of theoretical prediction, and also the time available for testing these predictions by experiment. For these reasons, it was decided at the outset to restrict attention to models which have simpler properties than real systems (and are therefore more amenable to analysis and computation), but nonetheless preserve those features which are believed to be essential to a fuller understanding of the effects of detuning.

To this end, the model which is subsequently considered incorporates the following simplifications:

- 1) the disc and blades are each of constant cross section;
- 2) all the blades have zero stagger, so that vibration is entirely normal to the plane of the disc;
- 3) the system is assumed to be stationary and the effects of rotation are ignored; and

4) only a small number of blades (5) will be considered, although subsequent work will deal with multibladed discs,

(Whereas calculations **may be** made for any number of blades, a smaller number enables more cases to be examined and assists in detecting patterns of behaviour.)

Any study of vibration in **detuned bladed discs**, **whether** real or hypothetical, can be subdivided as follows

- 1) calculation of normal modes and natural frequencies in the absence of damping;
- 2) calculation of response to forcing with damping;
- 3) search for pattern of behaviour in respect of detuning;
- 4) experimental assessment of the theoretical predictions.,

All these aspects are considered later in relation to the simplified model. Part (1) involves considerable preliminary analysis, using both receptance and matrix methods, and this forms the basis for the development of computer programs for obtaining numerical results. Part (2) is based upon the results obtained in part **(1)**, but because somewhat questionable assumptions have to be made concerning the damping, a comprehensive numerical study is not attempted. In part **(3)**, numerical results for detuned systems form the basis for formulating empirical 'laws' of behaviour, although the theoretical basis for these remains obscure. Nevertheless, it is relevant to note that there is no significant conflict with **experimental** evidence, To this extent, there are good grounds for believing that the theory **which** is used here to discuss a simplified model will be found to apply, with little change in its essentials, to real **bladed** discs.

CHAPTER 2A GENERAL ANALYSIS OF THE UNDAMPED VIBRATION OF A BLADED DISC2.1 Introduction

The work reported in this thesis forms part of a study which is being made of the vibration characteristics of bladed discs. It is particularly concerned with the manner in which these characteristics are affected by detuning, such as might arise from the presence of small differences between the blades. However, in order to undertake such a study, it is first necessary to develop a method for determining the natural frequencies, modal shapes and other properties of a vibrating bladed disc. Previous techniques are found to be inadequate for the present case of non-identical blades, so that it has been necessary to devise a more general form of solution. The present chapter is concerned with this task, and describes in general terms two analyses which are suggested as alternative methods of obtaining this solution. Both analyses apply to a system which is composed of a circular disc with a number of separate blades attached at points on its rim. It is assumed (for the purpose of this chapter) that data defining the vibratory properties of the subsystems is available in some convenient form, and it is in their requirements in this respect that the two methods of solution differ.

The first analysis, which is based on receptance techniques, is only useful when the information on the component subsystems is available as explicit algebraic expressions. The second method is based on normal mode theory, and it employs such data in an infinite series form. The numerical application of this latter analysis provides an approximate solution by truncating the series at some convenient level. This is a more practical approach when the required data must be computed for complex non-uniform components, although the accuracy of the resulting **approximate** solution has yet to be investigated,

The displacement of any element of the system may be considered as being composed of six components, namely,

- (i) translation normal to the plane of the element;
- (ii) translation along the disc radius through the element;
- (iii) translation in the plane of the disc, normal to the radius through the element;
- (iv) rotation about the normal;
- (v) rotation about a radial line; and
- (vi) rotation in a plane containing both the normal and the radius through the element.

In a general treatment of the **flexural** vibrations of a bladed disc, one of these six **displacements, (ii)**, usually becomes redundant.

Motion in the other two **directions** which are **in** the plane of the disc, **(iii)** and (iv), occurs as a result of staggered blades, In the present work, in which a simplified system is studied in detail, only motion which is normal to the plane of the disc will be considered, and furthermore, the torsional modes of vibration of the blades will be ignored so that the system is reduced to one in which only two displacements are relevant, (i) and (vi) above. This system is referred to as having 'two degrees of coupling'.

As mentioned earlier, the analyses in this chapter are presented in general terms, and in the interests of brevity, a matrix notation is used throughout. In the text, the 'displacement' of a point refers to the displacement vector (which is composed of the components described above), and not to the motion in any one particular direction (such as the normal displacement).

2.2 Receptances of blades and discs

Before proceeding with the analysis, a definition of the receptance expressions which are used throughout will be given. Consider first any one of the N blades which are attached to the disc. This blade will possess certain receptance properties which are determined by its dimensions and elastic properties. The general receptance for the i^{th} blade, $\underline{\Omega}_i(x, y)$, relates the displacement at any point x (defined by $r = a + x$, $\theta = \theta_i$) and a dynamic loading at any other point y ($r = a + y$, $\theta = \theta_i$). In the present work we shall be concerned only with displacements of the end of the blade which is attached to the disc, and which is subsequently referred to as the 'root'. Thus, the blade root receptance $\underline{\Omega}_i(y)$ is defined which relates the root displacement to any loading applied to the blade. If the load itself is applied at the root, then it is convenient to write the receptance simply as $\underline{\Omega}_i$. The order of the receptance matrix $\underline{\Omega}$ is determined by the number of degrees of coupling which are admitted to the analysis (see section 2.1). The elements on the leading diagonal are direct receptance terms and are the ratio of displacement to load in any one particular **direction**, while the other elements are cross receptances and these represent the ratios of displacement in **one direction to loading in another**.

If we next consider a freely supported disc, we shall define the general receptance for the disc $\underline{\alpha}(l, k)$ as the relationship between the displacement at a point defined by l ($r = r_l$, $\theta = \theta_l$), and a harmonic load applied at another point k ($r = r_k$, $\theta = \theta_k$). Much of the analysis requires only 'edge' receptances in which the two points (l, k) both lie on the rim of the disc. The following notation is adopted in order to simplify the algebraic expressions: points on the disc which are situated at the rim (i.e. $r = a$) are denoted by the suffices i and j , and the edge receptance between them is written as $\underline{\alpha}_{i,j}$. A further simplification is made by omitting the second suffix when the positions of the response and

2.2 Receptances of blades and discs

Before proceeding with the analysis, a definition of the receptance expressions which are used throughout will be given. Consider first any one of the N blades which are attached to the disc. This blade will possess certain receptance properties which are determined by its dimensions and elastic properties. The general receptance for the i^{th} blade, $\underline{\Omega}_i(x, y)$, relates the displacement at any point x (defined by $r = a+x$, $\theta = \theta_i$) and a dynamic loading at any other point y ($r = a+y$, $\theta = \theta_i$). In the present work we shall be concerned only with displacements of the end of the blade which is attached to the disc, and which is subsequently referred to as the 'root'. Thus, the blade root receptance $\underline{\Omega}_i(y)$ is defined which relates the root displacement to any loading applied to the blade. If the load itself is applied at the root, then it is convenient to write the receptance simply as $\underline{\Omega}_i$. The order of the receptance matrix $\underline{\Omega}$ is determined **by the number of degrees of coupling which are admitted** to the analysis (see section 2.1). The elements on the leading diagonal are direct receptance terms and are the ratio of displacement to load in any one particular **direction**, while the other elements are cross receptances and these represent the ratios of displacement in **one direction to** loading in another.

If we next consider a freely supported disc, we shall define the general receptance for the disc $\underline{\alpha}(l, k)$ as the relationship between the displacement at a point defined by l ($r = r_l$, $\theta = \theta_l$), and a harmonic load applied at another point k ($r = r_k$, $\theta = \theta_k$). Much of the analysis requires only 'edge' receptances in which the two points (l, k) both lie on the rim of the disc, The following notation is adopted in order to simplify the algebraic expressions: points on the disc which are situated at the rim (i.e. $r = a$) are denoted by the suffices i and j , and the edge receptance between them is written as $\underline{\alpha}_{i,j}$. A further simplification is made by omitting the second suffix when the positions of the response and

excitation are identical (i.e. $i=j$), so that $\underline{\alpha}_{i,i}$ is written simply as $\underline{\alpha}_i$.

It is to be remembered throughout that each of these receptance terms is a function of frequency of vibration as well as the system geometry. They may be derived from consideration of the basic equations describing the motion of the systems.

2.3 A receptance analysis of the undamped free vibration of a bladed disc

Consider a bladed disc vibrating in a direction normal to its plane. Fig.2.1 illustrates the system where i and j are two of the N stations around the rim of the disc at which the blades are attached.

The displacement of the disc at station i (Y_i) due to the combined effects of all loads F_j at each of the N stations, is given by

$$Y_i = \sum_{j=1}^N \alpha_{i,j} F_j \quad (2.1)$$

and there are N of these equations, corresponding to $i = 1(1)N$.

Next, consider the blade which is attached at station i . The corresponding expression for the displacement of the root is

$$y_i = \underline{\Omega}_i f_i \quad \text{for } i = 1(1)N \quad (2.2)$$

The boundary conditions for the whole system are those of compatibility and equilibrium at each station, i . First, since all the blades are rigidly attached to the disc, we have

$$Y_i = y_i \quad \text{for } i = 1(1)N \quad (2.3)$$

and secondly, equilibrium is maintained if

$$F_i + f_i = 0 \quad \text{for } i = 1(1)N \quad (2.4)$$

The combination of these four sets of equations leads to a set of homogeneous linear equations in which the variables are the individual forces and couples at the points of attachment, and the coefficients are the elements of the receptance matrices. This set of equations may be conveniently written as

$$\sum_{j=1}^N (\alpha_{i,j} F_j) + \Omega_i F_i = 0 \quad \text{for } i = 1(1)N \quad (2.5)$$

In order that a set of homogeneous equations may have a **non-trivial** solution, the determinant of the coefficients must vanish. Because the receptance terms are frequency dependent, this condition will be satisfied at particular values of frequency - the so-called natural frequencies - and these are given by the roots of the determinantal equation

$$\Delta(\omega) = 0 \quad (2.6)$$

The order of this determinant is the product of the number of blades and the number of degrees of coupling (usually 2 or 3: see section 2.1).

It may be shown that for a set of homogeneous equations, such as those in equation (2.5), no unique solution exists for the variables (F_j) . However, it is possible to obtain a set of relative values of these loads, or a form of the modal shape, at any particular natural frequency. The equations are reduced to an inhomogeneous form by an arbitrary choice of values for a specific number of the variables. For example, if the determinantal equation (2.6) possesses one root at $\omega = \omega_x$, we set one variable to unity, F_i say.

This condition and $\omega = \omega_x$ are substituted into the equation (2.5) and a set of inhomogeneous linear equations are formed. A unique solution is now possible for the ratios F_2/F_1 , F_3/F_1 , ... etc, and thus the pattern of the distribution of forces and couples around the disc is deduced.

However, if the determinantal equation possesses M coincident roots at $\omega = \omega_x$, the problem is somewhat more complex. It is then necessary to choose M variables (such as F_1, F_2, \dots) and assign to them a set of suitable values (e.g. $1, 0, 0, \dots, 0$). The relative values of the remaining variables may now be computed as before. This process must be repeated M times, each time using a different set of values for the M fixed variables (e.g. $0, 0, 1, 0, \dots, 0$), until the complete solution of M linearly independent modal patterns is obtained. The general solution at this frequency is any linear combination of these M modal patterns.

2.4 An analysis of undamped forced vibration

It is possible to determine the undamped response of the bladed disc to any form of excitation at any frequency other than a natural frequency.

Suppose that a number of external loads P_k are applied at points k on the disc (see Fig.2.2) together with a number of loads $i p_x$ acting at points x on the blades. In this case, equation (2.1) is written as

$$Y_i = \sum_{j=1}^N \alpha_{i,j} F_j + \sum_k \alpha_{(i,k)} P_k \quad (2.7)$$

and equation (2.2) becomes

$$y_i = \underline{\Omega}_i f_i + \sum_x \underline{\Omega}_i(x) i p_x \quad (2.8)$$

The boundary conditions of compatibility and equilibrium may be applied to the N stations i , as before, and this time form a set of inhomogeneous linear equations

$$\sum_{j=1}^N (\underline{\alpha}_{i,j} F_j) + \underline{\Omega}_i F_i = \sum_x (\underline{\Omega}_i(x) i p_x) - \sum_k (\underline{\alpha}(i,k) P_k) \quad \text{for } i = 1(1)N \quad (2.9)$$

In this case, the condition for a unique solution for F_j is that the determinant of the coefficients shall not vanish. Providing that the frequency equation (2.6) is not **satisfied** (i.e. that the system is not vibrating at a natural frequency), then each of the forces and couples at the stations i may be found in terms of externally applied loads P_k and $i p_x$ by solution of equation (2.9).

With the solution thus provided as a set of loads on the disc and blades, the response may be derived in any convenient form, such as disc or blade amplitudes of vibration, or blade root stress levels etc.

2.5 The normal modes of vibration of blades and discs

An alternative method of analysis will now be developed which is based upon normal mode theory and which expresses the vibration of the bladed disc as a set of equations of motion. For a numerical application of this method, it is necessary to make a number of simplifications but the method of solution employs powerful matrix techniques which may be readily programmed for a digital computer,

We consider first a free free blade oscillating freely in its normal **modes of** vibration, which are represented by the principal coordinate vector A . It is possible to write down expressions for the local amplitudes of vibration and for the kinetic and potential energy of the system in terms of the properties of the normal modes and their principal coordinates. In these expressions, the following

notation is used:

prefix i refers to the i^{th} blade;

$i \underline{h}_0$ is a vector whose elements are the principal coordinates for the rigid body motions of the i^{th} blade;

$i \underline{h}$ is a vector whose elements are the principal coordinates representing the normal modes of **flexural** vibration of the i^{th} blade;

l represents geometrical coordinates;

$i \underline{h}_0(l)$ and $i \underline{h}(l)$ are vectors of characteristic functions and correspond to the principal coordinates $i \underline{h}_0$ and $i \underline{h}$ respectively;

$[i \underline{\omega}^2]$ is a diagonal matrix of natural frequencies squared;

$i \underline{a}_0$ and $i \underline{a}$ are row vectors of characteristic inertial coefficients of the system when vibrating in its normal modes.

The displacement at any point in the blade which is specified by the coordinate A may be written as

$$i y(l) = i \underline{h}_0(l) i \underline{h}_0 + i \underline{h}(l) i \underline{h} \quad (2.10)$$

The kinetic and potential energy of the blade when it is vibrating in its normal modes may be written in terms of the properties of these modes as

$$2 i T = i \underline{a}_0 i \dot{\underline{h}}_0^2 + i \underline{a} i \dot{\underline{h}}^2$$

and

$$2 i V = i \underline{a} (i \omega^2) i \underline{h}^2 \quad (2.11)$$

respectively.

We next treat the disc in the same manner. The notation is similar to that used above, except that in this case the principal coordinates are represented by \underline{q} ; the characteristic functions by \underline{f} and the typical geometrical coordinate by $\underline{\xi}$. Natural frequencies and other properties are the same but lack the blade identification prefix.

The equation for the displacement of the disc becomes

$$\underline{Y}(\underline{\xi}) = \underline{f}_0(\underline{\xi}) \underline{q}_0 + \underline{f}(\underline{\xi}) \underline{q} \quad (2.12)$$

while the expressions for the kinetic and potential energies are

$$2 T_d = \underline{a}_0 \dot{q}_0^2 + \underline{a} \dot{q}^2 \quad (2.13)$$

and

$$2 V_d = \underline{a} [\underline{\omega}^2] \underline{q}^2$$

respectively.

2.6 Equations of motion for a bladed disc in matrix form

By using the compatibility conditions which were employed in the receptance analysis, a set of equations of motion will now be derived for the bladed disc in terms of the principal coordinates and the properties of the normal modes of vibration for the disc and the blades,

First, expressions for the kinetic and potential energies of the combined system may be obtained simply by addition of equations (2.11) and (2.13). Thus we have

$$2 T = 2 T_d + \sum_{i=1}^N 2_i T \quad (2.14)$$

and

$$2 V = 2 V_d + \sum_{i=1}^N 2_i V$$

For reasons which will become clear later, it is necessary to eliminate

from the analysis those coordinates which correspond to modes with zero natural frequencies (i.e. the rigid body modes). This is done in two stages, The first is to use the condition of compatibility at the blade roots as expressed by the equation

$$Y(i) = i y(o) \quad (2.15)$$

in conjunction with (2.10) and (2.12) to give

$$i \underline{h}_o = [i \underline{h}_o(o)]^{-1} [\underline{f}_o(i) \underline{q}_o + \underline{f}(i) \underline{q} - i \underline{h}(o) i \underline{h}] \quad (2.16)$$

(where $\xi = i$ is the position of attachment of the i^{th} blade). In this way, the coordinates referring to rigid body motions of the blades may be eliminated from any subsequent equations.

The second stage, the elimination of the coordinates q_o , which represent rigid body motions of the disc, is conveniently done by deriving the equations of motion for these coordinates by the Lagrangian method, The form of Lagrange's equation applicable to the system is

$$\frac{d}{dt} \left(\frac{\partial T}{\partial \dot{x}} \right) + \left(\frac{\partial V}{\partial x} \right) = 0 \quad (2.17)$$

where x is any principal coordinate, and if we apply this equation to $x = q_o$, the equation becomes

$$\begin{aligned} \ddot{q}_o \left\{ 2 a_o + \sum_{i=1}^N 2 [i \underline{h}_o(o)]^{-2} [\underline{f}_o(i)]^2 \right\} = \\ - \ddot{q} \left\{ \sum_{i=1}^N 2 [i \underline{h}_o(o)]^{-2} [\underline{f}_o(i)] [\underline{f}(i)] \right\} - \sum_{i=1}^N i \underline{h} \left\{ 2 [i \underline{h}_o(o)]^{-2} \right. \\ \left. [\underline{f}_o(i)] [i \underline{h}(o)] \right\} \end{aligned} \quad (2.18)$$

Thus in subsequent equations, we may substitute for \ddot{q}_o (or q_o) in terms of the principal coordinates of the modes of **flexural** vibration and thereby express the energy functions (2.14) in terms of q and h only,

If Lagrange's equation is applied to these modified expressions for x equal in turn to all the **flexural** coordinates, i.e. to all q and h , we arrive at a set of equations

$$\underline{A} \ddot{x} + \underline{B} x = 0 \quad (2.19)$$

where \underline{A} is the inertia matrix, \underline{B} is the stiffness matrix and x is the coordinate vector which contains all q and h .

It is convenient, both analytically and computationally, to combine the symmetric inertia and stiffness matrices into a single 'system' matrix. As is well known, the latter will not itself be **symmetric** unless the coordinate vector is subjected to the linear transformation $\underline{z} = \underline{B}^{-1/2} \underline{x}$, which serves to define a modified coordinate vector \underline{z} . Assuming harmonic oscillations, so that $\ddot{x} = -\omega^2 x$, we find that

$$\underline{A} x = \frac{1}{\omega^2} \underline{B} x$$

or, in terms of z ,

$$(\underline{B}^{-1/2} \underline{A} \underline{B}^{-1/2}) z = \frac{1}{\omega^2} (\underline{B}^{-1/2} \underline{B} \underline{B}^{-1/2}) z = \frac{1}{\omega^2} z$$

or

$$\underline{D} z = \frac{1}{\omega^2} z \quad (2.20)$$

where $\underline{D} = \underline{B}^{-1/2} \underline{A} \underline{B}^{-1/2}$ is the symmetrical 'system' matrix.

Inspection of \underline{B} shows that it is a diagonal matrix whose elements are the coefficients in the potential energy terms. The necessity for the elimination of the coordinates q_o and h_o is

now made clear, since their potential energy coefficients are zero. With such zero terms in \underline{B} , the matrix $\underline{B}^{-1/2}$ would possess infinite elements and render further manipulation impossible,

2.7 Solution of the equations of motion by matrix manipulation

In order to obtain a practical solution based on the matrix analysis described in the previous section, it is necessary to make one basic simplification. Because both the disc and the blades are continuous systems, they possess in theory an infinite number of normal modes of vibration. Consequently, the matrices and vectors in the previous sections are all of infinite order. We shall define the approximate system as one in which the disc and the blades each have a finite number of normal modes. Furthermore, we shall choose the properties of these modes of the approximate disc (for example) to be identical with those of the same number (Q say) of the normal modes of the continuous system. In practice, it is usually convenient to choose the first Q modes when they are arranged in ascending order of natural frequency. In this case, the approximation which is made consists of neglecting the effects of the higher frequency modes of vibration. Using this simplification, we reduce the matrices and vectors associated with \mathcal{A} to a finite order R , and those associated with the disc modes q to order Q . Thus, having eliminated \underline{u}_0 and q_0 , the order of the system matrices A, B and \underline{D} , and the vectors \underline{x} and \underline{z} becomes $Q + NR = M$ say, which may be made of realistic magnitude by a suitable choice of Q and R .

This done, the solution of equation (2.20) may be effected to produce M eigenvalues ω_m and the associated eigenvectors \underline{z}_m . These represent estimates of the natural frequencies (directly from ω_m), and the modal shapes (indirectly from \underline{z}_m) of the original system. The accuracy of these estimates will depend upon the

magnitudes of Q and R .

The modal shape may be most conveniently derived from the eigenvector \underline{z}_m in the form of the displacement pattern over the surface of the disc, by using equations (2.12) and (2.18) in conjunction with the eigenvector itself. Alternatively, the pattern of loads at the root of each blade may be determined using the root displacement (as computed above) together with the root receptance expression (as described in section 2.2). These loads provide estimates to the exact **values** which may be found according to the method described at the end of section 2.3. The remarks in that section concerning a number of normal modes with the same natural frequency apply equally in this case.

CHAPTER 3SOME PROPERTIES OF UNIFORM VIBRATING BEAMS AND DISCS3.1 Introduction

The analyses presented in Chapter 2 are intended to show, in general terms, two methods which can be usefully employed to study the behaviour of vibrating bladed discs, Before these methods may be used as a basis for computation, it is necessary to derive expressions for the receptances, natural frequencies etc, of both the blades and the disc, In general, this is a formidable task and is beyond the scope of the present work. However, it is possible to determine these properties for the components of a uniform system (**i.e.** a uniform disc with uniform bars to represent the blades), and this chapter describes various ways in which such information may be obtained.

The first part of the chapter is concerned with uniform free free beams or bars. None of the results nor the analysis in this section are new, and all the information could have been found in the relevant chapters of Bishop and Johnson - 'The Mechanics of **Vibration**'. Nevertheless, it has been thought worthwhile to include a derivation of these results on the ground that this serves to introduce the procedure which is adopted for the subsequent treatment of the freely supported disc, and which is much more difficult.

Receptances of a uniform disc were first derived by Armstrong in 1955 in the form of an infinite series. More recently (and after the completion of the work in this chapter), Bishop and **McLeod** published considerable information concerning the receptance expressions for uniform circular plates with various boundary conditions. Their expressions corresponding to Armstrong's receptances for a free disc are in a closed form, and as such they provide more accurate numerical values, However, their results are presented in

such a general form that application to a specific problem (in this case to a free disc) presents an extensive algebraic exercise,, In the second part of this chapter, these closed form receptances are derived from first principles, and the resulting expressions are found to be very much simpler than the general forma from Bishop and McLeod. Thus it is believed that the present analysis is a far more convenient approach for such a case, A large number of calculations were done to demonstrate the inaccuracy of the series form receptances when these series are truncated at various levels,

3.2 Flexural vibrations of a free free beam

The fundamental equation governing the free motion of a uniform prismatic beam, in the absence of rotary inertia and shear deflection effects, is

$$\frac{\partial^4 y}{\partial l^4} + \frac{A_0 \rho}{EI} \frac{\partial^2 y}{\partial t^2} = 0 \quad (3.1)$$

where y is a displacement coordinate normal to the length of the beam
 l is a displacement coordinate along the beam

A_0 , I , ρ and E are the sectional area, second moment of area, density and Young's modulus respectively of the beam,

The assumption of a harmonic solution to (3.1) in which

$$y = Y(l)e^{i\omega t} \quad (3.2)$$

leads to a general solution of the form

$$y = [A \cos(\lambda l) + B \sin(\lambda l) + C \cosh(\lambda l) + D \sinh(\lambda l)] e^{i\omega t} \quad (3.3)$$

where $\lambda^4 = \omega^2 A_0 \rho / EI$ and ω is the frequency of vibration,

The constants A , B , C and D in equation (3.3) are determined by four boundary conditions, Current interest is in a free free beam, in which the absence of restraining forces or couples at either end gives rise to the boundary conditions

$$\left\{ \frac{\partial^2 y}{\partial l^2} \right\} = \left\{ \frac{\partial^3 y}{\partial l^3} \right\} = 0 \quad l=0, L \quad (3.04)$$

where L is the length of the beam, When these conditions are applied to (3.3), they lead to the conclusion that a non trivial solution only exists if

$$\cos (\lambda L) \cosh (\lambda L) - 1 = 0 \quad (3.5)$$

The frequency equation (3.5) has an infinite number of roots which correspond to the natural frequencies of the beam, Corresponding to any such root, $\lambda = \lambda_{k}$, there is a normal mode of vibration whose shape may be found by substituting $\lambda = \lambda_{k}$ into any three of the four equations (3.4) and solving for the ratios B/A , C/A & D/A . This results in the characteristic function of the k^{th} normal mode which is

$$\phi_k(l) = C_k \left[\cosh (\lambda_k l) + \cos (\lambda_k l) - \sigma_k \{ \sinh (\lambda_k l) + \sin (\lambda_k l) \} \right] \quad (3.6)$$

where C_k is an arbitrary constant representing the amplitude of free vibration, and σ_k is the constant $\frac{[\cosh (\lambda_k L) - \cos (\lambda_k L)]}{[\sinh (\lambda_k L) - \sin (\lambda_k L)]}$

We shall now introduce a principal coordinate r_k which describes motion in the k^{th} normal mode such that

$$y_k(l) = r_k \phi_k(l) \quad (3.7)$$

It is convenient to normalise the characteristic function so that unit distortion in the principal coordinate r_k corresponds to a unit displacement at either end of the beam, From this, and equation (3.7), it follows that

$$C_k = 1/2 \quad \text{for all } k.$$

Because many relations in the theory of vibrations are most easily derived by Lagrangian methods, it is important to assess the contribution which each mode makes to the kinetic and potential energy, As to the first of these, the contribution from an elemental length of the beam is

$$\delta T_k = 1/2 \delta l \cdot A_0 \rho [\dot{y}_k(l)]^2$$

so that, for the whole beam,

$$2T_k = a_k \dot{r}_k^2 \quad (3.8)$$

where $a_k = A_0 \rho \int_0^l \phi_k^2(l) dl$ which, on substitution for $\phi_k(l)$ from (3.6), reduces to"

$$a_k = 1/4 m \quad \text{for all } k$$

m being the mass of the beam,

Similarly, the contribution of an element to the potential energy is

$$\delta V_k = 1/2 EI \delta l \left[\partial^2 y / \partial l^2 \right]^2$$

leading to

$$2V_k = C_k r_k^2 \quad (3.9)$$

where $C_k = EI \int_0^L [\phi_k''(x)]^2 dx$. Using the same substitution as before, this reduces to

$$C_k = a_k \omega_k^2 \quad (3.10)$$

Calculations

A number of solutions to the frequency equation (3.5) were computed together with a number of other characteristic properties, Although this information is available elsewhere, a computer program was written and tested which was to become a subroutine of the final program which is discussed in the next chapter, Most tabulated data on the characteristics of beam vibration are given to 5 significant figures, but the calculations which are described throughout this work are made (and required) to 7 figures,

3.3 End receptances of a free free beam in closed form

In order to derive expressions relating dynamic loading and response at an end of the beam, recourse is made to the general solution in equation (3.3). Suppose there to be an oscillating load $F e^{i\omega t}$ applied to the end of the beam ($x = 0$), then one of the four boundary conditions (3.4) will be altered so that

$$\left\{ \frac{\partial^3 y}{\partial x^3} \right\}_{x=0} = - \frac{F}{EI} \quad (3.11)$$

while the others remain unchanged, An explicit solution for the end displacement $y(0)$ may now be obtained using these modified boundary conditions, and this is

$$y(0) = \frac{F}{EI\lambda^3} \frac{\sin(\lambda L) \cosh(\lambda L) - \cos(\lambda L) \sinh(\lambda L)}{\cos(\lambda L) \cosh(\lambda L) - 1} \quad (3.12)$$

Also, the slope $(\partial y / \partial \ell)$ may be found at the same point, and is

$$\left(\frac{\partial y}{\partial \ell}\right)_{\ell=0} = \frac{F}{-EI\lambda^2} \frac{\sin(\lambda L) \sinh(\lambda L)}{\cos(\lambda L) \cosh(\lambda L) - 1} \quad (3.13)$$

In the same way, the result of applying an oscillating couple

$M_s e^{i\omega t}$ to the end of the beam may be deduced. Again, just one of the four boundary conditions (3.4) is affected so that

$$\left\{ \frac{\partial^2 y}{\partial \ell^2} \right\}_{\ell=0} = \frac{M}{EI} \quad (3.14)$$

The resulting displacement and slope at the end ($\ell = 0$) of the beam are

$$(y)_{\ell=0} = -\frac{M}{EI\lambda^2} \frac{\sin(\lambda L) \sinh(\lambda L)}{\cos(\lambda L) \cosh(\lambda L) - 1} \quad (3.15)$$

and

$$\left(\frac{\partial y}{\partial \ell}\right)_{\ell=0} = \frac{M}{EI\lambda} \frac{\cos(\lambda L) \sinh(\lambda L) + \sin(\lambda L) \cosh(\lambda L)}{\cos(\lambda L) \cosh(\lambda L) - 1} \quad (3.16)$$

The end receptances which we require are defined as the ratios of displacements to load, both measured at the root of a blade, which we take to be the end $\ell = 0$ of the beam. These receptances may be deduced directly from the four preceding equations, and are

$$y(0) = \frac{F}{EI\lambda^3} \frac{\sin(\lambda L) \cosh(\lambda L) - \cos(\lambda L) \sinh(\lambda L)}{\cos(\lambda L) \cosh(\lambda L) - 1} \quad (3.12)$$

Also, the slope $(\partial y / \partial l)$ may be found at the same point, and is

$$\left(\frac{\partial y}{\partial l}\right)_{l=0} = \frac{F}{-EI\lambda^2} \frac{\sin(\lambda L) \sinh(\lambda L)}{\cos(\lambda L) \cosh(\lambda L) - 1} \quad (3.13)$$

In the same way, the result of applying an oscillating couple $M e^{i\omega t}$ to the end of the beam may be deduced. Again, just one of the four boundary conditions (3.4) is affected so that

$$\left\{\frac{\partial^2 y}{\partial l^2}\right\}_{l=0} = \frac{M}{EI} \quad (3.14)$$

The resulting displacement and slope at the end ($l=0$) of the beam are

$$(y)_{l=0} = -\frac{M}{EI\lambda^2} \frac{\sin(\lambda L) \sinh(\lambda L)}{\cos(\lambda L) \cosh(\lambda L) - 1} \quad (3.15)$$

and

$$\left(\frac{\partial y}{\partial l}\right)_{l=0} = \frac{M}{EI\lambda} \frac{\cos(\lambda L) \sinh(\lambda L) + \sin(\lambda L) \cosh(\lambda L)}{\cos(\lambda L) \cosh(\lambda L) - 1} \quad (3.16)$$

The end receptances which we require are defined as the ratios of displacements to load, both measured at the root of a blade, which we take to be the end $l=0$ of the beam. These receptances may be deduced directly from the four preceding equations, and are

(i) the normal displacement - force receptance

$$\underline{\Omega} = (\lambda L) F_1 / m \omega^2 F_0 \quad (3.17)$$

(ii) the normal displacement - couple receptance, and the slope - force receptance (which are identical in conformity with Maxwell's principle of reciprocity)

$$\underline{\Omega}' = (\lambda L)^2 F_2 / m L \omega^2 F_0 \quad (3.18)$$

and (iii), the slope - couple receptance

$$\underline{\Omega}'' = (\lambda L)^3 F_3 / m L^2 \omega^2 F_0 \quad (3.19)$$

In these expressions,

$$\begin{aligned} F_0 &= \cos(\lambda L) \cosh(\lambda L) - 1 \\ F_1 &= \sin(\lambda L) \cosh(\lambda L) - \cos(\lambda L) \sinh(\lambda L) \\ F_2 &= -\sin(\lambda L) \sinh(\lambda L) \\ F_3 &= \cos(\lambda L) \sinh(\lambda L) + \sin(\lambda L) \cosh(\lambda L) \end{aligned} \quad (3.20)$$

The receptance matrix $\underline{\Omega}$ for the present case in which there are just two degrees of coupling (see section 2.2), is

$$\underline{\Omega} = \begin{bmatrix} \underline{\Omega} & \underline{\Omega}' \\ \underline{\Omega}' & \underline{\Omega}'' \end{bmatrix}$$

3.4 End receptances in a series form - an approximation

It is possible to express the end receptances of the previous section as an infinite series. Approximations to these receptances may then be obtained simply by truncating the series at some convenient level, and it is found in practice that reasonable estimates to the exact values are achieved by including a relatively small number of terms. This feature makes the approximate forms very convenient for numerical application,

With reference to the principal coordinates and normal modes of vibration which were discussed in section 3.2, the receptance for the k^{th} mode may be written

$$\Omega^{(k)} = 1 / a_k (\omega_k^2 - \omega^2) \quad (3.21)$$

and further, the receptance between two points on the beam, x & y , may be expressed in terms of such modal receptances as

$$\Omega(x, y) = \sum_{k=1}^{\infty} \Omega^{(k)} \left(\frac{\partial X}{\partial r_k} \right) \left(\frac{\partial Y}{\partial r_k} \right) \quad (3.22)$$

where X is the displacement (or slope) expression for the point at which the displacement (or slope) is measured ($l = l_x$);

and Y is the corresponding expression for the point at which the force (or couple) is applied ($l = l_y$).

Using the displacement function which is derived in equation (3.6), together with its derivative (for the slope), at $A, = l_y = 0$, the three end receptances of the previous section are derived in a series form in terms of the properties of the normal modes of vibration. These are

$$\Omega = \Omega_0 + \sum_{k=1}^{\infty} [\phi_k(0)]^2 / a_k (\omega_k^2 - \omega^2)$$

$$\Omega' = \Omega'_0 + \sum_{k=1}^{\infty} [\phi_k(0) \phi_k'(0)] / a_k (\omega_k^2 - \omega^2)$$

and

$$\Omega'' = \Omega''_0 + \sum_{k=1}^{\infty} [\phi_k'(0)]^2 / a_k (\omega_k^2 - \omega^2) \quad (3.23)$$

corresponding to (3.17), (3.18) and (3.19) respectively, where the three receptances Ω_0 , Ω'_0 and Ω''_0 represent the response of the beam as a rigid body. This motion is accounted for in the closed form receptance expressions, and arises as a special case in this series form as it corresponds to the particular solution $\lambda = 0$ of the frequency equation (3.5). The corresponding properties may be found from first principles, and are

$$\begin{aligned} \Omega_0 &= -1/m\omega^2 - 3/m\omega^2 = -4/m\omega^2 ; \\ \Omega'_0 &= 6/mL\omega^2 ; \quad \Omega''_0 = -12/mL^2\omega^2 . \end{aligned} \quad (3.24)$$

Calculations

As suggested previously, truncation of these infinite series can provide useful approximations to the exact, or closed form, receptances. A number of calculations were made to illustrate how the accuracy of these approximations varies with the number of terms included in the series. Typical results are shown in the four graphs in FIG.3.1 in which the ratio of series form estimate to closed form receptance is plotted against the number of terms in the series. Each of the three receptances Ω , Ω' and Ω'' is represented, and curves are shown which relate to four values of the frequency

parameter (AL). The results indicate that the approximations are not always highly accurate, but at the same time they do provide a very simple, and computationally fast, means of estimating these receptances,

3.5 Flexural vibrations of a freely supported circular disc

The analysis of the elastic vibrations of a uniform circular disc is basically the same as that described in section 3.2 for the free free beam, although it is considerably more complex. This analysis is presented in a number of works, most of which are derived from Prescott's 'Applied Elasticity'.

The basic equation of motion for a circular disc, expressed in polar (r, θ) coordinates, is

$$\nabla^4 w + k^4 \frac{\partial^2 w}{\partial t^2} = 0 \quad (3.25)$$

where w is the displacement of a typical element normal to the plane of the disc;

$$\nabla^2 = \left\{ \frac{\partial^2}{\partial r^2} + \frac{1}{r} \frac{\partial}{\partial r} + \frac{1}{r^2} \frac{\partial^2}{\partial \theta^2} \right\}; \quad k^4 = 2\omega^2 \rho h / \bar{D}; \quad \bar{D} = 2Eh^3 / 3(1-\sigma^2)$$

and h , ρ , E and σ are respectively the half thickness, density, Young's modulus and Poisson's ratio of the disc.

If we now assume a harmonic solution of the form

$$w = W(r, \theta) e^{i\omega t} \quad (3.26)$$

equation (3.25) may be rewritten as

$$(\nabla^2 + k^2)(\nabla^2 - k^2)W = 0 \quad (3.27)$$

and substitution of equation (3.26) leads to the general solution

$$w(r, \theta) = \sum_{n=0}^{\infty} \left\{ \begin{aligned} &\cos n\theta [A_n J_n(kr) + B_n Y_n(kr) + C_n I_n(kr) + D_n K_n(kr)] \\ &+ \sin n\theta [E_n J_n(kr) + F_n Y_n(kr) + G_n I_n(kr) + H_n K_n(kr)] \end{aligned} \right\} \quad (3.28)$$

In this equation, $A_n \rightarrow H_n$ are constants which depend upon boundary conditions, while $J_n(kr)$, $Y_n(kr)$, $I_n(kr)$ and $K_n(kr)$ are the standard notation for various types of Bessel functions of order n and argument (kr) . The boundary conditions which are to be used to determine A , etc. must hold for every integral value of n , so that subsequent work need only treat the general term of equation (3.28). However, it is found that $n = 0$ presents a special case which is most conveniently dealt with separately.

For a continuous plate, the displacement and slope, shear force and bending moment must all be finite at the centre, The expression for displacement (w) is given in (3.28) and the slope may be derived from this equation simply as $(\partial w / \partial r)$. The corresponding expressions for the shear force and bending moment are

$$P = -\bar{D} \left\{ \frac{\partial}{\partial r} (\nabla^2 w) + \frac{(1-\sigma)}{r} \frac{\partial}{\partial \theta} \left(\frac{1}{r} \frac{\partial^2 w}{\partial r \partial \theta} - \frac{1}{r^2} \frac{\partial w}{\partial \theta} \right) \right\}$$

[shear force/unit of circumference], (3.29)

and

$$M = \bar{D} \left\{ \nabla^2 w - \frac{(1-\sigma)}{r} \left(\frac{\partial w}{\partial r} + \frac{1}{r} \frac{\partial^2 w}{\partial \theta^2} \right) \right\}$$

[bending moment/unit of circumference] (3.30)

respectively. The substitution of the above mentioned conditions into the four equations results in the elimination of four of the constants. This arises since the terms containing Y_n and K_n (both of which tend to infinity as r tends to 0) must vanish, thus requiring the coefficients B_n , D_n , F_n and H_n to be **zero**. With this result,

we may rewrite the general solution (3.28) as

$$w_n(r, \theta) = W_n [J_n(\mu_n r) + \mu_n I_n(\mu_n r)] \cos(n\theta - \epsilon_n) \quad (3.31)$$

where $\cos(n\epsilon_n) = A_n / W_n = C_n / \mu_n W_n$

and $\sin(n\epsilon_n) = E_n / W_n = G_n / \mu_n W_n \quad (3.32)$

and W_n , μ_n and ϵ_n are constants which may be found from further boundary conditions. In the present case of a freely supported disc, the absence of restraining forces or couples at the rim gives rise to two more conditions which may be written as

$$[P]_{r=a} = [M]_{r=a} = 0 \quad (3.33)$$

When these conditions are applied to equations (3.29) and (3.30), using the general solution in (3.31), then we find that a non trivial solution can exist only if

$$\begin{aligned} & [b^4 + n^2(n^2 - 1)(1 - \sigma)^2] [I_{n-1}(b) J_{n+1}(b) + I_{n+1}(b) J_{n-1}(b)] \\ & - 2b^2 n(1 - a) [(n-1) I_{n-1}(b) J_{n-1}(b) + (n+1) I_{n+1}(b) J_{n+1}(b)] \\ & = 0 \end{aligned} \quad (3.34a)$$

or, for the special case of $n = 0$, if

$$\begin{aligned} & b^3 \left\{ 2(1 - \sigma) I_1(b) J_1(b) - b [I_1(b) J_0(b) + I_0(b) J_1(b)] \right\} \\ & = 0 \end{aligned} \quad (3.3413)$$

Each equation (3.34) has an infinite number of roots which define the natural frequencies of the disc. As in the case of the beam, to each solution $b = b_{n,s}$ (where s represents the $(s+1)^{th}$ root), there

corresponds a normal mode of vibration whose characteristic properties may be found by substituting $b = b_{ns}$ into equations (3.31) and (3.33). The characteristic function which defines the shape of the n, s mode, is

$$\begin{aligned} \phi_{ns}(r, \theta) &= \left[W_{ns} \left\{ J_n(b_{ns} r/a) + \mu_{ns} I_n(b_{ns} r/a) \right\} \right] \left[\cos(n\theta - \epsilon_{ns}) \right] \\ &= \left[f_{ns}(r) \right] \left[\cos(n\theta - \epsilon_{ns}) \right] \end{aligned} \quad (3.35)$$

where W_{ns} is an arbitrary constant representing the amplitude of free vibration, μ_{ns} is a constant which is equal to

$$\left\{ \frac{b^3 J_n'(b) + (1-\sigma)n^2 [b J_n'(b) - J_n(b)]}{b^3 I_n'(b) - (1-\sigma)n^2 [b I_n'(b) - I_n(b)]} \right\}_{b=b_{ns}} \quad (3.36)$$

and $f_{ns}(r)$ is the radial characteristic function.

If we now introduce a principal coordinate q_{ns} which describes motion in the n, s normal mode such that

$$w_{ns}(r, \theta) = q_{ns} f_{ns}(r) \cos(n\theta - \epsilon_{ns}) \quad (3.37)$$

we may then normalise the radial characteristic functions. Using a similar treatment to that described in the earlier case for the beam, we shall require that for unit distortion in the principal coordinate q_{ns} , the maximum rim amplitude shall be unity. Thus, we find that

$$W_{ns} = \left[J_n(b_{ns}) + \mu_{ns} I_n(b_{ns}) \right]^{-1} \quad (3.38)$$

With the present boundary conditions, it is not possible to establish a value for ϵ_{ns} , and this must consequently remain arbitrary. From equation (3.37), it is possible to deduce the physical form of the modal shapes. The cosine term vanishes at regular intervals of θ and thus gives rise to n nodal diameters

symmetrically disposed about $\theta = \epsilon_{ns}$. The radial characteristic function $f_{ns}(r)$, since it contains Bessel functions, is an oscillating function which is zero at a number of specific values of r . This results in a number (s) of nodal circles.

We shall now derive expressions for the kinetic and potential energy of the disc when it is vibrating in its n, s normal mode. For an element of the disc, the kinetic energy may be written as

$$\delta T_{ns} = \frac{1}{2} \rho \cdot 2h \cdot \delta r \cdot \delta \theta \cdot r [\dot{w}_{ns}(r, \theta)]^2 \quad (3.39)$$

so that for the whole disc

$$2 T_{ns} = 2 \rho h \int_0^{2\pi} \int_0^a r \dot{w}_{ns}^2 dr d\theta \quad (3.40)$$

$$\text{or} \quad = a_{ns} \dot{q}_{ns}^2 \quad (3.41)$$

where

$$a_{ns} = \left\{ \begin{matrix} 2 \\ 1 \end{matrix} \right\} \frac{1}{2} \int_0^{2\pi} \int_0^a r [f_{ns}(r) \cos(n\theta - \epsilon_{ns})]^2 dr d\theta \quad (3.42)$$

The integral in equation (3.42) may be expressed explicitly using a result given by McLachlan, as (see APPENDIX 2)

$$a_{ns}^* = \frac{a_{ns}}{M_d} = \left\{ \begin{matrix} 2 \\ 1 \end{matrix} \right\} \frac{1}{2} W_{ns}^2 \left\{ J_n^2 - J_{n-1} J_{n+1} \right. \quad \left. \begin{matrix} n=0 \\ n>0 \end{matrix} \right\} \\ + \frac{2\mu_{ns}}{b_{ns}} (J_n I_{n-1} - I_n J_{n-1}) + \mu_{ns}^2 (I_n^2 - I_{n-1} I_{n+1}) \quad (3.43)$$

where the argument of each Bessel function is (b_{ns}) .

For the corresponding potential energy expression, use is made of the relationship between the inertia and stiffness coefficients of a normal mode, in order to avoid further lengthy algebraic manipulation.

If c_{ms} is the stiffness coefficient, and a_{ms} the inertia coefficient for the m,s mode, then these two are related by the natural frequency (ω_{ms}) such that

$$c_{ms} = a_{ms} \omega_{ms}^2 \quad (3.44)$$

The potential energy of the disc, when vibrating in its m,s normal mode, is then simply

$$2V_{ms} = c_{ms} q_{ms}^2 = a_{ms} \omega_{ms}^2 q_{ms}^2 \quad (3.45)$$

Characteristic properties were computed for each of a large number of normal modes. FIG.3.2 shows a table of three of the more important quantities; dimensionless natural frequency (b_{ms}), inertia coefficient (a_{ms}^*) and slope at the rim ($a \left[\frac{\partial}{\partial r} (f_{ms}(r)) \right]_{r=a}$).

3.6 Edge receptances of a free disc in closed form

We shall now derive receptance expressions which relate the displacement (w) of the rim of the disc to excitation which is applied to the rim. A suitable form for this excitation is one which varies sinusoidally around the disc (e.g. $L = L_m \cos m\theta \cdot e^{i\omega t}$) since any other loading configuration may be achieved by the linear superposition of a number of such expressions.

Consider first the effect of applying a circumferential shear force, $P = P_m \cos m\theta \cdot e^{i\omega t}$. In this case, the boundary conditions are

$$\left[P \right]_{r=a} = P_m \cos m\theta ; \quad \left[M \right]_{r=a} = 0 \quad (3.46)$$

(omitting the $e^{i\omega t}$ term for convenience), where the expressions for P and M may be found in equations (3.29) and (3.30). Using the general form of the displacement function ($w_m(r, \theta)$) which is given

in equation (3.31), application of the conditions in (3.46) results in the solution (which is derived in APPENDIX 3)

$$w_n(r, \theta) = \frac{a^2}{\bar{D}} \frac{N_n(r)}{D_n} P_n \cos n\theta \quad (3.47)$$

where

$$D_n = [b^4 + n^2(n^2-1)(1-\sigma)^2] [I_{n-1} J_{n+1} + I_{n+1} J_{n-1}] \\ - 2b^2n(1-\sigma) [(n-1) I_{n-1} J_{n-1} + (n+1) I_{n+1} J_{n+1}]$$

and

$$N_n(r) = \frac{1}{b} \left\{ (R-b^2) J_{n-1} + (Q-b^2) J_{n+1} \right\} I_n(b\tau/a) \\ - \left\{ (R+b^2) I_{n-1} - (Q+b^2) I_{n+1} \right\} J_n(b\tau/a)$$

(omitting the argument of the Bessel functions when it is **b**):

The displacement at the rim, in which we are particularly interested, is.

$$w_n(a, \theta) = \frac{a^2}{\bar{D}} \frac{N_n}{D_n} P_n \cos n\theta \\ = W_n \cos n\theta \quad (3.48)$$

where

$$N_n = (1-\sigma) [I_{n-1} J_{n+1} + I_{n+1} J_{n-1}] - 4n I_n J_n$$

The radial slope ($\partial w / \partial r$) at the **rim** of the disc is also of interest, and this may be derived from equation (3.48) as

$$\left(\frac{\partial w}{\partial r} \right)_{r=a} = \frac{a}{\bar{D}} \frac{N_n'}{D_n} P_n \cos n\theta \\ = W_n' \cos n\theta \quad (3.49)$$

where

$$N_n' = a \left[\frac{d}{dr} N_n(r) \right]_{r=a} \\ = n^2(1-\sigma) [I_{n-1} J_{n+1} + I_{n+1} J_{n-1}] \\ - b^2 [I_{n-1} J_{n-1} + I_{n+1} J_{n+1}]$$

If we next consider a bending moment $M = M_n \cos n\theta e^{i\omega t}$ to be applied to the rim of the disc, then the boundary conditions become

$$[P]_{r=a} = 0 \quad ; \quad [M]_{r=a} = M_n \cos n\theta \quad (3.50)$$

When these conditions are applied to equations (3.29) and (3.30), the displacement at the rim of the disc is found (in APPENDIX 3) to be

$$w_n(a, \theta) = \frac{a}{D} \frac{N_n'}{D_n} M_n \cos n\theta = X_n \cos n\theta \quad (3.51)$$

The corresponding expression for the slope at the rim of the disc is

$$\left(\frac{\partial w}{\partial r}\right)_{r=a} = \frac{1}{D} \frac{N_n''}{D_n} M_n \cos n\theta = X_n' \cos n\theta \quad (3.52)$$

where

$$N_n'' = a^2 \left[\frac{\partial^2}{\partial r^2} N_n(r) \right]_{r=a}$$

or

$$N_n'' = n^2(1-\sigma) \left[J_{n+1} I_{n-1} + J_{n-1} I_{n+1} \right] \\ - b^2 n \left[J_{n-1} - J_{n+1} \right] \left[I_{n-1} + I_{n+1} \right]$$

The foregoing expressions for displacement and slope hold for any integral value of n except zero. When $n = 0$, it is found that the expressions for N_n , N_n' , N_n'' and D_n all vanish. However, non zero values for the corresponding functions N_0 , etc. may be determined, either by repeating the analysis for this special case, or by a limiting process. The former is quite straightforward and results in the following expressions:

$$\begin{aligned}
D_o &= b^3 \{ b [I_o J_1 + I_1 J_o] - 2 (1-\sigma) I_1 J_1 \} \\
N_o &= (1-\sigma) [I_o J_1 + I_1 J_o] - 2 b I_o J_o \\
N_o' &= b^2 [I_o J_1 - J_o I_1] \\
N_o'' &= 2 b^3 I_1 J_1 \\
N_o(r) &= \left\{ (1-\sigma) [I_1 J_o (br/a) \mp J_1 I_o (br/a)] \right. \\
&\quad \left. - b [I_o J_o (br/a) + J_o I_o (br/a)] \right\} \quad (3053)
\end{aligned}$$

We shall now introduce and define the disc edge receptances which give the displacement and slope at a point a, θ caused by a loading of the form $L_n \cos n\theta e^{i\omega t}$ applied to the rim of the disc. The receptance relating the normal displacement $w_n(a, \theta) = W_n \cos n\theta$ and a circumferential shear force of $P_n \cos n\theta$ is defined as

$$\alpha^{(n)} = \frac{W_n}{P_n} = \frac{a^2}{\bar{D}} \frac{N_n}{D_n} \quad (3054)$$

The normal displacement - circumferential couple, and the slope - circumferential shear force receptances are identical, and are

$$\alpha'^{(n)} = \frac{W_n'}{P_n} = \frac{X_n}{M_n} = \frac{a}{\bar{D}} \frac{N_n'}{D_n} \quad (3.55)$$

Finally, the slope - circumferential couple receptance is

$$\alpha''^{(n)} = \frac{X_n'}{M_n} = \frac{I}{\bar{D}} \frac{N_n''}{D_n} \quad (3.56)$$

It may be seen from this analysis that when the loading is symmetrical about $\theta = 0$, then so is the resulting displacement. We may extend this result to conclude that the constant ϵ_n is zero relative to the origin of the excitation, for all n .

3.7 Edge receptances in a series form

We shall now show that the edge receptances which were introduced in the previous section may also be represented by an infinite series. This analysis is summarised from that of Armstrong.

Let there be a normal force P applied at the rim such that $P = P_k \cos k\theta \cdot e^{i\omega t}$. We may determine the response in the n, s normal mode by considering the generalised force in that mode (Q_{ns}) which results from P . We shall also make use of the result in the previous section that for this type of loading, ϵ_{ns} is always 0. The total generalised force in the n, s mode due to P is

$$Q_{ns} = \int_0^{2\pi} P_k \cos k\theta [f_{ns}(r)]_{r=a} \cos n\theta \cdot d\theta \quad (3.57)$$

This integral has three possible solutions, viz.

$$\begin{aligned} Q_{ns} &= 0 & : k \neq n \\ Q_{ns} &= \pi P_k & : k = n \neq 0 \\ Q_{ns} &= 2\pi P_k & : k = n = 0 \end{aligned} \quad (3.58)$$

The magnitude of the principal coordinate q_{ns} is given by

$$q_{ns} = Q_{ns} \left\{ \frac{1}{a_{ns}(\omega_{ns}^2 - \omega^2)} \right\} \quad (3.59)$$

so that the displacement at the rim resulting from vibration in the n, s normal mode, is

$$\begin{aligned} w_{ns}(a, \theta) &= \begin{bmatrix} 2 \\ 1 \end{bmatrix} \frac{\pi P_m \cos n\theta}{a_{ns}(\omega_{ns}^2 - \omega^2)} & \begin{bmatrix} n=0 \\ n>0 \end{bmatrix} \\ &= W_{ns} \cos n\theta \end{aligned} \quad (3.60)$$

Similarly, an expression may be derived for the slope at the rim, and this is found to be

$$\begin{aligned} \left(\frac{\partial W_{ms}}{\partial r} \right)_{r=a} &= \begin{bmatrix} 2 \\ 1 \end{bmatrix} \frac{[\frac{\partial}{\partial r} (f_{ms}(r))]_{r=a} \pi P_n}{a_{ms} (\omega_{ms}^2 - \omega^2)} \cos n\theta \\ &= W_{ms}' \cos n\theta \end{aligned} \quad (3.61)$$

If we define the edge receptances for the n, s mode as

$$\alpha^{(ms)} = \frac{W_{ms}}{P_n} \quad (3.62)$$

and

$$\alpha'^{(ms)} = \frac{W_{ms}'}{P_n} \quad (3.63)$$

then the so-called 'closed form' receptances $\alpha^{(n)}$ and $\alpha'^{(n)}$ may be written as

$$\alpha^{(n)} = \sum_{s=0}^{\infty} \alpha^{(ms)} = \begin{bmatrix} 2 \\ 1 \end{bmatrix} \sum_{s=0}^{\infty} \frac{\pi}{a_{ms} (\omega_{ms}^2 - \omega^2)} \quad (3.64)$$

and

$$\alpha'^{(n)} = \sum_{s=0}^{\infty} \alpha'^{(ms)} \quad (3.65)$$

If the load at the rim is a couple $M = M_0 \cos k\theta \cdot e^{i\omega t}$, then a similar treatment to that described above results in the following receptance expressions:

$$\alpha^{I(ms)} = \begin{bmatrix} 2 \\ 1 \end{bmatrix} \frac{\pi \left[\frac{\partial}{\partial r} f_{ms}(r) \right]_{r=a}}{a_{ms} (\omega_{ms}^2 - \omega^2)}$$

and

$$\alpha^{II(ms)} = \begin{bmatrix} 2 \\ 1 \end{bmatrix} \frac{\pi \left[\frac{\partial}{\partial r} f_{ms}(r) \right]_{r=a}^2}{a_{ms} (\omega_{ms}^2 - \omega^2)} \quad (3.66)$$

As in the case of the free free beam, there are two rigid body, or zero frequency, modes of vibration. These are in fact included in the range $n, s = 0 \rightarrow \infty$, but their characteristic properties are best computed separately from those for the **flexural** modes. The first zero frequency mode corresponds to $n = 0, s = 0$, and represents translation of the disc as a rigid body. The second mode occurs when $n = 1, s = 0$, and constitutes rotation of the disc about a diameter. By considering the disc as a rigid body, it is possible to write down the properties of these two modes. We find

$$\omega_{00} = 0 ; a_{00} = M_d ; \left[f'_{00}(a) \right] = 0 \quad (3.67)$$

for the first case, and

$$\omega_{10} = 0 ; a_{10} = \frac{1}{4} M_d ; \left[f'_{10}(a) \right] = \frac{1}{a} \quad (3.68)$$

for the second.

Calculations

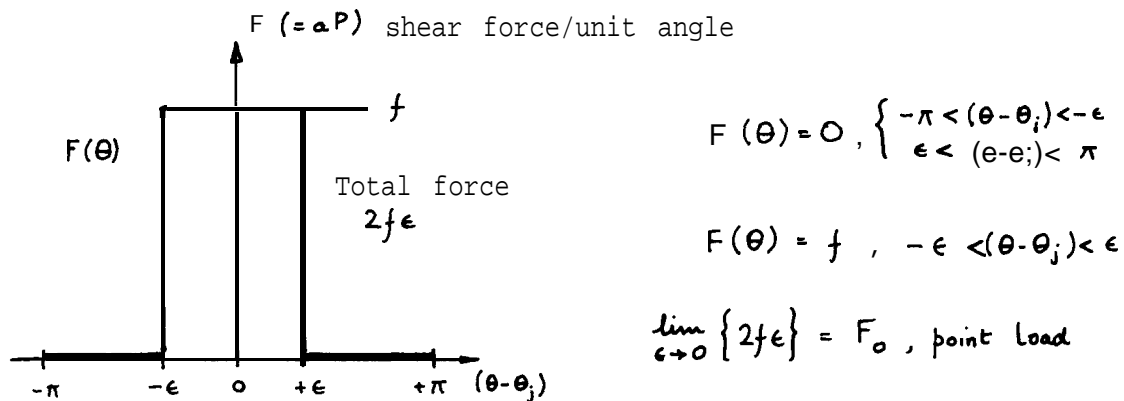
A number of calculations were made in order to study the accuracy of the truncated series form for the disc receptances. A large number of cases were necessary before a general pattern could be seen, and typical results are shown in FIG.3.3 where the estimate to the exact receptance is plotted against the number of terms included in the series.

The general conclusion to be drawn from these results is that the series form of disc receptance only provides a good approximation to the exact value when a large number of terms are included.

3.8 Point receptances

It was mentioned in section 3.6 that the edge receptances which were derived there could be used to provide receptances for any form of loading at the rim. In this section, the case of a point load applied at some position j ($r = a$, $\theta = \theta_j$) will be studied in detail since it is this type of load which is considered in the general analysis (Chapter 2).

Consider a distribution of shear force around the rim which is of the form $F(\theta)$;



If we represent this load by a Fourier series, then we may write

$$F(\theta) = \frac{1}{2} d_0 + \sum_{l=1}^{\infty} d_l \cos l(\theta - \theta_j) \quad (3.69)$$

where

$$d_l = \frac{2}{\pi} \int_0^{\pi} F(\theta) \cos l(\theta - \theta_j) d\theta = \frac{2f\epsilon}{\pi} \quad (3.70)$$

The limiting case as ϵ tends to 0 is a point load F_0 , and in this case

$$F(\theta)_{\text{POINT LOAD}} = \frac{F_0}{\pi} \left\{ \frac{1}{2} + \sum_{\ell=1}^{\infty} \cos \ell(\theta - \theta_j) \right\} \quad (3.71)$$

Now, the displacement of the rim of the disc due to a point load excitation, may be expressed in terms of the edge receptances as

$$w(a, \theta) = \frac{\alpha^{(0)} F_0}{2\pi} + \sum_{n=1}^{\infty} \frac{\alpha^{(n)} F_0 \cos n(\theta - \theta_j)}{\pi} \quad (3.72)$$

We shall now define the point receptances which relate the displacement and slope at a point i ($r=a, \theta=\theta_i$) on the rim of the disc to a point force or couple applied at j ($r=a, \theta=\theta_j$). These are

$$\alpha_{i,j} = \frac{1}{\pi} \left\{ \frac{1}{2} \alpha^{(0)} + \sum_{n=1}^{\infty} \alpha^{(n)} \cos n(\theta_i - \theta_j) \right\} \quad (3.73)$$

$$\alpha'_{i,j} = \frac{1}{\pi} \left\{ \frac{1}{2} \alpha'^{(0)} + \sum_{n=1}^{\infty} \alpha'^{(n)} \cos n(\theta_i - \theta_j) \right\} \quad (3.74)$$

$$\alpha''_{i,j} = \frac{1}{\pi} \left\{ \frac{1}{2} \alpha''^{(0)} + \sum_{n=1}^{\infty} \alpha''^{(n)} \cos n(\theta_i - \theta_j) \right\} \quad (3.75)$$

respectively.

Calculations

As in previous cases where an infinite series is truncated for practical reasons, it is necessary to check that convergence of the series is satisfactory, and that the truncation level which is proposed is suitable. A series of calculations was made in the present case in an attempt to establish a suitable rule for determining the number of terms required in the series in each of (3.73), (3.74) and (3.75) above.

The results (examples of which are shown in FIG.3.4) indicated that a suitable formula relating the number of terms to the frequency (b) at which the receptances are required would be $R = b + 15$, and this is used for all subsequent receptance calculations.

It may be noted that in this case, there is no exact or closed form expression with which to compare the series, nor is it envisaged that one may be obtained as it requires the summation of complicated Bessel functions of all integral orders from 0 to ∞ .

CHAPTER 4

A NUMERICAL STUDY OF A UNIFORM BLADED DISC

4.0 Summary

The results of Chapters 2 and 3 will now be used to obtain solutions to the vibration problem of a simplified bladed disc. This consists of a uniform circular disc which has a number of uniform rectangular bars attached at points on the rim to represent the blades. A receptance determinant is derived for this system and its properties are discussed prior to an extensive computational programme. An approximate system matrix is then formed, and the estimates of natural frequencies and modal shapes which its eigenvalues and eigenvectors provide are compared with those obtained by the 'exact' method. Applications of both methods are discussed. Finally the principal characteristics of the modes of vibration which emerge from the numerical study are summarised.

4.1 Application of the receptance method of solution to a uniform model of a bladed disc

We shall now apply the analysis presented in Chapter 2 to the uniform model whose component parts were discussed in the previous chapter. It will be convenient to refer only to those sections of the general analysis which are specifically relevant, and not to repeat each step in full. Since only straight blades are considered in this study, it was decided that the third degree of coupling - the tangential slope (section 2.1) - should be omitted as being of secondary importance. Thus, it is only the normal displacement and radial slope which have to be matched at each blade - disc fixing point. This is compatible with Armstrong's approach and is expected to provide good approximations for non-twisted blades. However, should it be necessary to consider the torsional modes of vibration of the blades, then this third form of coupling must be included.

The blade and disc receptance expressions which are used throughout this analysis were all derived and discussed in the previous chapter, and the symbols which were used for them there are retained. Only the so-called closed form receptances will be used.

With reference to FIG.2.1 and the analysis of section 2.3, we may express the normal displacement and radial slope of the point i on the rim of the disc in terms of the disc receptance terms and the forces (F_j) normal to the disc and couples (C_j) about tangents to the rim. These are

$$\begin{aligned} w_i &= \sum_{j=1}^N (\alpha_{ij} F_j + \alpha_{i,j}^{\prime} C_j) \\ w_i^{\prime} &= \sum (\alpha_{i,j}^{\prime} F_j + \alpha_{i,j}^{\prime\prime} C_j) \end{aligned} \quad (4.1)$$

respectively. Similarly, the displacement and slope at the root of the i^{th} blade expressed in terms of the force (f_i) and couple (c_i) acting at the same point are

$$\begin{aligned} y_i &= \Omega_i f_i + \Omega_i^{\prime} c_i \\ y_i^{\prime} &= \Omega_i^{\prime} f_i + \Omega_i^{\prime\prime} c_i \end{aligned} \quad (4.2)$$

If the displacements and slopes of both disc and blade are equated at each of the N fixing points, then a set of $2N$ linear equations are formed. These consist of a set of N similar pairs, and the general form of each pair is

$$\begin{aligned} \sum_{j=1}^N (\alpha_{ij} F_j + \alpha_{i,j}^{\prime} C_j) + \Omega_i F_i + \Omega_i^{\prime} C_i &= 0 \\ \sum_{j=1}^N (\alpha_{i,j}^{\prime} F_j + \alpha_{i,j}^{\prime\prime} C_j) + \Omega_i^{\prime} F_i + \Omega_i^{\prime\prime} C_i &= 0 \end{aligned} \quad (4.3)$$

The condition that these equations shall have a non trivial solution (i.e. not all F & C zero) is derived from the determinant of the coefficients of the equations (4.3), **A**. The general form of this determinant is given in FIG.4.2 and since every element in it is a frequency dependent receptance term, Δ itself is a function of frequency and it is the values of this parameter which cause it to vanish that provide the required solutions to (4.3). These values are known as the natural frequencies of the system, and they represent the frequencies at which undamped free vibration is possible.

To each such solution there corresponds a modal shape, or set of relative values of the variables F_j, C_j , although a unique solution for F_j and C_j does not exist. These modal shapes may be found by substitution of the natural frequencies into equations (4.3), removing one of the variables (F_1 say), and solving the resulting set of $(2N - 1)$ inhomogeneous equations for $F_j / F_1, C_j / F_1$ etc.

4.2 Properties of the receptance determinant

Before proceeding with a numerical treatment of this determinant, it is useful to examine the form which it takes,, Owing to the circular symmetry of the system, a disc receptance expression which relates point (i) with ($i + p$) is identical to one relating (i) with ($i + N - p$). Furthermore, this receptance is independent of the actual value of i and is purely a function of the separation of the two points, which is p . Thus

$$\alpha_{i, i+p} \equiv \alpha_{i, i+N-p} = \alpha_p \quad \text{for all } i \quad (4.4)$$

and it is this feature which is largely responsible for the interesting properties of the determinant. A second observation concerning the determinant Δ is that it may be seen to be composed of four quarters, each of which follows the same pattern, Using the result in equation (4.4) above, the receptance determinant for a symmetrical five bladed

disc has been written out in full (FIG.4.3), and with the four similar quarters indicated a rather curious symmetry is now evident.

Even with such a small number of blades as five, it is not practical to expand this determinant, but it is possible to show that it has some interesting properties. As a further simplification which is justified by the result, we shall consider the situation which would result from restricting the analysis to include just one degree of coupling. The receptance determinant for this case would be in fact one quarter of \mathbf{A} , and this reduced determinant is

$$\Delta_a = \begin{vmatrix} a_0 & a_1 & a_2 & a_2 & a_1 \\ a_1 & a_0 & a_1 & a_2 & a_2 \\ a_2 & a_1 & a_0 & a_1 & a_2 \\ a_2 & a_2 & a_1 & a_0 & a_1 \\ a_1 & a_2 & a_2 & a_1 & a_0 \end{vmatrix} \quad (4.5)$$

which, because of its symmetry, is a special type of circulant. As such, it may be factorised and expanded to the form given by Aitken,

$$\Delta_a = \prod_{j=1}^4 \left\{ a_0 + a_1 \omega_j + a_2 \omega_j^2 + a_2 \omega_j^3 + a_1 \omega_j^4 \right\} \quad (4.6)$$

where ω_j is the j^{th} complex root of $(1)^{1/5}$. On simplification, this product reduces to a simpler form in which there are only three different factors;

$$\Delta_a = [a_0 + 2a_1 + 2a_2] \left[a_0 + a_1(\omega + \omega^4) + a_2(\omega^2 + \omega^3) \right]^2 \times \left[a_0 + a_1(\omega^2 + \omega^3) + a_2(\omega + \omega^4) \right]^2 \quad (4.7)$$

and this in turn becomes

$$\Delta_a = [a_0 + 2a_1 + 2a_2] [a_0^2 - a_1^2 - a_2^2 - a_0 a_1 - a_0 a_2 + 3a_1 a_2]^2 \quad (4.8)$$

The three receptance terms, a_0 , a_1 and a_2 are all frequency dependent so that we may write

$$\Delta_a(\omega) = A_1(\omega) A_2(\omega) \quad (4.9)$$

in terms of the dimensionless frequency parameter ω . Now, the roots of Δ_a may be found by determining the roots of both A_1 and A_2 , and since the latter is a perfect square it may never be negative so that any roots it might possess will consist of coincident pairs. The significance of this is demonstrated in FIG.4.4 which shows what might be a typical section of a plot of Δ_a against ω . The first of the two roots shown is the result of A_1 vanishing and is known as a 'single' root, while the second one (or coincident pair) occurs because $A_2 = 0$, and this is termed a 'double' root.

Clearly, these double roots exist directly as a result of the circular symmetry of the disc and the uniformity of the set of blades. Further, it would appear that this result will hold for a disc with any number of equally spaced identical blades.

If now the system has its symmetry disturbed (i.e. is detuned) by varying the blades, then the diagonal terms of Δ_a will no longer all be identical. This necessarily destroys the circulant properties of the determinant but still leaves it symmetrical. It is reasonable to assume that the detuned system determinant will no longer necessarily exhibit double roots as two solutions at the same frequency, but as a pair of solutions with close natural frequencies,

Using this simplified model, two types of solution are predicted; those corresponding to single roots and those associated

with double roots. It is also postulated that a natural frequency splitting phenomenon might be associated with detuning.

If more than one degree of coupling between the disc and blades is admitted to the analysis, then the algebraic problem greatly increases in complexity while the physical system is virtually unchanged. The corresponding determinant for two degrees of coupling was shown in **FIG.4.3**, and whilst it is clearly not a circulant, a symmetry due to the circular properties of the system is still in evidence. It would seem reasonable to assume that the broad conclusions drawn for the simpler case above may be applied to this refinement of the same system.

4.3 Natural frequency solutions using the receptance method

Based upon the analysis in section 4.1 together with the computational experience reported in Chapter 3, a computer program was written to determine the natural frequencies of the uniform bladed disc. This it does simply by evaluating the frequency determinant of **an N b** laded disc of the type described above, assuming the two degrees of coupling, and the routines which were developed earlier for the calculation of the closed form disc receptance expressions (Chapter 3) now form the heart of this program.

Some apprehension was felt concerning the possible behaviour of the determinant in frequency regions near the natural frequencies of the disc alone. At these frequencies, each of the receptance terms which form the determinant is infinite, and whereas the value of the determinant itself would not necessarily be infinite, its evaluation might present a formidable computational problem. As it was not possible to estimate the extent to which such ill conditioning might affect the calculations, steps were taken to ensure **that** these difficulties were avoided.

The program was used to calculate the natural frequencies of a

number of different systems. Initially, a one bladed disc (of academic interest only!) was treated as the results could be checked quite easily by hand calculations. Then, the general program was tested with a three bladed disc and a programme of computing for the five bladed discs of interest was drawn up and carried out.

In the case of a tuned system, the pattern of the determinant - frequency relationship which had been predicted (section 4.2) was found to be accurate. Sections of a graph in which A is plotted against the frequency parameter (b) are shown in FIG.4.5, and from these the natural frequencies may be found. Using this method, the first dozen or so natural frequencies were computed to 5 significant figures, although not very efficiently owing to the failure of conventional root finding techniques to locate the double roots. A number of disc and blade sets with various geometrical ratios were treated in this way, and some of the results are presented graphically in FIG.4.6 where the natural frequencies of a five bladed disc are plotted for blades of varying length but constant width.

Next, the effect of detuning the system was investigated by making the blades slightly different one from another. This produced the result that was tentatively suggested in the previous section. Where the tuned system had a double root at one frequency, for the detuned system there was a pair of close natural frequencies. Single roots were largely unaffected. The system whose determinant produced the double root shown in FIG.4.5 was subjected to this type of detuning, and the corresponding section of the determinant - frequency plot is reproduced in FIG.4.7. The frequency splitting phenomenon, illustrated in this graph, is found to be a characteristic of every double root, and a detailed study of its mechanism may be found in Chapter 5.

There is one special case which has passed, so far, unmentioned. From consideration of the physical system, it may be seen that it is

possible for an N bladed disc to vibrate in a mode with N nodal diameters so disposed that the blades are all situated at nodal points and thus cannot participate in the motion. The natural frequencies and other characteristics of such modes of vibration of the bladed disc will be identical to those of the disc mode of the same shape. To each such mode, there will correspond a conjugate mode in which the blades will be situated at antinodes of a mode whose shape is similar, but not identical, to that of the pure disc mode. These latter conjugate modes appear as single roots to the determinant solution, but the former pure disc vibration modes are not detected by this solution since they constitute a trivial case in which $F_j, C_j = 0$.

The different types of solution and their corresponding modes are discussed in the last section of this chapter.

4.4 Calculation of modal shapes

Each root of the frequency determinant corresponds to a mode of vibration of the bladed disc. There are two properties of each of these modes which are defined by this solution, one being the natural frequency and the other the modal shape. The latter is found as a set of relative values for the forces and couples (F_j, C_j) and is conveniently expressed as $\{F_1 : F_2 : \dots : F_N : C_1 : C_2 : \dots : C_N\}$. From such a set of ratios, it is possible to derive other forms of the modal shape, such as the pattern of nodal lines which was used to describe the modes of a circular disc. However, it is the original version of modal shape which is the more convenient form for qualitative measurements and comparison.

The method by which these modal shapes are computed is basically quite straightforward, although difficulties do arise when there is more than one solution at a particular frequency, such as the double roots of the tuned system. If there is a single root of the determinant at frequency ω_x , then the modal shape corresponding to

that natural frequency is determined as follows. The equations represented by equation (4.3) may be written out with each receptance term completely defined by the value of ω_x . A unique solution for the variables F_j, C_j does not exist because the equations (4.3) are homogeneous, but a set of relative values may be found. By selecting one of these variables (C_N say) and setting it to unity, it is removed from the equations as a variable and replaced as a constant term. In this way, a set of $2N-1$ inhomogeneous equations are formed from which a solution for $F_1/C_N, F_2/C_N, \dots$ etc. may be obtained, and appears as a set of ratios $\{F_1 : F_2 : \dots : F_N : C_1 : C_2 : \dots : 1\}$.

If there is a double root at frequency ω_x , it is necessary to find two such sets of ratios which are linearly independent. The modal shape of free vibration at this frequency is then defined as any linear combination of these two modal shapes. In this case, it is necessary to fix two variables and slightly modify the procedure, but the results for these cases are so arbitrary that they are not very useful and in fact are not used in the subsequent sections.

Calculations have been made for a five bladed disc for a number of modes in which there is a unique root to the determinant. These include the single roots of the tuned systems, and all roots of the detuned versions. Consider first the single modes of the tuned model. In every case, the modal shape is found to exhibit complete circular uniformity and is always of the form $\{x : x : x : x : x : 1 : 1 : 1 : 1\}$ so that each blade experiences the same loading. When the system is detuned by varying (for example) the blade lengths about a mean value, then a similar variation in blade loading about the average value is found.

When examining the shapes of modes corresponding to double roots, it is convenient to confine the examples to detuned cases in order to simplify the computational procedure. Calculations were made for the mode shapes of the double mode whose pair of natural frequencies

is illustrated in FSG.4.7, and the results are tabulated in FIG.4.8. Although there seems to be little significance in these actual figures, it may be shown that the distribution of both force (F_j) and couple (C_j) around the disc correspond to a $\cos(2\theta + \phi)$ distribution for the first mode, and a $\sin(2\theta + \phi)$ distribution for the second (where θ is the angular position of the blades). The detailed study in Chapter 6 examines the full significance of these observations, and relates them to the specific form of detuning of which they are the result.

By considering the combined effect of five forces and couples (F_j, C_j) acting at the rim of the disc, it is possible to compute the normal displacement of any part of the disc using the general receptance expressions $\alpha(r, \theta)$ in Chapter 3. These calculations lead directly to defining the patterns of nodal lines which constitute an alternative expression of modal shape. However, the numerical procedure is somewhat lengthy and the results merely of passing interest, so that few calculations have been done. As an illustration of the technique, the nodal patterns which correspond to the pair of modes described above are given in FIG.4.9.

From both presentations of the modal shapes of this pair of modes, it is clear that not only are their natural frequencies almost identical, but also their modal shapes are identical in every aspect other than their angular orientation in the disc.

Chapter 6 deals with the properties of the modal shapes of detuned systems in much greater detail, and it is sufficient at this stage to have described the manner in which they may be found, together with one or two examples.

4.5 Application of the matrix method of solution to a uniform model

Having established that the receptance determinant solution provides a somewhat inefficient means of computing natural frequencies, we shall now investigate the potential of the alternative approximate solution. This expresses the motion of the system in a matrix form which readily lends itself to numerical application on a digital computer. However, we have yet to establish whether the estimates of natural frequency which the approximate method yields are sufficiently accurate to be useful.

The **salient** points of the analysis in section 2.6 will now be expressed in terms of the properties of the uniform model which, in turn, were derived in Chapter 3. Considering first the blades, which are represented by rectangular beams, the displacement functions of the i^{th} blade (equation 2.12) may be written as

$$y_i(l) = i h_T + \left(\frac{L_i}{2} - l\right) i h_R + \sum_{k=1}^S i \Phi_k(l) i h_k \quad (4.10)$$

$$y_i'(l) = -i h_R + \sum_{k=1}^S i \Phi_k'(l) i h_k \quad (4.11)$$

where $y_i(l)$ and $y_i'(l)$ are the displacement and slope of the beam;

l is the coordinate along the length of the beam with an origin at the root;

L_i is the length of the beam;

$i h_T$ and $i h_R$ are the principal coordinates representing rigid body translation and rotation;

$i h_k$ is the principal coordinate for the k^{th} **flexural** mode;

$i \Phi_k(l)$ is the characteristic function of that mode, and

$i \Phi_k'(l)$ is its derivative with respect to l ;

S represents the number of **flexural** modes which are admitted to the approximation.

The potential and kinetic energy may be expressed in terms of the same properties as

$$2V = \frac{1}{4} \sum_{k=1}^S m_i \omega_k^2 i r_k^2 \quad (4.12)$$

$$2T = m_i \dot{i}_r^2 + \frac{1}{3} m_i \left(\frac{L_i}{2}\right)^2 \dot{i}_R^2 + \frac{1}{4} \sum_{k=1}^S m_i i \dot{r}_k^2 \quad (4.13)$$

Turning now to the disc, we find that a similar treatment is less straightforward in this case. The normal displacement function for a single **flexural** mode was derived in equation (3.37) and is

$$w_{ns}(r, \theta) = q_{ns} f_{ns}(r) \cos(n\theta - \epsilon_{ns}) \quad (4.14)$$

where r and θ are the geometrical coordinates;
 a is the radius of the disc;
 q_{ns} is the principal coordinate for the n, s mode which has n nodal diameters and s nodal circles;
 $f_{ns}(r)$ is the radial characteristic function of that mode and is derived in equation (3.40), and
 $\cos(n\theta - \epsilon_{ns})$ is the angular characteristic function.

In this equation there are two unknown parameters, q_{ns} and ϵ_{ns} , and it is found that a more convenient way of expressing the equation is obtained by introducing a pair of principal coordinates, q_{ns} and p_{ns} , so that

$$w_{ns}(r, \theta) = f_{ns}(r) \{ q_{ns} \cos n\theta + p_{ns} \sin n\theta \} \quad (4.15)$$

The double suffix n, s which identifies the **flexural** modes may be replaced by the single suffix j which is chosen for convenience so that $j = 1, 2, 3 \dots$ etc. corresponds to the modes arranged in ascending order of their natural frequency. Thus:

j	b_j^2	n_j	s_j
1	5.398968	2	0
2	8.974141	0	1
3	12.52070	3	0
4	20.45769	1	1
:			

ETC.

On the inclusion of the rigid body modes of vibration (discussed at the end of section 3.6), the final form of the expressions for the normal displacement and slope of the disc is obtained:

$$\begin{aligned}
 w(r, \theta) &= q_{00} + r \{ q_{10} \cos \theta + p_{10} \sin \theta \} \\
 &\quad + \sum_{j=1}^Q f_j(r) \{ q_j \cos n_j \theta + p_j \sin n_j \theta \} \\
 w'(r, \theta) &= \{ q_{10} \cos \theta + p_{10} \sin \theta \} + \sum_{j=1}^Q f_j'(r) \{ q_j \cos n_j \theta + p_j \sin n_j \theta \} \quad (4.16)
 \end{aligned}$$

where q_{00} is the principal coordinate representing rigid body translation
 q_{10} and p_{10} are the principal coordinates for rigid body rotation about perpendicular diameters
and Q is the number of **flexural** modes of vibration considered in the approximation

The potential and kinetic energy of the vibrating disc, in terms of these coordinates, is

$$2V_d = \sum_{j=1}^Q \omega_j^2 a_j (q_j^2 + p_j^2) \quad (4.17)$$

and

$$2T_d = M_d \dot{q}_{00}^2 + \frac{1}{4} M_d a^2 (\dot{q}_{10}^2 + \dot{p}_{10}^2) + \sum_{j=1}^{\infty} a_j (\dot{q}_j^2 + \dot{p}_j^2) \quad (4.18)$$

The equivalent energy expressions for the bladed disc are simply the sums of the respective energy terms of each of the constituent parts of the system. Thus,

$$\begin{aligned} 2V &= 2V_d + \sum_{i=1}^N 2{}_iV \\ 2T &= 2T_d + \sum_{i=1}^N 2{}_iT \end{aligned} \quad (4.19)$$

where both expressions are functions of all the principal coordinates p , q and r , including those representing the rigid body modes of vibration. As explained earlier, the zero-natural-frequency property of these latter modes necessitates the elimination of their coordinates from the equations of motion. In order to eliminate ${}_i r_T$ and ${}_i r_R$ from the kinetic energy term ${}_i V$, two equations may be derived by equating the displacement and slope of the root of the i^{th} blade to the same quantities for the point on the rim of the disc at which it is attached. Thus

$$\begin{aligned} y_i(0) &= w(a, \theta_i) \\ y_i'(0) &= w'(a, \theta_i) \end{aligned} \quad (4.20)$$

and from these equations ${}_i r_T$ and ${}_i r_R$ may be found in terms of ${}_i r_A$ and all b and q . The three disc coordinates q_{00} , q_{10} and p_{10} may be eliminated by the application of Lagrange's equation to the energy expressions (4.19) for each coordinate in turn. The algebraic manipulation of the three resulting equations of motion may be found in APPENDIX 4.1 where q_{00} , q_{10} and p_{10} are expressed

in terms of coordinates representing only **flexural** modes of vibration.

The energy expressions (4.19) may now be written in terms of the coordinates of **flexural** modes only, and further application of the Lagrangian technique to the modified equation (4.19) for each of these coordinates in turn leads to the set of equations of motion of the approximate system. These provide the required system matrix whose eigenvalues and eigenvectors may be computed by one of a number of standard methods. The general forms of the equations of motion are derived in APPENDIX 4.2 for reference.

4.6 Eigenvalue estimates of natural frequency

A series of calculations was done on Titan in order to find the accuracy of the eigenvalue estimates of natural frequency which resulted from various degrees of approximation, as defined by the parameters **Q** and **S**. All the results which are described in this section relate to five bladed discs. A detailed study was made on the particular model in which the five identical blades had a length equal to $1/3$ of the diameter of the disc, and the results from this study were found to be typical of those for other configurations. Natural frequencies computed according to the 'exact' receptance method (section 4.3) provided a standard of comparison.

The first step in each calculation was the formation of the system matrix (or order $P \times P$, where $P = 2Q + NS$, and $N = 5$), after the fashion described in sections 2.7 and 4.5. The eigenvalues and eigenvectors for this matrix were then found by a library routine which is based on the well known Jacobi process described in Wilkinson (1965). From this solution, the natural frequencies and modal shapes were determined from the relationships given in Chapter 2.

Results pertaining to the natural frequencies are displayed in FIG.4.10 for various combinations of **Q** and **S**. The eigenvalue estimates are invariably on the high side and tend to the exact values

as Q and S increase. However, even when $Q = 16$ and $S = 5$, the estimates are in error by as much as 20% in some cases, which points to the need for caution when applying the method*. On the other hand, the present matrix method yields natural frequencies very much more quickly than does the receptance method. Experience has shown that the two methods may be usefully combined, the one rapidly providing estimates which make the root-finding procedure in the other much more efficient. The apparently random variation from mode to mode in the accuracy of the results (see FIG.4.10) is discussed later in the present section.

A second series of calculations was designed to assess the accuracy of the eigenvalue method in estimating the magnitude of the natural frequency splits which occur in the double modes of detuned systems. Results shown in FIG.4.11 show that these estimates are acceptable in that they are of the right order of magnitude.

FIG.4.12 shows the results of further computations which illustrate the effect of variation in blade length on the natural frequencies of a tuned five bladed disc. The eigenvalue method was used with $Q = 16$ and $S = 5$, and the disc thickness, blade width and disc diameter were kept constant in the ratio **1:2:48**. Because the range of blade length extends to zero (so including a disc without any blades) it is possible to identify each mode of a bladed disc with the unbladed disc mode from which it is generated. This is a convenient way of identifying modes when there are only a small number of blades and the composite system does not, in consequence, possess such geometrically simple modal shapes as an unbladed disc.

* In any one particular case, both the matrix and receptance methods yield identical results if, instead of using the closed form receptances, we use the series form truncated at the same values of Q and S . Thus this result also indicates the need for caution when using series form receptances,

There appears to be some connection between the results shown in FIG.4.12 and the variation in accuracy of eigenvalue estimates which was mentioned earlier. While it would be difficult to establish a numerical relationship, it may be noted that those modes in which the eigenvalues provided the poorest natural frequency estimates correspond to the lines in FIG.4.12 whose slope (at the appropriate point on the abscissa) is greatest. In fact there would seem to be a qualitative connection between the slope of the frequency curves in that graph and the accuracy of the natural frequency estimates provided by the matrix method of solution. However, as it seems unlikely that a more convenient form of this method will be found, the matter will be pursued no further.

4.7 Eigenvector estimates of modal shape

In the same way that the matrix method supplies approximations to the natural frequencies of a bladed disc, it also provides estimates of the modal shapes. The determinant solution for modal shapes consists of a distribution of blade load around the rim of the disc from which the displacement shape, or nodal lines, of the surface of the disc may be deduced. In the matrix solution, the eigenvectors which are computed simultaneously with the eigenvalues lead directly to this displacement shape. From this, the more convenient form of a blade load distribution may be found.

The normal displacement of the disc was derived in equation (4.16) and is

$$w(r, \theta) = q_{00} + r(q_{10} \cos \theta + p_{10} \sin \theta) + \sum_{j=1}^{\infty} f_j(r) \{ a_j \cos n_j \theta + p_j \sin n_j \theta \} \quad (4.21)$$

This may also be written

$$w(r, \theta) = \underline{F}(r, \theta) q \quad (4.22)$$

in which q is a vector containing all the **flexural** principal coordinates p , q and A (but not those of rigid body motion, q_{00} etc.); and \underline{F} is a matrix of coefficients which include not only the terms such as $\{f_j(r) \cos n_j \theta\}$ above, but also those resulting from the elimination of the three coordinates q_{00} , q_{10} and p_{10} . The form which \underline{F} takes is shown in APPENDIX 4.1,

Each eigenvalue (or natural frequency ω_x) of the system matrix has an associated eigenvector, q_x . The displacement shape of the mode corresponding to this natural frequency is simply

$$w_x(r, \theta) = \underline{F}(r, \theta) \underline{q}_x \quad (4.23)$$

and by substituting various values of r and θ in the matrix \underline{F} , the relative displacement at the corresponding points may be found. Solution of the equation

$$w_x(r, \theta) = 0$$

produces the patterns of nodal lines which are a familiar description of modal shapes. Furthermore, by finding the relative values of the normal displacement and slope at the points on the rim at which the blades are attached, and using the series form receptance expressions for the blades, it is possible to obtain the distribution of blade load around the disc.

However, both these processes are cumbersome in numerical execution and the few results which are described here demonstrate that the matrix method of solution has no advantage either in speed or accuracy over the determinant solution in the evaluation of modal shapes. This is the reverse of the situation described in the previous section for natural frequency calculations,

A number of calculations were performed for a five bladed disc and were analysed in a similar manner to the eigenvalues. Owing to the amount of time required to perform these calculations, it was not convenient to study many different modes of vibration, and we shall in fact confine our discussion to the results for one double and one single mode. The results relating to a double mode were from a detuned system and those for a single mode from a tuned system, The graphs in **FIG.4.13** show how the five individual blade loads vary with the values of Q and S , and unlike the results of the previous section we find them to be almost completely independent of either parameter. One surprising result apparent in the graph for the single mode is the fact that the blade load estimates appear to worsen as the approximation is improved'. Whilst the determinant solutions corresponding to these results are marked on these graphs, there is a better form of comparison for the double mode which is shown in **FIG.4.14**. In these two graphs the blade loads are plotted as a histogram against the angular positions of the blades around the disc, From these discrete values, it is possible to deduce a simple cosine distribution, and this is shown alongside the corresponding curve deduced from the determinant calculations so that the two may be compared. For the first case, good agreement is observed between the two methods of solution (the amplitude of each curve is arbitrary and must not be considered in the comparison), but the second set of results is somewhat confusing. Certainly both solutions indicate a similar cosine variation of blade load around the rim, but the approximate solution has a mean value which differs considerably from zero, the value which it should take.

No explanation for this discrepancy, nor for the seemingly ill-conditioned single mode case was immediately forthcoming, and since this method of solution has no advantages over the exact solution, a more detailed investigation was not made,

However, it is as well to bear in mind that the determinant solution is not possible unless the roots of the determinant are known,

and it is only with the assistance provided by the eigenvalue estimates that these roots may be readily found,

4.8 Vibration characteristics of bladed discs

The results reported in this chapter may be summarised quite briefly as characteristics of the **flexural** vibrations of bladed discs in general. The two methods of solution which were used both demonstrated the existence of two distinct types of **flexural** vibration mode. These are called '**single**' and 'double*' modes after the form taken by the corresponding solution to the equations of motion,

There are two aspects in which single and double modes are fundamentally different, and these are both concerned with detuning. The first of these is a property of the natural frequencies. A single mode has just one natural frequency associated with it, although the actual value of this frequency may vary slightly as the nature and magnitude of detuning varies. However, there are always two natural frequencies associated with each double mode. These are very close in a detuned system and identical in a tuned system, as shown by the existence of equal eigenvalues of the system matrix and double roots of the frequency equation found by the receptance method. The phenomenon of 'frequency splitting' is a consequence of detuning, and cannot under any circumstances occur in a single mode,

The second difference concerns the modal shapes. It is a property of a single mode that in a tuned system each blade experiences the same loading, or that the modal shape is circumferentially symmetrical. Detuning causes this symmetry to be slightly disturbed, but the individual variation of blade load is small compared to the **mean**, or tuned system, value. The modal shapes corresponding to a double mode are essentially the same in both tuned and detuned systems. In any one case, the distribution of blade load follows a cosine variation around the rim and consequently has a mean value of zero,

exactly the reverse of that for a single mode.

Single modes include all those bladed disc modes which are associated with the symmetric disc modes (*i.e.* those with no nodal diameters) as seen in **FIG.4.12**, and also those special cases with the same number of nodal diameters as there are blades (or any multiple thereof). These were described as 'conjugate' modes earlier in the text, but as they are found to exhibit all the properties of single modes, they may be classified as such. All other modes fall into the category of double modes.

CHAPTER 5

DETUNING A FIVE BLADED DISC - (I) NATURAL FREQUENCIES

5.1 Introduction

Calculations described in the previous chapter show that when the symmetry of a tuned bladed disc system is slightly disturbed, certain of the normal **modes** of vibration split into a pair of modes with similar characteristics and very close natural frequencies. The asymmetry was introduced in that case by varying the sizes of the blades so that they were no longer identical (as had previously been the case). Similar results would also be obtained by disturbing the circular symmetry of the disc itself, or the angular positions of otherwise identical blades. Detuning may thus be defined generally as the process of making small variations to a basically symmetrical system, and this work will seek to investigate the specific effects of detuning on the properties of a vibrating bladed disc. Because the precise mechanism seemed unimportant, it was decided that for the purpose of all subsequent computation, the system would be detuned by varying the blade lengths only, keeping all other dimensions constant,

The general form of detuning will be represented by a distribution of blade length around the disc so that the length of any one blade is defined by the equation

$$L(\theta) = L_0 \{ 1 + \sigma f(\theta) \} \quad (5.1)$$

where $f(\theta)$ is the detuning function, and is within the range $-1 \leq f(\theta) \leq +1$;

σ represents the degree of detuning, and determines upper and lower limits of blade length;

L_0 is the length of each blade in the tuned system;

and θ is the angular position of a blade.

Subsequent sections in this chapter deal with the effect of using a variety of forms for the detuning function $f(\theta)$, and in particular with the frequency splitting which then **occurs**.

Basically, there are two problems associated with the frequency splitting phenomenon which must be solved. The first is concerned with the mechanism of such splitting, and the second with the consequences. A physical explanation of this phenomenon has not been found. However, by considering the effect of adding small detuning masses to the rim of a uniform circular disc, it is possible to predict a natural frequency split and to estimate its magnitude. This analysis is given in APPENDIX 5, and the results are discussed in relation to their possible extension to include bladed discs. Given that certain modes of vibration do split on detuning, we wish to establish a relationship between the type of detuning ($f(e)$), the degree of detuning (σ) and the magnitude of the resulting splits in each mode. The present chapter is concerned with this problem only, while in the next chapter a study is made of the properties of a pair of modes with close natural frequencies.

In order to tackle the problem numerically, a large number of calculations must be performed. It may be seen from the previous chapter that the matrix or eigenvalue approximation to the natural frequency solution is an ideal tool for this investigation. In such an application, this method scores heavily over the alternative receptance determinant method by virtue of its speed and convenience of **use**. A five bladed disc with dimensions in the **ratio** $\lambda = 0.3$, and $W_0/2a = .04167$ was selected for this study. For all calculations, 16 disc modes (**Q**) and 5 modes per blade (**S**) are considered in the approximation; reference may be made to the previous chapter concerning the accuracy attained with this set of data. The natural frequencies of the tuned version of the chosen model are found on FIG.4.12 at the point corresponding to $\lambda = .3$, and this particular

case is of special interest because the natural frequencies of modes 3 and 4 (corresponding to the 3/0 and 1/1 modes of the unbladed disc) are extremely close together. Their separation is of the same order of magnitude as the splitting phenomenon which is under investigation. This makes possible a study of the effects of interference between one pair of modes and another.

Finally, we note that when it is required to derive a general form of a function, in this case the detuning function $f(\theta)$, there are two principal methods which may be employed. One is to form a polynomial such that

$$f(\theta) = \sum_{n=0}^{\infty} a_n \theta^n \quad (5.2)$$

and the other is to assume a Fourier series,

$$f(\theta) = \sum_{n=0}^{\infty} \{ a_n \cos n\theta + b_n \sin n\theta \} \quad (5.3)$$

Because of the circular nature of the system, this latter form is the obvious choice, and the present chapter is devoted to developing this idea.

It has been found convenient throughout to identify each mode of the bladed disc with the shape of the unbladed disc mode from which it has degenerated. This system is illustrated in FIG.4.12.

5.2 A systematic analysis of detuning

When a study of the effects of detuning was first considered, it was decided to make a statistical analysis of randomly detuned systems. This work was largely completed, but the results led to the belief that a systematic study could illustrate much more clearly the patterns of behaviour of a bladed disc subjected to detuning.

The blade length equation which was used for random detuning was simply

$$L = L_0 \{ 1 + \sigma K_i \} \quad (5.4)$$

where K_i could take any value at random within the range $-1 \leq K \leq 1$. Now, it is possible to derive a function of the type shown in equation (5.3) which has the same values at the five points $\theta_i = 2\pi i/5$, for $i = 1(1)5$, as the corresponding random numbers K_i . As there are only five variables, the function needs only five terms and may be written either as

$$f(\theta) = a_0 + a_1 \cos \theta + a_2 \sin \theta + a_3 \cos 2\theta + a_4 \sin 2\theta \quad (5.5)$$

or, in a more convenient form, as

$$f(\theta) = b_0 + b_1 \cos(\theta + \phi) + b_2 \cos 2(\theta + \psi) \quad (5.6)$$

The five constants, a_0 to a_4 in the first case and b_0, b_1, b_2, ϕ and ψ in the second, may be found by solving the set of five linear equations which are formed by equating $f(\theta_i)$ and K_i for each value of i . Thus, any five blade lengths may be represented by (5.6), and this equation is the general form of $f(e)$ for the case of a five bladed disc.

We shall now study the effect of each of the three terms in equation (5.6) individually. The first of these is a constant term, b_0 , and provides an almost trivial case in that it serves only to lengthen (or shorten) each blade by the same amount. This does not disturb the circular symmetry of the system and thus will not cause splitting in the double modes, although it will raise (or lower) the natural frequency of each mode. Calculations were made to assess the magnitude of this effect and the results are shown as a set of curves in FIG.5.1. For each of a number of modes, the detuned natural frequency is plotted against the total extension or contraction of the

blades. The straight lines which result correspond to the slopes of the respective curves in FIG.4.12 at the point $\lambda = 0.3$.

Next consider a detuning function of the type

$$f(\theta) = b, \cos(\theta + \phi)$$

A set of calculations was carried out for a variety of values of $(\sigma b,)$ and ϕ , and the results may be summarised as follows:

(i) the natural frequencies of single modes are unaffected by this form of detuning; (ii) the value of ϕ has no effect whatsoever on any of the natural frequencies, and (iii) certain of the double modes exhibit a splitting of their natural frequencies which is symmetrical about the tuned system value, while others do not. The results are shown graphically in FIG.5.3 where natural frequency is plotted against the component of $\cos\theta$ detuning, $(\sigma b,)$. With the exception of modes 3 and 4 (1/1 and 3/0), which present a special case by virtue of their proximity, it is found that all those modes which do exhibit a split are associated with unbladed disc modes possessing $(5j \pm 2)$ nodal diameters (j is any integer). Also all modes which show no splitting are associated with disc modes which have $(5j \pm 1)$ nodal diameters. This indicates that each double mode of the five bladed disc belongs to one of two categories, depending on the shape of the unbladed disc mode from which it degenerates. The existence of two distinct groups is also evident in the general form of the detuning function for the five bladed disc (5.6), where it is necessary and sufficient to include terms of $\cos\theta$ and $\cos 2\theta$ types only. The reason for this may be illustrated by reference to the diagrams in FIG.5.2. The first of these, FIG.5.2a, shows how a detuning function of $\cos\theta$ results in the same set of blades as does a function of $\cos 4\theta$, or, generally, $\cos(5j \pm 1)\theta$. The second diagram shows the identity of the $\cos 2\theta$ detuning function with all others included in the general term $\cos(5j \pm 2)\theta$. Modes and detuning expressions of these two types are referred to as belonging to either the ' $\cos\theta$ ' or ' $\cos 2\theta$ ' family.

The other type of basic detuning function,

$$f(\theta) = \cos 2(\theta + \psi)$$

produces a similar set of results. Once again, no change is observed in the natural frequencies of the single modes; nor does the value of ψ affect the natural frequencies of any mode. In this case however, it is the modes of the $\cos \theta$ family which do split, while those of the $\cos 2\theta$ family do not. The computed results are shown in **FIG.5.4** alongside those from the previous case. Both sets of results are combined and presented graphically in **FIG.5.5** where the degree of splitting in each mode is plotted against the component of the relevant cosine term (σb_1 or σb_2).

In this graph, the results for the 1/1 and 3/0 modes are omitted since they do not conform to the regular pattern. It is clear from **FIGS.5.3** and 5.4 that some form of interference is present between these two modes, and further calculations for a slightly modified system (one in which λ was .275 instead of .3 and the natural frequencies of these two modes are not so close) show the expected behaviour (**FIGS.5.3a** and 5.4a).

The general conclusion which might be drawn from these results is that detuning of the $\cos \theta$ type does not produce any splitting in those modes which belong to the $\cos \theta$ family, whereas it does cause the modes of the other family to split. A reciprocal relationship holds for $\cos 2\theta$ detuning.

One further empirical relationship has been observed. For any particular bladed disc, there are just two parameters for each mode of vibration which define the behaviour of that mode under any detuned conditions. The first of these we shall call the 'frequency factor', Φ , and is the slope of the appropriate line in **FIG.5.1**. It is a measure of the rate at which the natural frequency of the tuned system varies with blade length. The second parameter is termed the 'split factor', Ψ , and this is a measure of the degree by

which splitting occurs, as indicated by the slope of the corresponding line in FIG.5.5. From the table of values which has been drawn up for the system currently under investigation, it appears that, apart from a difference in **sign**, these two parameters have substantially the same value.

MODE	FREQUENCY FACTOR Φ	SPLIT FACTOR Ψ
2/0	.474	.477
2/1	.824	.806
6/0	.610	.602
3/1	.350	.348
1/2	.330	.331

In order to demonstrate the application of the above results to a general example, one of the randomly detuned cases of the statistical analysis was taken, The five random numbers K_i specifying the individual blade lengths were analysed to determine the constants b_0, b_1, b_2, ϕ and ψ in the Fourier series of equation (5.6). Using the values of Φ and Ψ in the above table, the natural frequencies of each of the double modes were deduced by superposition of the relationships described above,, These frequencies were then compared with the values which were computed directly from the same blade and disc data. Details of this example, which is just one of several treated in the same way, are tabulated in FIG.5.6 where the extremely close agreement between 'deduced' and 'computed' natural frequencies is clear.

5.3 Calculations made using the receptance method

Having established a number of relationships between blade variations and their effects on the natural frequencies by using the approximate matrix solution, it was decided that they should be verified by test cases computed according to the more precise receptance determinant method. This would confirm that the relationships are not peculiar to the approximate solution, and also furnish more accurate values for the frequency and split factors, defined in the previous section.

In order to provide values for comparison with later experimental work, the blade length ratio (λ) was taken as 0.275 (rather than 0.3), and calculations were made for the same model as before. The results of these calculations confirm those of the earlier analysis, and as an illustration, a portion of the determinant - frequency plot is shown in FIG.5.7. These curves are drawn in the region of the natural frequency of the fundamental mode (2/0), and correspond to (i) the tuned system; (ii) the detuned system when $f(\theta) = \cos \theta$ and $\sigma = 0.01$; and (iii) a second detuned system in which $f(\theta) = \cos 2\theta$ and $\sigma = 0.01$. Curves (i) and (iii) are indistinguishable from one another, while curve (ii) demonstrates a definite split of natural frequency which is symmetrical about the tuned system value. Furthermore, it was found that a detuning function of $\cos(\theta + \phi)$ produced exactly the same curve for any arbitrarily chosen value of ϕ . This was also a result of the earlier analysis.

As had been the case earlier, it was found that for larger degrees of detuning (of the order of $\sigma = .02$), a detuning function of the $\cos \theta$ type would in fact produce a small degree of split in modes of the $\cos \theta$ family, but once again the order of magnitude of this split in such a mode is insignificant when compared to that due to $\cos 2\theta$ detuning. This would seem to confirm the suspicion that there is a second order, or nonlinear, effect causing these small

splits, rather than these being the result of computational errors.

Finally, a set of calculations were undertaken in order to obtain more accurate values for the frequency and split factors (Φ and Ψ) which were defined in section 5.2. Based on these calculations, a table of values for these parameters was drawn up and is shown below,

MODE	FREQUENCY FACTOR Φ	SPLIT FACTOR Ψ
2 / 0	- .475	.478
1 / 1	- 1.405	1.443
3 / 0	- .719	.672
2 / 1	- .572	.564
4 / 0	- .034	.035
6 / 0	- .382	.371
1 / 2	- .473	.481

For the system used in these calculations, the natural frequencies of the 1/1 and 3/0 modes were not as close as had been the case for the earlier study,, However, they were sufficiently close to produce slight interference one with the other, and it is thought that the proximity of their natural frequencies is responsible for the larger discrepancies which are found between Φ and Ψ for these particular modes. The figures relating to the other five modes show the same degree of similarity as those computed by the matrix method, so that it is not possible to attribute the differences found there to the approximate nature of the solution. However, it is difficult to be sure whether or not the discrepancies found between the two constants Φ and Ψ , being as small as they are, are due to rounding errors in computation. It must be remembered that each of these

factors is found from the difference of two almost identical frequencies, and is of the order of $\frac{1}{2}\%$ of the magnitude of either frequency, The order of magnitude of the discrepancies with which we are concerned is in turn just 1% of this difference, and thus only a very small fraction of the original values,, Although all the computation is done with seven significant figures, it is doubtful whether all the disc receptance terms attain this degree of accuracy. Thus it is felt that computational errors of the same order of magnitude as the discrepancies observed between Φ and Ψ are quite possible.

In this chapter, we have established that for a five bladed disc there are just two types of mode; the $\cos \theta$ and $\cos 2\theta$ families. From the results it is possible to deduce two alternative general rules of detuned behaviour, One is that the modes of the $\cos n\theta$ family are split by any detuning function except one which belongs to the $\cos n\theta$ family. The alternative rule is that modes of the $\cos n\theta$ family are only split by detuning functions belonging to the $\cos 2n\theta$ family. In the case of the five bladed disc these two rules amount to the same result, but it is the latter which is supported by the theoretical predictions in APPENDIX 5, Test calculations for a seven bladed disc, in which there are three such families, substantiate this prediction,

CHAPTER 6

DETUNING A FIVE BLADED DISC - (II) MODAL SHAPES AND VIBRATION LEVELS

6.1 Introduction

The previous chapter was concerned solely with the natural frequencies of detuned systems, and did not describe the corresponding shapes of the modes of vibration. In this chapter, a study is made of these modal shapes, along much the same lines as that for natural frequencies, and the practical significance of the results is discussed. All the numerical examples upon which this chapter is based result from calculations which were made using the receptance method of solution. The relative merits of the two methods for obtaining modal shapes were discussed in Chapter 4, and it was found that it is the receptance method which provides the more efficient and accurate means of computing this information,

Each modal shape, as computed by this receptance method, is in the form of a set of values for the forces and couples which act at the root of each blade. It was considered necessary to devise a more concise form for the presentation of this information, and a number of possibilities were examined. One of these - the pattern of nodal lines on the disc - was rejected since it provides very little quantitative information. The shape of the displacement at the rim was also considered to be unsuitable as its specification is, if anything, less concise than the original set of blade loads. Finally, it was decided to define a modal shape function (or, blade load distribution) which is of a similar form to that of the detuning function $f(\theta)$, and which represents the distribution of either

blade forces or couples around the disc*, The modal shape function is written as

$$F(\theta) = A \left\{ \beta_0 + \beta_1 \cos(\theta + \gamma) + \beta_2 \cos 2(\theta + \delta) \right\} \quad (6.1)$$

and the five constants β_0 , β_1 , β_2 , γ and δ are determined by the couples on each of the five blades. The constant A is an arbitrary scaling factor, and may be chosen to have any convenient value,

It is convenient to study the behaviour of single and double modes separately, Their characteristics are dissimilar, and so, it is found, are their reactions to detuning.

6.2 Single modes

Although it is a property of single modes that they do not split under any detuned conditions, it appears that their modal shapes are affected by detuning, and then often to an appreciable extent. The present section attempts to establish the precise manner in which the single modal shapes of a detuned system are related to the form and degree of the detuning arrangement, In order to achieve this, a numerical study was made on four such modes of the five bladed disc, those selected being associated with the 0/1, 5/0, 0/2 and 0/3 modes of the unbladed disc. As before, this classification is used to identify the bladed disc modes.

First, the shapes of these four modes were computed for a tuned system, in order to provide a standard of comparison for subsequent detuned cases. The result was the same for each mode, and the modal

* It is found that in any modal shape, the pattern of blade root forces is identical with that of blade root couples. The couple is a more useful parameter since the bending stress at the root is directly proportional to it.

shape function was found to be simply

$$F(\theta) = \{1\} \quad (6.2)$$

where \mathbf{A} is chosen in this case so that the constant term is 1. This result illustrates clearly the circular uniformity which is a property of single modes, and which was discussed in Chapter 4,

In order to discover how these modal shapes are affected by detuning, it was found convenient yet again to consider individually the effect of each of the three terms which constitute the general detuning function $f(\theta)$, (5.6). The first of these, a constant term, is clearly a trivial case and has no effect on the modal shapes simply because it does not upset the circular symmetry of the system, However, when a detuning function of the form

$$f(\theta) = b, \cos(\theta + \phi)$$

was applied to the system, and calculations made for various degrees of detuning, it was found that the shape of each mode followed the same pattern in which the modal shape was of the form

$$F_j(\theta) = \{1 + j\beta_1 \cos(\theta + \phi)\} \quad (6.3)$$

(where j refers to the j^{th} single mode), By plotting a number of results (see FIG.6.1), it was possible to establish a simple relationship between $j\beta_1$ and (σb_1) , and it is found that for each mode: $j\beta_1 = jK_1(\sigma b_1)$. A similar result is obtained by using the third type of detuning function:

$$f(\theta) = b_2 \cos 2(\theta + \psi)$$

for which modal shapes were all of the form

$$F_j(\theta) = \{1 + j\beta_2 \cos 2(\theta + \psi)\} \quad (6.4)$$

In this case, the coefficients ${}_j\beta_2$ and (σb_2) are related for each mode by a second constant ${}_j k_2$, so that ${}_j\beta_2 = {}_j k_2 (\sigma b_2)$ (FIG.6.2). These results show that for each of the two basic forms of detuning, there is a linear relationship between the variation in blade length and the variation in blade load around the disc, The consequences of this effect appear to be considerably more serious for the higher frequency modes,

If we now consider the general form of detuning, represented by

$$f(\theta) = b_0 + b_1 \cos(\theta + \phi) - t b_2 \cos 2(\theta + \psi) \quad (6.5)$$

it is possible to deduce the modal shapes for this arrangement by superposition of the above results. As mentioned above, the constant b_0 will have no effect on the modal shapes, The effect of each of the two cosine components may be derived from equations (6.3) and (6.4), so that the modal shape resulting from any detuning arrangement is:

$$F_j(\theta) = \left\{ 1 + ({}_j k_1 \sigma b_1) \cos(\theta + \phi) + ({}_j k_2 \sigma b_2) \cos 2(\theta + \psi) \right\} \quad (6.6)$$

In this case, a simple linear relationship between blade length and load, such as was found for the two simpler detuning functions, does not exist. However, since the two constants for any one mode, ${}_j k_1$, and ${}_j k_2$, have similar values, the overall effect is much the same. A variation in blade length gives rise to a variation in the blade loads about a mean value.

The practical significance of this result may only be appreciated by considering the response of a system which is lightly damped to various forms of excitation. Suppose that a bladed disc is excited in some given manner at the natural frequency of a single mode, The response to this excitation might be conveniently measured as the distribution of blade root stresses around the rim of the disc, and

the presence of light damping is necessary in order to maintain finite stress levels at the natural frequencies. If the damping is light, we may express this form of the response as

$$R_j(\theta) = j p_o F_j(\theta) \quad (6.7)$$

where $F_j(\theta)$ is the modal shape, and $j p_o$ represents the mean stress level and is directly proportional to the excitation level.

If we may assume that this given excitation will give rise to the same mean stress level ($j p_o$) for various detuned versions of the same basic system, then it is possible to make a direct comparison between tuned and detuned systems. The conclusion which may be drawn from such a comparison is that, for a single mode, detuning always causes one or more blades to experience higher stress levels than they do in the tuned system under the same excitation conditions. The extent of this effect depends upon both the form and the degree of detuning, but the variation in stress levels (about their mean) is usually several times that of the blade lengths about their nominal (tuned system) value,

It is difficult to ascertain whether this assumption is justified. It is unlikely to be valid in a case where the position of excitation (if this is at a point) is close to a node. In this case, slight variations in the nodal pattern, which will result from detuning, may cause large variations in the effective excitation.

6.3 Double modes

The behaviour of double modes under detuned conditions is somewhat more complex than that described in the previous section for single modes. It was first observed in Chapter 2 that when there are two or more coincident roots to the receptance determinant, there is no unique modal shape corresponding to that frequency, This is the

situation which exists in respect of the double modes of a tuned system, and for these modes, the modal shapes or patterns depend upon an external influence (such as the excitation) for their complete specification. However, as soon as the system is detuned, and no matter how small the degree of detuning, the pairs of coincident roots of the frequency determinant are replaced by pairs of very close roots and corresponding to each of these is a unique modal shape which is defined completely. Thus, it is only in the limit of detuning (*i.e.* in the tuned case) that analytical difficulties arise,

As in previous cases, we shall begin by considering the simple form of detuning where

$$f(\theta) = b, \cos(\theta + \phi) \quad (6.8)$$

The modes which are studied in the numerical investigation are those which are identified with the **2/0**, **3/0** and **2/1** modes of the unbladed disc. The other double modes which lie in this frequency range, the **1/1** and **6/0** modes, are omitted since they do not exhibit the frequency splitting phenomenon under this type of detuning (see section 5.2).

It is found that the results pertaining to each of these three modes follow the same pattern, For each pair of modes (constituting a double mode), the shape of the one with the lower natural frequency may be expressed as

$${}_j F_1(\theta) = \cos 2(\theta - \frac{1}{4} \phi), \quad (6.9)$$

while that for the higher frequency mode is

$${}_j F_2(\theta) = \sin 2(\theta - \frac{1}{4} \phi) \quad (6.10)$$

A set of results for the **2/0** mode, typical of those from which these expressions were derived, is shown in **FIG.6.3**. It may be seen in this

table that the coefficient β_1 increases with $0-b$, but since its magnitude is always very much less than that of β_2 , it is omitted from the modal shape functions, (6.9) and (6.10), as being negligible. Since there is thus only one term in either of these expressions, the value of its coefficient in each case (β_2) is of no consequence, and is chosen for convenience to be unity.

A similar study was made for the 1/1 and 6/0 modes by using a detuning function which is known to cause them to split. Calculations made for these two modes, with

$$f(\theta) = b_2 \cos 2(\theta + \psi)$$

produced a similar set of results. The two modal shapes for any double mode in this category are typified by the results tabulated in FIG.6.4 for the 6/0 mode. The modal shape functions which are derived from these results are

$${}_j F_1(\theta) = \cos(\theta + \psi) \quad (6.11)$$

and

$${}_j F_2(\theta) = \sin(\theta + \psi) \quad (6.12)$$

(corresponding to (6.9) and (6.10) respectively), and these demonstrate the same properties as those described above for modes of the other family*

As a general rule, it may be considered that it is the natural frequency of each mode which determines its shape. In the case of a double mode of a detuned system, there are two modes which have almost identical natural frequencies so that they possess correspondingly similar modal shapes. The form of the detuning, and in particular the constant ϕ or ψ , provides the specific angular orientation of each of these two virtually identical modal patterns. As the degree of detuning increases, the natural frequencies of the two modes will

differ appreciably, and this, in turn, will give rise to differences of a similar order of magnitude between the shapes of the corresponding modes. It is believed that the nonlinearity which is evident in the tabulated results in **FIGS.6.3** and 6.4 (in which the coefficient β , (or β_2) increases with σ) might be attributed to this effect, and this suggestion is further substantiated by the behaviour of the **1/1** and **3/0** modes, in which the nonlinearity is considerably more pronounced than in the other modes. The natural frequencies of these two modes in the tuned version of the system are quite close together, so that a variation of modal shape with frequency would be more marked in their vicinity than elsewhere, Thus, one might expect that any second order effect which arises from such a variation would be more prominent in these two modes than in the others.

The alternative expressions of modal shape were computed for one particular case (for the pair of **2/0** modes) in order to provide a comparison between them. From the basic form of a set of blade loads, the modal shape was computed in the form of (i) a blade load distribution; (ii) the disc rim displacement shape and (iii) as a pattern of nodal lines on the disc, A further expression was obtained by computing the blade root displacement distribution, This was found by considering the displacement of the rim of the disc at the five points corresponding to the positions of the blades as five discrete values, and then deducing a function of the same form as the modal shape function $F(\theta)$. The results are presented in two sets of graphs, The first, **FIG.6.5**, shows the individual blade loads and their deduced distribution, the disc rim displacement shape and the **deduced** blade root displacement distribution. The second simply shows the nodal patterns: **FIG.6.6**. In both sets of results the orthogonality property of the pair of modes is evident. The deduced blade load and blade root displacement distributions for each mode consist of similar $\cos 2\theta$ -type curves and are in phase with each other. The disc rim displacement, although it exhibits a

somewhat complex shape, may be seen to be basically a $\cos 2\theta$ variation around the disc, and this also is in phase with the two distribution curves, The results shown in these graphs serve to illustrate the close similarity which exists between the various expressions of modal shape, and this is a feature which may be used to advantage in the next section,

6.4 A simplified double mode

Once again, it is necessary to consider the response of a bladed disc to damped forced vibration in order to realise the practical implications of the results obtained in the previous section. It has been found convenient to study the behaviour of double modes by considering a simplified analytical model which has basically similar properties, Using this model, the response of a simplified system may be determined for a wide range of detuning arrangements under various damping and excitation conditions. Subject to the limitations of the simplifications, results obtained in this way may be related to the real system to predict the behaviour of a bladed disc when it is detuned.

The basic assumption which is made in the construction of the model is that the response of a bladed disc double mode may be considered in isolation from the effects of other modes. Thus the system is reduced to one in which there are just two degrees of freedom. The normal modes of vibration which correspond to these two degrees of freedom have properties typical of those of the pair of modes which constitute the double mode of a bladed disc, These two modes are represented by principal coordinates q_1 and q_2 , and their natural frequencies (ω_1 and ω_2) are very close. The shape of each mode is defined by the rim displacement shape, and this is assumed to be

$$w_1(\theta) = \cos n\theta \quad (6.13)$$

for the mode with the lower natural frequency (ω_1), and

$$w_2(\theta) = \sin n\theta \quad (6.14)$$

for the higher frequency mode. These are typical of a bladed disc double mode with n nodal 'diameters', It will be assumed that the inertia and stiffness coefficients of the two modes are identical,

We shall now derive expressions for the response of this system to various forms of excitation. It is convenient to consider first the possible forms which the excitation might take, In Chapter 3 it was shown that the only type of loading at the rim of the disc which could excite a mode with n nodal diameters is one of the form

$$P(\theta) = P_0 \cos n\theta e^{i\omega t} \quad (6.15)$$

Any configuration of loading at the rim may be represented in a Fourier series, and generally this will contain a term such as that in (6.15). It is found that a point loading is a typical example in that its Fourier series representation contains a $\cos n\theta$ term for every integral value of n . We shall thus confine our interest to this type of excitation. For a point load F_0 situated at a point $\theta = \eta$ on the rim, the general term in the Fourier series expansion is

$$P_n(\theta) = \frac{F_0}{\pi} \cos n(\theta - \eta) e^{i\omega t} \quad (6.16)$$

The total generalised force in the two modes due to the point load F_0 may be determined (as in section 3.7), and is found to be

$$Q_1 = F_0 \cos(n\eta) \quad (6.17)$$

in the first case, and

$$Q_2 = F_0 \sin(n\eta) \quad (6.18)$$

in the second,

Damping may be included in the analysis, and c_1 and c_2 will be used to represent the fraction of critical damping which is present in each mode. The two **equations of motion** corresponding to q_1 and q_2 may now be written as

$$\ddot{q}_1 + 2c_1\omega_1 \dot{q}_1 + \omega_1^2 q_1 = Q_1 / a_0 \quad (6.19)$$

and

$$\ddot{q}_2 + 2c_2\omega_2 \dot{q}_2 + \omega_2^2 q_2 = Q_2 / a_0 \quad (6.20)$$

where a_0 is the inertia coefficient of either mode. These equations may be readily solved for q_1 and q_2 , and the response of the system to excitation at a point $\theta = \eta$ may be obtained in some suitable form. It is convenient to express this response as a receptance function $R(\theta)$ which relates the displacement at any point on the rim to the point load F_0 at $\theta = \eta$. This receptance may be written generally as

$$R(\theta) = [w_1(\theta) q_1 + w_2(\theta) q_2] / F_0 \quad (6.21)$$

where $w_1(\theta)$ and $w_2(\theta)$ are the modal shapes defined in (6.13) and (6.14) respectively. On substitution for q_1 and q_2 (which are found by solving the equations of motion (6.19) and (6.20)), the response becomes

$$R(\theta) = W_0(\eta) \cos n(\theta - \epsilon) \quad (6.22)$$

where

$$W_0 = \sqrt{W_1^2 + W_2^2}; \quad \epsilon = \tan^{-1}(W_2 / W_1)$$

and

$$W_1(\eta) = \cos(n\eta) / \sqrt{[1 - (\omega/\omega_1)^2]^2 + 4c_1^2(\omega/\omega_1)^2};$$

$$W_2(\eta) = \sin(n\eta) / \sqrt{[1 - (\omega/\omega_2)^2]^2 + 4c_2^2(\omega/\omega_2)^2}$$

(W_0 is the maximum response and θ the position around the rim at which it occurs),, It was shown in the previous section that the variation of blade load around the disc corresponded to the rim displacement shape. Thus it may be considered that W_0 is representative of the maximum blade load (and θ of its position), and it will be used subsequently as the significant parameter in comparing tuned and detuned systems.

Having obtained a measure of the response of the simplified system, it now remains to investigate the properties of this solution for a variety of conditions. The three parameters which might be most usefully varied are (i) the split, or difference between the two natural frequencies ω_1 and ω_2 ; (ii) the position of the excitation η , and (iii) the level of the damping.

First, we shall study the significance of the position, or origin of the excitation, For a given split and damping levels (assuming $c_1 = c_2 = c$), the amplitude of the response (W_0) was computed at frequencies in the region of the natural frequencies, for different values of η . Typical results for a system with a split of .01 and with .01 critical damping are shown in the graph in FIG.6.7 where the three curves correspond to excitation positions of $\eta = 0, \pi/2n, \pi/n$. Clearly, for the second of these three curves the maximum response attained throughout is lower than for the other two, illustrating that the maximum response of a detuned system is a function of the position of the excitation. This function is shown in FIG.6.8 where the maximum response (\hat{W}_0) of systems with different splits but a constant level of damping is plotted against the angular position (η) of the excitation, Each curve in FIG.6.8 shows there to be an optimum position of η , at $\pi/2n$, where the reduction in W_0 is at its greatest, A further graph, FIG.6.9, shows how this reduction varies with both the split and the level of damping present in the two modes. The curves represent the maximum

amplitude attained in the response for the optimum position of excitation at $\eta = \pi/2\mu$. Each curve is asymptotic to 0,707 times the worst, or tuned, case, and the speed of convergence to this value is governed by the split and damping.

The conclusion which may be drawn from this study of a simplification of the real system is straightforward, Detuning cannot produce higher levels of response in a double mode than those present in the tuned **case**. The degree of the reduction which is possible depends on the position of the excitation, the split of the two natural frequencies (or the degree of detuning), and the level of damping present in the system,

It is believed that the simplified system which has been studied in this section will represent closely the behaviour of most double modes of a bladed disc, In certain cases where there are a number of modes all with similar natural frequencies, the assumptions may not be justified, However, the results of an experimental investigation, which is described in Chapter 8, indicate the validity of the simplification,

It has been found that the simplified analytical model, which has been formulated in this section based upon a large number of calculations of an 'exact' analysis, corresponds to that assumed by **Tobias** and Arnold (1957) in their discussion on the vibration of rotating imperfect discs.

CHAPTER 7THE DESIGN AND DEVELOPMENT OF THE EXPERIMENTAL EQUIPMENT7.1 Requirements of an experimental model

The basic requirement of an experimental model is that it should represent as closely as possible the system which was studied in the theoretical analysis. If this requirement is met, a realistic comparison might be made between the results of the analysis as described in the earlier sections and those obtained from an experimental investigation,

Since this work is primarily concerned with a uniform disc which is bladed with five uniform rectangular bars, such is the form that the model should take., Furthermore, it was observed at the outset of the study that the inclusion of blade stagger as a variable parameter would be an inessential complication, so that no provision for the adjustment of stagger is necessary on the model,

It is necessary to suspend the disc in such a manner that it is effectively freely supported in space, This simply means that the natural frequencies of the bladed disc when it is vibrating as a rigid body on its suspension should be much lower than those of the **flexural** modes of vibration with which we are concerned,

Detuning is the principal factor of interest in this work, so that a means of controlling it must be incorporated which is at the same time precise and convenient, In the analytical **study**, detuning was both effected and measured by the variation of the individual blade lengths, and the same technique may be used experimentally,,

Finally, it was believed that the inclusion of a source of damping which may be varied up to a level such as is experienced in a running turbine (of the order of $Q = 50$), would be a desirable feature, This would serve to ensure that the response in the

vicinity of a resonant frequency would be restrained to a reasonable level, Experience shows that on this type of freely supported system, inherent damping is very low ($Q > 1000$) so that the response at a natural frequency is extremely high. In practice this is manifest by the applied exciting force becoming very small, under which conditions electronic noise levels render accurate or consistent measurements very difficult, if not impossible. Thus, the inclusion of damping which is heavy enough to overcome this difficulty but sufficiently light so as not to interfere with the general patterns of behaviour, is advantageous,

7.2 The design of a model

The first design consideration is clearly that of the five bladed disc itself, Several forms which this might take were considered before it was finally decided to machine this item in one piece, from a sheet of steel, The main advantage of this form of construction is that it avoids discontinuities of geometry or material properties at the blade to disc junctions, and thus provides what is perhaps the best possible representation of the analytical model. The actual dimensions of the model are of some importance in that it is preferable to arrange for the working frequency range to lie between 100 cps and 3000 cps. The **flexural** natural frequencies of the bladed disc are of course highly dependent upon its size, and the following dimensions were those eventually chosen:

Disc diameter	=	24"
Disc thickness	=	$\frac{1}{2}$ "
Blade width	=	1"
Blade thickness	=	$\frac{1}{2}$ "
Blade length	=	(initially) 8"
		(subsequently) 6"

The original model, with 8" blades ($L./2a = 1/3$), had a fundamental natural frequency of about 125 cps, and the later version a slightly higher value, Vibration data for the experimental

model have been computed, and are discussed in APPENDIX 7.

In order to control the detuning process, it was decided to vary the effective length of each blade by the addition of shims with the same cross section as the blades but of various thickness, to its tip. Also fixed to the tip of each blade is an aluminium plate which forms part of the damping arrangements which are discussed later. It was decided that the standard blade throughout the detuning tests should be effectively 6.6" long ($L_0/2\alpha = .275$), and this should be attained by adding to the tip of the 6" blade the damping plate and a 'detuning block' (basically a large shim). The size of this block is chosen so that the fundamental frequency of a free free bar, 6" long and with a mass at one end equal to the total mass of the block and the damping plate, is the same as that for a uniform free free bar which is 6.6" long. The assembly is illustrated in FIG.7.1a. On detuning, an overall blade length of $L_0(1 + \sigma\alpha)$ might be required, where σ represents the degree of detuning and α may be any value between -1 and +1. In this case, a detuning block corresponding to the chosen value of σ is used which makes the effective blade length up to $L_0(1 - \sigma)$, and then the number of **shims** which constitute the increment of blade length ($\{1 + \alpha\}\sigma L_0$) are added as shown in FIG.7.1b. A set of nine shims were made for each blade in sizes of 1, 2, 4, 8, 16, 32, 64, 128 and 256 units, where one unit is equivalent to a length increment of $L_0/20000$. Also for each blade, a set of detuning blocks were made which corresponded to five degrees of detuning ($\sigma = 0, .0025, .005, .01$ and $.025$). For each assembly, the shims, block and damping plate are all fixed to the tip of the blade by two Allen screws which locate in holes tapped in the end of the blade. The detuning 'kit' for one blade is shown in FIG.7.2, and a typical assembly may be seen in the photograph in FIG.7.3. For convenience, two tables were drawn up, one of which provided the total number of units corresponding to any combination of σ and α , while

the other gave the only combination of shims which add up to this total.

Turning now to the damping arrangements, there are basically two mechanisms which might be employed to produce a viscous damping effect on the vibrating system. One of these, based on the resistance offered by a highly viscous fluid to the motion of a body through it, was considered as impractical owing to the difficulties which would be involved in varying or controlling the damping level. The method which was adopted depends on the fact that a conductor moving in a magnetic field experiences retarding forces proportional to its velocity. An aluminium plate is attached to the tip of each blade so that it moves in its own plane as the blade vibrates. An electromagnet is then placed in position with the aluminium plate situated in the gap between the two poles of the magnet, as illustrated in **FIG.7.3**. The magnetic flux in this gap, and hence the magnitude of the retarding or damping forces which result from eddy currents induced in the plate, is controlled by the current flowing in the winding of the magnet. Pilot tests, which are described in the next section, showed that an arrangement of this type was capable of providing damping whose magnitude could be readily varied up to the required level, in this case to $Q = 50$. A magnet was designed which is intended for use with a disc and any number of blades, and consists of a single winding to which may be added a number of pole pieces (see **FIG.7.4**). A magnetic circuit with a high flux density air gap may be obtained simply by the addition of a pole piece as illustrated in **FIG.7.4** and in detail in the photograph of **FIG.7.3**. It is appreciated that there will be edge effects arising from the simplifications which it was found convenient to adopt for manufacturing, but these are not expected to impair performance. This design has several advantages over the alternative of a number of smaller individual magnets, and these are increasingly apparent for greater numbers of blades. In particular,

very little effort is required in setting up the magnet ready for a test, and the ampere-turns associated with each of the individual magnetic circuits is automatically the **same**. Also, for a larger number of blades there is a considerable saving in the quantity of copper which is needed for the magnet windings: for 30 blades, the individual magnets would take double the amount required by the present design, The adopted design may be seen in **FIG.7.5**.

The final item which required careful attention at the design stage was the means of suspension of the disc, The necessity for low natural frequencies of the rigid body vibrations was mentioned earlier, and to obtain these, a previous worker (Armstrong) suspended his model with 'shock-proof' elastic cord. However, this has the disadvantage that it provides virtually no lateral restraint (**i.e.** in the plane of the disc) which in turn would render the proposed damping arrangements impractical, An alternative method of resting the system on rubber blocks was ruled out owing to the high level of damping which would result, A suggestion that some form of air cushion might be employed led to the discovery that a partially inflated automobile inner tube provides an excellent support for the disc by combining the required low stiffness in a direction normal to the plane of the disc with a fairly high lateral stiffness, Tests described in the next section showed the inner tube to be ideal for this purpose, and experience has since borne out its suitability and convenience in use, It may be seen in position in **FIG.7.5**.

7.3 Suspension and damping tests

Prior to the acceptance of the suspension and damping arrangements described above, simple tests were carried out to examine their suitability,

The suspension was required to provide a free support for the disc while at the same time introducing no significant energy

dissipation. The first set of tests were made to study the effect of variation of air pressure in the tube on the natural frequencies of the bladed disc which it supported,, For pressures ranging from 3 cm to 12 cm of Mercury, a number of the natural frequencies were measured from free vibrations of the disc. The signal from a piezoelectric strain gauge on the surface of the disc was passed through a frequency analyser, and on impact excitation of the disc each individual component of the gauge signal could be isolated and measured. No variation in these frequencies could be detected with change of pressure, and as they agreed well with the theoretically computed values, it was concluded that the inner tube did not influence the stiffness of the system to an appreciable extent.

A second set of tests was carried out using the same technique in order to measure the level of damping present in each mode, A record was taken of the decaying oscillations of the disc in each mode of vibration in turn. Analysis of these decay curves showed that in every case the level of damping was less than 0.0005 times the critical damping for that mode (corresponding to a Q factor of greater than 1000). Damping of this low order might very well be attributed to mechanical losses in the specimen itself, which again seems to indicate that the inner tube is not contributing to the motion.

In order to test the proposed damping arrangements, it was necessary to construct a separate rig, This consisted simply of a bar of the same dimensions as the blades which had one end embedded in a large block of steel and an **aluminium** plate attached to the free end. A small electromagnet was then placed in position with its two pole pieces on either side of the plate. By plucking the free end of the bar, it could be excited to free vibration as a cantilever with the attached plate moving in its own plane, Depending upon the strength of the magnetic field in the gap between the poles, the

plate, and consequently the bar, would experience a retarding force proportional to the instantaneous velocity of the plate, The effective damping offered by this source of energy dissipation was measured as before by the analysis of decay **curves**. A strain gauge fixed to the 'root' of the bar was used to detect the vibrations, and photographic records of its signal were made for various magnetizing currents. **The** results from this experiment indicated that viscous damping was introduced which was substantially proportional to the magnetizing current, The maximum current which was considered as permissible from considerations of heat dissipation in the winding, was found to correspond to a level of damping of the same order of magnitude as that required (**i.e.** .01 critical, or a **Q** factor of **50**).

7.4 Instrumentation and other equipment

Experimental equipment other than the basic items described above falls into three distinct categories. The first of these concerns the means of vibration excitation; the second includes all the equipment necessary for the measurement and recording of the response of the system, and the third constitutes the power supply for the damping magnet,

In order to excite the bladed disc to vibration, an electromagnetic vibration generator was used and the moving coil of this unit was rigidly fixed to a point on the rim of the disc by means of a simple clamp arrangement, This method of attachment was designed so that the excitation could be applied to any point on the rim, The receptance transducers were also mounted on the clamp assembly, which is shown in **FIG.7.6**. A **Muirhead** decade oscillator was used to supply a signal at the required frequency to a power amplifier which, in turn, drove the vibrator, The frequency stability of this signal is **very** important (for reasons discussed in the next

section) and an electronic counter was used to measure its frequency to an accuracy of 6 significant figures,

The basic requirements of the instrumentation are to measure (i) the excitation force applied to the disc and (ii) the response of the disc, both as the normal displacement or acceleration at the point of excitation (the driving point) and also as a distribution of blade loading around the rim. It was decided that the most suitable transducers for use in each case would be those of a piezoelectric type, since they are more sensitive and less demanding on ancillary electronics than passive types of transducer. A short description of piezoelectric charge generating transducers and their use in vibration work is given in APPENDIX 6. A force gauge and accelerometer were used for the accurate measurement of receptance, while barium titanate strain gauges were attached to the root of each blade in order to provide an indication of stress levels. **These** gauges are not suitable for accurate measurements of strain, nor may they be calibrated owing to the variation in their sensitivity both one from another and with environmental conditions. **They** may, however, be used to illustrate the distribution of blade stress around the rim of the disc, and are ideal for comparing the responses of different systems,

Many of the experimental results were recorded by a Solartron data logger, and as this instrument measures **d.c.** levels only, it was necessary to rectify the **a.c.** outputs from the transducers. **The** circuitry associated with a single strain gauge signal is shown in the diagram in **FIG.7.7**, while the corresponding circuit for the receptance transducers will be discussed in the next section,,

Finally, we come to the equipment used to control the application of damping. In order to vary the intensity of the damping, a **d.c.** power supply was used which was capable of delivering 10 amps at 24 **volts**. The circuit is shown in **FIG.7.8** and consists of a rheostat for controlling the current level, and a reversing

switch for demagnetising the magnet while switching off the power.,

7.5 Development of receptance measuring technique

One of the principal objectives of the experiments is the observation and measurement of the natural frequency splits which result from detuning (see Sections 4.3, 5.2). It was decided that this could be best accomplished by measurement of the response of the bladed disc to forced vibration, In order to measure a split of the order of **1%**, it is necessary to know each of the two natural frequencies to within at least **0.1%**. This in turn requires that the frequency of any point on the response curve (from which the natural frequencies are deduced) should be known to within about **0.01%**. The stability of the oscillator signal and the electronic measurement of its frequency are both capable of maintaining this degree of **accuracy**. However, it is necessary that other aspects of the measurement technique should be examined in detail to ensure that such a level of accuracy is in fact attainable.

If it is assumed that the acceleration and force transducers are accurate (in their measurement of the quantities they are experiencing), it is necessary to establish that these quantities are in fact those that we wish to measure, Since the transducer and clamp assembly is very stiff in a longitudinal direction, it is reasonable to assume that the displacement (and acceleration) in that direction is the same throughout its length. This being so, the acceleration level indicated by the accelerometer is the same as that of the point on the rim at which the excitation is applied, and at which the response is required, However, the force level measured by the force gauge is not the (true) exciting force which is applied to the disc, on account of the separation of the point of force measurement and the disc itself by part of the clamp assembly, In the vicinity of a resonance of the bladed disc (which is virtually undamped), the true

excitation force which is required to sustain a working vibration level is **almost zero**. In this situation, the inertia force of the mass of metal between the points of force measurement and application will be several times greater than the applied force which is to be measured. The transducer will give a reading which is a combination of both the inertia force and the (true) excitation force, so that measurements in the regions of greatest interest (*i.e.* near natural frequencies) are incorrect. Fortunately, it is possible to correct the force gauge readings so as to measure the excitation force which is required. Suppose the force gauge reading is F , the accelerometer reading is \ddot{x} and the angle by which F leads \ddot{x} is measured as ϕ . We shall assume that the inertial load (*i.e.* the mass of metal between the points of force measurement and application) may be estimated or measured, and that its mass is m_o . The true excitation force which is applied to the disc, P , is obtained simply by the vector subtraction of the inertia force $m_o \ddot{x}$ from the measured force F , and this, in terms of the measured parameters is

$$P^2 = F^2 + (m_o \ddot{x})^2 - 2 m_o \ddot{x} F \cos \phi \quad (7.1)$$

Other workers (**ref.** Schloss) have proposed an alternative method of making this correction which is both more convenient and more accurate. The amplified outputs from the force gauge and accelerometer provide signals which are directly proportional to the physical quantities they are measuring. Now, the vector subtraction described above may be performed electronically with the aid of operational amplifiers, similar to those used as charge amplifiers (see APPENDIX 6), thus forming a miniature analogue computer. A fraction of the acceleration signal is subtracted from the force signal using a circuit which is shown in FIG.7.9, and this fraction may be chosen to correspond to any particular value of the inertial load m_o .

To illustrate the importance of this correction, and the identity of the two methods of making it for a given load m_o , the results of a test are shown in FIG.7.10. Of the three curves of receptance plotted against excitation frequency, one illustrates the uncorrected results (i); a second shows the curve drawn from the electronically corrected receptance (ii), while the third is the result of numerical correction according to equation (7.1) (iii)., Clearly the two methods of correction provide almost identical results, but the former process is much more convenient to use, A further advantage of this technique is that it provides a means of obtaining a good estimate of the mass of the inertial load, m_o . In order to make this estimate, the vibrator and transducer assembly is driven without attaching it to the disc, The electronically corrected force level should be zero since in this case there is no load, and the fraction of the acceleration signal which is subtracted may be adjusted until the (corrected) force is at a minimum. In practice, this minimum will not be exactly zero, but it is usually at least two orders of magnitude less than the uncorrected force (i.e. than the inertia force of the mass m_o). A calibration test was performed to determine this inertial load, and to examine its variation with frequency of vibration, The results, shown in FIG.7.11, indicate a fairly consistent relationship between these two parameters with the inertial mass approximately equal to 0.29 lb, except near two frequencies (200 and 800 cps). The deviation from a constant value near these two frequencies indicates that the inertial load is not simply a mass, but that it has elastic properties of its own which result in the behaviour shown on the graph, It is found in practice that there are two similar narrow frequency regions in which the receptance measurements by the transducers are inconsistent, The cause of this is believed to be this flexural behaviour of the clamp assembly and such regions are arranged so as not to interfere with any measurements which are required,

Electronic mass cancellation was employed in all the tests which are described in the next chapter,

7.6 Calibration of the damping assembly

The most convenient way of calibrating the damping assembly is by measuring the level of damping in each mode of vibration and relating it to the magnetizing current, The experimental procedure which is employed to do this is based on the recording and analysis of decay curves resulting from free vibrations of the system, and is now described in detail,

Before any measurements may be made, it is necessary to determine the natural frequencies of the bladed disc, and this may be done either by calculation or by experiment. The output from a piezoelectric strain gauge attached to the surface of the disc is fed into a wave analyser which is tuned to the natural frequency of the mode which is currently of interest, If the disc is struck, it will vibrate in every normal mode (except any which might have a node at the point of excitation), and the decaying oscillations in the selected mode will be filtered out of the complex strain gauge signal, These oscillations may then be recorded in the form of a decay curve, such as the one shown in **FIG.7.12**, and analysed to provide a measurement of the level of damping present, The reproduction also shows the details of this analysis,,

A series of tests was carried out for a number of different modes of vibration at each of three different magnetizing currents, From the results, which are shown in **FIG.7.13**, a roughly linear relationship between magnetizing current and damping was found for each mode. In general, the damping resulting from a given current falls off for the higher natural frequency modes, although it appears that single modes are more effectively damped than double modes.

CHAPTER 8

THE EXPERIMENTAL PROGRAMME, PROCEDURE AND RESULTS

8.1 Objectives of the experimental investigation

The experimental investigation was undertaken in order to provide a check on the calculations and observations which had resulted from the theoretical analysis. These fall into two categories, one concerned with a method of natural frequency calculation and the other with the behaviour characteristics of detuned systems; and the experimental programme is similarly divided.

The first objective of the experiments is to provide an estimate of the accuracy of the natural frequencies which were computed by the receptance determinant method. The experimental model **was** designed so as to represent the analytical model as closely as possible, and comparison of measured and computed natural frequencies is considered to be a realistic check on the accuracy of the method of solution.

The second and more important series of tests are intended to confirm, both qualitatively and quantitatively, the patterns of behaviour of detuned systems which were examined in detail in chapters 5 and 6. These experiments involve observation and measurement of the frequency splitting which occurs in certain modes under detuned conditions. They are also designed to verify that the two types of cosine detuning do in fact have the effects which are predicted by the 'theory'. The modal shapes may also be measured, and in certain cases the validity of the proposed 'simplified double mode' (Section 6.4) may be investigated. An extensive study of modal shapes is less readily made experimentally than by computation owing to the necessity of making measurements from forced vibration response in the former case, while the latter is based on a consideration of free vibrations. It is in this aspect also that both the advantages and the

limitations of having just five blades become noticeable, While there are only five blade stresses to be measured and recorded, a discrepancy in a single reading has a much greater effect on the deduced modal shape than if there were a large number of blades, however, the subsequent work which is planned for a multibladed disc should overcome this difficulty,

The series of tests which were carried out are listed here and described in detail later in the chapter, and in the same order,

1. Tuned systems: various λ *
 - Series A. Natural frequencies $\lambda = 0.3333$
 - Series B. **Natural** frequencies $\lambda = 0.25$
 - Series C. Natural frequencies $\lambda = 0.275$
2. Detuned systems: $\lambda = 0.275$
 - Series D. Natural frequencies: cosine detuning
 - Series E. **Damped** response: single modes
 - Series F. **Damped** response: double modes

8.2 Experimental procedure

The experimental procedure was basically the same for every test described in this chapter, The various parameters, such as excitation position and frequency, detuning and damping arrangements etc, were varied from one test to another according to the requirements of the **programme** outlined above, but in each case the results were obtained in the form of response curves,

Prior to each test, it was necessary to set up the system with the detuning blocks and shims which were specified for the current detuning arrangement as described in the previous chapter (7.2).

* λ is the 'blade length ratio'; being the ratio of blade length to disc diameter,

Having established which mode of vibration was currently of interest, the mass cancellation adjustment was corrected for the natural frequency of that mode, either by inspection (as described in the calibration; 7.5) or direct from the calibration curve **FIG.7.11**. Then, the vibrator and receptance transducers could be attached to the point on the rim of the disc which that particular test specified, by means of the clamp arrangement which was also described in the previous chapter, It was found to be convenient to locate accurately the natural frequency (or frequencies) which were to be measured during the test, so that the values of frequency at which readings should be made in order to produce an acceptable response curve could be most efficiently spaced, These natural frequencies could be detected by inspection of the force and acceleration signals, which were monitored on valve voltmeters, and noting the value(s) of frequency at which the ratio of acceleration to force reached a maximum. When this had been done, the specific values of frequency at which the response should be recorded were selected, the number of points ranging from about 20 for a single resonance to 30 or more for a double-peaked resonance.

With the damping magnet switched on at the required current level, the response at each of the excitation frequencies was obtained and recorded in the following **manner**. The oscillator signal was set at the appropriate frequency (its exact value being measured by the electronic counter) and the strength of the signal supplied by the power amplifier to the vibrator was adjusted to provide satisfactory force and acceleration levels, In the vicinity of a resonance, it was necessary to maintain a reasonably high level of vibration in order to make the exciting force signal large enough to be free from electronic noise, **As** the resonant frequency was approached, this became increasingly difficult, and the measurements of force at frequencies very close to this value are subject to considerable errors,, However, only one or two points on the response curve were affected, and these usually lay outside the bounds of the graph, A similar situation

arose near antiresonances where the acceleration fell to a very low level, The maximum level of vibration was determined by the acoustic noise level in the laboratory near resonant conditions, and by the power limitations of the equipment which became evident near **anti-resonances**.

As soon as the monitored transducer signals showed that transient effects had died away, the outputs from the two transducers and the five strain gauges could be recorded, In the majority of cases this was done directly onto punched tape by the data logger, ready for processing. In the few cases when this instrument was not available, these outputs had to be measured individually on the voltmeter, written down and then punched out onto tape; this procedure took almost 100 times as long as when using the data logger.

Finally the results were processed by computer to provide measurements of receptance, blade stress response and relative blade stress levels around the rim at the various excitation frequencies.

8.3 Experiments on tuned systems

The experiments in this category are intended to provide accurate measurements of the natural frequencies of three five-bladed disc sets, In each case, the natural frequencies were first measured by an impact technique similar to that used in the damping calibration tests (7.6). The filtered strain gauge signal was compared with one of known frequency from an oscillator for each mode in turn, and the natural frequency deduced by matching the two signals. The resolution of this method proved to be poor and ineffectual for close natural frequencies, so the measurement of the response to forced vibration was adopted as the means of determining natural frequencies.

Series A: Blade length ratio = **0.3333**.

The original model was machined with five 8" blades and the response of this system was measured over a wide range of frequency

during the development of the receptance measuring technique (7.5). The response in the vicinity of each resonant frequency was examined in greater detail so that the natural frequencies could be measured to within **0.02 cps**. The results of these tests are tabulated in **FIG.8.1** alongside the theoretically computed values, with which they show good agreement, Owing to a lack of precise information concerning the physical properties of the steel from which the model was made (see APPENDIX 7), it is necessary to quote upper and lower bounds on the constant (κ) which relates the dimensionless and dimensional forms of frequency, and this results in the upper and lower limits which are quoted for the 'theoretical values' in this and subsequent tables,

Series B: Blade length ratio = **0.25**.

The model was then subjected to further machining prior to the detuning tests and the blade lengths were reduced from 8" to **6"**. A series of tests was performed, identical to those of Series A, in order to determine the natural frequencies of this modified system, Results are tabulated in **FIG.8.2**.

Series C: Blade length ratio = 0,275.

When each blade had its damping plate and 0% detuning block added to its tip, the system was an approximation to a bladed disc with a blade length ratio of **0.275***. The natural frequencies of this model were then measured and compared with those computed for a system with $\lambda = 0,275$ as shown in **FIG.8.3**. As might be expected*, the results do not show such close agreement as for the two earlier cases, although the correlation is still very good.

The results from all three series of tests are presented on a single graph, **FIG.8.4**, in which the measured natural frequency is

* The assumption is made that these composite blades behave as uniform bars, 6.6" long, when vibrating at low frequencies. This will become less valid at higher frequencies,

plotted against the computed dimensionless natural frequency for each mode. If the analysis is accurate, then the experimental results should all lie on a straight line, the slope of which is the constant K and depends upon the elastic and dimensional properties of the model. **However**, this constant may only be determined to within about **$\pm 5\%$** , thus making a direct comparison of the two sets of results difficult. Two lines corresponding to the upper and lower bounds on the constant are shown as broken lines on the graph and all the experimental points are seen to lie on or between them. It is also clear that these experimental points lie very close to the straight line which has been drawn through them, and this fact serves not only to illustrate a good agreement between experimental and computed natural frequencies, but also to provide a much better estimate of the constant K . Using this result, a further table has been prepared in which the deviation of each experimental frequency from this straight line is shown: FIG.8.5. Finally, the results are shown superimposed upon a graph from one of the earlier sections, **FIG.4.6**, which illustrates the variation of natural frequency with blade length,

In every case, the results show an exceptional agreement between the computed and measured natural frequencies, and thus provide confirmation of the accuracy of the analytical solution.

8.4 Detuned systems - I. Natural frequency measurements

In performing a series of experiments with the intention of confirming the predicted behaviour under detuned conditions, there are two problems to be **overcome**. The first of these is to locate and measure a natural frequency split in those modes for which 'theory' predicts such a split will occur with the given detuning. The second and more difficult task is that of demonstrating that there is **no** split in those modes which theory again specifies. The difficulty here is that in selecting a point on the rim of the disc at which to

apply the excitation, it is quite possible to choose a point which is on, or very close to, a node of one or other of the pair of modes. This results in only one mode being apparent in the response curve. If a second excitation position is chosen, say 10 to 20 degrees from the first, then a second mode may well be detected in the response, in which case the existence of a split is confirmed together with a measure of its magnitude. Such a case is illustrated in **FIG.8.7** where the response in the vicinity of the pair of 2/0 modes is shown for two positions of excitation. However, this second position will not necessarily produce a significant change in the response, such as the case illustrated by the curves in **FIG.8.8**. In this case there is in theory no split, but a third and perhaps even fourth excitation position might be necessary in order to furnish sufficient evidence to make this observation conclusive. There is, however, one feature which indicates whether or not a split is to be found by further measurements. Marked on both graphs is the natural frequency of the tuned system, and as the detuning is in both cases of a cosine nature, theory predicts that any splitting which results will be symmetrical about this tuned system value. In **FIG.8.7**, the curve corresponding to $\Theta = 50^\circ$ indicates a single resonance, but as this occurs at a frequency which is substantially higher (0.3%) than the tuned system value, it suggests that that particular excitation position is producing response in just one of a pair of modes. Excitation at a different point proves this to be the case by displaying two natural frequencies symmetrically placed about the tuned system frequency. On the other hand, the curve corresponding to $\Theta = 50^\circ$ in **FIG.8.8** also shows a single resonance but this time it coincides with the tuned system natural frequency, suggesting no split. The second excitation position produces an identical response to the first, substantiating this result. Although this provides a useful indication, it must be used with some caution since, if there is a constant term in the detuning function, then the splits will

not be symmetrical about the tuned system values.

Series D: Various forms of detuning, $\lambda = 0.275$

During the course of these tests it was found necessary to alter the damping plates slightly and this resulted in a shift of about 1X in each tuned system natural frequency. In the detuning tests we are concerned only with the difference or split between pairs of close natural frequencies, and not so much with the absolute values, so that the results from all the tests are included in this section. In each 'test' described below, the natural frequencies and splits of the first five double nodes were measured.

D1. In this series, the first tests used a simple $\cos \theta$ detuning function with $\sigma = .01$. These were followed by $\cos (\theta + 30)$; $\sigma = .025$, $\cos (\theta + 30)$; $\sigma = .01$ and then by $\cos (\theta + 90)$; $\sigma = .01$. The results from these tests are tabulated in FIG.8.9 and they illustrate the same pattern of behaviour as that predicted in the theoretical sections. The modes which belong to the second family (i.e. those which are associated with $(5j+2)$ nodal diameter disc modes) exhibit a split which is dependent upon σ but not on ϕ , while the double modes of the other category show no signs of splitting at all,

D2. The second series of tests used the complementary detuning functions based on $\cos 2(\theta + \psi)$, with a similar selection of values for σ and ψ . These results are given in the table in FIG.8.10, and once again they conform to the behaviour specified in Chapter 5 for this type of detuning.

D3. Finally, a third set of tests incorporated detuning functions formed by the sum of two different types of detuning. The first used a detuning function of $f(\theta) = 0.2 + \cos(\theta + 30)$ with $\sigma = .025$. In addition to the expected splitting which occurred in this case, the mean natural frequency of each mode was lowered as a result of the positive constant term ($\sigma b_0 = .005$), thus providing an opportunity

to estimate the frequency factor Φ (defined in Chapter 6), as well as the split factor Ψ , for various modes.

The second test of this type used a combination of both types of cosine detuning with $\frac{1}{2} \{ \cos(\theta + 30) + \cos 2(\theta + 15) \}$ and $\sigma = .025$. In this case a split was observed in every double mode, and the results from this and the previous test are given in FIG.8.11..

Having satisfactorily established agreement between experimental and predicted patterns of behaviour, the results were then analysed to provide a quantitative measure of the split and frequency factors of some of the modes. These are shown in the table in FIG.8.12 alongside values which result from the computational study described in Chapter 5. With due consideration to the order of magnitude of the quantities being measured, it is felt that agreement between the experimental and computed values of these properties is very good, and that the behaviour predicted by the analysis is confirmed by the experiments.

Throughout the course of these tests, measurements were made to check that splitting is a property of double modes only. In no case was splitting detected in any single mode.

8.5 Detuned systems - II. Damped response

The experimental study next sought to compare the response of the system when it was subjected to various detuning arrangements in the presence of light damping. Many of the experimental observations relevant to this section were measured from the strain gauges, and consequently the results are considerably less accurate than those concerned with frequency measurements. As it was found convenient in the analytical sections to separate the treatments of single and double modes, so it was decided to divide the experimental work in the same way. In the previous section (8.4), only double modes were of interest and single modes were hardly mentioned. However, theory predicts that it is these latter modes which are adversely affected by

detuning from a consideration of stress levels, so that a number of tests were carried out to check this result,

Series E: Single modes

This series of tests was performed to measure the variation in blade stresses resulting from various forms of detuning in each of three single modes, Only the blade stresses at the resonant frequency were required and in order to overcome the difficulties which are encountered when taking measurements near these frequencies (Section 8.2), light damping was applied using a magnetizing current of 4 amps in every case, The position of the excitation was also the same for every test, so that realistic comparisons could be made between systems with various detuning arrangements.

The first tests were made on the tuned version in order to determine the natural frequencies and also to trim the strain gauge outputs so that each blade was indicating the same stress level, This trimming was found to be necessary to take account of variation in gain between channels due to differences in the sensitivity of the gauges and associated circuitry. Cosine variations were then made on the blade lengths, much as in the earlier natural frequency tests, and the response at resonance was measured under the same excitation and damping conditions for each detuning arrangement, The collected results are shown in a table in **FIG.8.13** and graphically in **FIG.8.14** where the variation in relative stress levels is plotted against the variation in blade length for (i) $\cos 10^\circ$ detuning and (ii) $\cos 20^\circ$ detuning, These graphs are arranged so as to enable a direct comparison to be made with the computed values of Chapter 6, which are reproduced in this instance as the solid lines,

Although on first sight the correlation between the experimental points and the theoretical lines is not very good, it is clear that there is qualitative agreement, When it is considered that it would be necessary to measure each stress to better than 1% in order to obtain

'good' agreement, the results are thought to provide qualitative confirmation of the behaviour predicted in Chapter 6.

It was observed in Section 6.2 that a conclusion could be drawn concerning the effects of detuning on single modes on the basis of one assumption viz. that the mean stress or response level for given excitation and damping conditions would be largely unaffected by detuning. The experiments also sought to produce evidence of the validity of this assumption, but difficulty was again encountered in attaining a sufficiently high degree of accuracy. The results presented in the table in **FIG.8.13** show that although there is a variation in the mean stress level from one test to the next, it does not appear to conform to any particular pattern, nor are the variations of any significant magnitude, This would seem to indicate that the assumption is justified.

Series F: Double modes

The analytical treatment of the effects of detuning on double modes (Chapter 6) resulted in the construction of a simplified model of this type of mode. If the assumptions and approximations relating to this model can be justified, it provides a simple method of examining the properties of the double modes of bladed discs with arbitrary detuning, This was in fact done in Section 6.4, and the present series of experiments attempt to provide the required justification.

It was considered impracticable to attempt an extensive experimental study along the same lines as that made numerically with the aid of the simplified model. Instead, it was decided that a typical bladed disc double mode should be studied in detail and that a direct comparison should be made between these results and those of a numerical treatment of the simplified model under the same conditions of detuning and excitation.

The investigation reported here was conducted on the 2/0 modes of the experimental model with a detuning function of $\cos(\theta + 30)$ and with $\sigma = .01$. The response of this system was measured at four positions of excitation at each of two levels of damping. These four positions were chosen such that one produced a response in just one of the two modes, a second produced a similar level of response in both modes, while the third and fourth were situated between these two. The response is shown as a number of graphs, the first two of which (FIG.8.16) show the driving point receptance plotted against frequency at each of the two levels of damping. It was noticed in these graphs that the damping levels appeared to be somewhat lower than was suggested from the calibration tests. The receptance curves corresponding to $\theta = 100^\circ$ may be used to measure damping by the 'half power' method since they indicate response in only one mode of vibration, and application of this technique shows the damping to be approximately one half of the calibrated value: a possible explanation is discussed at the end of this section. The blade stress response is also plotted, although only for the lighter damping, and appears as a set of five graphs in FIG.8.18a.

It was shown in Chapter 6 that a relationship existed between the coefficients in the detuning function $f(\theta)$ and those in the modal shape functions $F(\theta)$. When this relationship is applied to this experimental case, the modal shape functions for the pair of 2/0 modes are defined as $\cos 2(\theta - 7.5)$ for the lower frequency mode, and $\sin 2(\theta - 7.5)$ for the higher frequency mode. Results are shown in the form of nodal patterns in FIG.8.15, and also indicated on this diagram are the positions of the four experimental excitation points which were discussed above. The first of these points was chosen so that it was situated at a node of the higher frequency mode (thus fixing the complete nodal pattern), and it may be seen from FIG.8.15 that the experimental and theoretical position for the nodal lines agree very closely,

Calculations **were** made using the simplified double mode analysis for the above experimental conditions, For these conditions, the basic theory predicts a split of **0.5%** and the modal shapes given above, and this information is incorporated in the model. Other data, such as excitation and damping arrangements, was drawn from the experimental conditions.

The results of these calculations are presented as a set of graphs which may be compared directly with the experimental observations. The driving point receptance is plotted in two graphs on **FIG.8.17**, and the blade response in a series of five graphs, **FIG.8.18b**.

The general form of the two sets of graphs is remarkably similar. The twin peaked response predicted by the simplified double mode calculations (**FIG.8.17**) is reproduced in the experimental curves (**FIG.8.16**), and the correlation between the curves relating to the four specific excitation positions is very good. The only disparity between these results is in the minimum response which is situated between the two natural frequencies, as this drops to a somewhat lower value in the experimental graphs. It is thought possible that this might be due to a non-linear effect in the damping assembly in which the value of the damping is amplitude-dependent. Such an effect has not been investigated in detail, but it might also account for the discrepancies found between the damping levels indicated by the calibration and those measured from the response **curves**. In order to eliminate any such effects from the present series of tests, each of the four tests in the two graphs were recorded at approximately the same level of vibration,

Turning now to the two sets of five graphs (**FIG.8.18**) showing the response curves for each blade, we find a similar degree of correlation between the computed values and experimental measurements. Owing to the lower order of precision of the recording transducers in

this case (strain gauges), the experimental response curves are less well defined. however, only second order differences may be found between the two graphs for each blade.

8.6 Summary of experimental results

The experimental apparatus performed well in general, but some difficulty was encountered in obtaining accurate measurements of blade stress levels due, presumably, to variations in the sensitivities of the strain gauges. The damping arrangement was not as effective as had been expected, and considerable variations from the calibration curve were observed in various forced vibration tests.

The natural frequencies measured on a number of tuned systems agreed very closely with the values computed from the receptance determinant. The collected results provided a useful estimate of the constant K , whose value could not be determined accurately owing to a lack of precise physical data for the model.

Extensive measurements of the natural frequency splitting phenomenon provided confirmation of the patterns of behaviour which were predicted in Chapter 5. Values of the frequency and split factors $(\Phi \Delta \Psi)$ of certain modes were found to agree very well with those computed for this model.

Although measurements of blade stress levels were considerably less accurate than those of natural frequencies, it was possible to demonstrate that detuning always has a disadvantageous effect on single modes, as was predicted in Chapter 6.

Measurement of the response of double modes for detuned systems provides confirmation of the validity of the 'simplified double mode' model. Taking a specific case, good agreement was found between experimental measurements and calculations made using this model. The conclusion drawn from this section is that detuning cannot produce

higher stress levels than are experienced in a tuned system under the same conditions of excitation.

CHAPTER 9

CONCLUSIONS

9.0 General conclusion

A procedure has been developed for investigating the vibration properties of a bladed disc which has been detuned in an arbitrary manner. The techniques have been applied to make a detailed study of a uniform five bladed disc, and the results from numerical and experimental tests have agreed in every case. It is concluded that these methods may be used to make a similar study on any system, and that some of the results obtained are general and apply to any bladed disc .

9.1 Vibrations of a tuned bladed disc

A general method for determining the natural frequencies and modal shapes of a bladed disc has been developed in terms of receptance **expressions**. In a detailed investigation which has been made for uniform five-bladed discs, the natural frequencies of experimental models were measured and compared with values computed according to this method . The close agreement which was achieved in every case led to the conclusion that the assumptions made in the analytical approach are justified,

Because of the numerical difficulties which would be encountered in applying this method to practical cases, an approximate method of solution was devised which is based on matrix techniques and readily programmed for efficient digital computation. During the course of the development of this method, a large number of calculations were made to assess the accuracy of the truncated series form receptances, and also of natural frequency estimates which result from using them. It was found that a much greater number of terms are required in order to obtain good estimates of either receptances or natural frequencies,

than had been expected,

The receptance analysis from which the natural frequencies were computed shows there to be two distinct types of solution, or vibration mode. The first of these, single modes, are associated with symmetrical vibrations of the bladed disc in which all the blades vibrate in phase and with the same amplitude. In double modes the blade amplitudes vary sinusoidally around the disc, although they are vibrating in phase, and these modes are related to those of an unbladed disc in which there are nodal diameters.

9.2 The effects of detuning

When a bladed disc is detuned, the two types of mode are affected in different ways. The natural frequency of a single mode is unaffected by small variations of blade length (provided that the mean length is unchanged), but the symmetry of the modal shape is disturbed and the blades no longer all have the same amplitude of vibration. However, such a variation in the blading causes a double mode to split into a pair of modes with virtually identical modal shapes and very close natural frequencies. The magnitude of this natural frequency split depends upon the nature and amplitude of the variation of the blades. In the case of a five-bladed disc, it was found that a cosine variation of blade length produced either the maximum or minimum possible split, according to the frequency of the cosine expression and the shape of the double mode. It was also found that the behaviour of each double mode could be defined by a single property called the 'split factor'. An extensive experimental investigation on a number of detuned models confirmed without exception the patterns of behaviour predicted by the analytical treatment.

It is of considerable importance to appreciate the practical significance of the changes which are brought about by detuning. For single modes, a variation in the blades always results in one or more

blades experiencing higher loads than others, and it is concluded that in practice the maximum blade stress level for given conditions will always be raised by detuning, Results from experimental tests suggest that this is probably true, but owing to inaccuracies in the stress measurements, these results are not conclusive. In a double mode, there is **a pair** of similarly shaped, but orthogonally orientated modes whose respective natural frequencies are very close. It has proved possible to devise a simplification of a double mode by ignoring the effects of all other modes. Using this model, it has been shown that detuning cannot cause an increase in the maximum blade stress in this case above that found in a perfectly tuned system. In fact, with favourable excitation conditions, the maximum blade stress attained on resonance may be reduced by as much as **30%**, depending on the extent of detuning and on the damping level. Measurements of the response of experimental models to forced vibration in the presence of damping and detuning provide good agreement with calculations made with the facility of the simplified double mode, which suggests that this analytical model may be used to study the response of a typical double mode under more complex excitation and damping,,

9.3 Application of the results to other systems

Although a comprehensive study may be made for any uniform bladed disc, many of the results described above **are** general and apply equally to uniform and non-uniform systems alike. Any bladed disc in which the disc is flexible and symmetric will possess both single and double modes of vibration, This property results from the circular symmetry of the disc and the regular spacing of the blades. Consequently, all such systems will exhibit frequency splitting when the blades are detuned. The consequences of this property in a detuned system are expected to be similar to those described in detail for a five-bladed disc, although exceptions will probably arise when a number of distinct modes have natural frequencies that are almost the same.

The pattern of behaviour of detuned systems which has been established in this work is largely in agreement with experimental observations made by Armstrong. In a number of tests on detuned models, he observed splitting in most of those modes which, by the present classification, are double modes, while no such behaviour was detected in any of the single modes. However, possible patterns of behaviour were not investigated, nor are the results sufficiently comprehensive to deduce such a pattern. **Measurements** of response on the detuned model produced results which were very similar to those obtained in the present investigation.

A qualitative comparison may be made between the results of the present work and those of Whitehead and Stratford, described in the introduction (section 1.2). In a single mode, the effect of the coupling through the flexible disc is that in a tuned system each blade vibrates with the same amplitude. This situation also results from coupling through the rigid body motions of the disc, such as that described by Stratford. The effects of detuning on this type of vibration are found in both studies to be unfavourable, but owing to the diversity of the basic assumptions in the two approaches a numerical comparison may not be usefully made.

9.4 Limitations and extension of the work

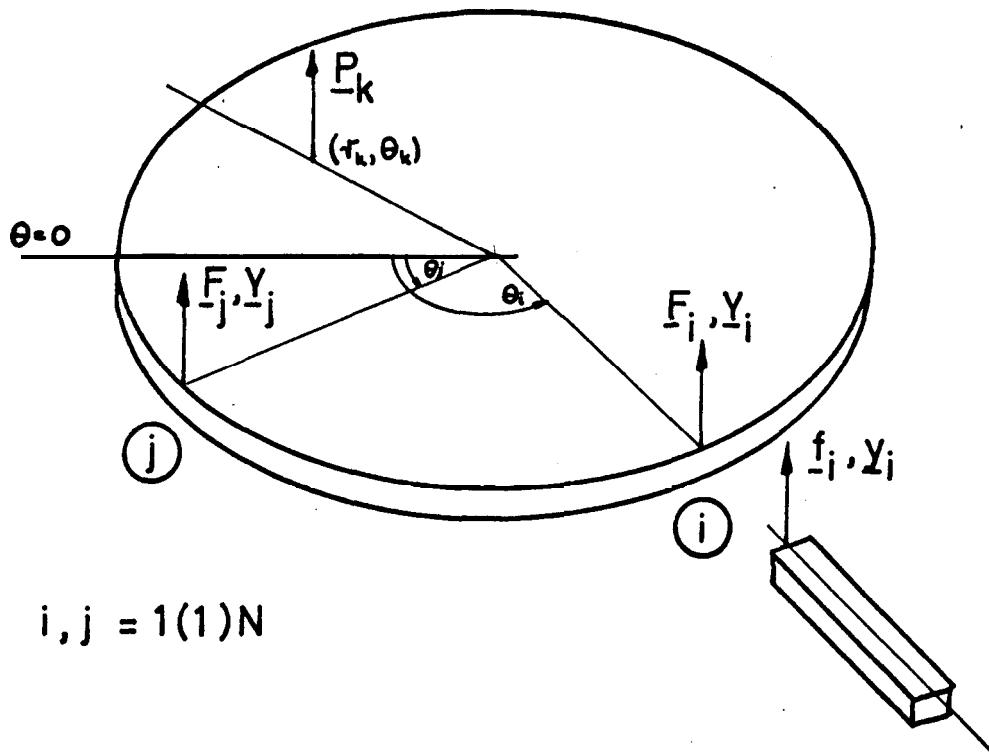
The most important limitation of this work arises because it has not been possible in the time available to investigate the properties of a bladed disc which are peculiar to systems with a large number of blades. It is known, for example, that a multibladed disc has a number of (double) modes whose natural frequencies are all just below the blade cantilever frequencies, and the behaviour of these modes under detuned conditions might well differ from that described above for isolated double modes by virtue of the proximity of several natural frequencies. Any extension of this research must first examine these

properties of multibladed discs, However, the results of the present work provide information which is essential to the planning of an efficient numerical study of such a system, The computation time for a natural frequency solution increases with the cube of the number of blades, so that an investigation of the same scale as the one reported here would not be practicable for large numbers of blades.

It is felt that the other principal assumptions, those of uniformity and zero stagger, do not seriously restrict the generality of the results. The inclusion of stagger and components of non-uniform cross section would present a considerable numerical problem in the derivation of accurate receptance expressions, Whilst an extension of the work to include such additions is not envisaged in the immediate future, it might be extremely useful to consider in greater detail the mechanism of excitation, Such a development of the theory might be made possible by analysis **of** the simple analytical model of a double mode which was devised in this work.

An attempt has been made to include the effects of damping in both the numerical and experimental studies. In both cases, some measure of success was attained, but it is believed that a more detailed study is required of the precise form of the damping which is to be simulated, The experimental damping assembly did not provide a sufficiently accurate source of damping for this quantity to be included as a parameter in the study, although it did serve to facilitate accurate and consistent measurements of response at resonant conditions,

Finally, the techniques which were used to measure the effects of detuning on an experimental model did not permit sufficiently accurate measurements to be made of the blade stress levels,, This limitation could be overcome by the use of more accurate strain gauges,



$i, j = 1(1)N$

upper case refers to the disc
 lower case refers to the blades

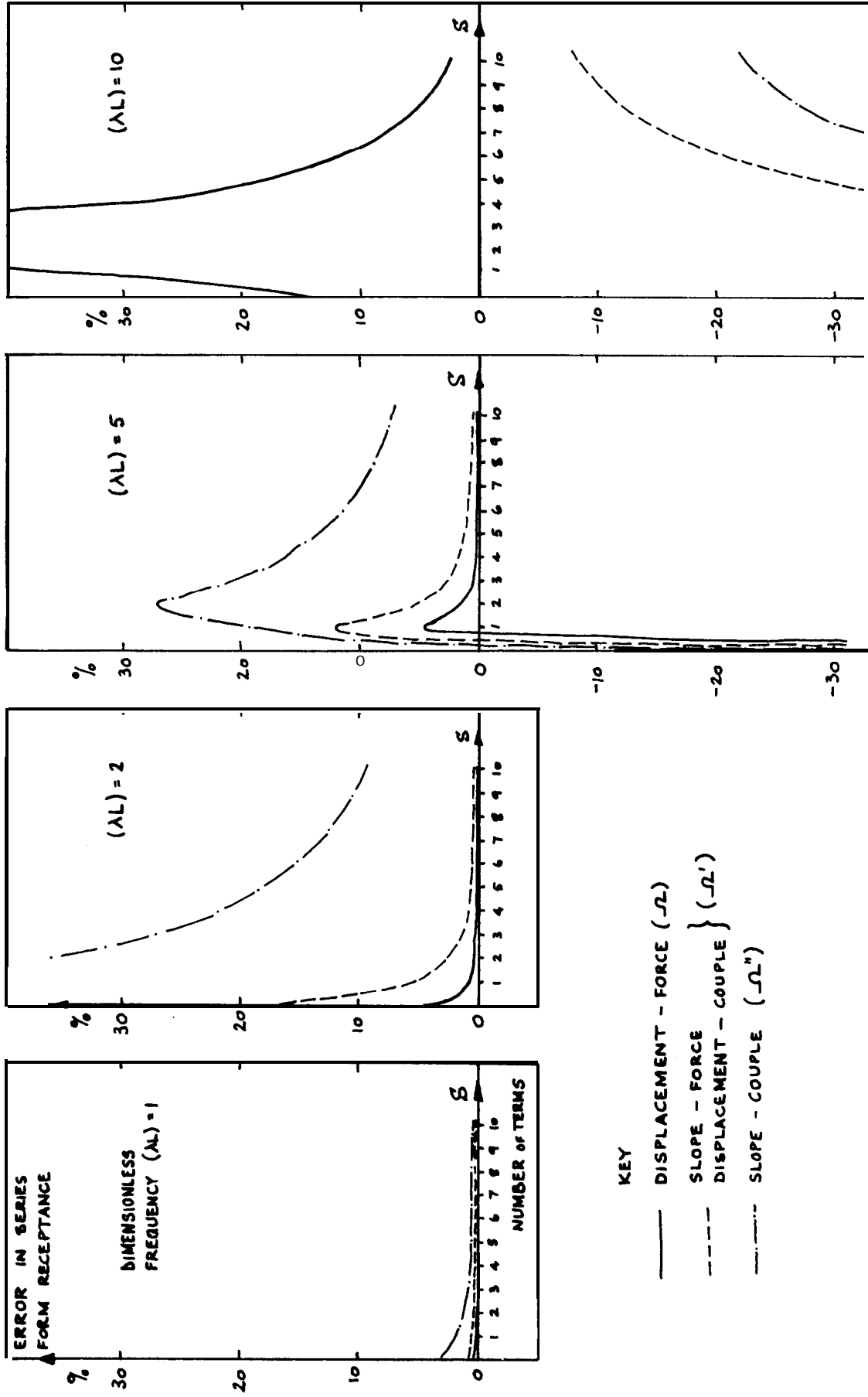
\underline{Y} and \underline{y} are displacement vectors

\underline{F} and \underline{f} are load vectors

\underline{P} is an externally applied load

BLADED DISC SYSTEM

FIG 2.1



ACCURACY OF SERIES FORM END RECEPTANCES FOR A FREE FREE BEAM

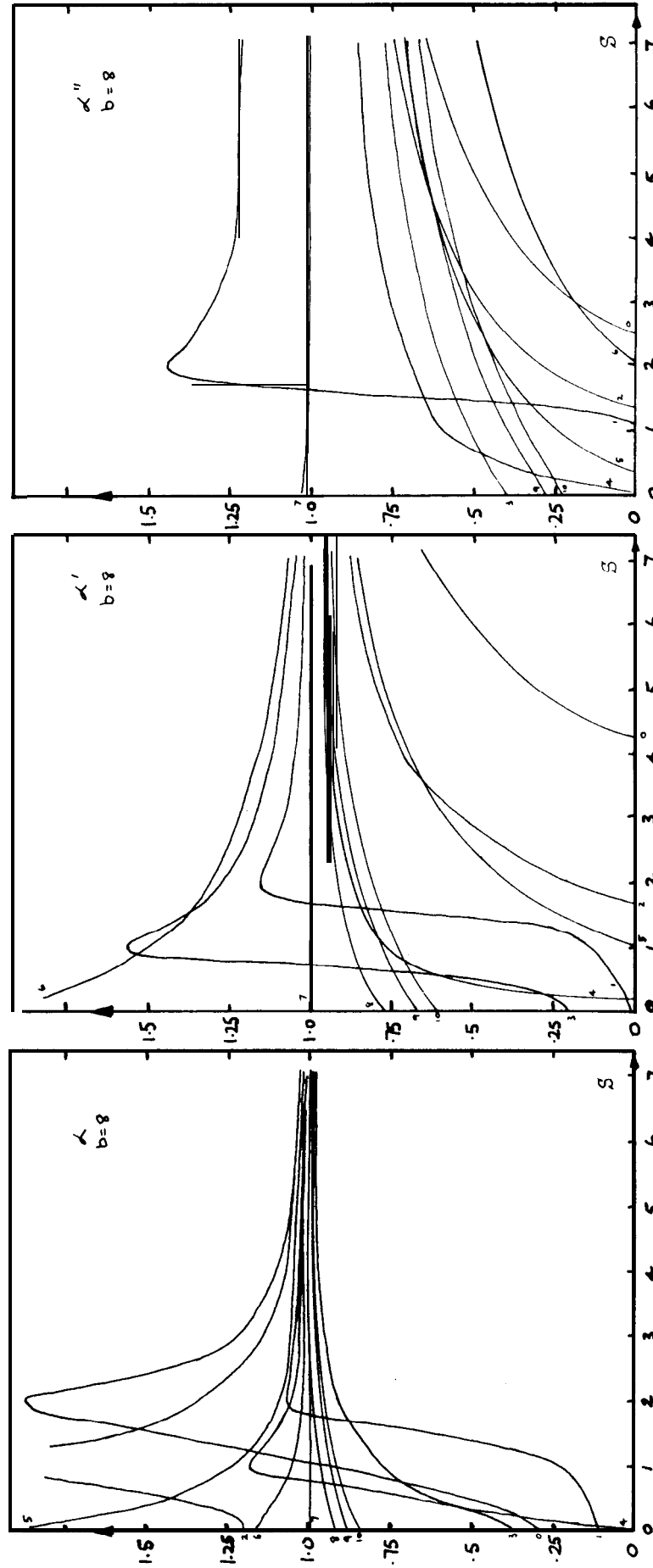
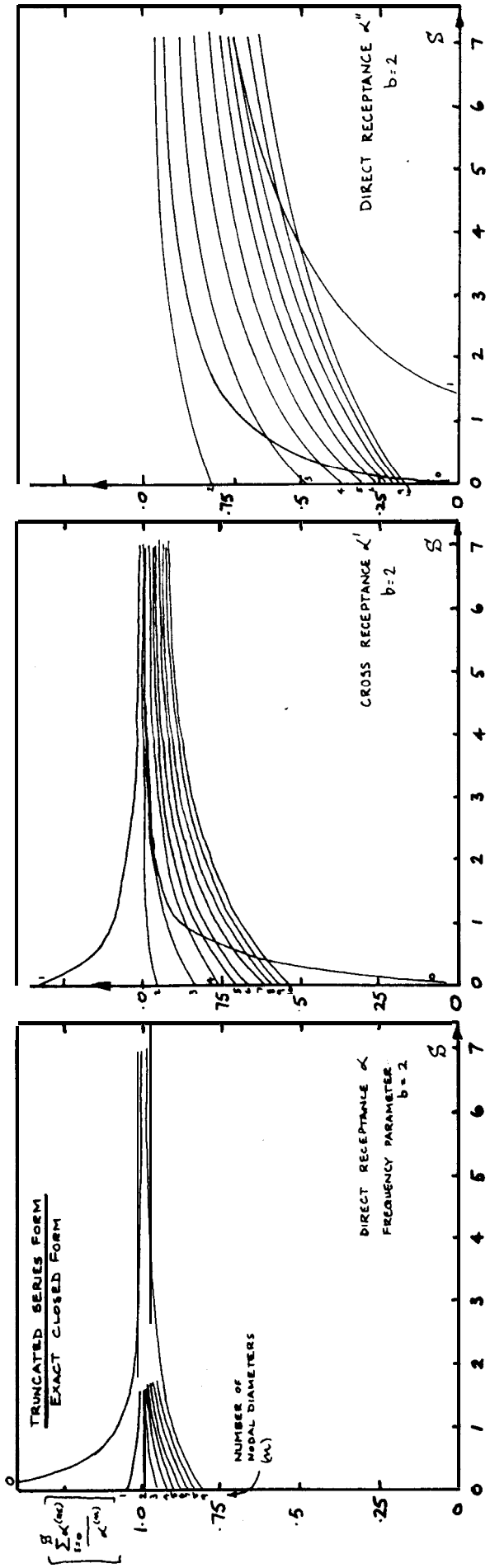
FIG 3.1

**SOME PROPERTIES OF THE NORMAL MODES OF VIBRATION OF A FREELY SUPPORTED
UNIFORM CIRCULAR DISC**

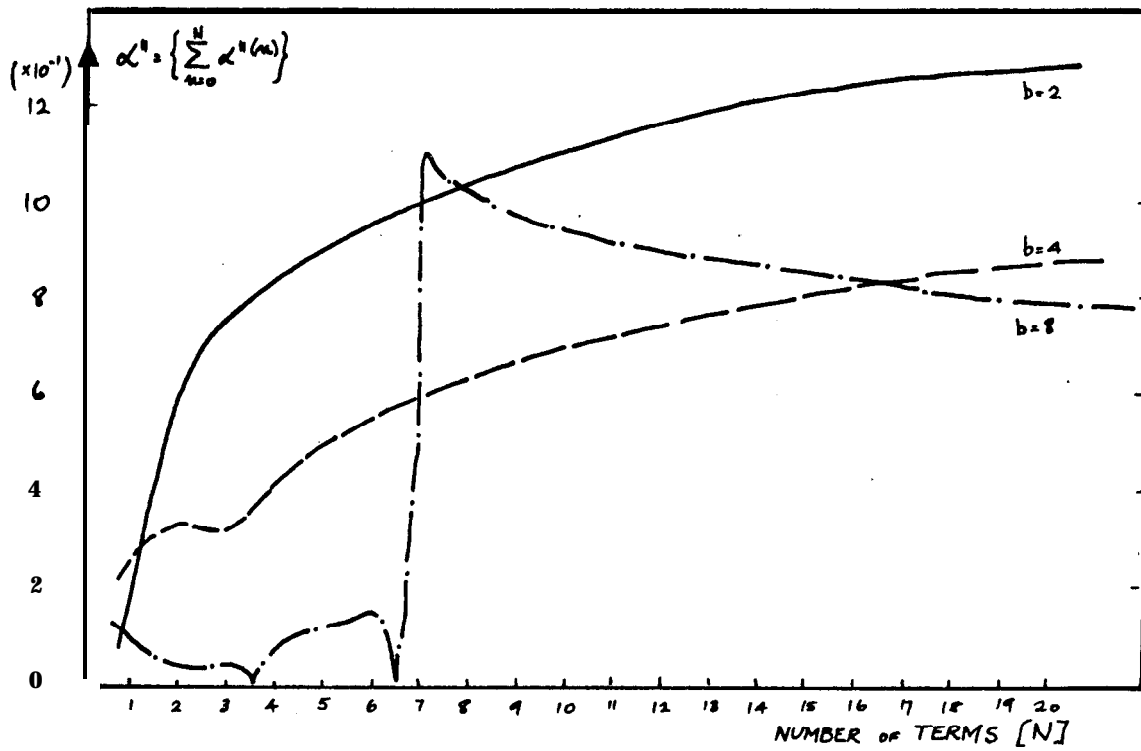
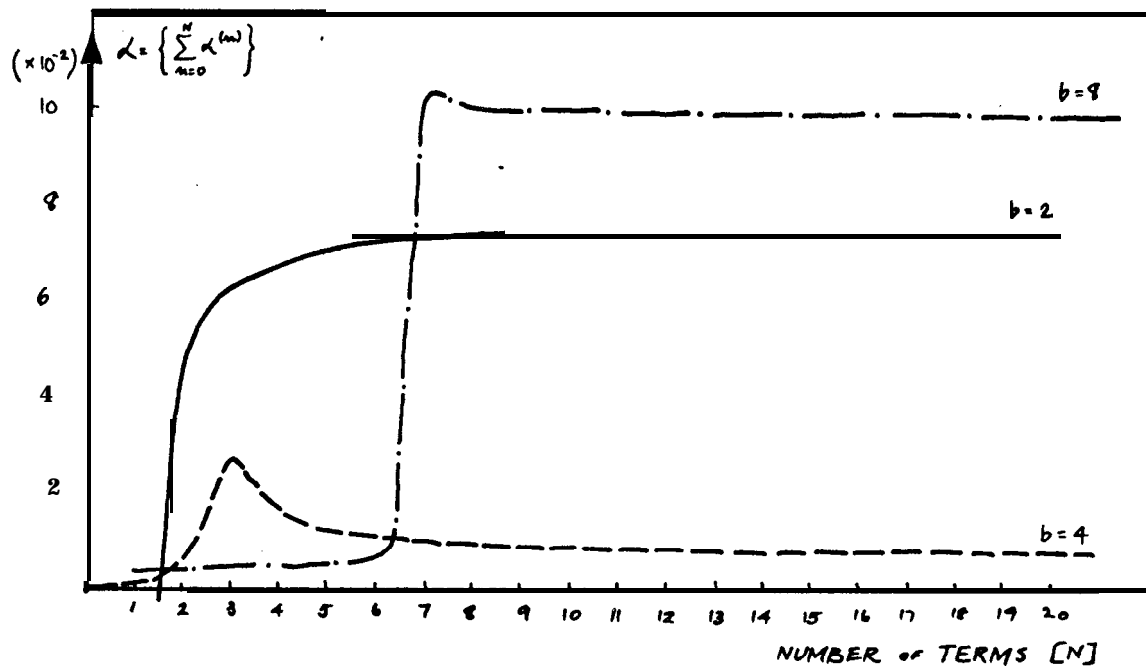
S	NUMBER OF NODAL DIAMETERS															
	0	1	2	3	4	5	6	7	8	9	10	11	13	14		
0	0.0000	0.0000	2.3236	3.5385	4.6865	5.8030	6.9002	7.9843	9.0588	10.1258	11.1870	12.2432	13.122954	14.3442	15.3900	16.43; ;
	0.50000	0.25000	0.18696	0.15578	0.13623	0.12245	0.11203	0.10378	0.09702	0.09135	0.08651	0.08230	0.07860	0.07531	0.07236	0.06970
1	0.0001j	1.0000	1.6044	2.0913	2.5213	2.9173	3.2903	3.6467	3.9905	4.3243	4.6501	4.9691	5.2825	5.5910	5.8953	6.1960
	2.9957	4.5230	5.9387	7.2832	8.5798	9.8419	11.0776	12.2928	13.4911	14.6756	15.8483	17.0110	18.1649	19.3112	20.4507	21.5841
2	0.22429	0.23267	0.22497	0.21462	0.20483	0.19613	0.18849	0.18175	0.17576	0.17039	0.16554	0.16112	0.15708	0.15335	0.14989	0.14667
	3.0045	4.5182	5.6264	6.5306	7.3152	8.0206	8.6696	9.2761	9.8492	10.3955	10.9195	11.4247	11.9139	12.3893	12.8524	13.3048
3	6.1980	7.7325	9.1849	10.5813	11.9363	13.2593	14.5566	15.8327	17.0910	18.3342	19.5641	20.7825	21.9907	23.1898	24.3807	25.5643
	0.24375	0.24242	0.23630	0.22887	0.22145	0.21449	0.20911	0.20230	0.19702	0.19220	0.18778	0.18372	0.17997	0.17649	0.17325	0.17021
4	6.3409	7.7985	9.0192	10.0808	11.0299	11.8959	12.6977	13.4489	14.1588	14.8344	15.4811	16.1030	16.7035	17.2852	17.8503	18.4005
	9.3661	10.9057	12.3813	13.8094	15.2006	16.5622	17.8992	19.2154	20.5138	21.7968	23.0661	24.3234	25.5699	26.8066	28.0345	29.2543
5	0.24729	0.24585	0.24158	0.23619	0.23050	0.22489	0.21953	0.21450	0.20980	0.20542	0.20134	0.19755	0.19401	0.19069	0.18758	0.18466
	9.5371	11.0105	12.3002	13.4554	14.5008	15.4807	16.3885	17.2432	18.0535	18.8261	19.5663	20.2783	20.9656	21.6310	22.2769	22.9052
6	12.5216	14.0659	15.5571	17.0070	18.4237	19.8128	21.1785	22.5243	23.8526	25.1655	26.4648	27.7519	29.0279	30.2938	31.5507	32.7991
	0.24849	0.24739	0.24434	0.24032	0.23589	0.23136	0.22689	0.22256	0.21843	0.21450	0.21079	0.20728	0.20397	0.20084	0.19788	0.19507
7	12.7046	14.1935	15.5302	16.7496	17.8755	18.9255	19.9126	20.8465	21.7351	22.5846	23.3999	24.1852	24.9438	25.67%	26.3919	27.0558
	15.6718	17.2196	18.7222	20.1861	21.6237	23.0337	24.4217	25.7904	27.1422	28.4789	29.8021	31.1131	32.4130	33.7028	34.9833	36.2552
8	0.24904	0.24822	0.24595	0.242%	0.23935	0.23564	0.23139	0.22818	0.22457	0.22108	0.21772	0.21451	0.21144	0.20852	0.20573	0.20306
	15.8615	17.3622	18.7328	19.9901	21.1799	22.2892	23.3381	24.3350	25.2869	26.1992	27.0767	27.9232	28.7419	29.5356	30.3066	31.0570
9	18.8133	20.3699	21.8809	23.3590	24.8094	26.2359	27.6415	29.0288	30.3997	31.7559	33.0989	34.4298	35.7497	37.0594	38.3598	39.6515
	0.24934	0.24870	0.24696	0.24452	0.24168	0.23862	0.23545	0.23225	0.22909	0.22599	0.22297	0.22005	0.21723	0.21452	0.21191	0.20940
10	19.0132	20.5229	21.9189	23.2211	24.4446	25.6011	26.6997	27.7481	28.7522	29.7171	30.6470	31.5456	32.4158	33.2604	34.0815	34.8812
	21.9651	23.5179	25.0355	26.5234	27.9856	29.4254	30.8456	32.2481	33.6350	35.0075	36.3671	37.7149	39.0517	40.3785	41.6960	43.0049
11	0.24952	0.24901	0.24763	0.24567	0.24333	0.24076	0.23805	0.23529	0.23251	0.22976	0.22705	0.22439	0.22181	0.21930	0.21687	0.21452
	22.1619	23.6788	25.0945	26.4250	27.6827	28.8775	30.0172	31.1084	32.1565	33.1660	34.1409	35.0844	35.9994	36.8884	37.7535	38.5967

- 1 dimensionless natural frequency b_{ns}
- 2 dimensionless inertial coefficient a_n
- 3 dimensionless slope at the rim $a[\partial/\partial r f(r)]_{r=a}$

FIG 3.2

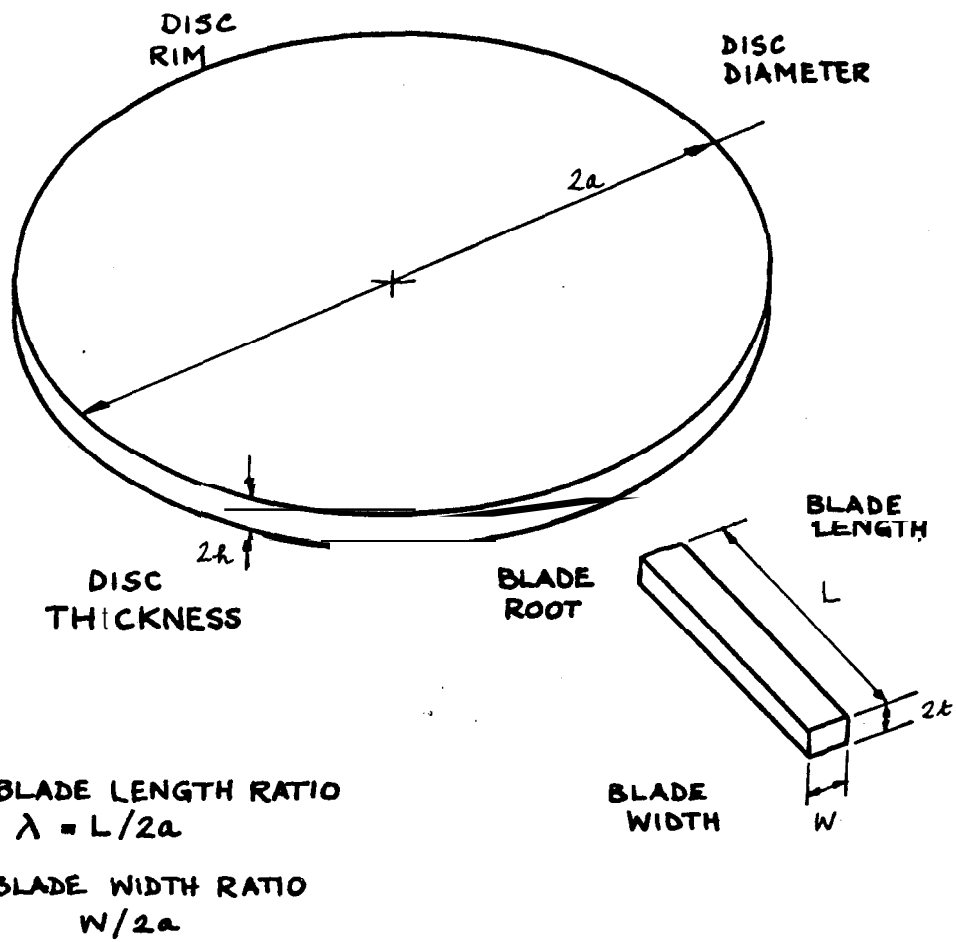


ACCURACY OF TRUNCATED SERIES FORM RECEPTANCES FOR A FREE DISC



POINT RECEPTANCES FOR A FREE DISC

FIG 3.4



TERMS USED IN THE ANALYSIS

FIG. 4.1

$$\begin{array}{cccccccc}
 \left\{ \alpha_{1,1} \right\} & \alpha_{1,2} & \alpha_{1,3} & \dots & \alpha_{1,N} & \left\{ \alpha'_{1,1} \right\} & \alpha'_{1,2} & \alpha'_{1,3} & \dots & \alpha'_{1,N} \\
 \vdots & \vdots & & & \vdots & \vdots & \vdots & & & \vdots \\
 \alpha_{i,1} & \alpha_{i,2} & \dots & \left\{ \alpha_{i,i} \right\} & \dots & \alpha_{i,N} & \alpha'_{i,1} & \alpha'_{i,2} & \dots & \left\{ \alpha'_{i,i} \right\} & \dots & \alpha'_{i,N} \\
 \vdots & \vdots & & & \vdots & \vdots & \vdots & & & \vdots & & \vdots \\
 \alpha_{N,1} & \alpha_{N,2} & \alpha_{N,3} & \dots & \left\{ \alpha_{N,N} \right\} & \alpha'_{N,1} & \alpha'_{N,2} & \alpha'_{N,3} & \dots & \left\{ \alpha'_{N,N} \right\} \\
 \left\{ \alpha'_{1,1} \right\} & \alpha'_{1,2} & \alpha'_{1,3} & \dots & \alpha'_{1,N} & \left\{ \alpha''_{1,1} \right\} & \alpha''_{1,2} & \alpha''_{1,3} & \dots & \alpha''_{1,N} \\
 \vdots & \vdots & & & \vdots & \vdots & \vdots & & & \vdots \\
 \alpha'_{i,1} & \alpha'_{i,2} & \dots & \left\{ \alpha'_{i,i} \right\} & \dots & \alpha'_{i,N} & \alpha''_{i,1} & \alpha''_{i,2} & \dots & \left\{ \alpha''_{i,i} \right\} & \dots & \alpha''_{i,N} \\
 \vdots & \vdots & & & \vdots & \vdots & \vdots & & & \vdots & & \vdots \\
 \alpha'_{N,1} & \alpha'_{N,2} & \alpha'_{N,3} & \dots & \left\{ \alpha'_{N,N} \right\} & \alpha''_{N,1} & \alpha''_{N,2} & \alpha''_{N,3} & \dots & \left\{ \alpha''_{N,N} \right\}
 \end{array}$$

GENERAL RECEPTANCE DETERMINANT FOR
AN N BLADED DISC ASSUMING TWO
DEGREES OF COUPLING

FIG 4.2

a_0	a_1	a_2	a_2	a_1	b_0	b_1	b_2	b_2	b_1
a_1	a_0	a_1	a_2	a_2	b_1	b_0	b_1	b_2	b_2
a_2	a_1	a_0	a_1	a_2	b_2	b_1	b_0	b_1	b_2
a_2	a_2	a_1	a_0	a_1	b_2	b_2	b_1	b_0	b_1
a_1	a_2	a_2	a_1	a_0	b_1	b_2	b_2	b_1	b_0
b_0	b_1	b_2	b_2	b_1	c_0	c_1	c_2	c_2	c_1
b_1	b_0	b_1	b_2	b_{21}	c_1	c_0	c_1	c_2	c_2
b_2	b_1	b_0	b_1	b_{21}	c_2	c_1	c_0	c_1	c_2
b_2	b_2	b_1	b_0	b_1	c_2	c_2	c_1	c_0	c_1
b_1	b_2	b_2	b_1	b_0	c_1	c_2	c_2	c_1	c_0

where

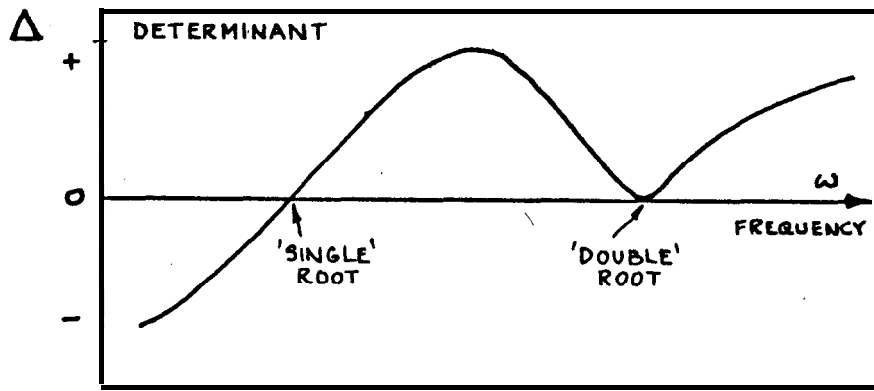
$$a_0 = \alpha_{0,0} + \Omega ; \quad b_0 = \alpha'_{0,0} + \Omega' \quad c_0 = \alpha''_{0,0} + \Omega''$$

$$a_1 = \alpha_{0,2\pi/5} ; \text{ etc.}$$

$$a_2 = \alpha_{0,4\pi/5} ; \text{ etc.}$$

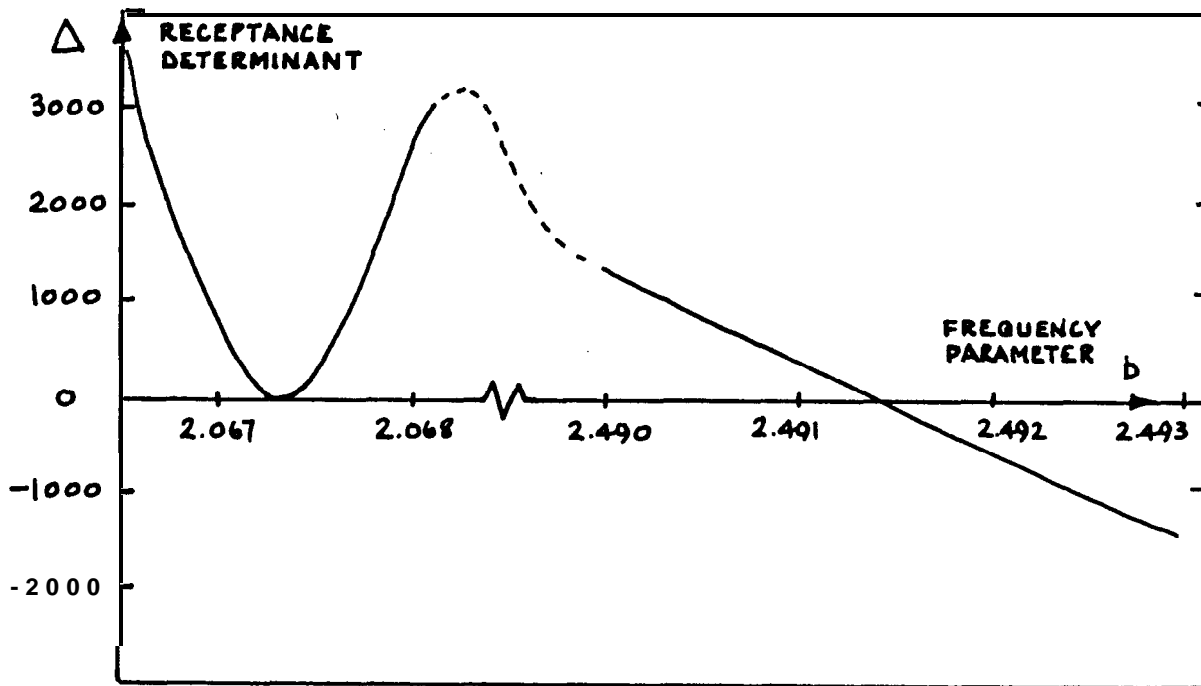
RECEPTANCE DETERMINANT FOR A 5 BLADED DISC

FIG 4.3



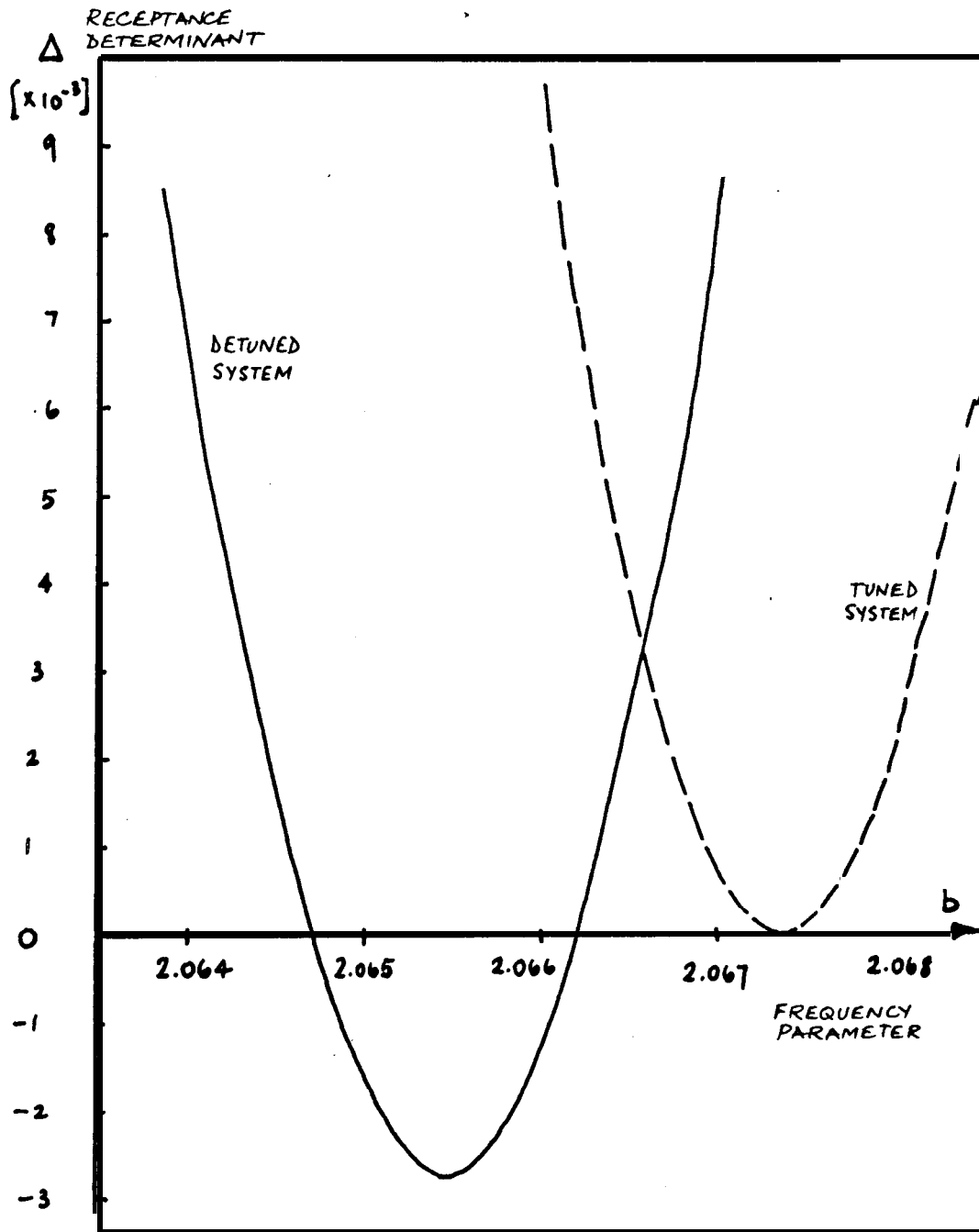
SECTION OF THE PREDICTED DETERMINANT~
FREQUENCY RELATIONSHIP

FIG 4.4



SECTION OF THE DETERMINANT- FREQUENCY PLOT
FOR A TUNED FIVE BLADED DISC

FIG 4.5



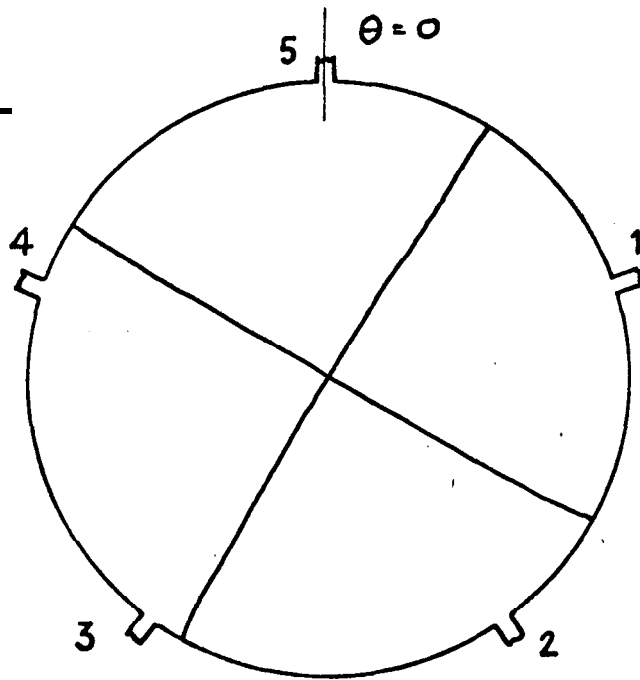
SECTION OF THE DETERMINANT ~ FREQUENCY PLOT
FOR A DETUNED FIVE BLADED DISC

FIG.4.7

lower frequency mode

i	F_i	C_i
1	-.978	-.313
2	.719	.227
3	-.200	-.064
4	-.393	-.124
5	.853	.273

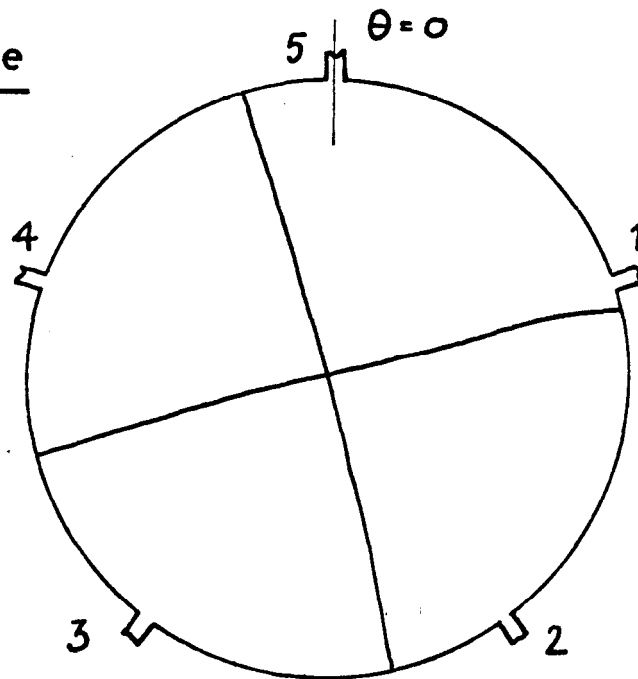
$\cong \cos 2(\theta+15)$



higher frequency mode

i	F_i	C_i
1	.111	.036
2	-.664	-.210
3	.978	.312
4	-.895	-.282
5	.503	.161

$\cong \sin 2(\theta+15)$

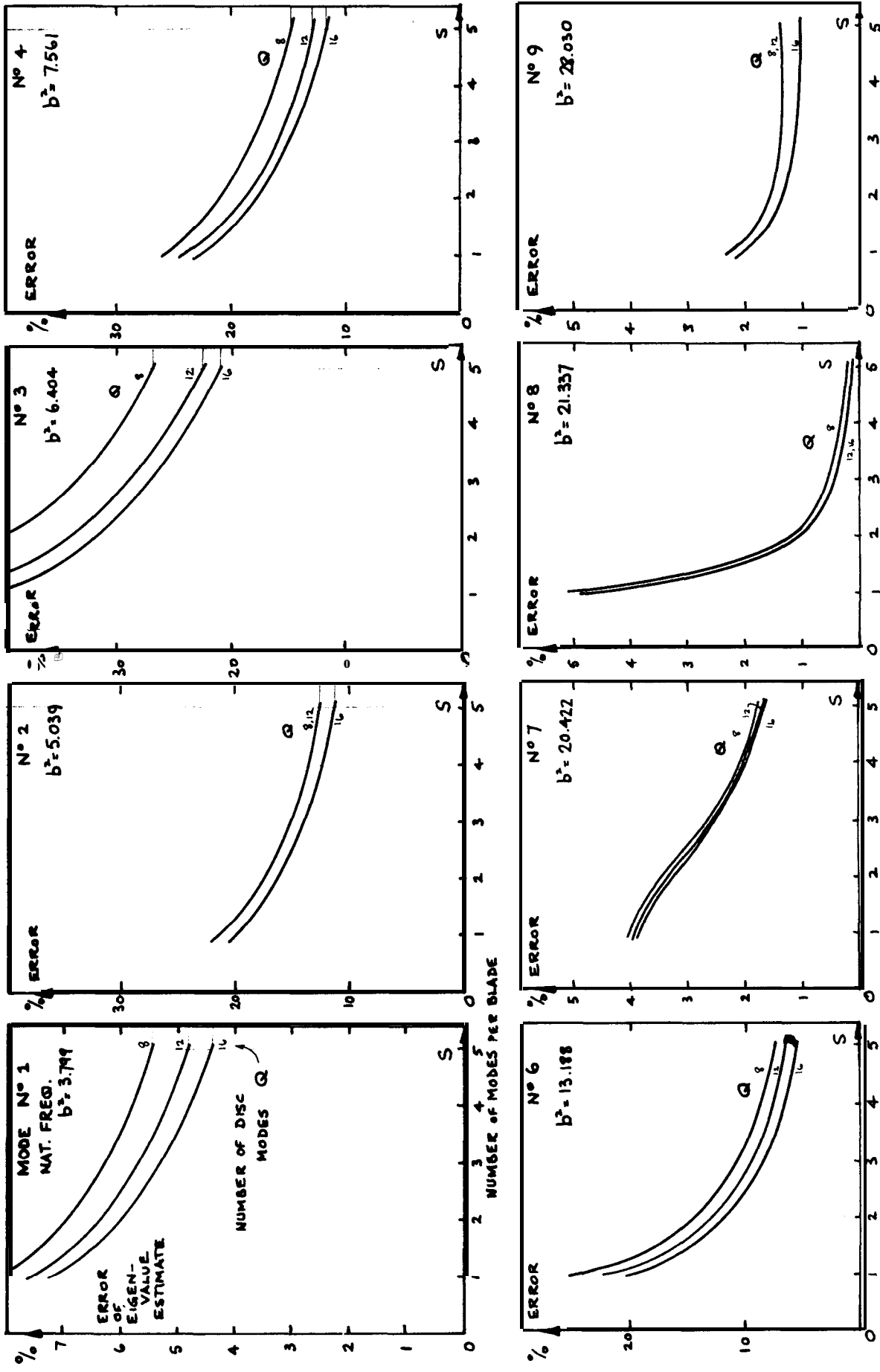


MODAL SHAPES FOR
DETUNED 2/0 MODES

FIG 4.0

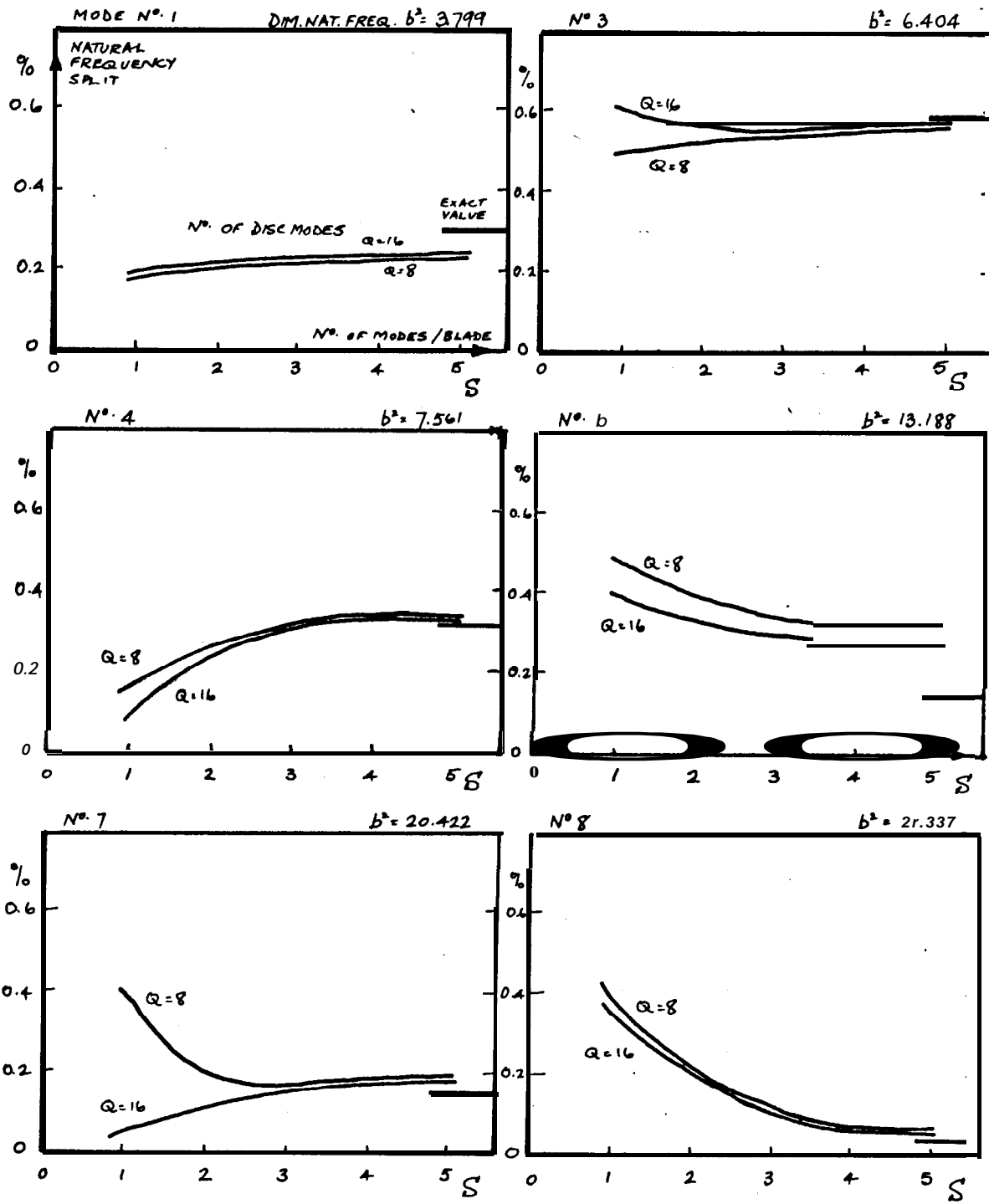
NODAL PATTERNS FOR
DETUNED 2/0 MODES

FIG 4.9



ACCURACY OF EIGENVALUE ESTIMATES OF NATURAL FREQUENCY
 FIVE BLADED DISC $\lambda = 0.3333$

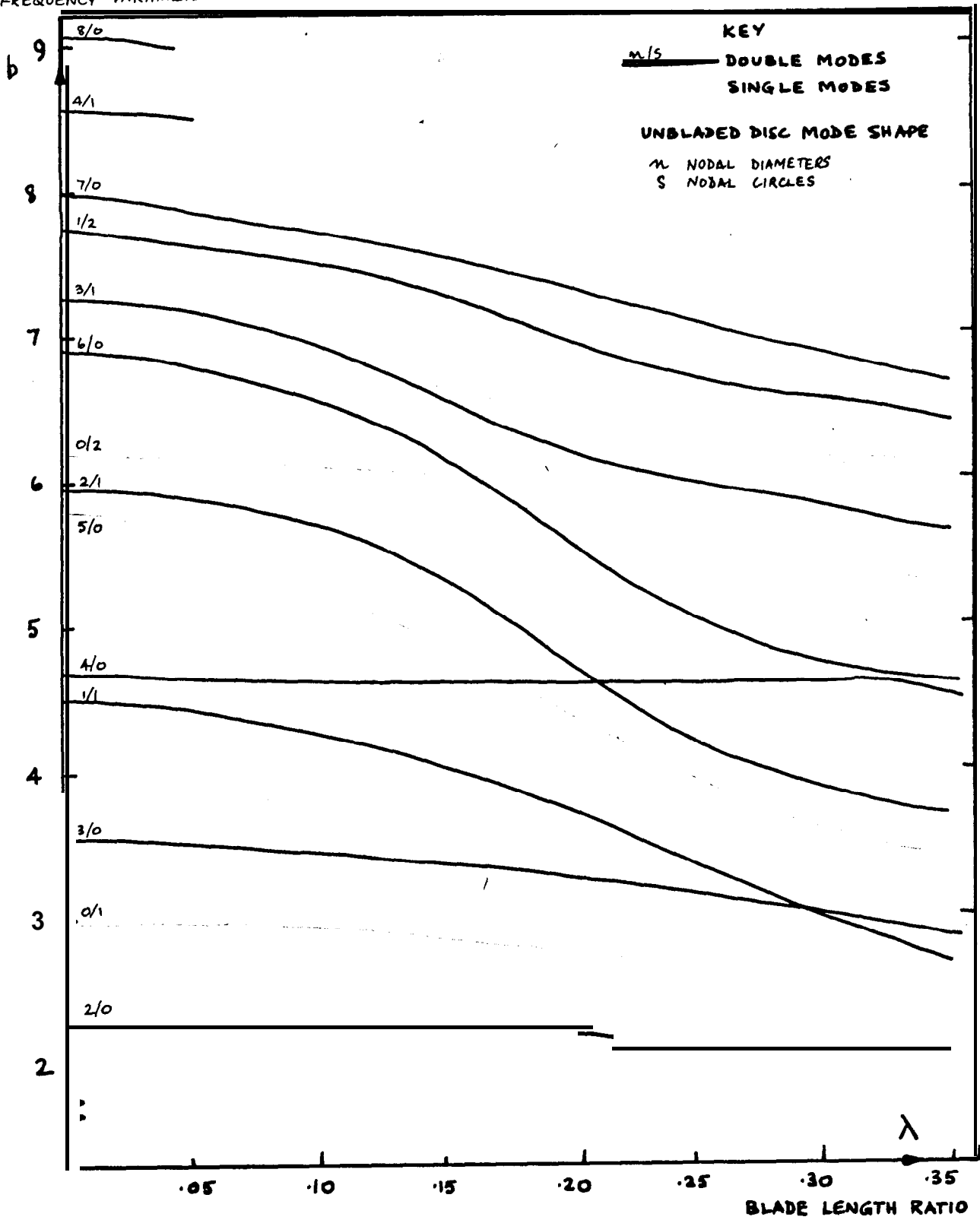
FIG 4.10



TYPICAL GENVALUE ESTIMATES OF NATURAL FREQUENCY SPLITS 5 BLADED DISC $\lambda = 0.3333$

FIG 4.11

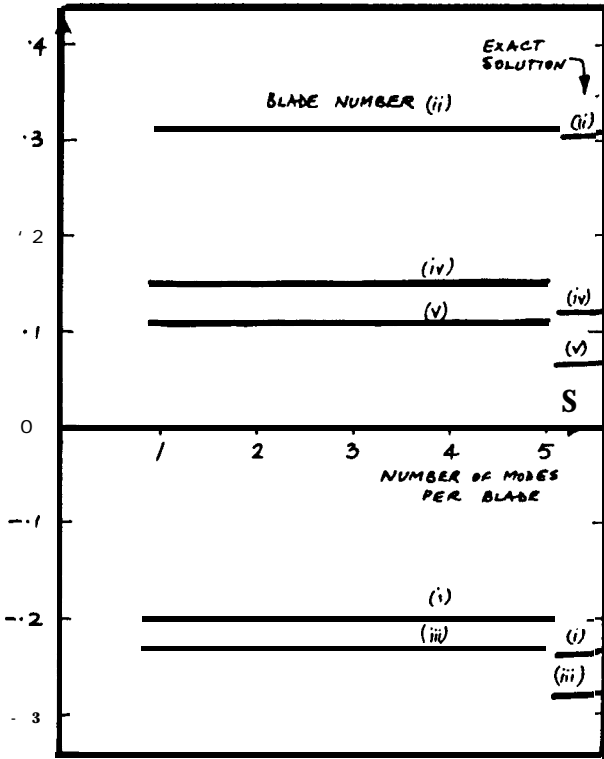
FREQUENCY PARAMETER



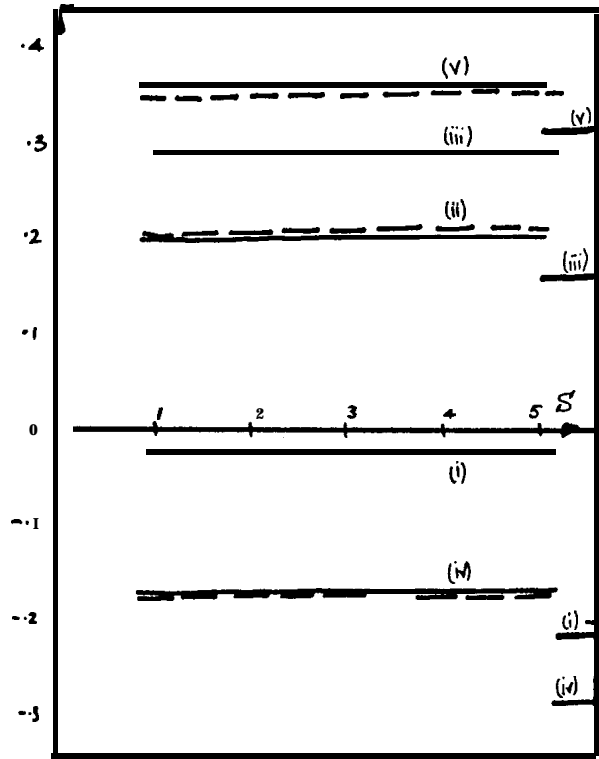
VARIATION OF THE EIGENVALUES FOR A FIVE BLADED DISC WITH THE BLADE LENGTH

FIG. 4.12

RELATIVE BLADE LOAD



DOUBLE MODE (1)
(LOWER NATURAL FREQUENCY)

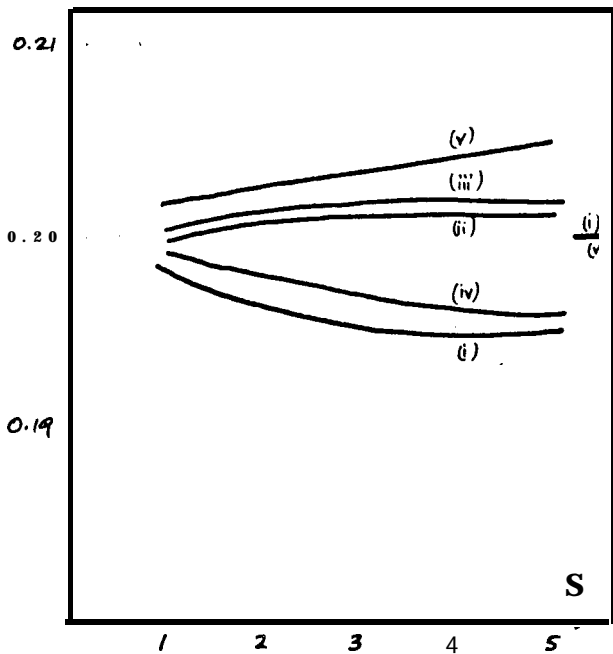


DOUBLE MODE (2)
(HIGHER NATURAL FREQUENCY)

KEY

- Q (NUMBER OF DISC MODES) = 8
- - - Q = 16

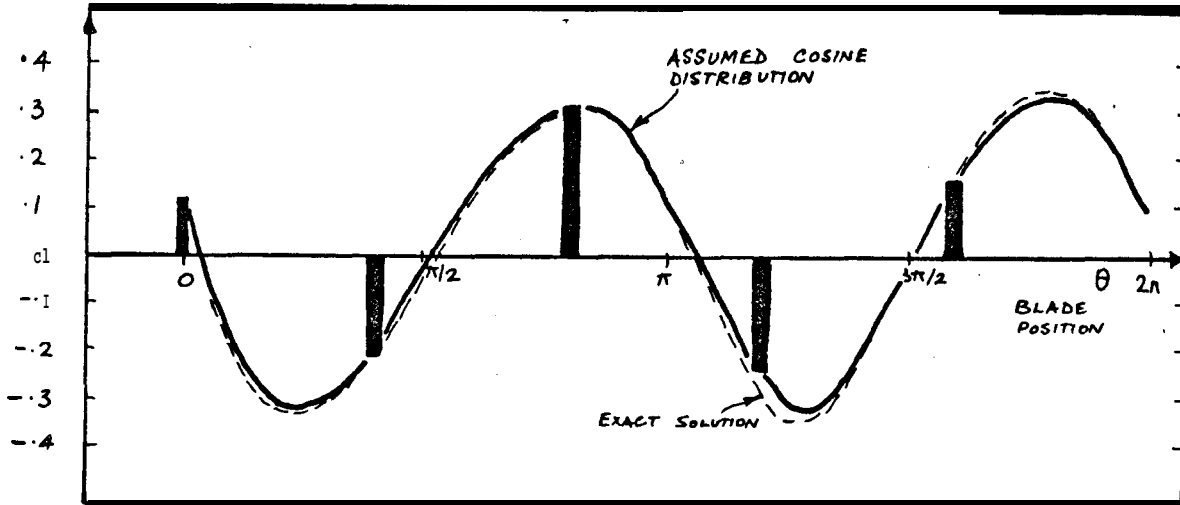
SINGLE MODE



VARIATION OF EIGENVECTOR
ESTIMATES OF MODAL
SHAPE WITH Q AND S

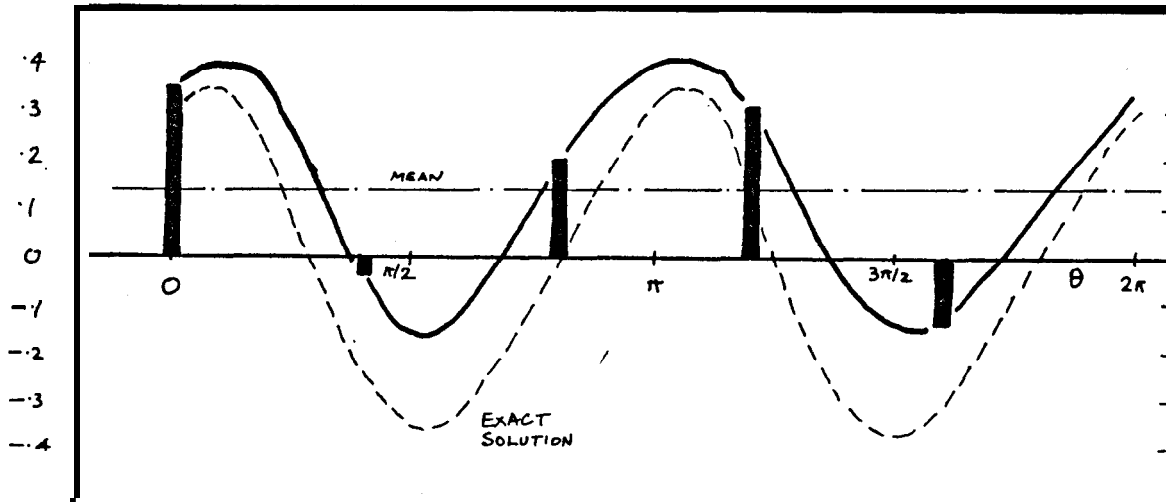
FIG. 4.13

RELATIVE
BLADE LOAD



LOWER FREQUENCY MODE

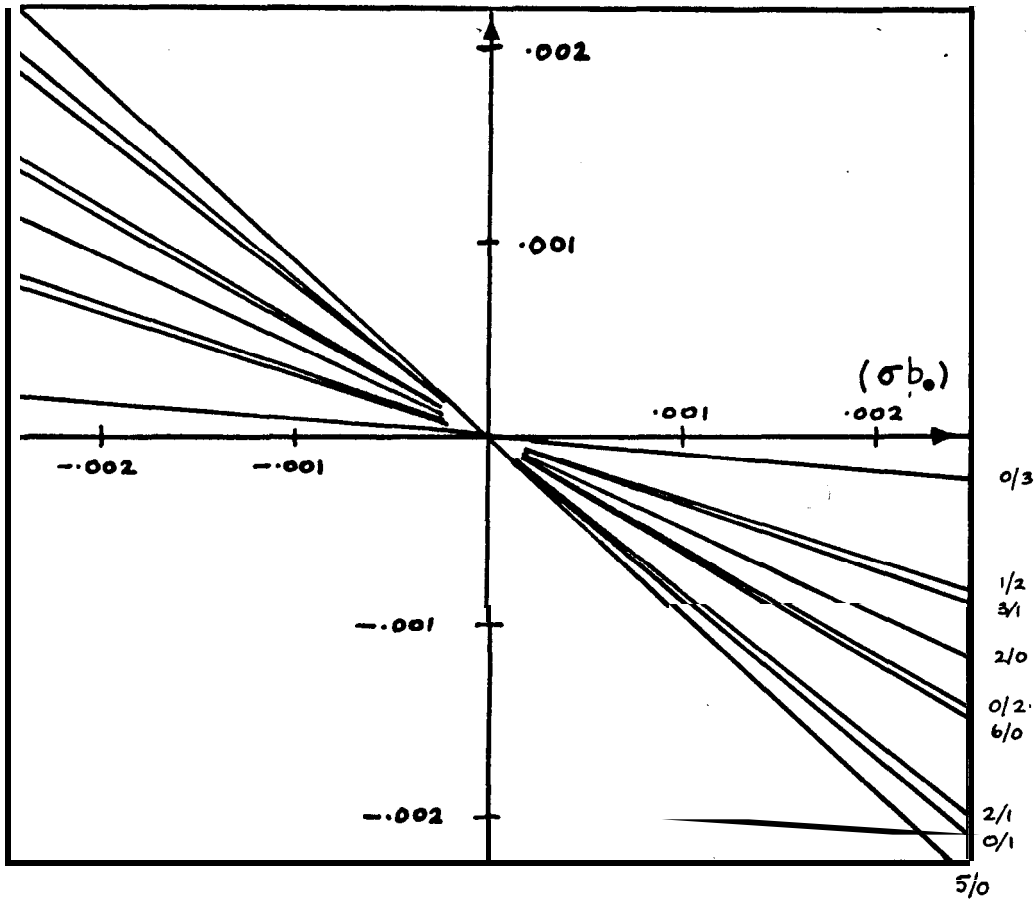
HIGHER FREQUENCY MODE



EIGENVECTOR ESTIMATES OF MODAL SHAPE FOR
A DOUBLE MODE

FIG. 4.14

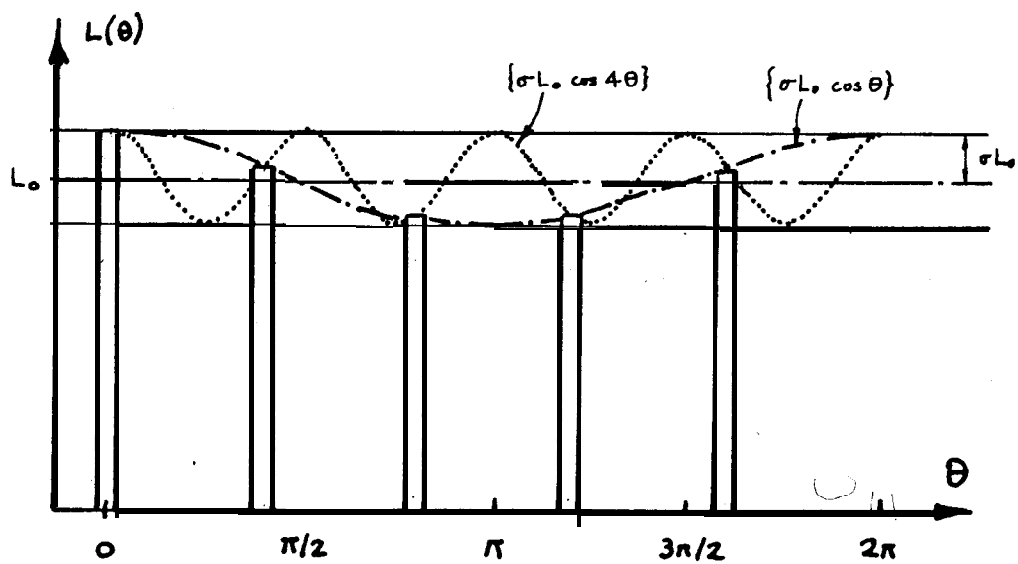
VARIATION OF THE DETUNED NATURAL
FREQUENCY FROM THE TUNED VALUE



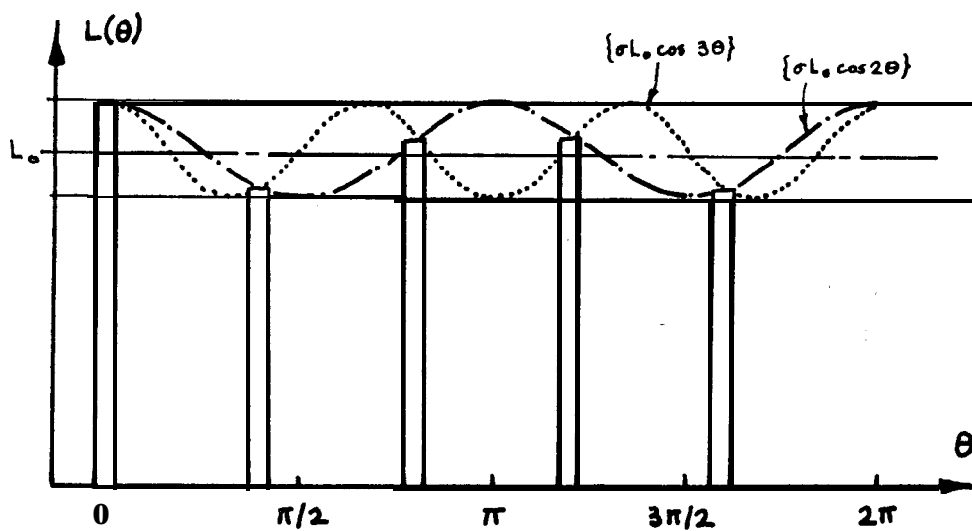
UNBLADED DISC MODES BY WHICH THE
BLADED DISC MODES ARE IDENTIFIED.

VARIATION OF NATURAL FREQUENCIES
WITH CONSTANT DETUNING (σb_0)

FIG 5.1



(a) $\cos 1\theta$ detuning function



(b) $\cos 2\theta$ detuning function

BLADE LENGTHS FOR COSINE DETUNING

FIG 5.2

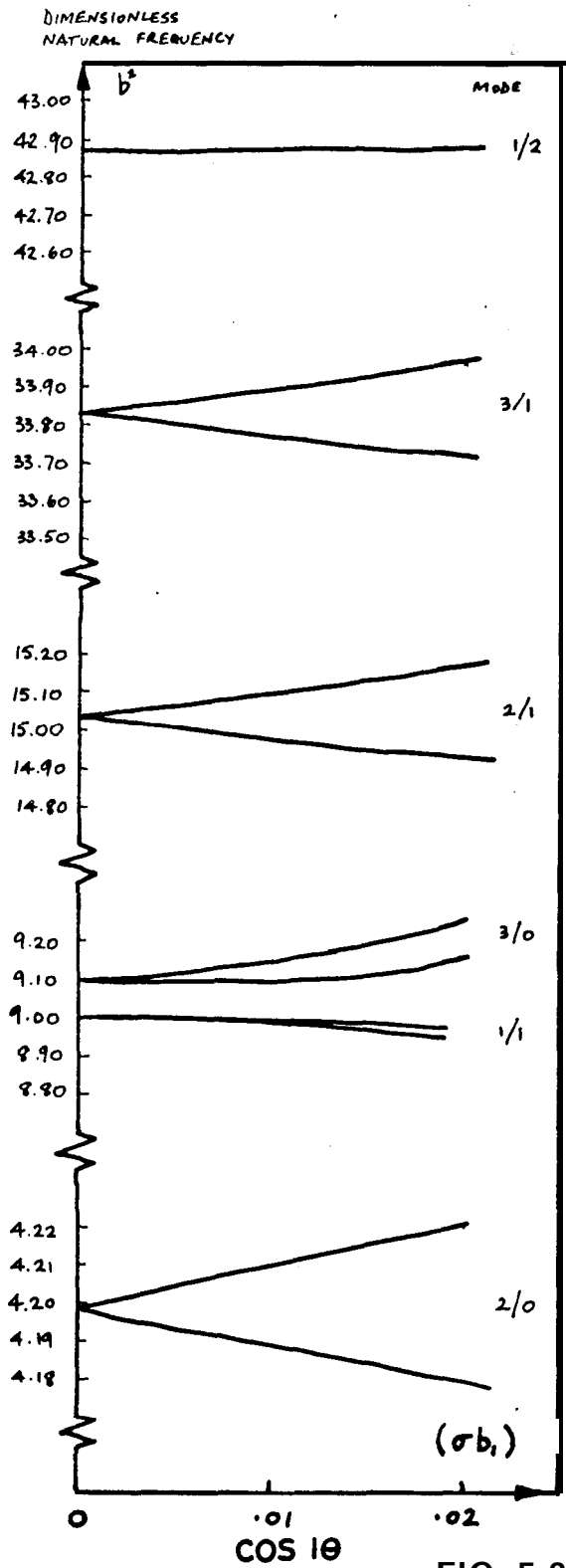


FIG 5.3

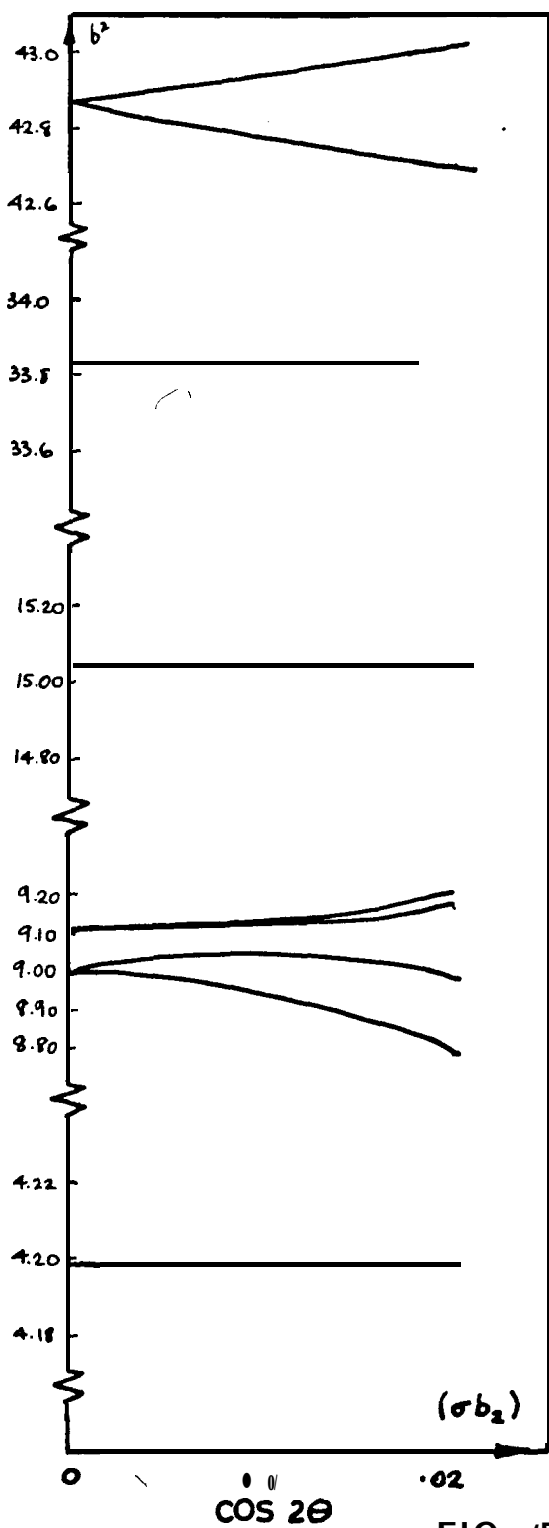


FIG 5.4

VARIATION OF NATURAL FREQUENCIES WITH COSINE DETUNING

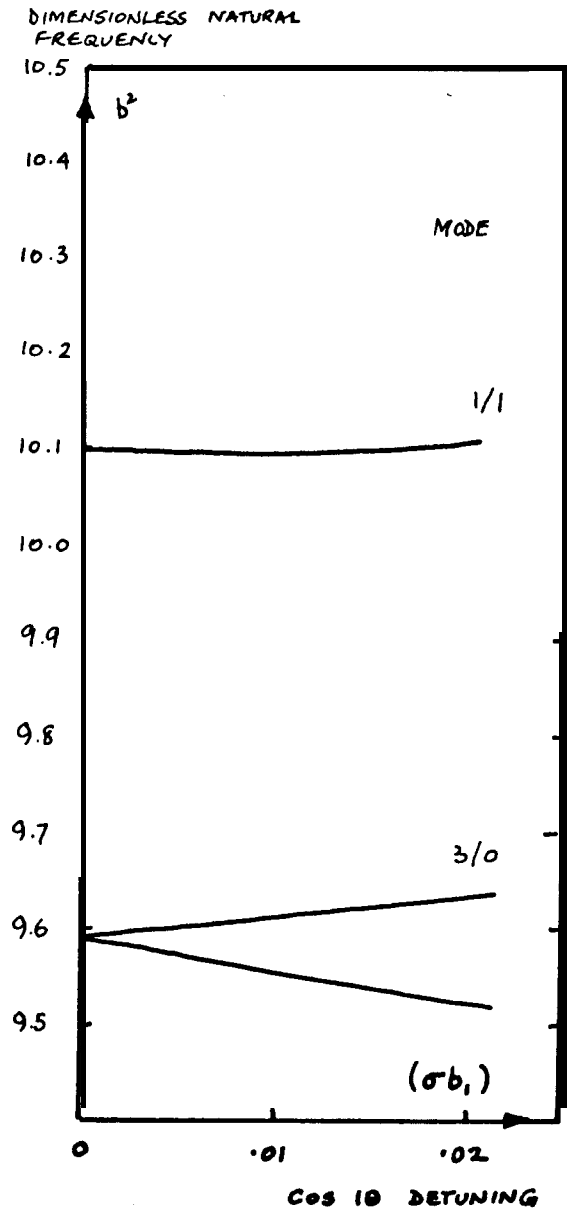


FIG 5.3a

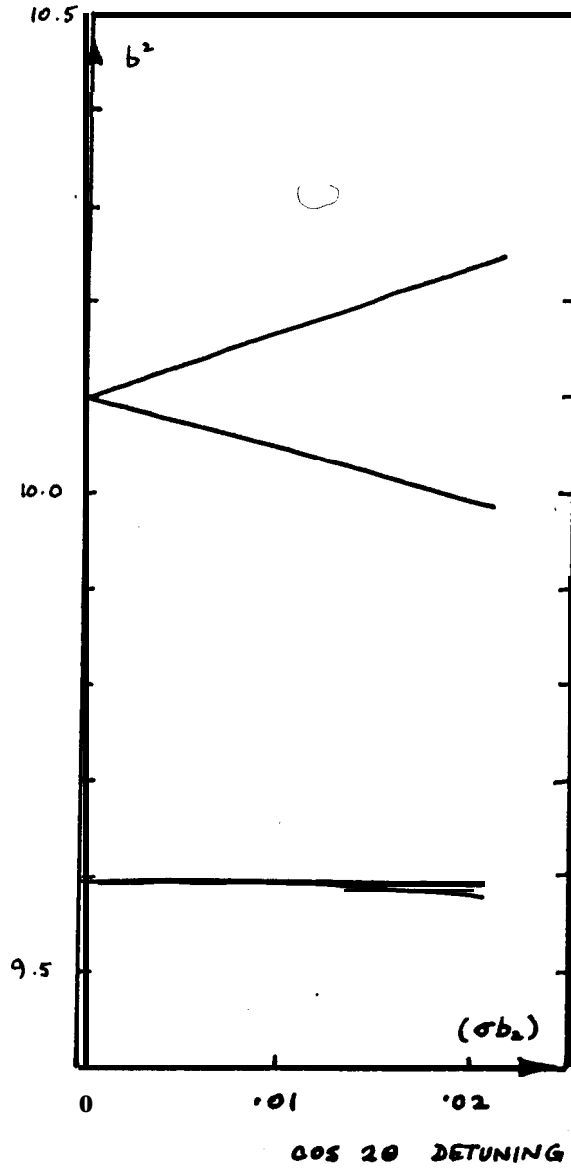
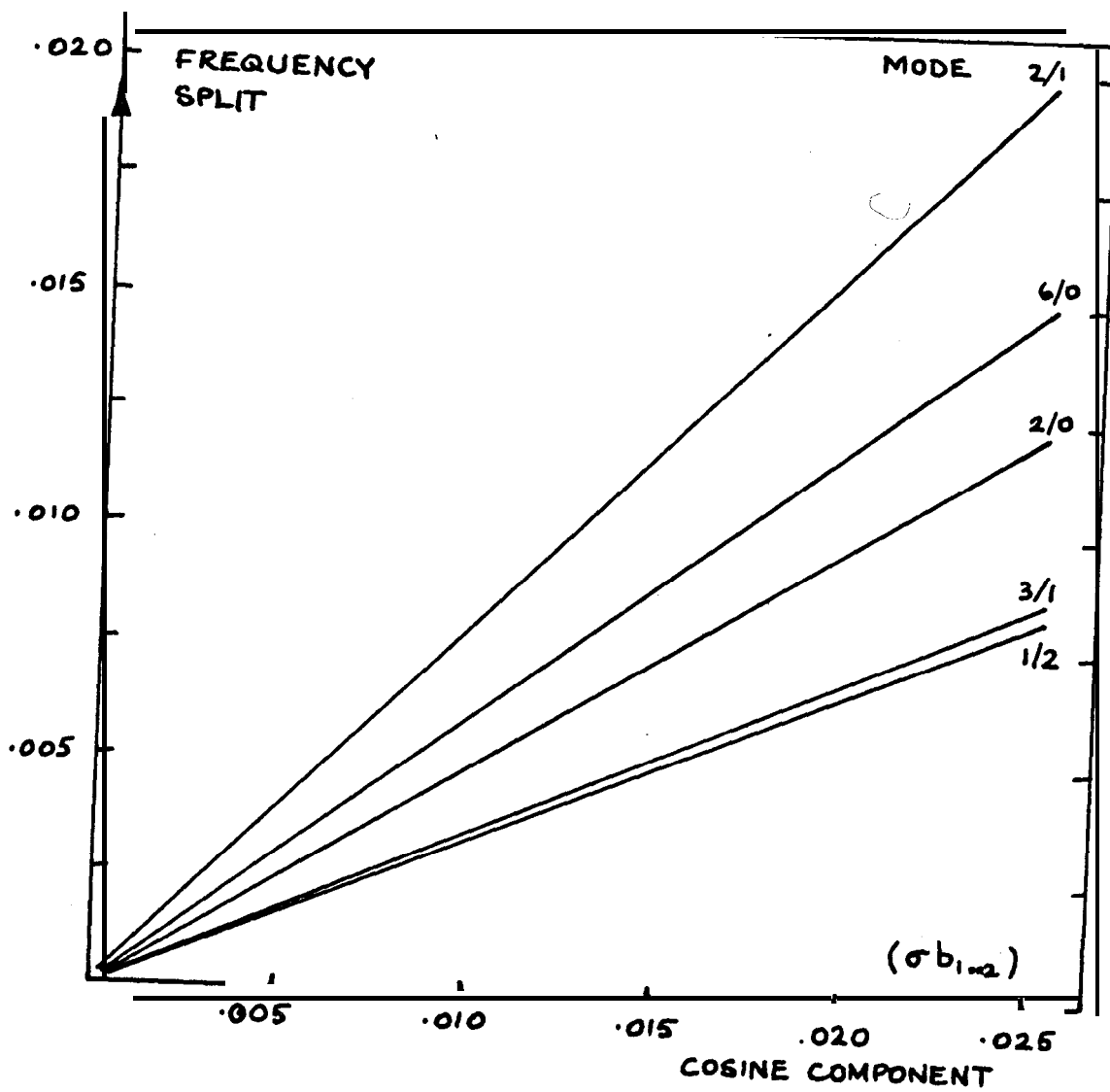


FIG 5.4a

FREQUENCY SPLITTING IN THE
1/1 AND 3/0 MODES WITH $\lambda=0.3$



VARIATION OF FREQUENCY SPLIT WITH
COSINE COMPONENT

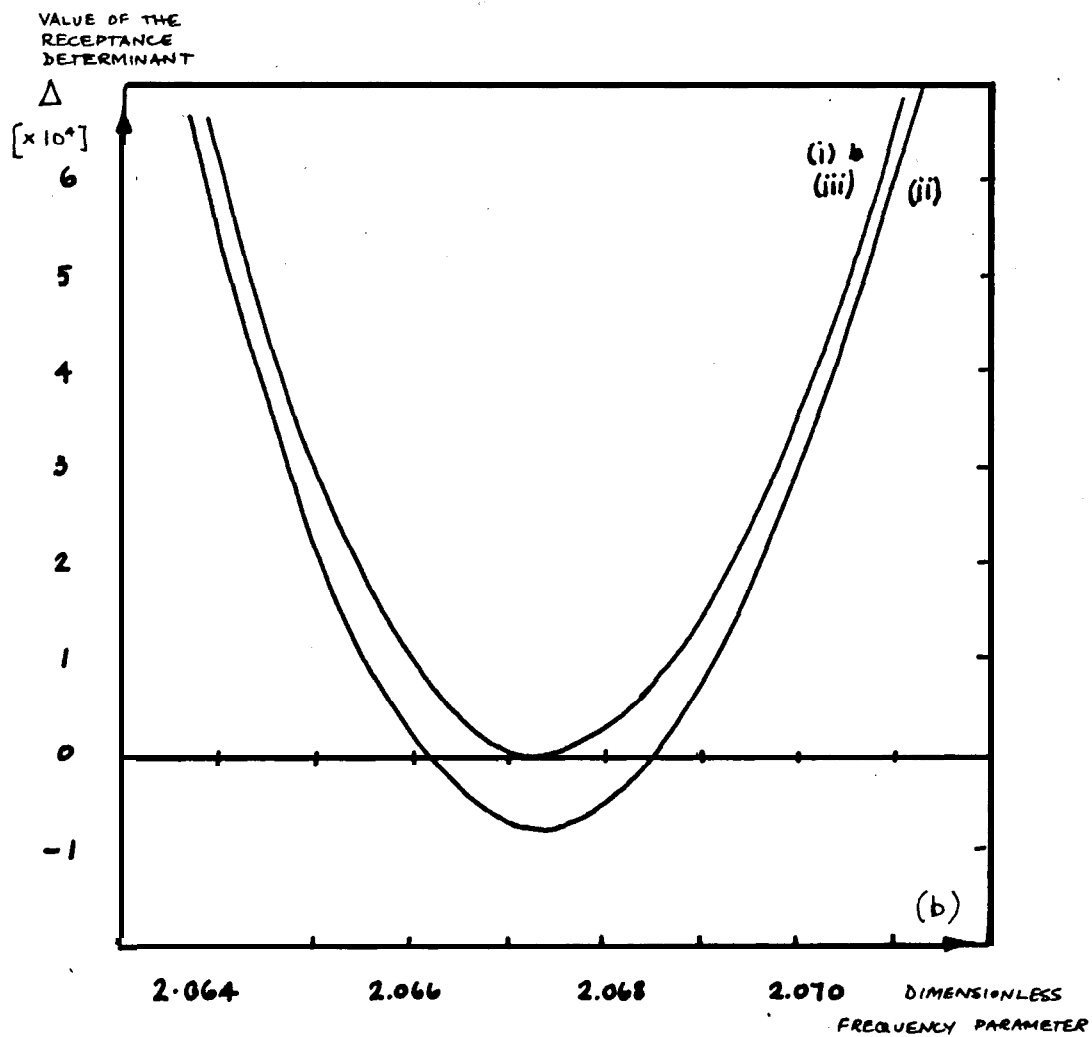
FIG. 5

Random Numbers k_i	Cosine Components	Predicted Split (percent) Mode No.				
		1	6	8	11	13
1 $-.0152$	$b_0 = .1696$ $b_1 = .3150$ $b_2 = .4799$					
2 $+.4768$						
3 $+.0570$.151	.252	.288	.110	.158
4 $+.7488$						
5 $-.4194$						
Split computed for this system		.151	.250	.286	.109	.160

RANDOM **DETUNING, ANALYSIS** OF RANDOMLY CHOSEN BLADES

AND PREDICTED SPLIT

FIG 5.6



key

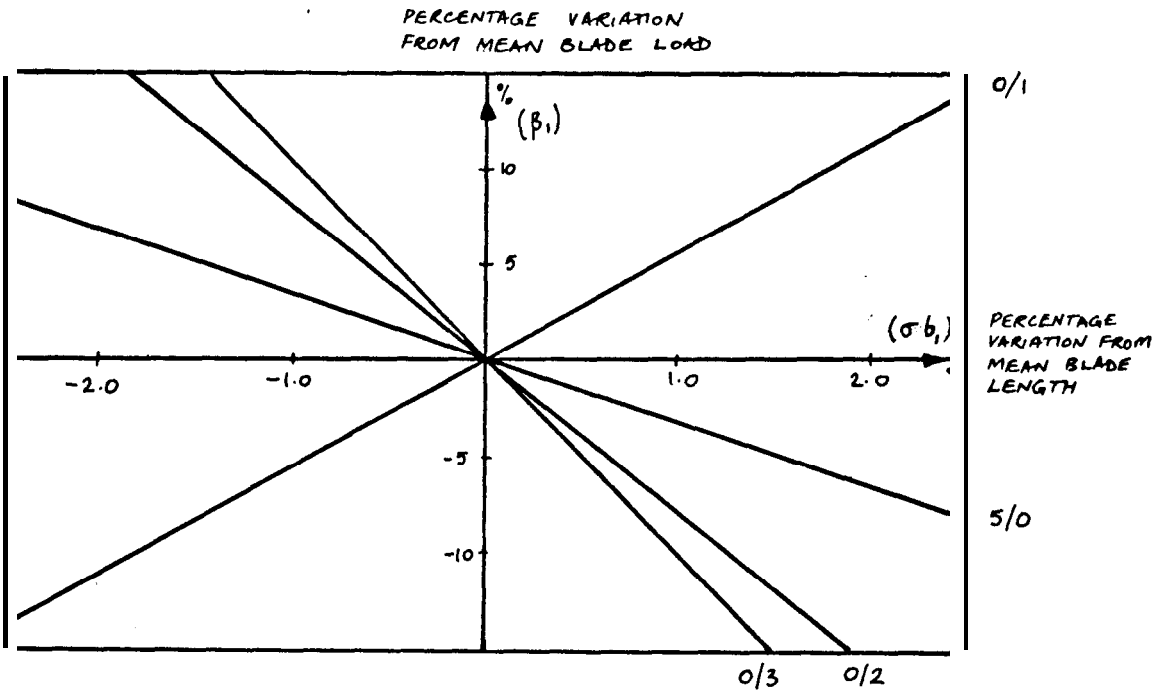
(i) tuned case

(ii) detuned: $\sigma = 0.01$; $f(\theta) = \cos \theta$

(iii) detuned: $\sigma = 0.01$; $f(\theta) = \cos 2\theta$

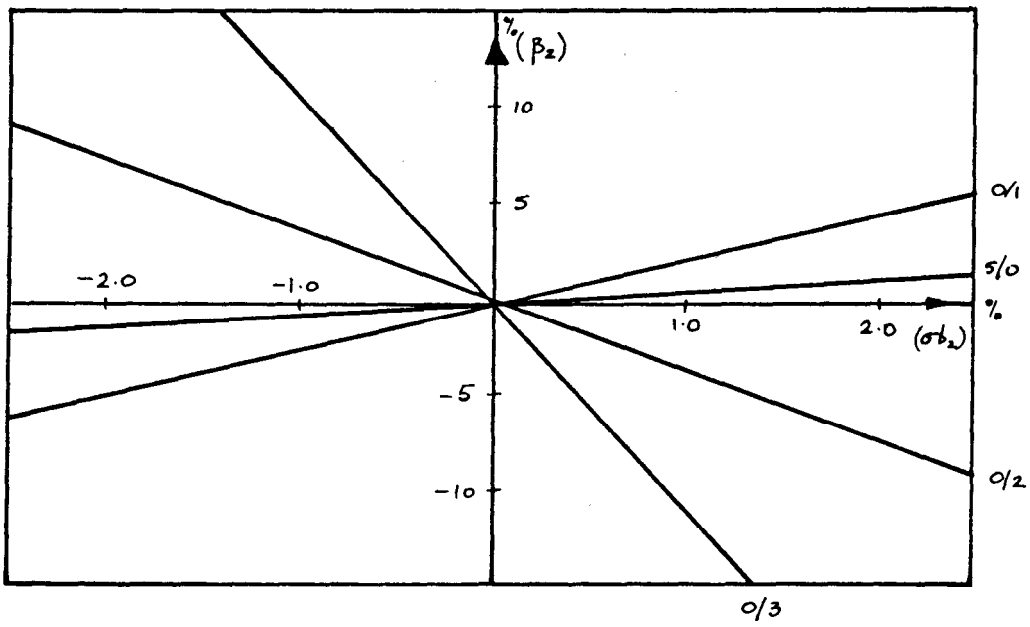
RECEPTANCE DETERMINANT VALUES
FOR DETUNED SYSTEMS: 2/0 MODE

FIG 5.7



COS 10 DETUNING

FIG 6.1



COS 20 DETUNING

FIG 6.2

VARIATION OF SINGLE MODE SHAPES WITH
COSINE DETUNING

σb_1	ϕ	σb_2	ψ	β_0	β_1	γ	β_2	δ	
DETUNING FUNCTION $f(\theta)$				$F(\theta)$ MODAL SHAPE FUNCTIONS					
.0001	$\pi/3$	0	-	0	0	-	.311	$\pi/12$	(i)
				0	0	-	.316	$-\pi/6$	(ii)
.001	$\pi/3$	0	-	0	0	-	.311	$\pi/12$	
				0	0	-	.316	$-\pi/6$	
.005	$\pi/3$	0	-	0	.002	-	.312	$\pi/12$	
				0	.002	-	.315	$-\pi/6$	
.01	$\pi/3$	0	-	0	.005	-	.312	$\pi/12$	
				0	.005	-	.314	$-\pi/6$	
.025	$\pi/3$	0	-	0	.012	-	.315	$\pi/12$	
				0	.012	-	.312	$-\pi/6$	

2/0 MODES

(i) lower frequency mode
(ii) higher frequency mode

FIG 6.3

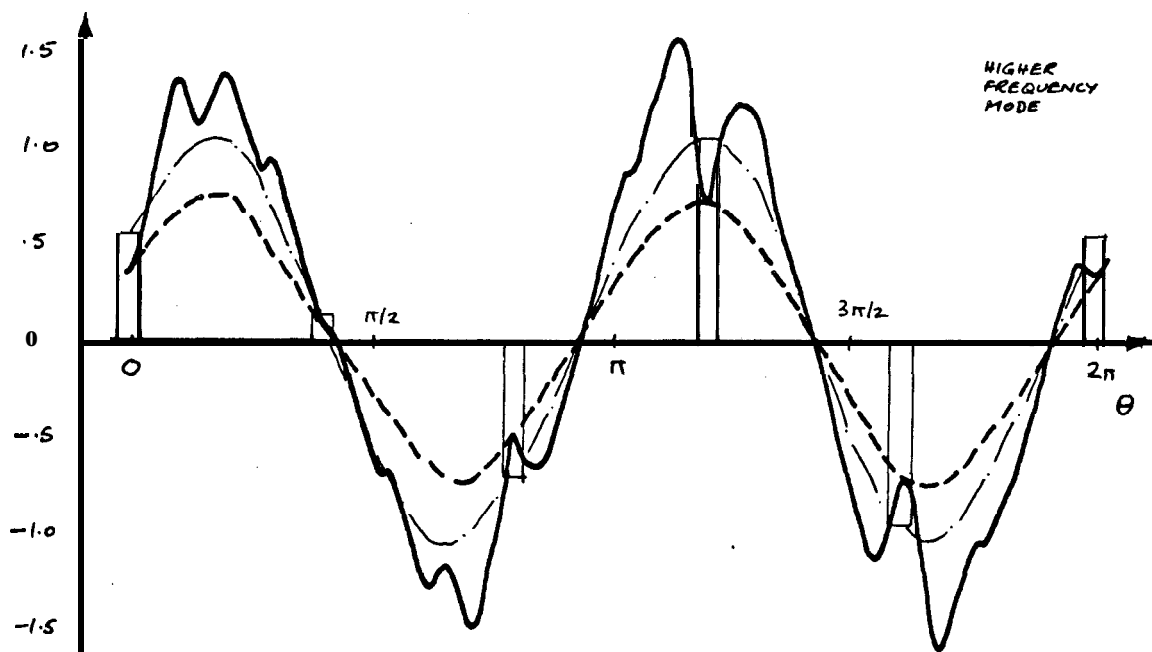
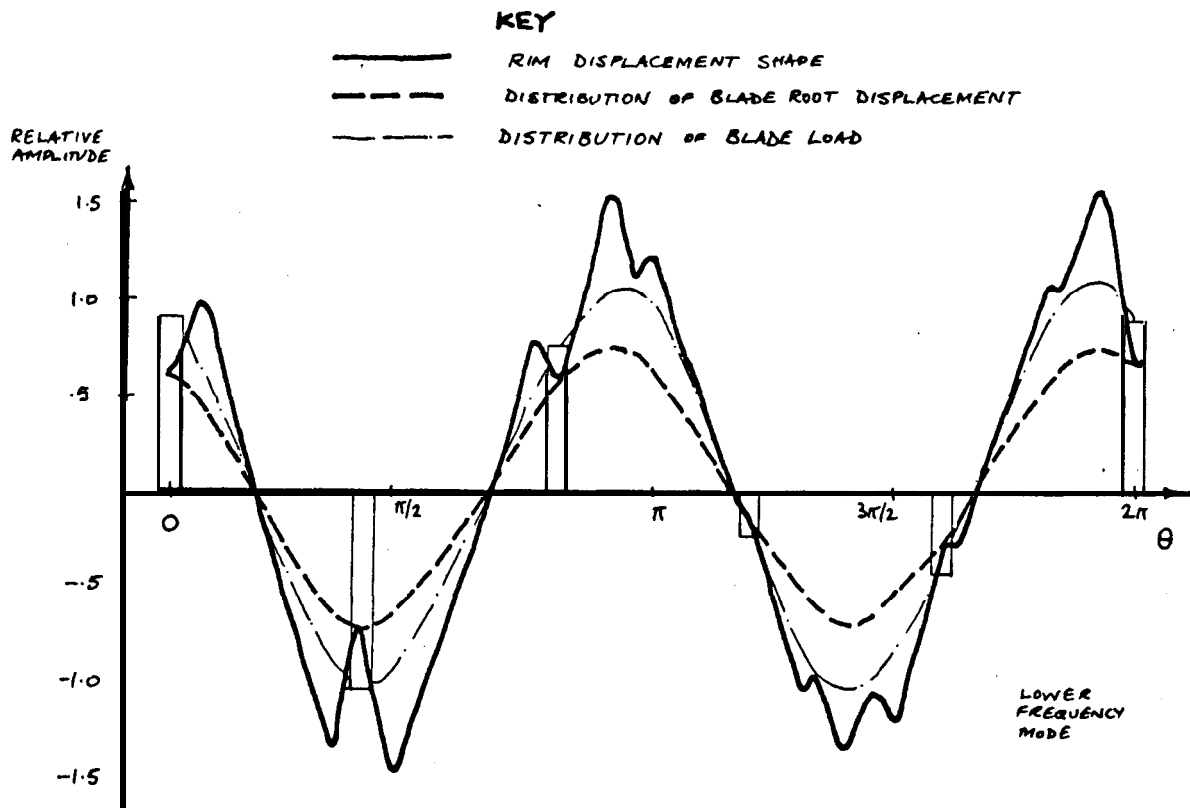
σb_1	ϕ	σb_2	ψ	β_0	β_1	γ	β_2	δ	
0	-	.0001	$\pi/6$	0	.311	$\pi/6$	0	-	(i)
				0	.316	$-\pi/3$	0	-	(ii)
0	-	.001	$\pi/6$	0	.311	$\pi/6$	0		
				0	.316	$-\pi/3$	0		
0	-	.005	$\pi/4$	0	.317	$\pi/4$.002	-	
				0	.311	$-\pi/4$.002	-	
0	-	.01	$\pi/6$	0	.309	$\pi/6$.005	-	
				0	.317	$-\pi/3$.005	-	

6/0 MODES

FIG 6.4

BLADE LOAD DISTRIBUTIONS FOR DETUNED WUBLE MODES

FIGS 6.3&6.4

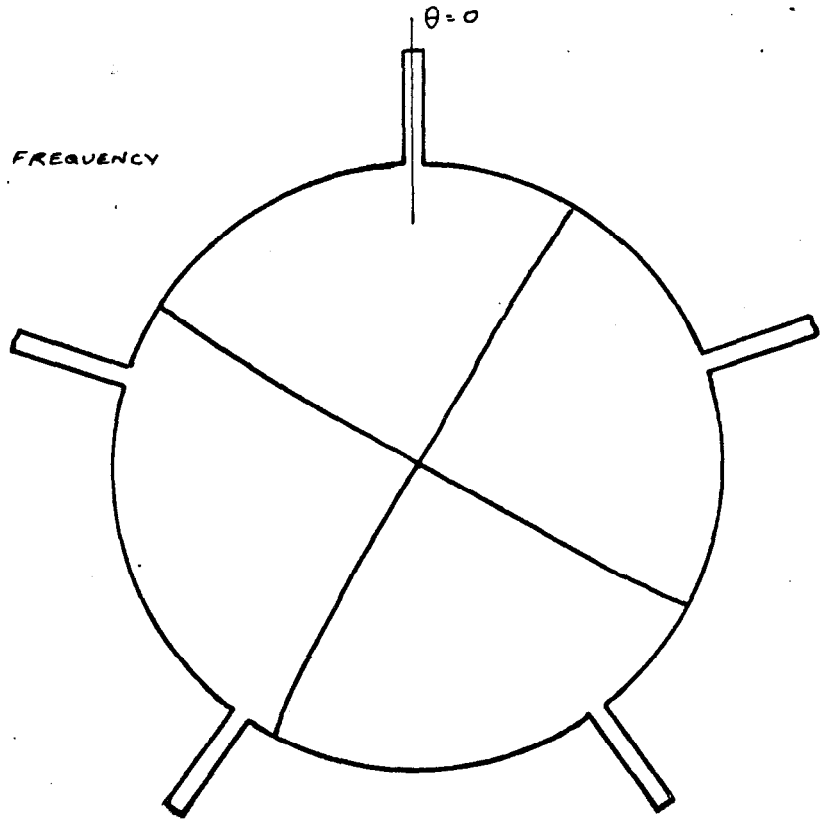


RIM DISPLACEMENT AND BLADE LOADS

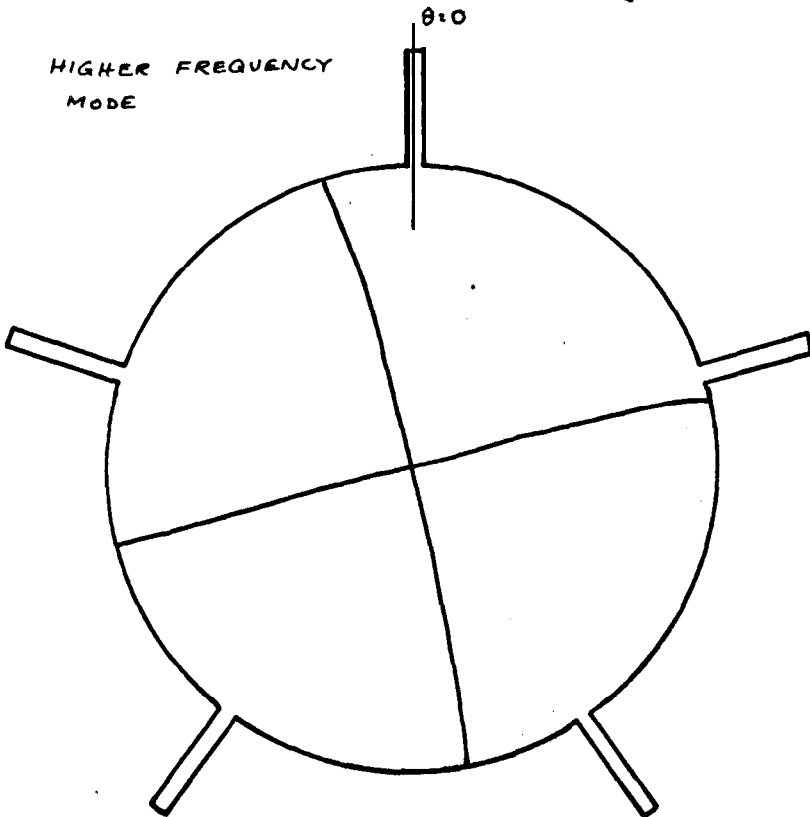
DETUNED 2/0 MODES

FIG 6.5

LOWER FREQUENCY
MODE



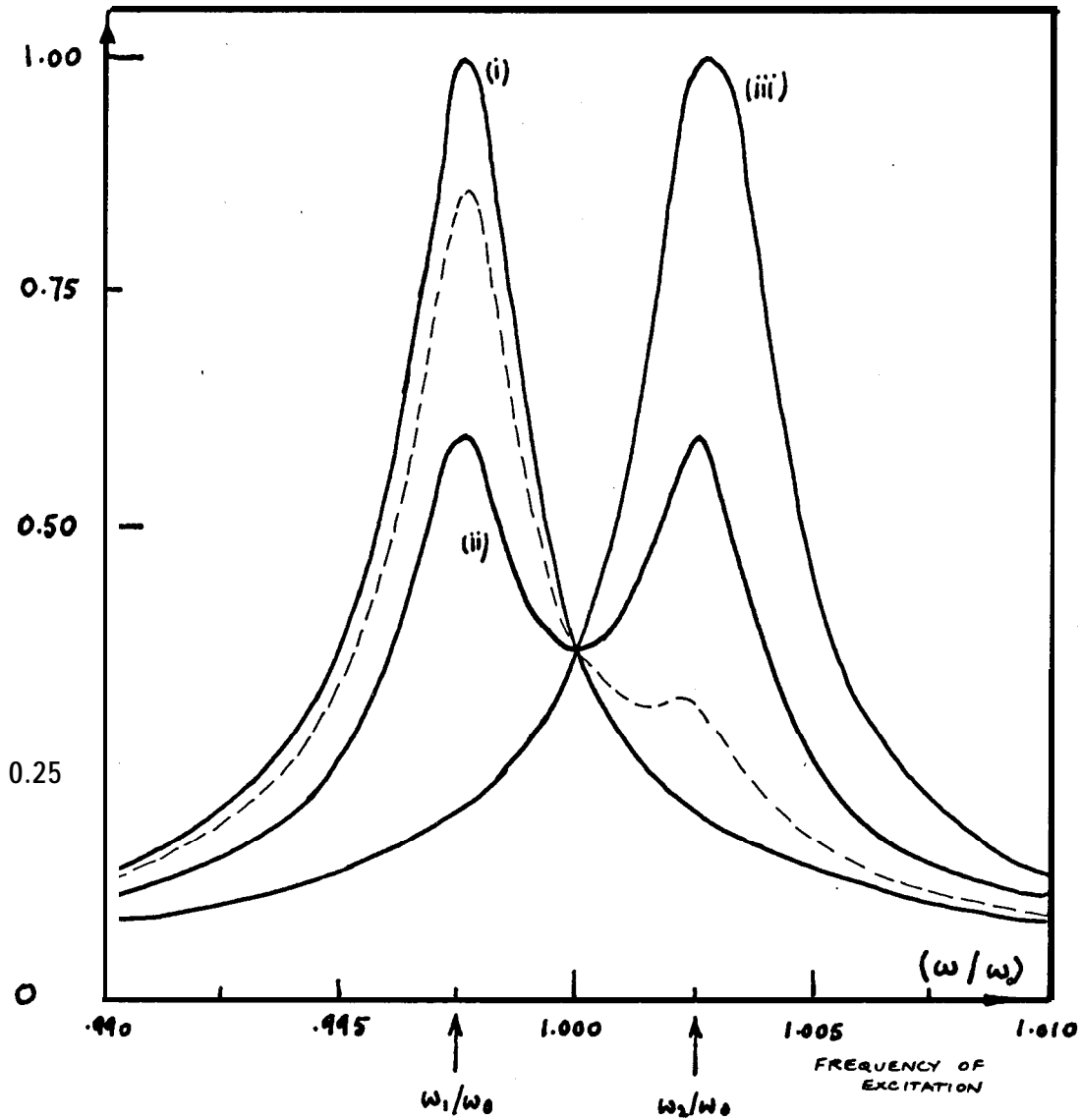
HIGHER FREQUENCY
MODE



NO DAL PATTERNS
DETUNED
2/0 MODES

FIG 6.6

AMPLITUDE AT THE POINT OF
EXCITATION RELATIVE TO
TUNED CASE



DAMPING

.001 CRITICAL IN EACH MODE

EXCITATION POSITIONS

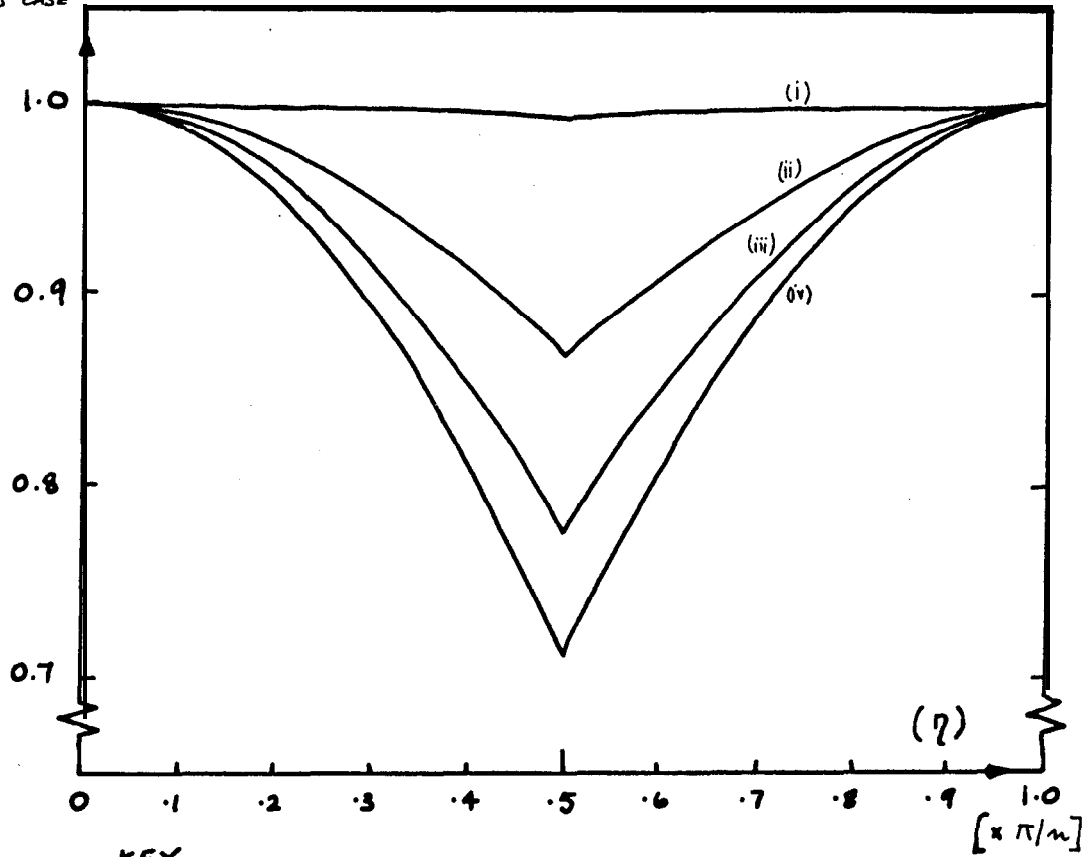
(i) 0 (ii) $\pi/2\pi$ (iii) π/π

SIMPLIFIED DOUBLE MODE

VARIATION OF RESPONSE WITH POSITION
OF EXCITATION

FIG 6.7

MAXIMUM RESPONSE
RELATIVE TO THAT IN THE
TUNED CASE



KEY.

NATURAL FREQUENCY SPLIT

(i) 0.1%

(ii) 0.5%

(iii) 1.0%

(iv) 5.0%

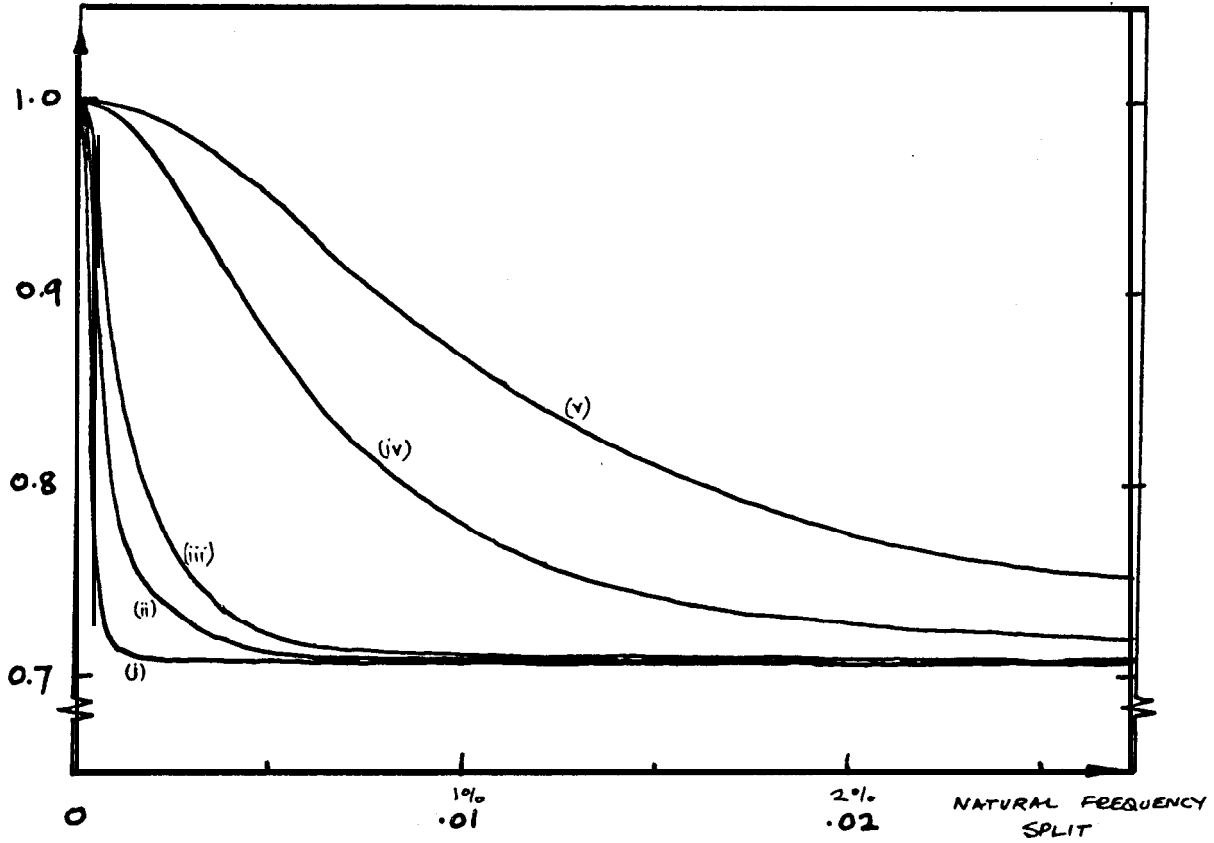
DAMPING = 0.005 CRITICAL

SIMPLIFIED DOUBLE MODE

VARIATION OF MAXIMUM RESPONSE WITH POSITION OF EXCITATION

FIG 6.8

MAXIMUM RESPONSE WITH EXCITATION
 AT OPTIMUM POSITION ($\eta = \pi/2m$)
 RELATIVE TO TUNED CASE



KEY

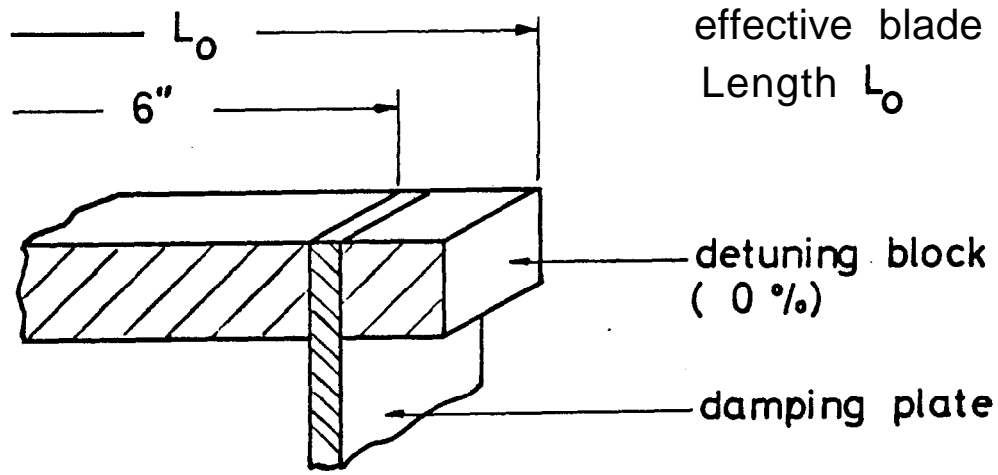
DAMPING RATIO

- (i) .0001
- (ii) .0005
- (iii) .0010
- (iv) .0050
- (v) .0100

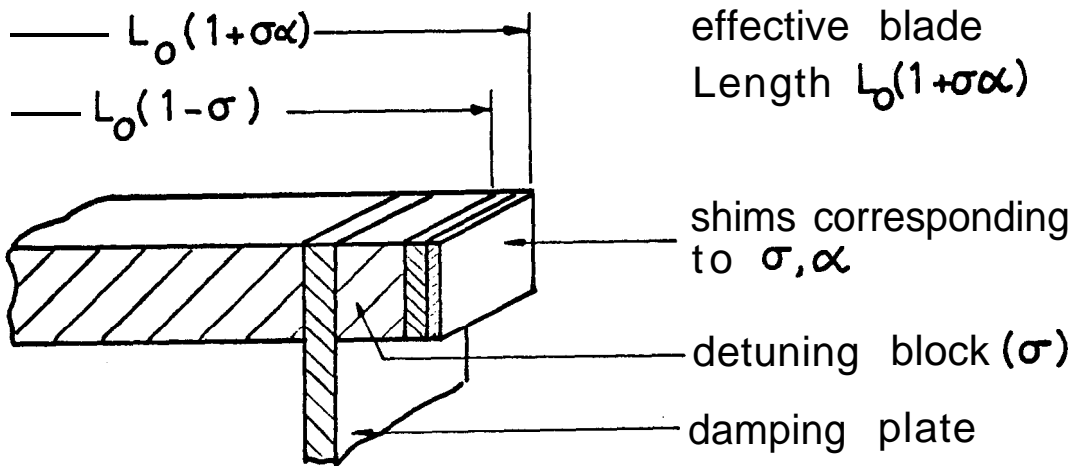
SIMPLIFIED DOUBLE MODE

VARIATION OF OPTIMUM RESPONSE WITH
DEGREE OF DETUNING AND DAMPING

FIG 6.9



TUNED SYSTEM

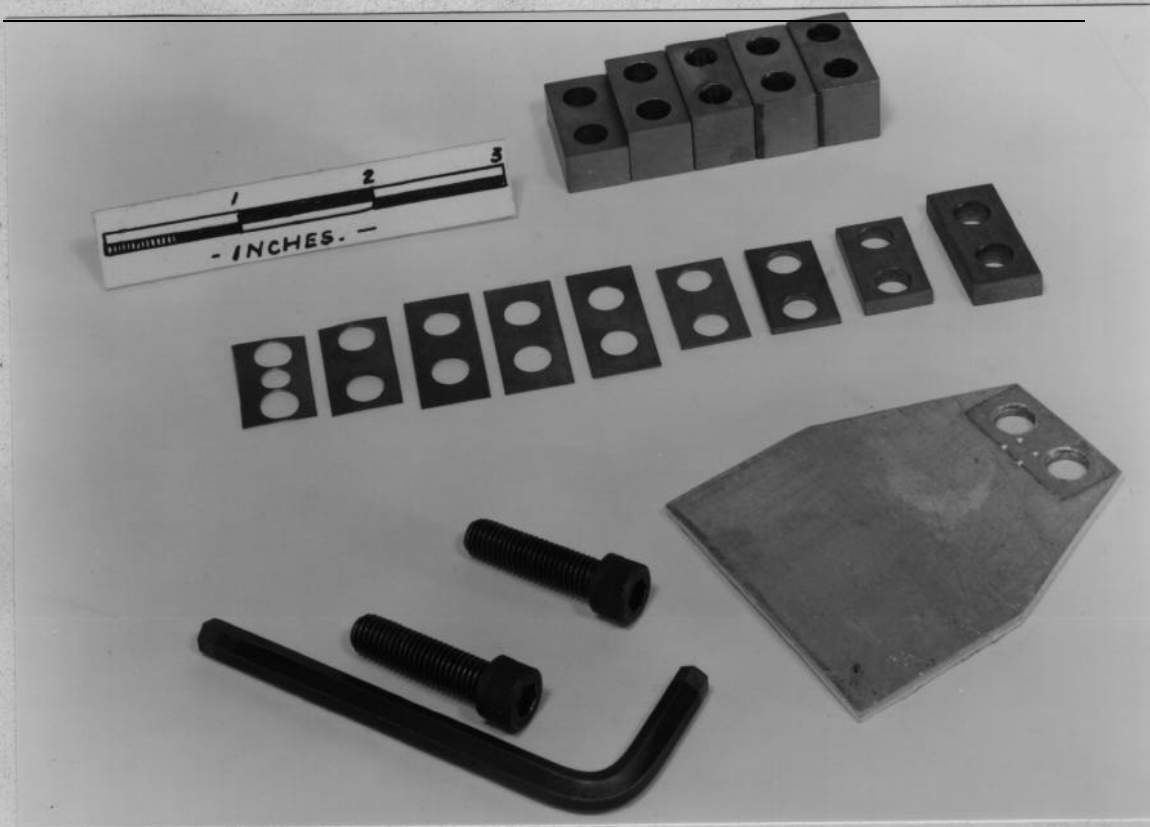


DETUNED SYSTEM

BLADE DETUNING ARRANGEMENT

FIG 7.1

DETUNING BLOCKS SHIMS



DAMPING PLATE

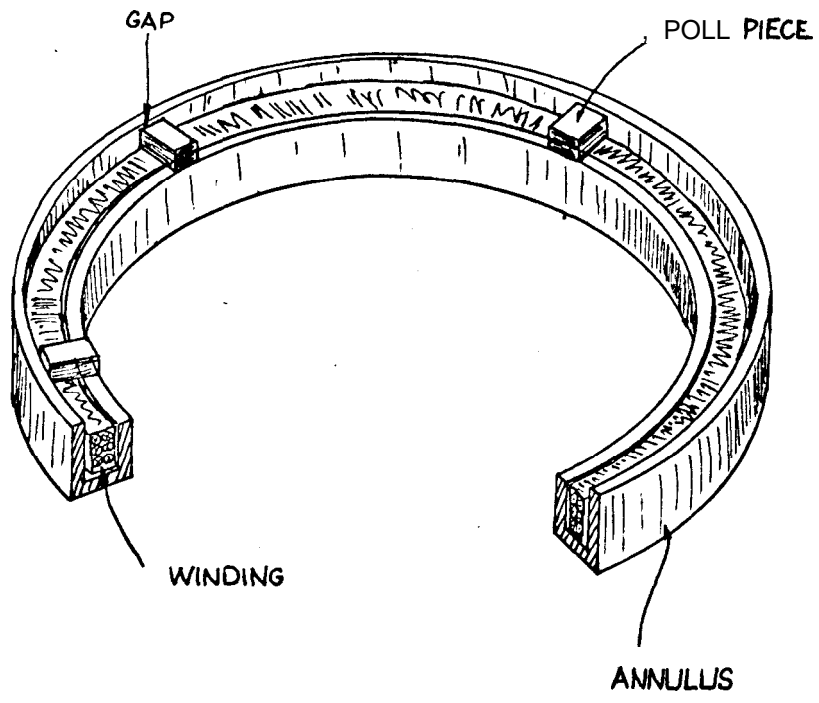
DETUNING KIT FOR ONE BLADE

FIG 7.2



A TYPICAL BLADE ASSEMBLY

FIG 7.3



THE DAMPING MAGNET

FIG. 7.4

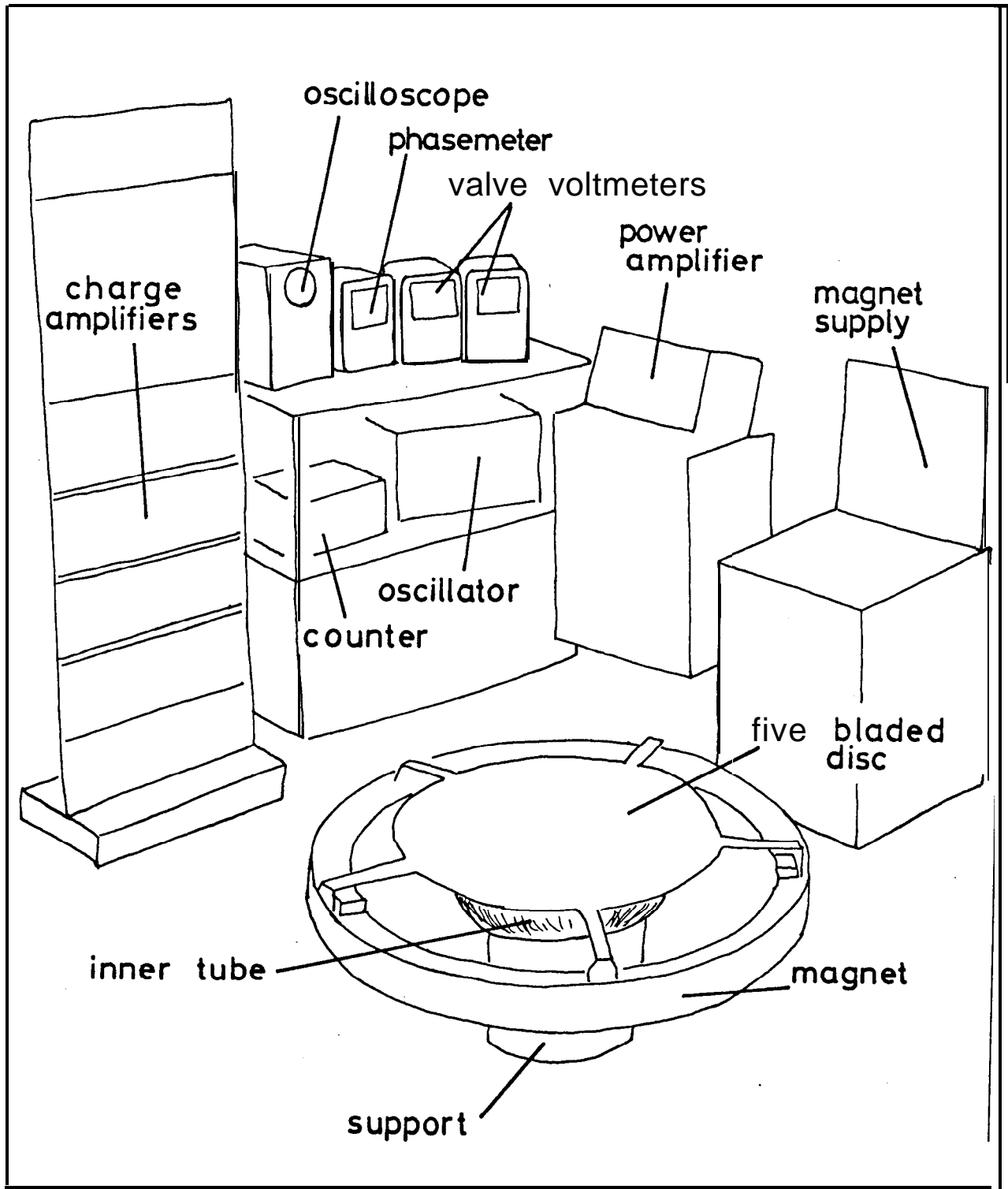
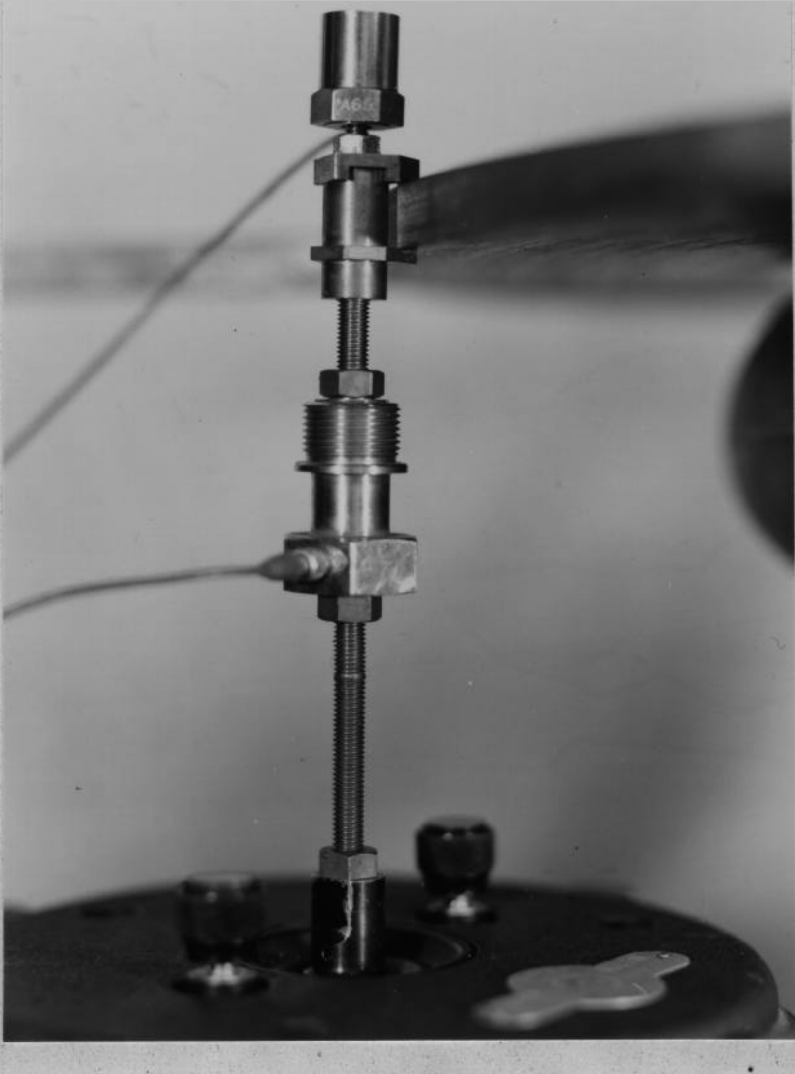


FIG 7.5 (opposite)



THE EXPERIMENTAL APPARATUS

FIG 7.5



ACCELEROMETER

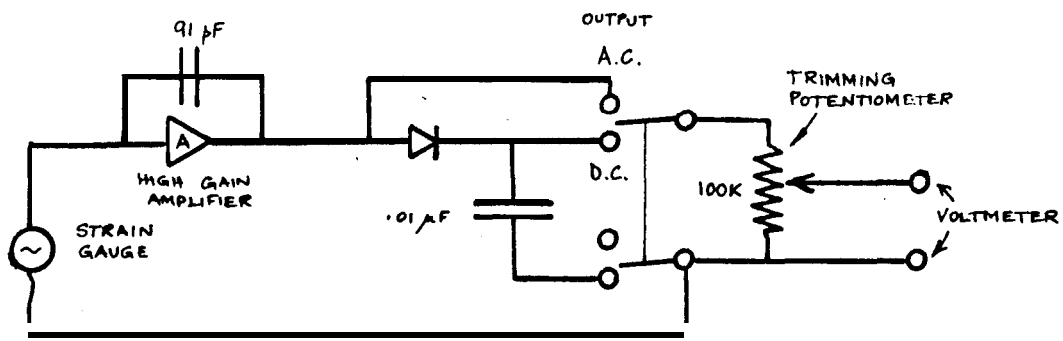
CLAMP

FORCE GAUGE

VIBRATOR

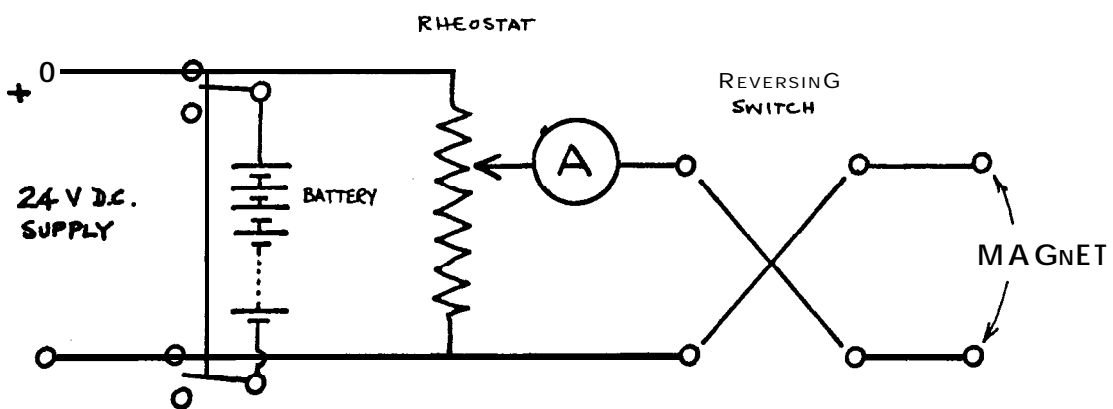
THE TRANSDUCER AND CLAMP ASSEMBLY

FIG 7.6



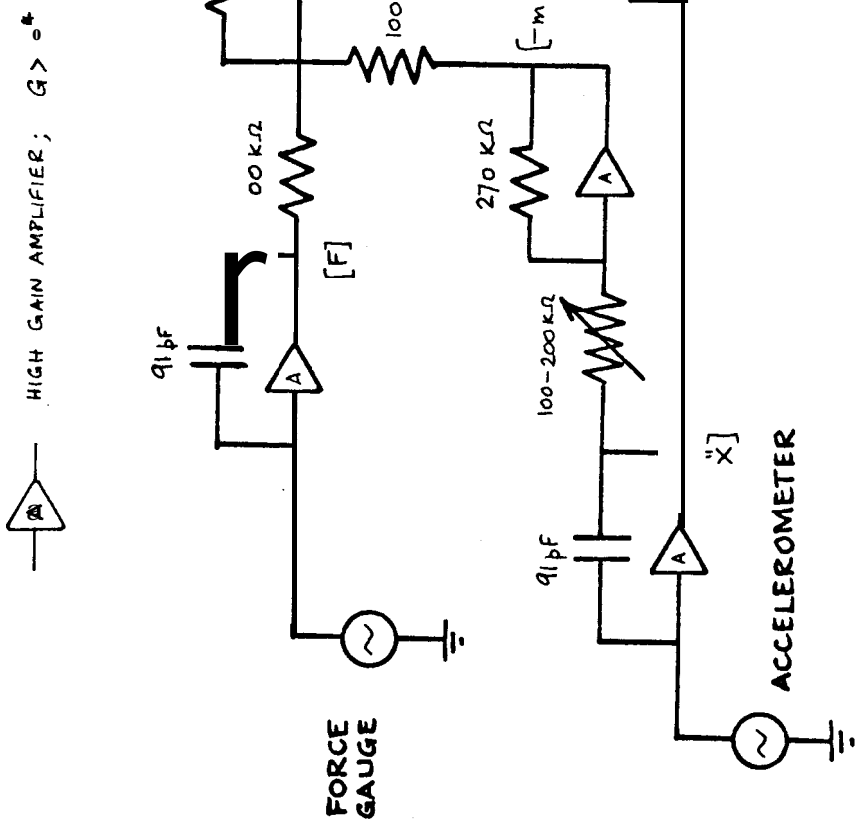
CIRCUIT DIAGRAM FOR ONE STRAIN GAUGE

FIG 7.7



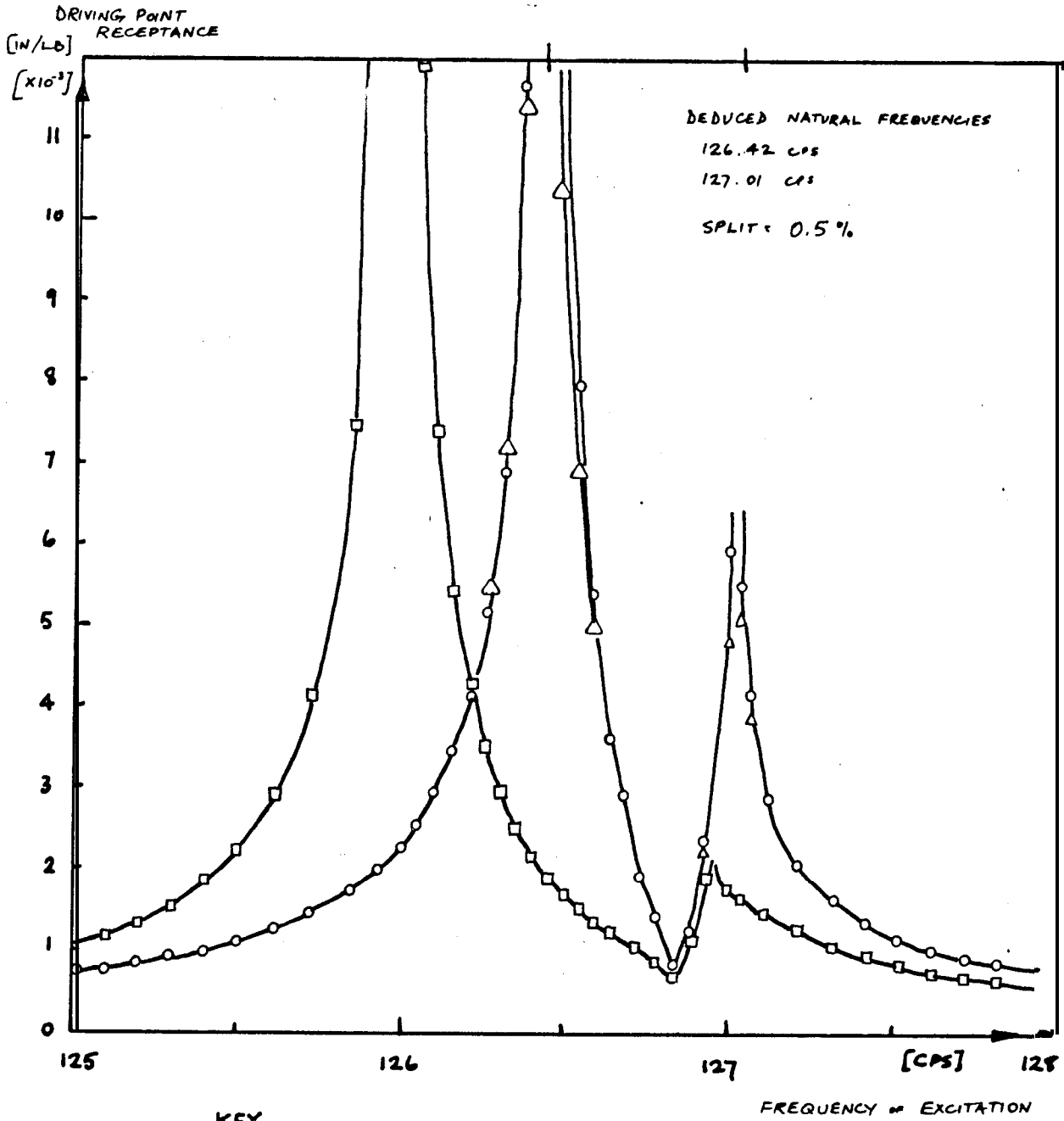
CIRCUIT DIAGRAM FOR THE MAGNET SUPPLY

FIG 7.8



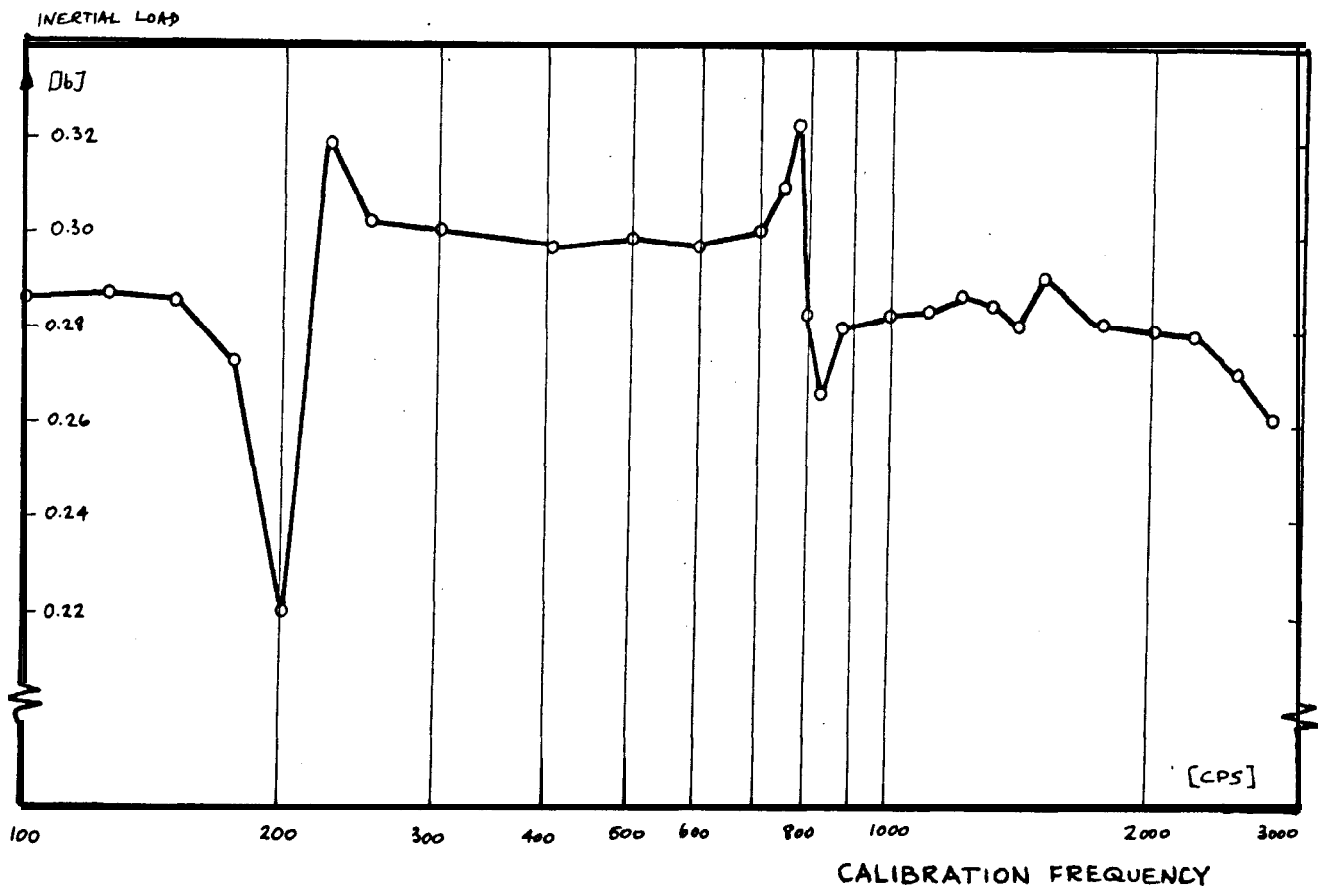
CIRCUIT DIAGRAM FOR THE RECEPTANCE TRANSDUCERS

FIG 7.9



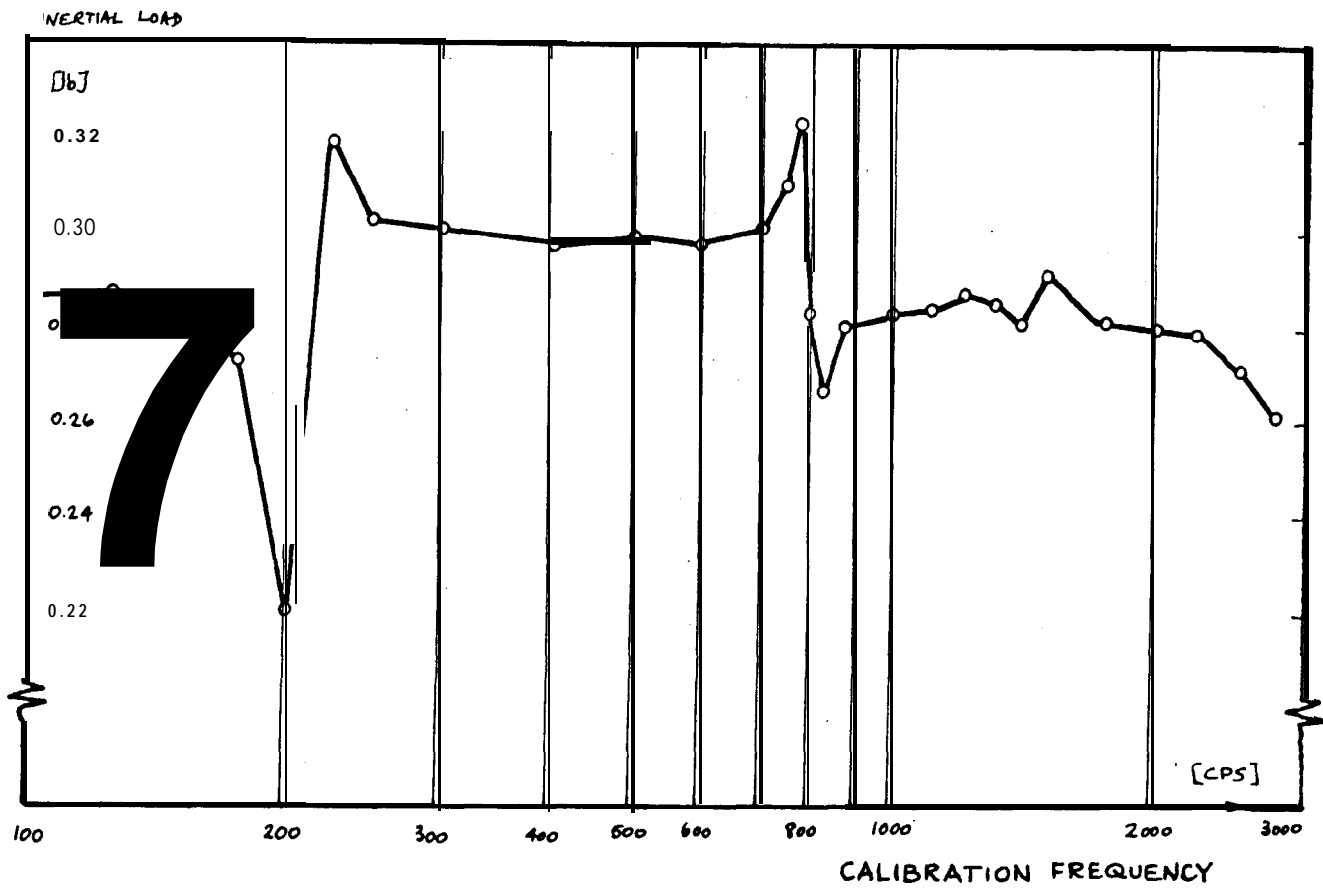
RECEPTANCE MEASUREMENT ON A BLADED DISC

FIG 7.10



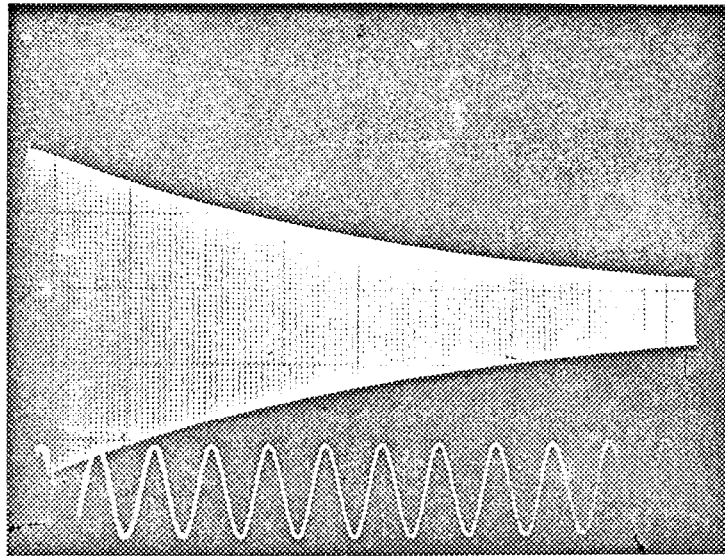
CALIBRATION OF THE MASS
CANCELLATION TECHNIQUE

FIG 7.11



CALIBRATION OF THE MASS
CANCELLATION TECHNIQUE

FIG 7.11

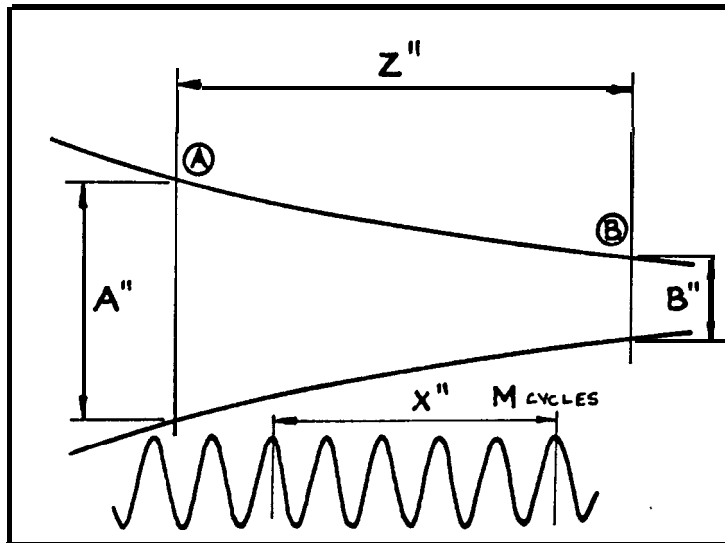


MODE : 0/1

CURRENT : 0A

FREQUENCY
194 cps

STANDARD
FREQUENCY
10 cps



FREQUENCY
F cps.

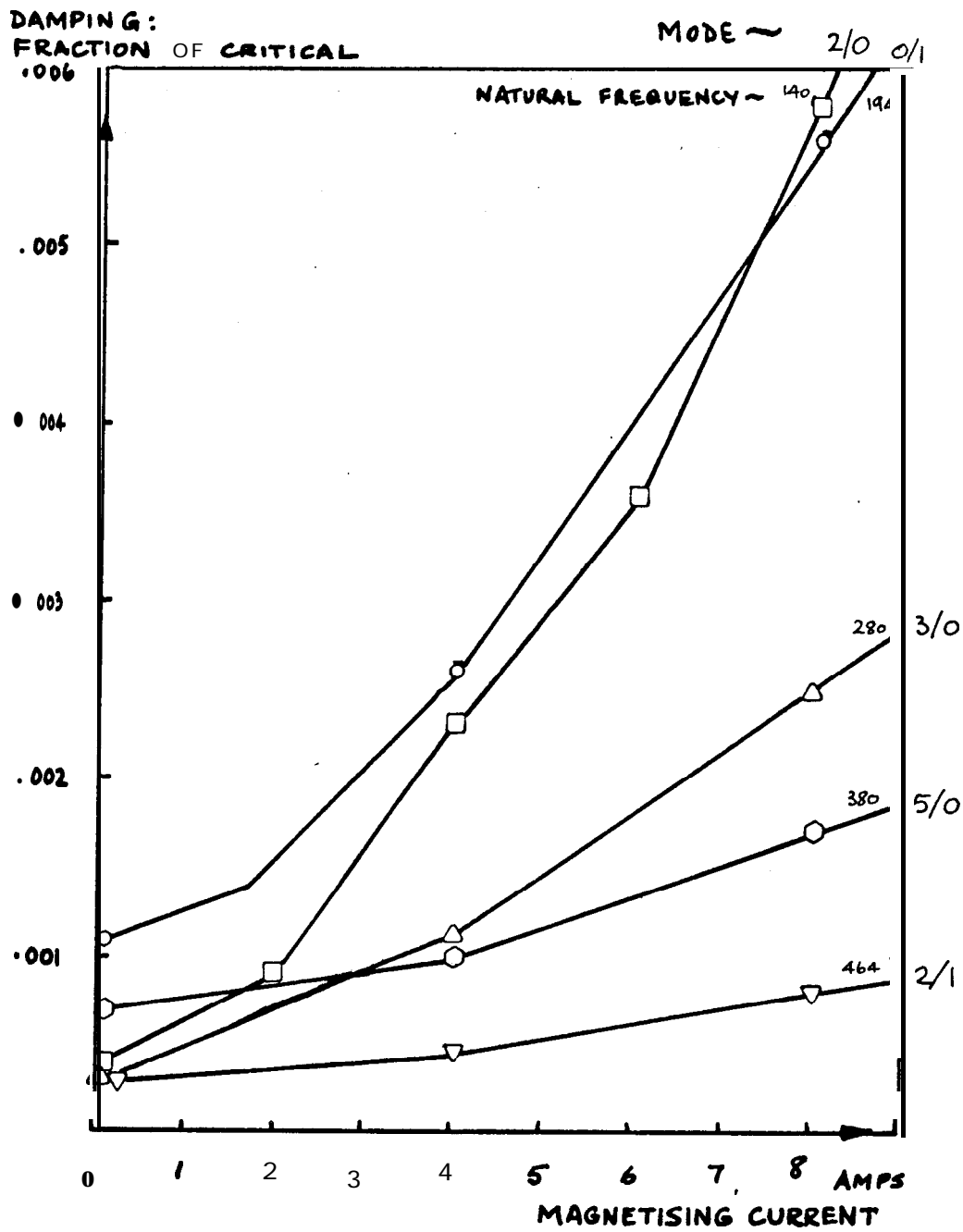
FREQUENCY
G cps.

$$Q \text{ FACTOR} = \frac{\pi \{ F Z M / X G - 1 \}}{\log_e (A/B)}$$

$$\text{CRITICAL DAMPING RATIO } C = 1 / 2.9$$

TYPICAL DECAY CURVE WITH ANALYSIS

FIG 7.12



DAMPING MAGNET CALIBRATION CURVE

FIG 7.13

EXPERIM. FREQ.	LIMITS ON COMPUTED FREQ.	SERIES A : $\lambda = 0.3333$			
		126.89	121.80 134.64	677.69	654.75 723.77
165.32	161.54 178.57	711.49	684.06 756.18	1363.88	1334.30 1475.0
208.28	205.30 226.95	933.18	898.64 995.79	1607.72	1579.0 1745.5
250.38	242.39 267.95	1058.54	1027.39 1135.70	1669.73	1632.5 1804.6
351.54	342.23 378.31	1110.49	1079.60 1193.42	1813.90	1774.3 1961.4
440.3	422.82 467.40	1236.86	1196.07 1322.17	2107.93	1986.4 2195.8

FIG 8.1

SERIES B : $\lambda = 0.25$					
149.2	142.59 154.82	312.8	308.02 340.49	703.5	677.21 748.61
220.5	214.85 237.80	424.0	418.35 462.46	775.0	748.30 827.19
312.8	301.14 332.89	505.7	491.84 543.70		

FIG 8.2

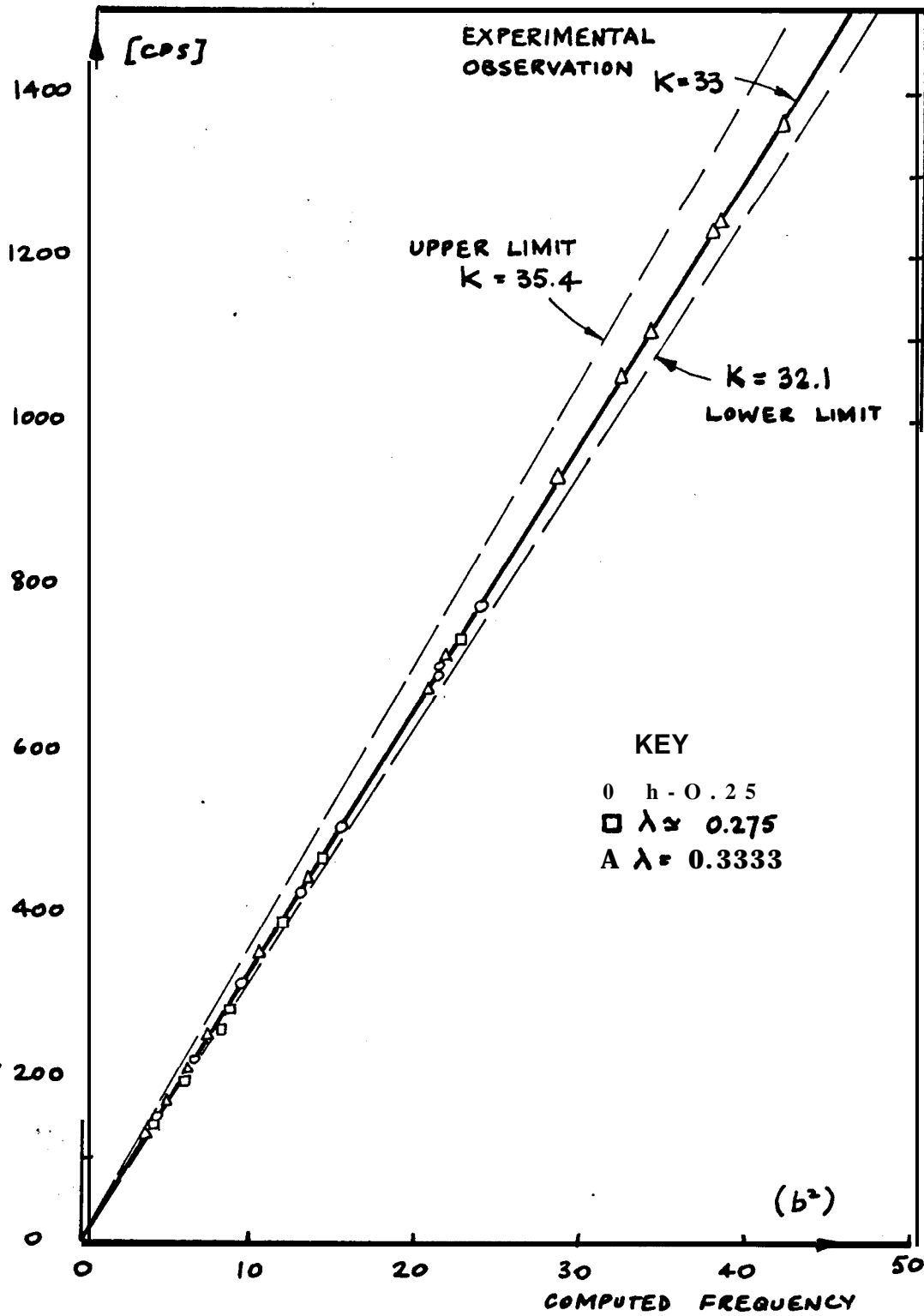
SERIES C : $\lambda = 0.275$					
140.25	137.02 151.47	280.3	281.71 311.41	696.3	675.79 747.03
196.5	198.99 219.97	383.6	386.74 427.51	733.7	720.2 796.12
259.6	270.90 299.46	467.7	462.23 570.96		

FIG 8.3

NATURAL FREQUENCIES OF TUNED SYSTEMS

FIGS 8.1- 8.3

EXPERIMENTAL FREQUENCY



EXPERIMENTAL NATURAL FREQUENCY MEASUREMENTS

FIG 8.4

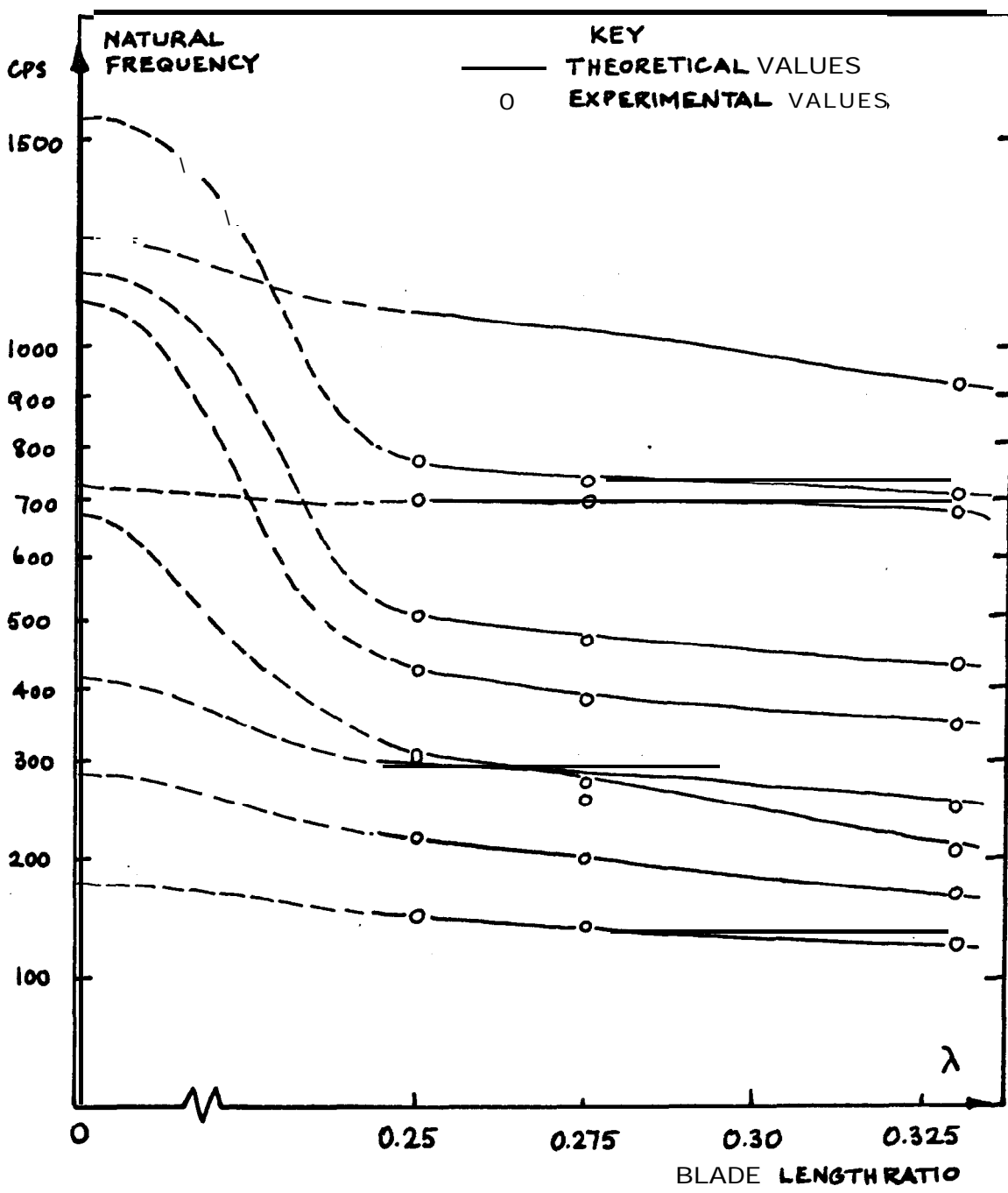
EXPTL. FREQ.	ERROR OF COMP. FREQ. (%)	SERIES A: $\lambda = 0.3333$			
126.89	-1.2	677.69	-0.6	1245.80	+0.4
165.32	+0.6	711.49	-1.0	1363.88	+0.7
208.28	+1.5	933.18	-0.9	1607.72	+1.1
250.38	-0.4	1058.54	-0.1	1669.73	+0.6
351.54	+0.2	1110.49	0	1813.90	+0.7
440.30	-1.2	1236.86	-0.5	2107.93	-2.0

SERIES B: $\lambda = 0.25$					
149.2	-1.6	312.8	+1.4	703.5	-0.9
220.5	+0.3	424.0	+1.6	715.0	-0.6
312.8	-0.9	505.7	+0.1		

SERIES C: $\lambda = 0.275$					
140.25	+0.6	280.3	+3.4	696.3	0
196.5	+4.2	383.6	+3.8	733.7	+1.0
259.6	+7.4	467.7	+1.7		

ACCURACY OF NATURAL FREQUENCY CALCULATIONS
(BASED ON $K = 33$)

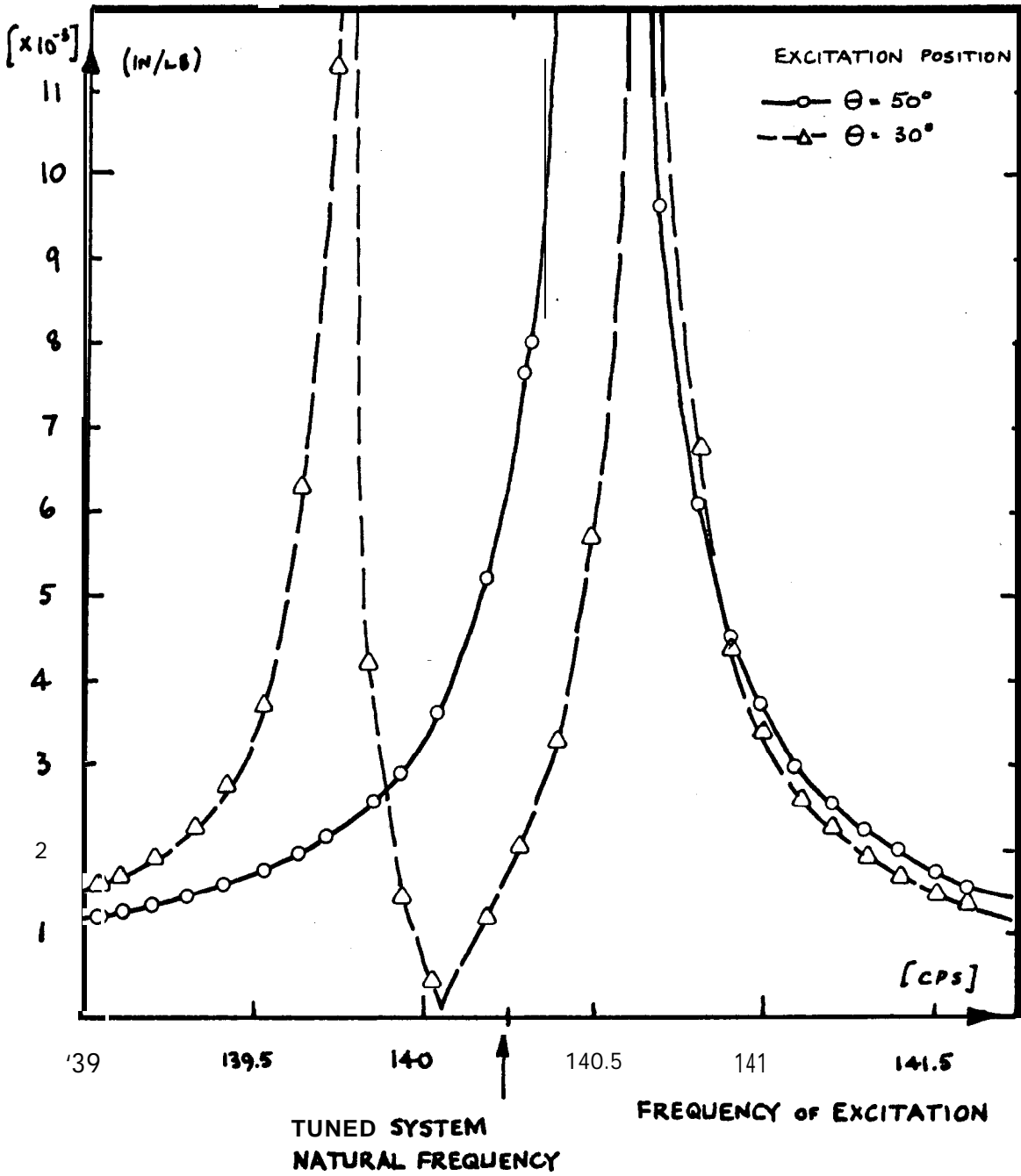
FIG 8.5



VARIATION OF NATURAL FREQUENCIES WITH
BLADE LENGTH

FIG 8.6

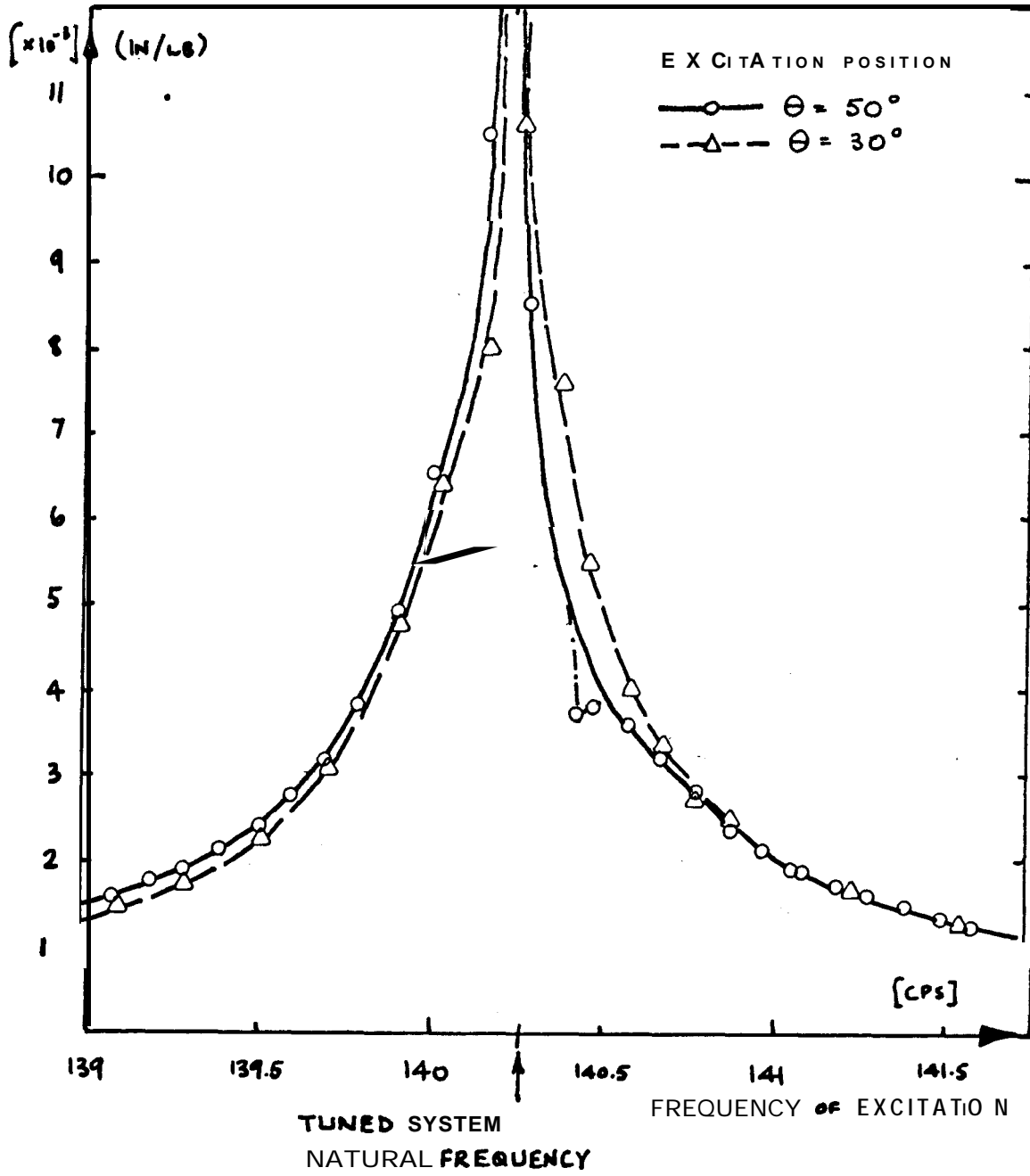
DRIVING POINT
RECEPTANCE



RESPONSE IN THE 2/0 MODE WITH $\cos \theta$
DETUNING

FIG 8.7

DRIVING POINT
RECEPTANCE



RESPONSE IN THE 210 MODE WITH COS 28
DETUNING

FIG 8.8

SERIES D

$\lambda = 0.275$

		TEST No.	E1,1	E1,2	E1,3	E1.4
		$\phi, \sigma b_1$	0, .01	$\frac{\pi}{2}, .01$	$\frac{\pi}{6}, .01$	0, .025
Mode	N.Freq.		(i)	(i)	(ii)	(ii)
2/0	(i) 140.25		139.75	139.95	139.05	138.6
	(ii) 139.4		140.6	140.7	139.8	140.4
			0.6%	0.5%	0.5%	1.3%
1/1	(i) 259.6		258.95	259.0	254.9	-
	(ii) 255.0		0%	0%	0%	-
3/0	(i) 380.3		279.88	280.03	277.2	-
	(ii) 278.0		281.65	281.55	279.85	-
			0.6%	0.5%	0.9%	-
2/1	(i) 467.7		466.7	466.25	463.05	-
	(ii) 463.9		468.9	466.85	464.55	-
			0.5%	0.6%	0.3%	-
6/0	(i) 733.7 (ii) 750.5		-	-	-	-

DETUNED NATURAL FREQUENCIES - (I) COS 10 DETUNING

FIG 8.9

SERIES D

$\lambda = 0.275$

		TEST No.	E2,1	E2,2	E2,3
		$\psi, \sigma b_2$	0, .01	$\frac{\pi}{4}, .01$	$\frac{\pi}{12}, .01$
Mode	N.Freq.		(i)	(i)	(ii)
2/0	(i) 140.25		140.1	140.2	139.4
	(ii) 139.4				
1/1	(i) 259.6		257.15	257.13	252.8
	(ii) 255.0		260.50	260.35	256.4
			1.3%	1.2%	1.4%
3/0	(i) 280.3		280.23	-	277.48
	(ii) 278.0		0%		0%
2/1	(i) 467.7		-	-	463.6
	(ii) 463.9				0%
6/0	(i) 733.7		732.0	732.5	-
	(ii) 750.5		735.5	735.0	
			0.5%	0.4%	

DETUNED NATURAL FREQUENCIES -(II) COS 2θ DETUNING

FIG 8.10

Mode	Test No.	E3,1	E3,2
		0.2, .025 , $\frac{\pi}{6}$, 0, 0	0, .0125 , 0, .0125 , 0
2/0	139.4	131.05 139.95 1.4%	139.05 139.90 0.6%
1/1	255.0	—	252.6 257.1 1.7%
3/0	278.0	—	278.0 279.1 0.4%
2/1	463.9	460.40 465.15 1.1%	463.1 465.2 0.5%
6/0	750.5	—	749.7 755.6 0.8%

SERIES D.

$$\lambda = 0.275$$

DETUNED NATURAL FREQUENCIES-(III) GENERAL DETUNING

FIG 8.11

Mode	SPLIT FACTOR			FREQUENCY FACTOR	
	min max	of mean () tests	computed value	one case	computed value
2/0	.50 .60	0.5 (6)	0.5	0.6	0.5
1/1	1.2 1.4	1.32 (4)	1.4	—	—
3/0	0.4 0.5	0.6 (4)	0.7	—	—
2/1	0.3 0.4	0.5 (5)	0.55	0.5	0.55
6/0	0.4 0.6	0.5 (4)	0.5	—	—

SERIES D

$\lambda = 0.275$

EXPERIMENTAL AND COMPUTED VALUES OF
SPLIT AND FREQUENCY FACTORS

FIG 8.12

	RELATIVE STRESS					MEAN STRESS RESPONSE
	1	2	3	4	5	
TEST 1	.2	.2	.2	.2	.2	.51
TEST 2	.204	.199	.187	.205	.206	.43
TEST 3	.209	.186	.177	.208	.219	.46
TEST 4	.199	.207	.197	.195	.203	.50

*TEST 1	.2	.2	.2	.2	.2	2.6
TEST 2	.198	.206	.206	.200	.190	2.7
TEST 3	.197	.213	.210	.198	.182	2.7
TEST 4	.202	.204	.202	.204	.189	2.8

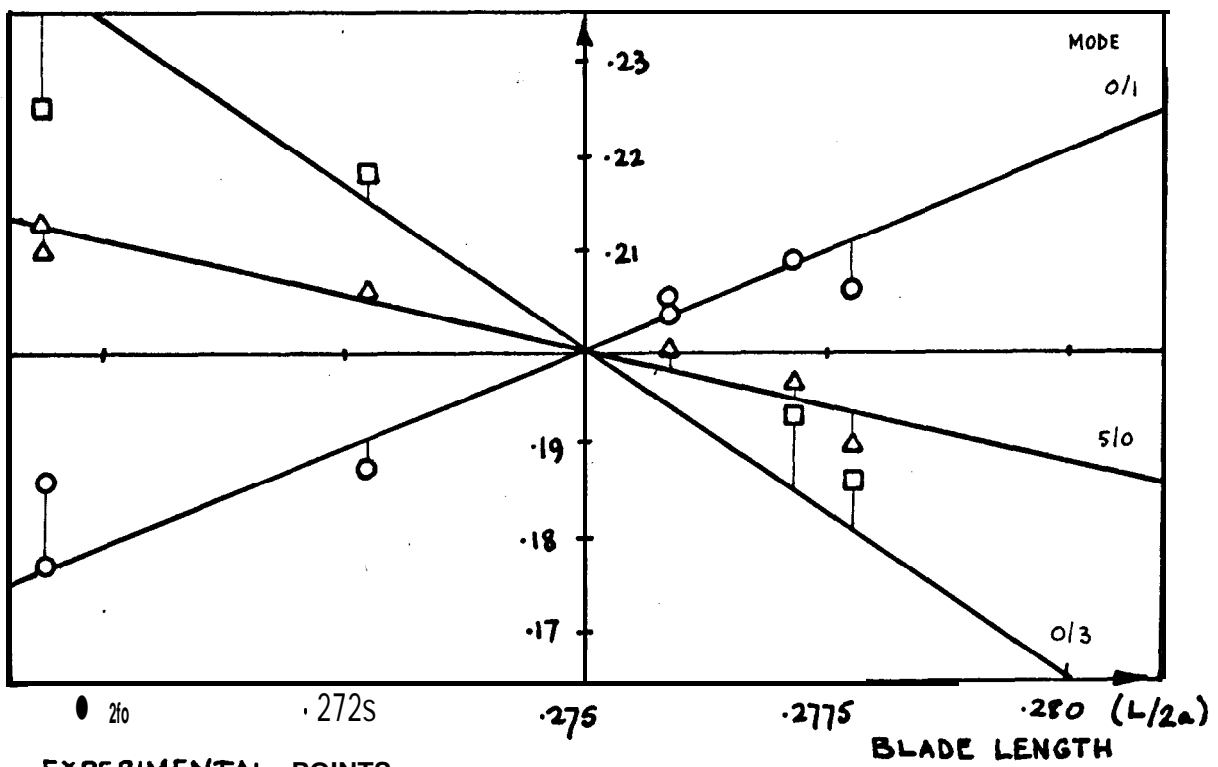
*TEST 1	.2	.2	.2	.2	.2	.072
TEST 2	.199	.199	.218	.199	.186	.071
TEST 3	.193	.225	.225	.197	.161	.075
TEST 4	.233	.189	.189	.233	.155	.071

***TEST 1** $f(\theta) = 0$; $\sigma = 0$
 TEST 2 $f(\theta) = \cos \theta$; $\sigma = .01$
 TEST 3 $f(\theta) = \cos \theta$; $\sigma = .025$
 TEST 4 $f(\theta) = \cos 2\theta$; $\sigma = .025$

RESPONSE MEASUREMENTS ON SINGLE MODES

FIG 8.13

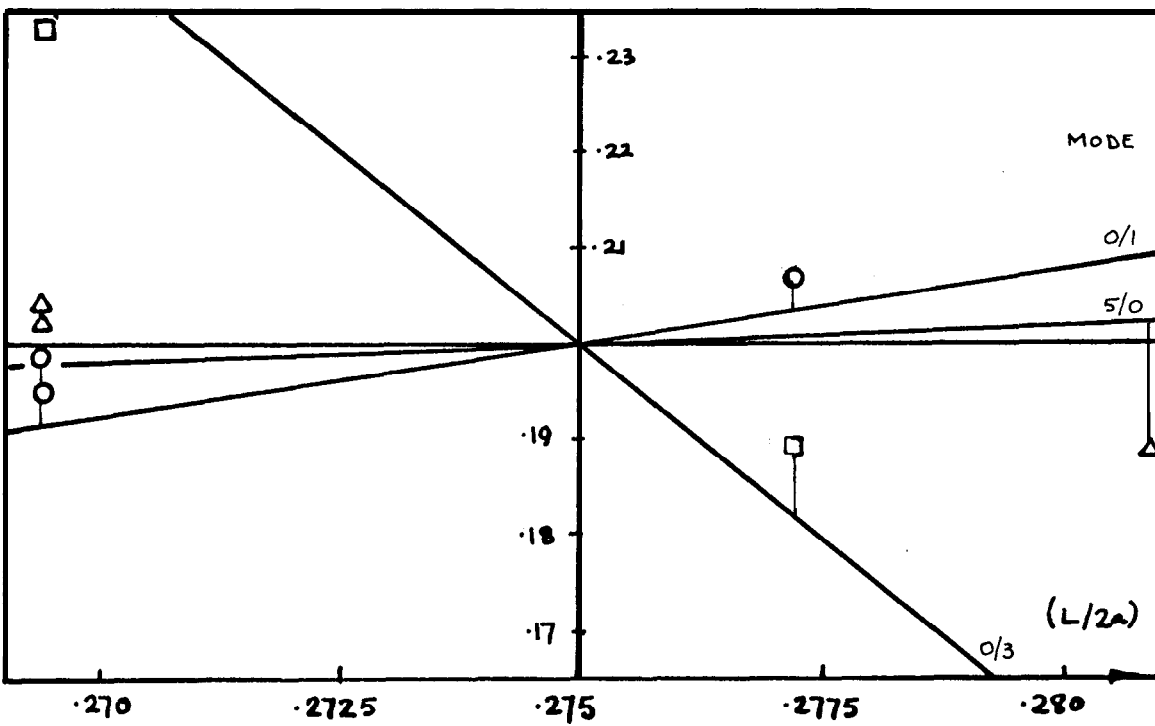
RELATIVE STRESS LEVEL $\cos 10^\circ$ DETUNING



EXPERIMENTAL POINTS

- — 0/1 MODE
- △ — 5/0 MODE
- — 0/3 MODE

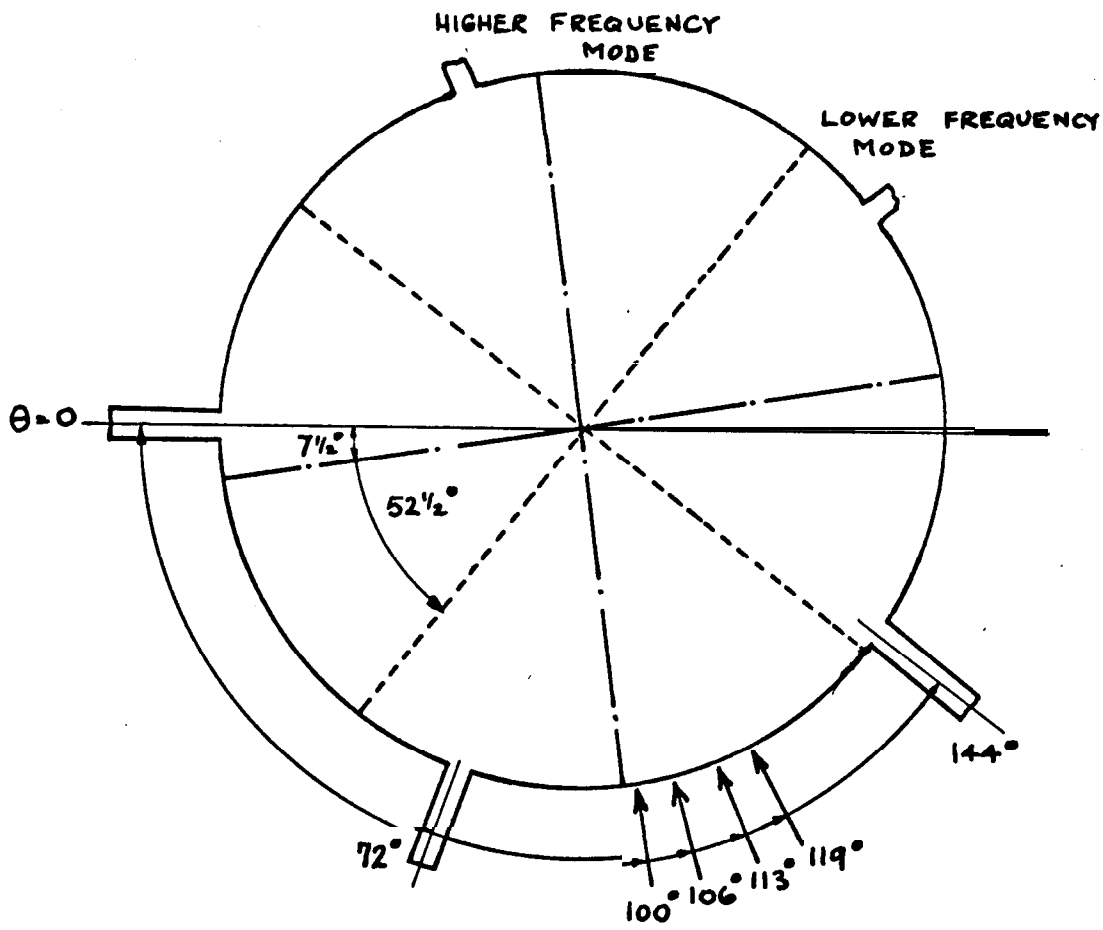
RELATIVE STRESS LEVEL $\cos 20^\circ$ DETUNING



STRESS MEASUREMENTS IN DETUNED SINGLE MODES

FIG 8.14

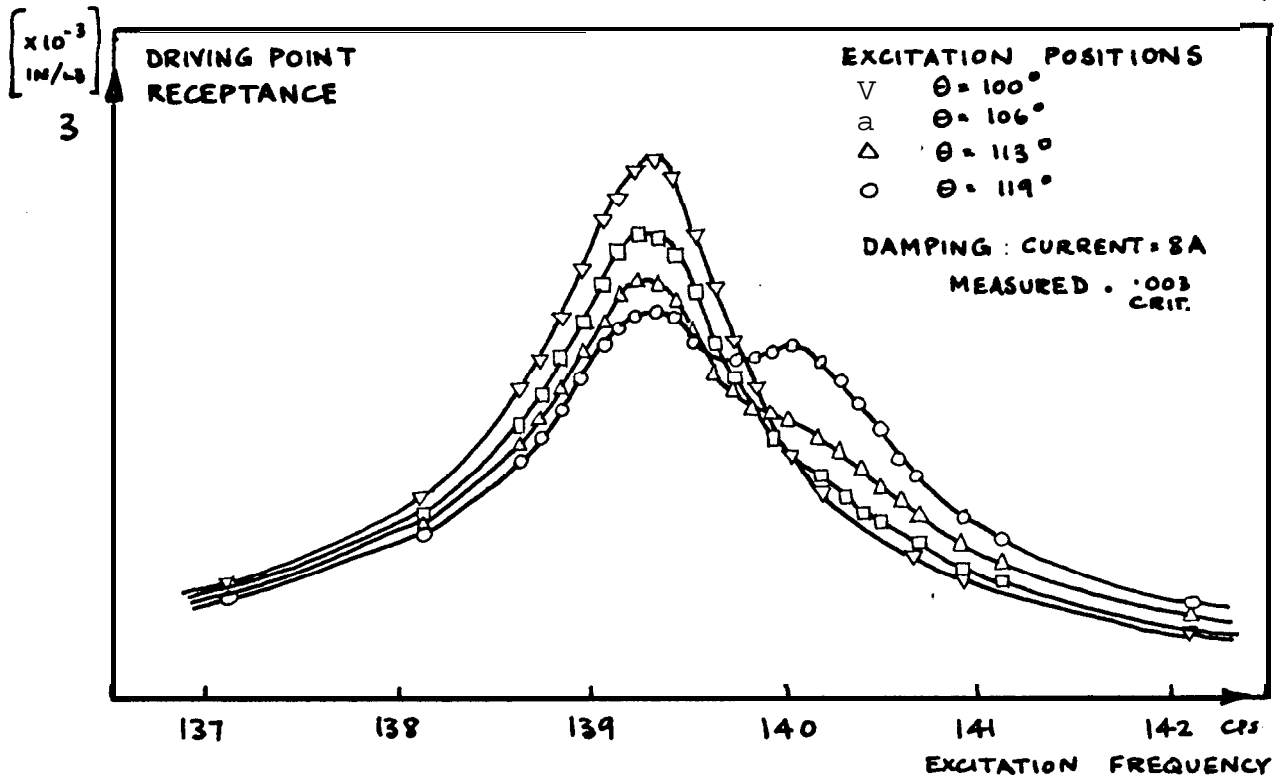
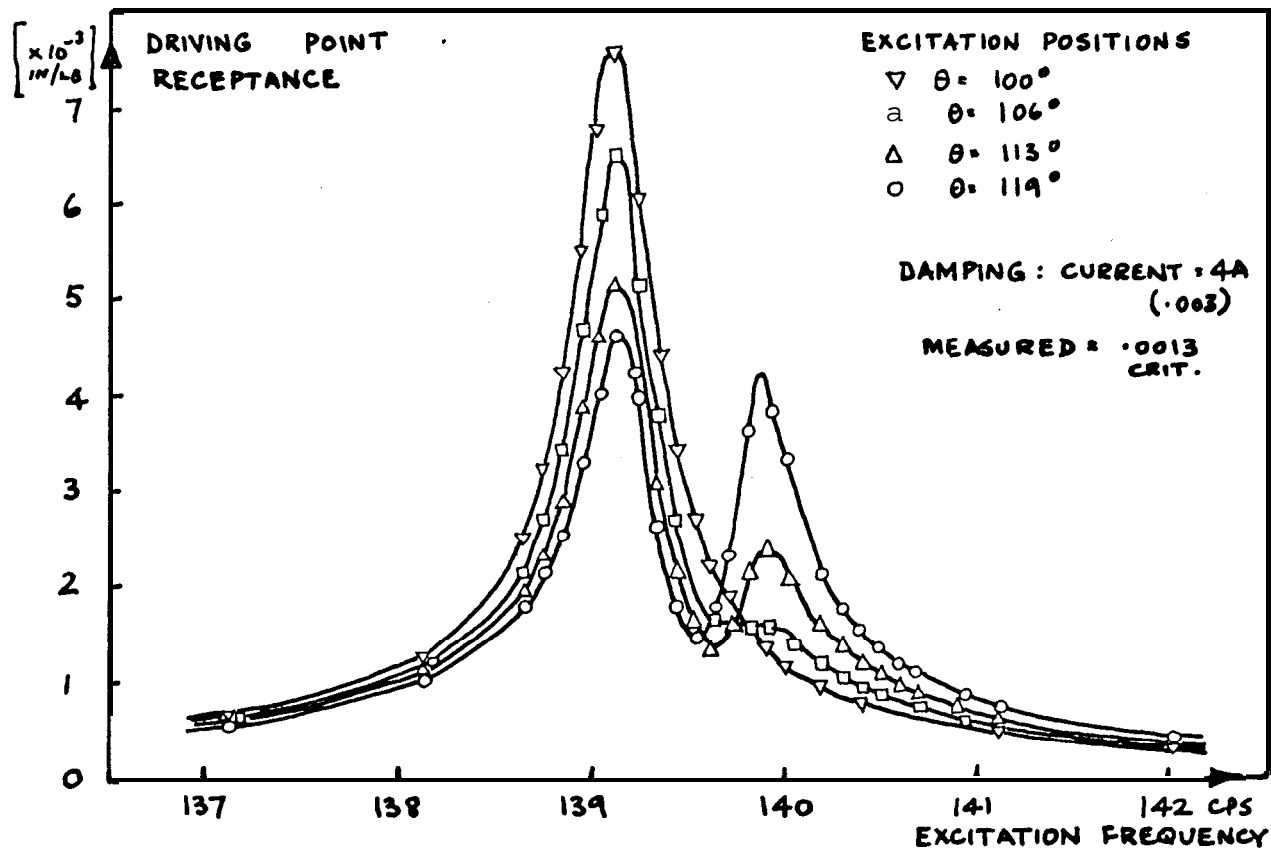
theoretical nodal lines



experimental excitation positions

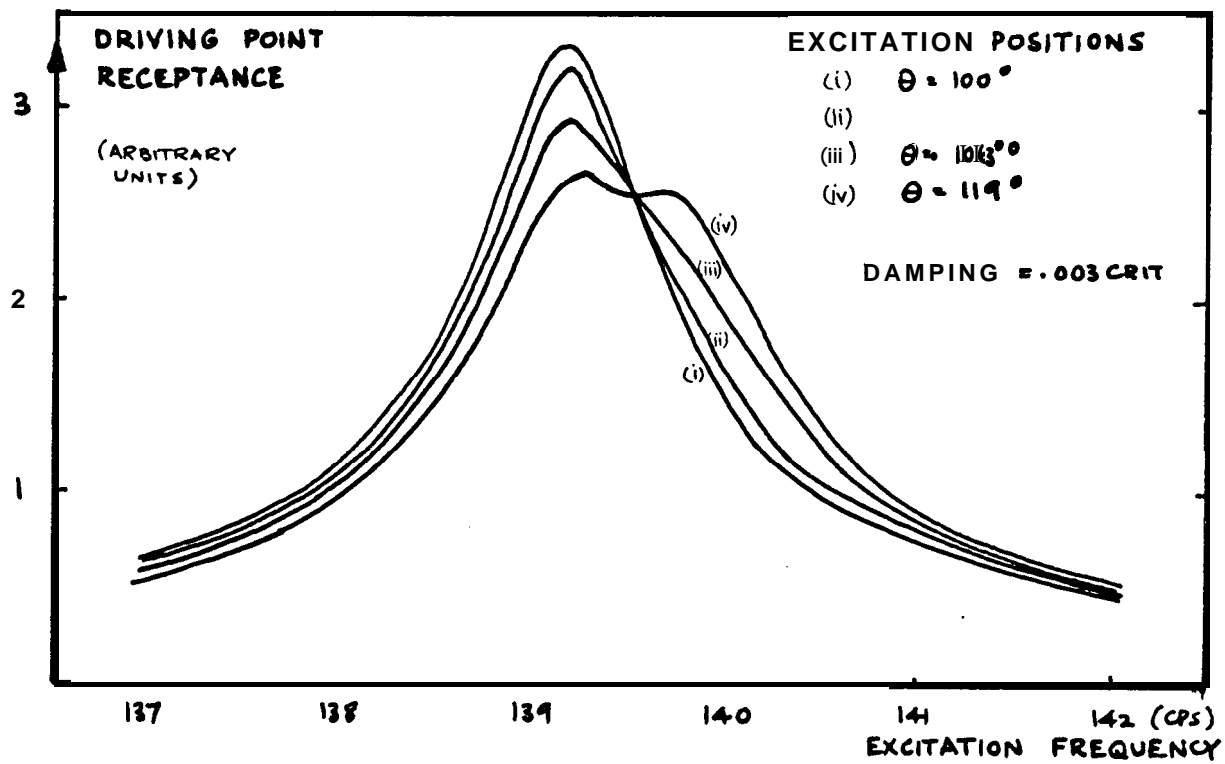
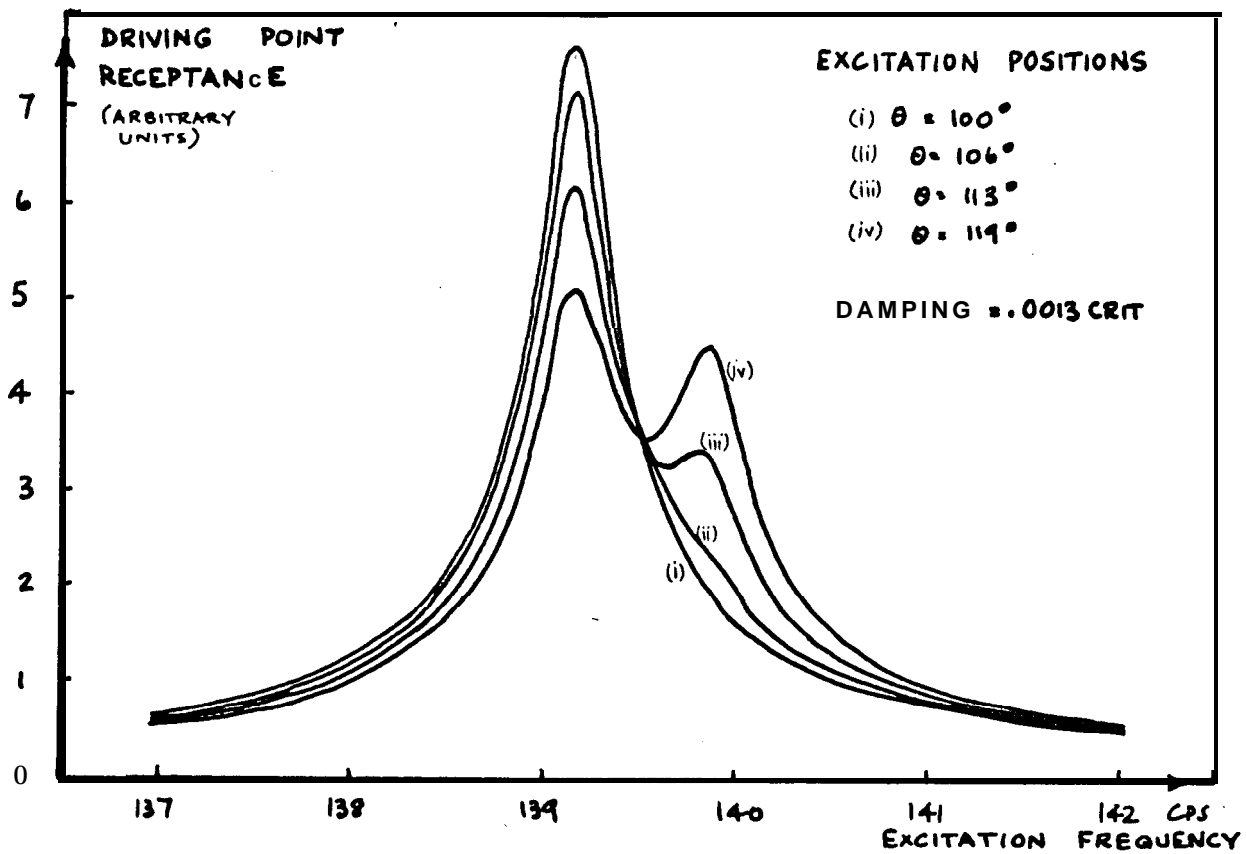
EXPERIMENTAL AND THEORETICAL STUDY
OF THE DETUNED DOUBLE MODE

FIG 8.15



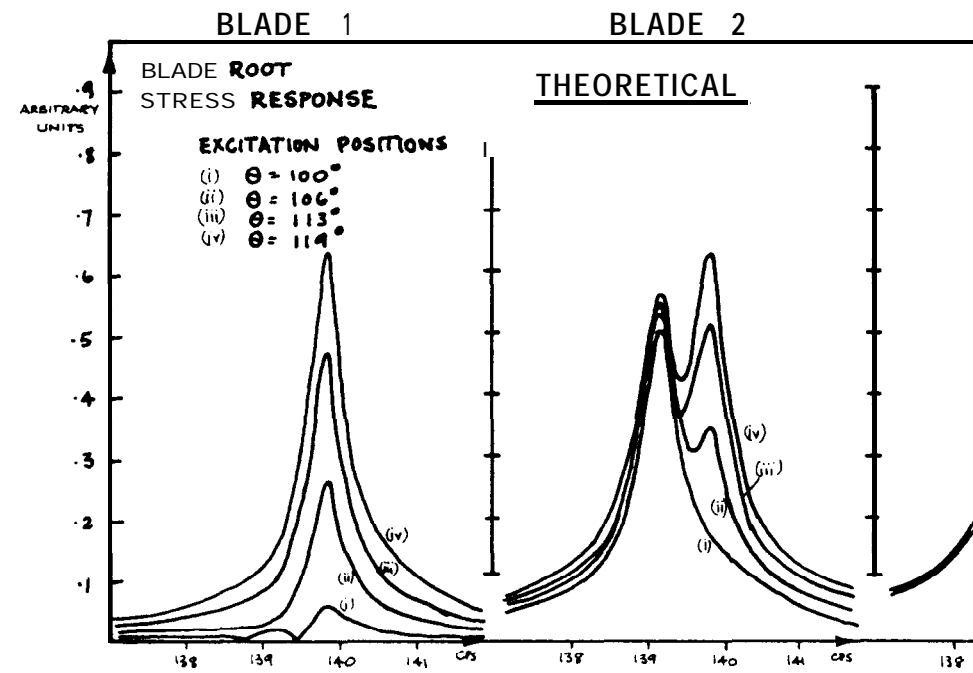
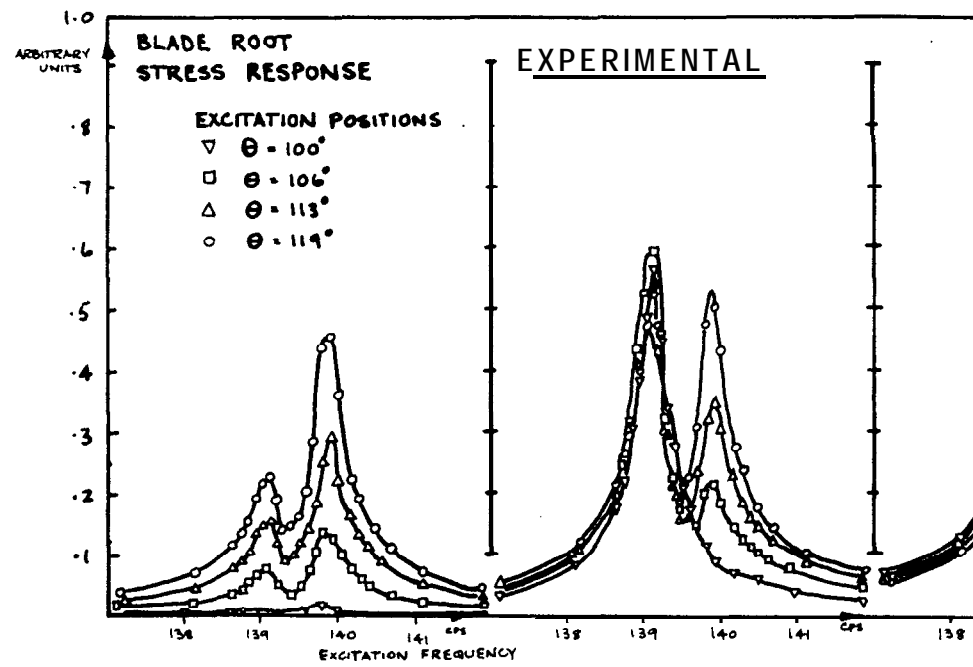
EXPERIMENTAL RESPONSE OF DETUNED 2/0 MODE

FIG 8.16



COMPUTED RESPONSE FOR DETUNED 2/0 MODE

FIG 8.17



EXPERIMENTAL AND THEORETICAL BLADE STRESS RESPONSE

APPENDIX 1NOTATION

The following list refers to those symbols which are used frequently throughout the text. Other notation is often adopted locally, but this is clearly defined in the text. Numbers in brackets refer to the appropriate chapters.

a	radius of the disc
a_j	inertia coefficient of a vibration mode defined by j
A	constant, cross sectional area (3)
b	dimensionless frequency parameter
b_{ms}	dimensionless natural frequency of the m, s mode
b_0, b_1, b_2	coefficients in detuning function
B	constant (3)
c_i	reaction couple on the i^{th} blade (2)
c_j	inertia coefficient of the j^{th} mode (3)
C_i	reaction couple on the disc (2)
C, D	constants (3)
E	Young's modulus, constant
f_i	reaction force on the i^{th} blade (2)
$f(\theta)$	detuning function
$f_{ms}(\tau)$	characteristic function of the m, s mode
F	constant (3)
F_i	reaction force on the disc (2)
$F(\theta)$	modal shape function
G	constant (3)
h	half thickness of the disc and blades
H	constant (3)
I, J, K, Y	Bessel functions (3)
l	length coordinate along a blade
L	length of a blade
L_0	length of blades in a tuned system

$L(\theta)$	blade length equation
m_i	mass of the i^{th} blade
M	bending moment in a plate
M_d	mass of disc
n	number of nodal diameters
N	number of blades on a disc
p, q, r	principal coordinates
P_x	externally applied force on a blade (2)
P_d	externally applied force on the disc (2)
P	order of the approximate system matrix $(2Q + NS)$
Q	number of disc modes in the approximate system
r	radial coordinate
s	number of nodal circles
S	number of modes per blade in approximate system
t	time coordinate
T	kinetic energy
V	potential energy
w	normal displacement of disc
y	normal displacement of blade
$\alpha, \alpha', \alpha''$	disc receptance terms
$\beta_0, \beta_1, \beta_2$	coefficients in modal shape function
γ, δ	constants in modal shape function
Δ	receptance determinant
θ	angular coordinate
λ	blade length ratio $(L/2a)$ (4 et seq)
λ	dimensionless frequency parameter in blade frequency eq.(3)
ρ	density
σ	Poisson's ratio
σ	degree of detuning (5 et seq)
ϕ, ψ	constants in detuning function
Φ	frequency factor (5)

$\bar{\Psi}$ split factor (5)
 ω frequency of vibration
 ω_j natural frequency of the j^{th} mode
 $\Omega, \Omega', \Omega''$ blade receptance terms

APPENDIX 2

INERTIA COEFFICIENTS FOR THE NORMAL MODES OF A DISC

The equation for the inertia coefficient of the n, s mode, given in (3.42), is

$$a_{ns} = \begin{Bmatrix} 2 \\ 1 \end{Bmatrix} \frac{M_d}{\pi a^2} \int_0^{2\pi} \int_0^a r [f_{ns}(r) \cos n(\theta - \epsilon_{ns})]^2 dr d\theta \quad \begin{cases} n=0 \\ n>0 \end{cases} \quad (\text{A2.1})$$

The integration over θ may be made directly, and upon substitution for $f_{ns}(r)$ from (3.35), equation (A2.1) may be rewritten as

$$a_{ns} = \begin{Bmatrix} 2 \\ 1 \end{Bmatrix} \frac{M_d}{a^2} \int_0^a r W_{ns}^2 [J_n(b_{ns}r/a) + \mu_{ns} I_n(b_{ns}r/a)]^2 dr \quad (\text{A2.2})$$

We shall now introduce the dimensionless inertia coefficient, $a_{ns}^* = a_{ns} / M_d$, and rewrite (A2.2) in general terms, so that

$$a_{ns}^* = \begin{Bmatrix} 2 \\ 1 \end{Bmatrix} W_{ns}^2 \int_0^1 \eta [J_n(\eta b_{ns}) + \mu_{ns} I_n(\eta b_{ns})]^2 d\eta; \quad (\text{A2.3})$$

($\eta = r/a$).

McLachlan gives three results which enable this integral to be evaluated explicitly. In the present notation, these are

$$\int_0^1 \eta [J_n(\eta b_{ns})]^2 d\eta = \frac{1}{2} \{ [J_n]^2 - J_{n-1} J_{n+1} \}$$

$$\int_0^1 \eta J_n(\eta b_{ns}) I_n(b_{ns} \eta) d\eta = \frac{1}{2b_{ns}} \{ J_n I_{n-1} - J_{n-1} I_n \}$$

$$\int_0^1 \eta [I_n(\eta b_{ns})]^2 d\eta = \frac{1}{2} \{ I_n^2 - I_{n-1} I_{n+1} \}$$

(A2.4)

Thus,

$$a_{ms}^* = \begin{Bmatrix} 2 \\ 1 \end{Bmatrix} \frac{W_{ms}^2}{2} \left\{ J_n^2 - J_{n-1} J_{n+1} + \frac{2\mu_{ms}}{b_{ms}} (J_n I_{n-1} - I_n J_{n-1}) \right. \\ \left. + \mu_{ms}^2 (I_n^2 - I_{n-1} I_{n+1}) \right\} \quad (\text{A2.5})$$

where all Bessel functions are of argument (b_{ms}) .

APPENDIX 3

CLOSED FORM RECEPTANCE EXPRESSIONSA3.1 General

Note: In this appendix we shall write $J_n(ka) = J_n$ etc., and $\partial/\partial r \{ J_n(kr) \} = J_n'(kr)$ etc.

The general displacement function, equation (3.31), may be written as

$$w_n(r, \theta) = U_n \cos n\theta + V_n \sin n\theta \quad (\text{A3.1})$$

where

$$\begin{aligned} U_n &= A_n J_n(kr) + C_n I_n(kr) \\ V_n &= E_n J_n(kr) + G_n I_n(kr) \end{aligned} \quad (\text{A3.2})$$

We shall also use the expressions for shear force and bending moment in the disc which were given in equations (3.29) and (3.30), but it must be noticed that the units of these expressions are shear force and bending moment per unit circumference. It is convenient for later work to deal in terms of force etc. per unit angle and thus appropriate corrections will be made to the expressions for shear force and bending moment.

Substitution of (3.31) into (3.29) gives

$$-\frac{[P]_{r=a}}{D a} = X_n \cos n\theta + Y_n \sin n\theta \quad (\text{A3.3})$$

(and P is now force per unit angle), where

$$\begin{aligned} X_n &= [A_n \gamma_n + C_n \delta_n] b/2a^3 \\ Y_n &= [E_n \gamma_n + G_n \delta_n] b/2a^3 \end{aligned} \quad (\text{A3.4})$$

where

$$\begin{aligned} \gamma_m &= -(R+b^2) J_{m-1} + (Q+b^2) J_{m+1} ; \\ \delta_m &= -(R-b^2) I_{m-1} - (Q-b^2) I_{m+1} ; \\ R &= n(n-1)(1-\sigma) ; \quad Q = n(n+1)(1-\sigma) \end{aligned} \quad (\text{A3.5})$$

Next, on substitution of (3.31) into (3.30), we find that

$$\frac{[M]}{\bar{D} a} \Big|_{r=a} = \bar{W}_m \cos n\theta + \bar{Z}_m \sin n\theta \quad (\text{A3.6})$$

where

$$\begin{aligned} \bar{W}_m &= [A_m \gamma_m + C_m \beta_m] b/2n \\ \bar{Z}_m &= [E_m \eta_m + G_m \beta_m] b/2n \end{aligned} \quad (\text{A3.7})$$

$$\begin{aligned} \eta_m &= (R-b^2) J_{m-1} + (Q-b^2) J_{m+1} \\ \beta_m &= (R+b^2) I_{m-1} - (Q+b^2) I_{m+1} \end{aligned} \quad (\sim 3.8)$$

A3.2 Normal displacement - edge shear force

In this case, the boundary conditions (given in equation (3.46)) are

$$[P]_{r=a} = P_m \cos n\theta ; \quad [M]_{r=a} = 0 \quad (\text{A3.9})$$

so that, from (A3.6), (A3.7) and (A3.8), we find that

$$\bar{W}_m = \bar{Z}_m = 0 \quad \text{also} \quad \bar{X}_m = \bar{Y}_m = 0, \quad m \neq n \quad (\text{A3.10})$$

Because the shear force boundary condition;

$$\bar{X}_m \cos n\theta + \bar{Y}_m \sin n\theta = -P_m \cos n\theta / \bar{D} a \quad (\text{A3.11})$$

must hold for all θ , it follows that

$$\begin{aligned} Y_n &= 0 \\ X_n &= -P_n / \bar{D} a \end{aligned} \quad (\text{A3.12})$$

The equation for the displacement at any point r, θ is thus

$$w_n(r, \theta) = [A_n J_n(kr) + C_n I_n(kr)] \cos n\theta \quad (\text{A3.13})$$

We may solve two of the boundary conditions, (A3.10) and (A3.13) above, for A_n and C_n since

$$\begin{aligned} A_n \eta_n + C_n \beta_n &= 0 \\ A_n \gamma_n + C_n \delta_n &= -\frac{2a^2 P_n}{\bar{D} b} \end{aligned} \quad (\text{A3.14})$$

Thus, the displacement becomes,

$$\begin{aligned} w_n(r, \theta) &= -\frac{2a^2 P_n}{\bar{D} b} \frac{[\beta_n J_n(kr) - \eta_n I_n(kr)]}{[\beta_n \gamma_n - \eta_n \delta_n]} \cos n\theta \\ &= \frac{a^2}{\bar{D}} \cdot \frac{N_n(r)}{D_n} P_n \cos n\theta \end{aligned} \quad (\text{A3.15})$$

where

$$\begin{aligned} N_n(r) &= -\frac{1}{b} J_n(kr) [(R+b^2) I_{n-1} - (Q+b^2) I_{n+1}] \\ &\quad + \frac{1}{b} I_n(kr) [(R-b^2) J_{n-1} + (Q-b^2) J_{n+1}] \\ D_n &= [b^4 + n^2(n^2-1)(1-\sigma)^2] [I_{n-1} J_{n+1} + I_{n+1} J_{n-1}] \\ &\quad - 2b^2 n(1-\sigma) [(n-1) I_{n-1} J_{n-1} + (n+1) I_{n+1} J_{n+1}] \end{aligned} \quad (\text{A3.16})$$

A3.3 Normal displacement - edge couple

The boundary conditions for this case are given in (5.50) as

$$[P]_{r=a} = 0 ; [M]_{r=a} = M_n \cos n\theta \quad (\text{A3.17})$$

Substitution of the first of these into (A3.3) gives

$$X_n = Y_n = 0 \quad (\text{A3.18})$$

and into (A3.6), results in

$$W_n \cos n\theta + Z_n \sin n\theta = M_n \cos n\theta / \bar{D} a ;$$

$$W_n = Z_n = 0 , \quad m \neq n \quad (\text{A3.19})$$

The requirement that this equation shall hold for all θ is that Z_n is identically zero, and that

$$W_n = M_n / \bar{D} a \quad (\text{A3.20})$$

In order to eliminate A_n , and C_n from the displacement equation (A3.13), two equations may be derived from (A3.18) and (A3.20) such that

$$A_n \gamma_n + C_n \delta_n = 0$$

$$A_n \eta_n + C_n \beta_n = \frac{2n M_n a}{b a \bar{D}} \quad (\text{A3.21})$$

Thus, the displacement at the rim may be written as

A3.3 Normal displacement - edge couple

The boundary conditions for this case are given in (5.50) as

$$[P]_{r=a} = 0 ; [M]_{r=a} = M_n \cos n\theta \quad (\text{A3.17})$$

Substitution of the first of these into (A3.3) gives

$$X_n = Y_n = 0 \quad (\text{A3.18})$$

and into (A3.6), results in

$$W_n \cos n\theta + Z_n \sin n\theta = M_n \cos n\theta / \bar{D} a ;$$

$$W_n = Z_n = 0 , \quad m \neq n \quad (\text{A3.19})$$

The requirement that this equation shall hold for all θ is that Z_n is identically zero, and that

$$W_n = M_n / \bar{D} a \quad (\text{A3.20})$$

In order to eliminate A_n and C_n from the displacement equation (A3.13), two equations may be derived from (A3.18) and (A3.20) such that

$$A_n \gamma_n + C_n \delta_n = 0$$

$$A_n \eta_n + C_n \beta_n = \frac{2n M_n a}{b a \bar{D}} \quad (\text{A3.21})$$

Thus, the displacement at the rim may be written as

$$\begin{aligned}
 w_n(a, \theta) &= - \frac{2na}{D b} \frac{[\delta_n J_n - \gamma_n I_n]}{[\gamma_n \beta_n - \eta_n \delta_n]} \cos n\theta \cdot M_n \\
 &= \frac{a}{D} \cdot \frac{N_n'}{D_n} M_n \cos n\theta
 \end{aligned}
 \tag{A3.22}$$

where

$$\begin{aligned}
 N_n' &= n^2(1-\sigma) [I_{n-1} J_{n+1} + I_{n+1} J_{n-1}] \\
 &\quad - b^2 [I_{n-1} J_{n-1} + I_{n+1} J_{n+1}]
 \end{aligned}
 \tag{A3.23}$$

APPENDIX 4

EQUATIONS OF MOTION IN MATRIX FORM

A4.1 Rigid body modes of vibration

If Lagrange's equation is applied to each of the three rigid body coordinates q_{00} , q_{10} and p_{10} in turn, then we have, for q_{00} :

$$M_d \ddot{q}_{00} + \sum_{i=1}^N \left\{ m_i \left[\ddot{w}_i + \lambda_i \ddot{s}_i - \sum_{k=1}^S (i\psi_k + i\phi_k)_i \ddot{\eta}_k \right] \left[\frac{\partial w_i}{\partial \dot{q}_{00}} + \lambda_i \frac{\partial s_i}{\partial \dot{q}_{00}} \right] + \frac{1}{3} m_i \left[-\lambda_i \ddot{s}_i + \sum_{k=1}^S i\psi_k \ddot{\eta}_k \right] \left[-\lambda_i \frac{\partial s_i}{\partial \dot{q}_{00}} \right] \right\} = 0 \quad (A4.1)$$

for q_{10} :

$$\frac{1}{4} M_d a \ddot{q}_{10} + \sum_{i=1}^N \left\{ m_i \left[\ddot{w}_i + \lambda_i \ddot{s}_i - \sum_{k=1}^S (i\psi_k + i\phi_k)_i \ddot{\eta}_k \right] \left[\frac{\partial w_i}{\partial (a\dot{q}_{10})} + \lambda_i \frac{\partial s_i}{\partial (a\dot{q}_{10})} \right] + \frac{1}{3} m_i \left[-\lambda_i \ddot{s}_i + \sum_{k=1}^S i\psi_k \ddot{\eta}_k \right] \left[-\lambda_i \frac{\partial s_i}{\partial (a\dot{q}_{10})} \right] \right\} = 0 \quad (A4.2)$$

and a similar expression corresponding to p_{10} , (A4.3)

where

$$\begin{aligned} w_i &= w(a, \theta_i) \quad ; \quad s_i = a \left\{ \frac{\partial w}{\partial r} [w(r, \theta)] \right\}_{r=a, \theta = \theta_i} \\ m_i &= \text{blade mass} \quad ; \quad \lambda_i = L_i / 2a \\ i\phi_k &= [i\phi_k(l)]_{l=0} \quad ; \quad i\psi_k = \frac{1}{2} L_i \left\{ \frac{\partial \phi_k}{\partial l} [i\phi_k(l)] \right\}_{l=0} \end{aligned}$$

By substituting for w_i and s_i from equation (4.16) the three equations (A4.1), (A4.2) and (A4.3) may be expressed as

$$\underline{R} \begin{bmatrix} \ddot{q}_{00} \\ a\ddot{v}_{10} \\ a\ddot{p}_{10} \end{bmatrix} + \sum_{j=1}^Q \{ \underline{C}_j \ddot{q}_j + \underline{S}_j \ddot{p}_j \} + \sum_{i=1}^N \left\{ \sum_{k=i}^Q \underline{V}_k \ddot{q}_k \right\} = 0 \quad (\text{A4.4})$$

where \underline{R} is a 3x3 matrix and \underline{C}_j , \underline{S}_j and \underline{V}_k are 3x1 column vectors. Introducing $\mu_i = m_i / M_d$ and $g_j = a \left[\frac{\partial}{\partial r} [f_j(r)] \right]_{r=a}$, we find, after some manipulation, that

$$\underline{R} = \begin{bmatrix} 1 + \sum_i \mu_i & , & \sum_i \mu_i (1 + \lambda_i) \cos \theta_i & , & \sum_i \mu_i (1 + \lambda_i) \sin \theta_i \\ \sum_i \mu_i (1 + \lambda_i) \cos \theta_i & , & \frac{1}{4} + \sum_i \mu_i \left\{ (1 + \lambda_i)^2 + \frac{1}{3} \lambda_i^2 \right\} \cos^2 \theta_i & , & \sum_i \mu_i \left\{ (1 + \lambda_i)^2 + \frac{1}{3} \lambda_i^2 \right\} \cos \theta_i \sin \theta_i \\ \sum_i \mu_i (1 + \lambda_i) \sin \theta_i & , & \sum_i \mu_i \left\{ (1 + \lambda_i)^2 + \frac{1}{3} \lambda_i^2 \right\} \cos \theta_i \sin \theta_i & , & \frac{1}{4} + \sum_i \mu_i \left\{ (1 + \lambda_i)^2 + \frac{1}{3} \lambda_i^2 \right\} \sin^2 \theta_i \end{bmatrix}$$

$$\underline{C}_j = \begin{bmatrix} \sum_i \mu_i (1 + \lambda_i g_j) \cos \alpha_j \theta_i \\ \sum_i \mu_i \left\{ (1 + \lambda_i)(1 + \lambda_i g_j) + \frac{1}{3} \lambda_i^2 g_j \right\} \cos \alpha_j \theta_i \cos \theta_i \\ \sum_i \mu_i \left\{ (1 + \lambda_i)(1 + \lambda_i g_j) + \frac{1}{3} \lambda_i^2 g_j \right\} \cos \alpha_j \theta_i \sin \theta_i \end{bmatrix}$$

$$\underline{S}_j = \begin{bmatrix} \sum_i \mu_i (1 + \lambda_i g_j) \sin \alpha_j \theta_i \\ \sum_i \mu_i \left\{ (1 + \lambda_i)(1 + \lambda_i g_j) + \frac{1}{3} \lambda_i^2 g_j \right\} \sin \alpha_j \theta_i \cos \theta_i \\ \sum_i \mu_i \left\{ (1 + \lambda_i)(1 + \lambda_i g_j) + \frac{1}{3} \lambda_i^2 g_j \right\} \sin \alpha_j \theta_i \sin \theta_i \end{bmatrix} \quad \underline{V}_k = \begin{bmatrix} -\mu_i (\phi_k + i \psi_k) \\ -\mu_i \left\{ (1 + \lambda_i) \phi_k + (1 + \frac{2}{3} \lambda_i) \psi_k \right\} \cos \theta_i \\ -\mu_i \left\{ (1 + \lambda_i) \phi_k + (1 + \frac{2}{3} \lambda_i) \psi_k \right\} \sin \theta_i \end{bmatrix}$$

(A4.5)

If (as always proves to be the case) the three rigid body modes are **represented** in another equation of motion by a matrix product

$\underline{X} \begin{bmatrix} \ddot{q}_{00} \\ a\ddot{q}_{10} \\ a\ddot{p}_{10} \end{bmatrix}$, where \underline{X} is a **row** vector, then they may be eliminated by writing (from (A4.4))

$$\underline{X} \begin{bmatrix} \ddot{q}_{00} \\ a\ddot{q}_{10} \\ a\ddot{p}_{10} \end{bmatrix} = - \sum_{j=1}^a \left\{ (\underline{X}\underline{R}^{-1}\underline{C}_j) \ddot{q}_j + (\underline{X}\underline{R}^{-1}\underline{S}_j) \ddot{p}_j \right\} - \sum_{i=1}^N \left\{ \sum_{k=1}^S (\underline{X}\underline{R}^{-1}\underline{V}_{ik})_i \ddot{x}_k \right\} \quad (\text{A4.6})$$

Thus we may use this result to express the displacement $w(r, \theta)$, (4.16), in terms of the coordinates of the **flexural** modes only. If we write

$$w(r, \theta) = \left[1, \frac{r}{a} \cos \theta, \frac{r}{a} \sin \theta \right] \begin{bmatrix} q_{00} \\ aq_{10} \\ ap_{10} \end{bmatrix} + \sum_{j=1}^a \left\{ q_j [f_j(r) \cos n_j \theta] + p_j [f_j(r) \sin n_j \theta] \right\} \quad (\text{A4.7})$$

then $\underline{X} = \left[1, \frac{r}{a} \cos \theta, \frac{r}{a} \sin \theta \right]$ so that (A4.7) becomes

$$w(r, \theta) = \underline{F}(r, \theta) \underline{q}$$

where

$$\underline{F} = \begin{vmatrix} \{ f_j(r) \cos n_j \theta - \underline{X}\underline{R}^{-1}\underline{C}_j \} \\ \{ f_j(r) \sin n_j \theta - \underline{X}\underline{R}^{-1}\underline{S}_j \} \\ \{ -\underline{X}\underline{R}^{-1}\underline{V}_{ik} \} \end{vmatrix}; \quad \underline{q} = \begin{vmatrix} \{ q_j \} \\ \{ p_j \} \\ \{ x_k \} \end{vmatrix} \quad (\text{A4.8})$$

A4.2 Flexural modes of vibration

In constructing the inertia and stiffness matrices (and subsequently the system matrix, \underline{D}), there are three general cases to consider, namely, the equations of motion corresponding to

- (i) q_e , (ii) p_e and (iii) $e^k m$ (say). The equation for q_e is found by letting $\frac{d}{dt}(\delta T/\delta \dot{q}_e) + (\delta V/\delta q_e) = 0$:

$$\begin{aligned} & (a_e \omega_e^2) q_e + (a_e) \ddot{q}_e \\ & + \sum_{i=1}^N m_i \left\{ \left[\ddot{w}_i + \lambda_i \ddot{s}_i - \sum_{k=1}^S (\psi_k + i \phi_k)_i \ddot{\lambda}_k \right] \left[\cos n_i \theta_i \cdot (1 + \lambda_i g_e) \right] \right. \\ & \quad \left. + \frac{1}{3} \left[-\lambda_i \ddot{s}_i + \sum_{k=1}^S \psi_k \ddot{\lambda}_k \right] \left[-\cos n_i \theta_i \cdot \lambda_i g_e \right] \right\} \\ & = 0 \end{aligned} \quad (\text{A4.9})$$

On substitution for \ddot{w}_i and \ddot{s}_i (from (4.16)), and for the rigid body coordinates (from (A4.6)), this equation becomes

$$\begin{aligned} & a_e \omega_e^2 q_e + a_e \ddot{q}_e \\ & - \sum_{i=1}^N \sum_{k=1}^S \left\{ i \ddot{\lambda}_k \left[\mu_i \cos n_i \theta_i \{ i \phi_k (\lambda_i g_e + 1) + i \psi_k (1 + \frac{4}{3} \lambda_i g_e) \} + \underline{C}_e^T \underline{R}^{-1} \underline{V}_k \right] \right\} \\ & + \sum_{j=1}^Q \left\{ \dot{q}_j \left[\sum_i \mu_i \cos n_i \theta_i \cos n_j \theta_i \{ (1 + \lambda_i g_e)(1 + \lambda_i g_j) + \frac{1}{3} \lambda_i^2 g_e g_j \} - \underline{C}_e^T \underline{R}^{-1} \underline{C}_j \right] \right. \\ & \quad \left. + p_j \left[\sum_i \mu_i \cos n_i \theta_i \sin n_j \theta_i \{ (1 + \lambda_i g_e)(1 + \lambda_i g_j) + \frac{1}{3} \lambda_i^2 g_e g_j \} - \underline{C}_e^T \underline{R}^{-1} \underline{S}_j \right] \right\} \\ & = 0 \end{aligned} \quad (\text{A4.10})$$

Similarly the equation for p_e may be written as

$$\begin{aligned}
& a_e \omega_e^{-1} \dot{p}_e + a_e \ddot{p}_e \\
& - \sum_{i=1}^N \sum_{k=1}^S \left\{ i \ddot{\lambda}_{ik} \left[\mu_i \sin n_i \theta_i \left\{ i \phi_k (1 + \lambda_i g_e) + i \psi_k (1 + \frac{4}{3} \lambda_i g_e) \right\} + \underline{S}_e^T \underline{R}^{-1} \underline{V}_{ik} \right] \right\} \\
& + \sum_{j=1}^Q \left\{ \ddot{q}_j \left[\sum_i \mu_i \sin n_i \theta_i \cos n_j \theta_i \left\{ (1 + \lambda_i g_e)(1 + \lambda_i g_j) + \frac{1}{3} \lambda_i^2 g_e g_j \right\} - \underline{S}_e^T \underline{R}^{-1} \underline{C}_j \right] \right. \\
& \quad \left. + \dot{p}_j \left[\sum_i \mu_i \sin n_i \theta_i \sin n_j \theta_i \left\{ (1 + \lambda_i g_e)(1 + \lambda_i g_j) + \frac{1}{3} \lambda_i^2 g_e g_j \right\} - \underline{S}_e^T \underline{R}^{-1} \underline{S}_j \right] \right\} \\
& = 0 \tag{A4.11}
\end{aligned}$$

Finally, if we apply Lagrange's equation to ${}_e \dot{\lambda}_m$, the corresponding equation of motion becomes

$$\begin{aligned}
& e \omega_m^2 e a_m e \dot{\lambda}_m + e a_m e \ddot{\lambda}_m \\
& + \sum_{k=1}^S e \ddot{\lambda}_{km} \left[\mu_e \left\{ e \phi_m (e \phi_k + e \psi_k) + e \psi_m (e \phi_k + \frac{4}{3} e \psi_k) \right\} \right] \\
& + \sum_{j=1}^Q \left\{ \ddot{q}_j \left[-\cos n_j \theta_e \cdot \mu_e \left\{ e \phi_m (1 + \lambda_e g_j) + e \psi_m (1 + \frac{4}{3} \lambda_e g_j) \right\} - e \underline{V}_m^T \underline{R}^{-1} \underline{C}_j \right] \right. \\
& \quad \left. + \dot{p}_j \left[-\sin n_j \theta_e \cdot \mu_e \left\{ e \phi_m (1 + \lambda_e g_j) + e \psi_m (1 + \frac{4}{3} \lambda_e g_j) \right\} - e \underline{V}_m^T \underline{R}^{-1} \underline{S}_j \right] \right\} \\
& + \sum_{i=1}^N \sum_{k=1}^S i \ddot{\lambda}_{ik} \left[-e \underline{V}_m^T \underline{R}^{-1} e \underline{V}_{ik} \right] \\
& = 0 \tag{A4.12}
\end{aligned}$$

APPENDIX 5

A MECHANISM OF NATURAL FREQUENCY SPLITTING

In an attempt to predict a possible mechanism of natural frequency splitting, it is convenient to consider the simple system of a disc without any blades. The results may then be extended in principle to the more complex arrangement of a bladed disc.

Consider the disc to be vibrating in its normal mode with n nodal diameters and S nodal circles, which we shall identify as the j^{th} mode. This vibration may be expressed in terms of two principal coordinates, q_j and p_j , whose properties are as follows:

$$a_{p_j} = a_{q_j} = a_j ; \quad c_{p_j} = c_{q_j} = c_j ; \quad \omega_{p_j} = \omega_{q_j} = \omega_j ;$$

$$\phi_{p_j} = f_j(r) \cos(n\theta + \alpha) ; \quad \phi_{q_j} = f_j(r) \sin(n\theta + \alpha)$$

As in previous work we shall choose $f_j(a) = 1$, and it **should** be noted that α may be chosen as any convenient value. The potential and kinetic energy expressions for this motion are

$$2V_j = c_j (p_j^2 + q_j^2)$$

and

$$2T_j = a_j (\dot{p}_j^2 + \dot{q}_j^2) = a_j^* M_d (\dot{p}_j^2 + \dot{q}_j^2) \quad (\text{A5.1})$$

respectively.

Now suppose that a distribution of mass is added to the rim of the disc such that $M = M_0 \cos m\theta$ where $M_0 \ll M_d$, the disc **mass**. It will be supposed that the addition of this mass will only affect the vibration of the disc slightly, in that it will only alter the kinetic energy term and not contribute to the potential energy. The normal velocity of the rim of the disc, and hence of the added mass,

is given by the equation

$$\dot{w} = \dot{p}_j \cos(n\theta + \alpha) + \dot{q}_j \sin(n\theta + \alpha) \quad (\text{A5.2})$$

so that the kinetic energy of the added mass may be written as

$$2T_M = \int_0^{2\pi} M_0 \cos m\theta [\cos^2(n\theta + \alpha) \dot{p}_j^2 + \sin^2(n\theta + \alpha) \dot{q}_j^2] d\theta \quad (\text{A5.3})$$

There are two possible values for this expression. If $m \neq 2n$, then T_M is zero, indicating that the added mass has no effect whatsoever on the vibration of the disc. If, however, $m = 2n$, then we find that

$$2T_M = \frac{3}{2} M_0 \pi \cos 2\alpha [\dot{p}_j^2 - \dot{q}_j^2] \quad (\text{A5.4})$$

In this case the natural frequencies of the modified p_j and q_j modes will no longer be identical. If we consider the p_j mode first, we have

$$\omega_{p_j}' = \frac{c_j}{a_j + \frac{1}{2} M_0 \pi \cos 2\alpha} \quad (\text{A5.5})$$

In this expression, we may choose α to be any convenient value but as yet have no criterion upon which to base such a choice. However, Rayleigh's principle provides such a criterion, in that **any** value which is chosen will result in a value for ω_{p_j}' which is either greater than or equal to the exact value. Since in this analysis we assume that the solution is exact in every respect other than the value of α , then it follows that that value which makes ω_{p_j}' a minimum, yields the exact natural frequency. Thus,

$$\omega_{p_j}' = \frac{c_j}{a_j + \frac{1}{2} M_0 \pi} \quad (\text{A5.6})$$

and having established the value of α , we may determine the modified natural frequency ω_{q_j}' as

$$\omega_{q_j'} = \frac{c_j}{a_j - \frac{1}{2} M_o \pi} \quad (\text{A5.7})$$

The relationship between $\omega_{q_j'}$ and $\omega_{p_j'}$ may be examined as follows. Since $M_o \ll M_d$, we shall assume that $a_j^2 \gg \frac{1}{4} M_o^2 \pi^2$ and that $\omega_{p_j'} \approx \omega_{q_j'}$. Thus

$$(\omega_{q_j'})^2 - (\omega_{p_j'})^2 = \frac{M_o \pi c_j}{a_j^2} = \omega_j^2 \frac{M_o \pi}{a_j} \quad (\text{A5.8})$$

and

$$\omega_{q_j'} - \omega_{p_j'} = \omega_j \frac{M_o \pi}{2a_j} \quad (\text{A5.9})$$

so that we may define the 'split' as

$$\frac{\omega_{q_j'} - \omega_{p_j'}}{\omega_j} = \frac{M_o \pi}{M_d 2a_j^*}$$

and introduce a 'split factor' which is

$$\frac{(\omega_{q_j'} - \omega_{p_j'}) / \omega_j}{M_o / M_d} = \frac{\pi}{2a_j^*} \quad (\text{A5.10})$$

and consequently a property of the j^{th} mode.

The result of this simple analysis is the demonstration that a mode with n nodal diameters will only be split by a detuning function which takes the form $\cos(2n\theta)$, in which case the magnitude of the natural frequency split is dependent upon the amplitude of the detuning function and the properties of the disc mode. The modes of vibration of a bladed disc are essentially similar to those of the unbladed disc, and the same result is expected to hold in principle when applied to bladed discs.

It has been found that an analysis by **Zenneck (1899)**, also based on Rayleigh's principle, predicts the same type of behaviour for an imperfect disc.

APPENDIX 6

PIEZOELECTRIC TRANSDUCERS

Piezoelectric transducers were chosen for force and acceleration measurements on account of their high sensitivity and fundamentally simple (although sometimes costly) demands on ancillary electronic equipment. These transducers have been developed to overcome the considerable temperature sensitivity which was an early inherent disadvantage, and accurate and reliable devices are now available for the measurement of most dynamic properties. The advantage of their high sensitivity lies in the fact that less power need be supplied to the vibrating system (than for an equivalent passive type of pickup) in order to obtain a signal level 1 which is readily measurable, and thus they tend to be relatively free of electrical noise problems. This fact, in the present work at least, means that the acoustic noise level is not the nuisance that it might have been had larger amplitudes of vibration been required.

The piezoelectric transducer is essentially a charge-generating capacitive source (see **FIG.A6.1**), in which a charge is generated proportional to the physical quantity being measured. In order to

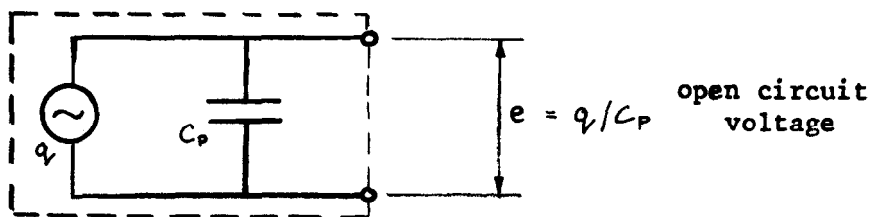


FIG.A6.1 EQUIVALENT CIRCUIT OF A PIEZOELECTRIC TRANSDUCER

measure this charge, two alternative systems are available. The more common of these requires a voltage amplifier whose input impedance is of the order of 100 Megohms in order that the lower frequency limit

of the system be at a reasonable level. The low frequency response of such transducers is critically dependent upon the measuring equipment, and the high figure quoted for an amplifier input impedance is absolutely necessary. From FIG.A6.1, it may be seen that the open circuit voltage (e) of the transducer is given by the ratio of the charge (q) to the source capacitance (C_p). The next diagram (FIG.A6.2) shows a transducer in a typical voltage amplifier system,

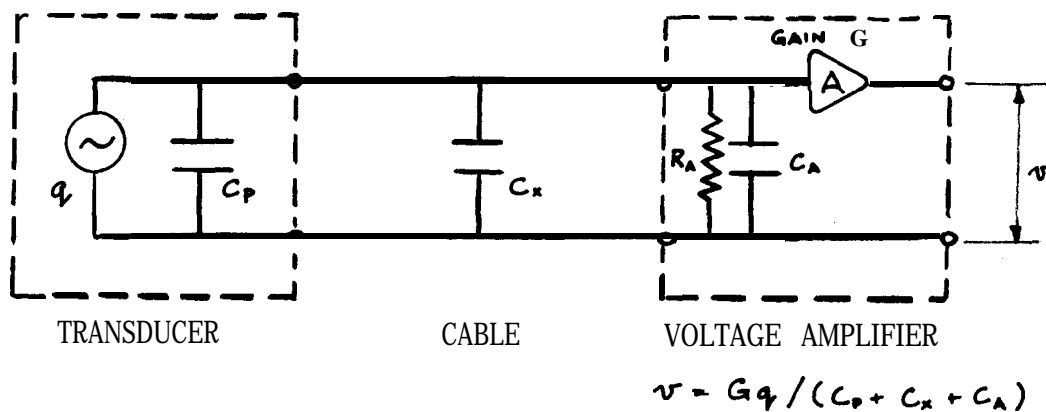


FIG.A6.2 VOLTAGE AMPLIFIER MEASURING SYSTEM

and it may be seen that the voltage amplifier measures the voltage across its input, which has now been reduced from e by the addition of the external capacitance of the cable, and still further by any input capacitance that the amplifier itself might possess. Clearly then, the sensitivity of the transducer will be highly dependent upon the external circuitry imposed between it and the amplifier, and although cathode follower units could be employed, they really only serve as an additional unknown quantity, rather than solve the difficulties.

In spite of such drawbacks, the voltage amplifier system may be used to measure charge. However, there exists another technique which seems basically more sound and appropriate for the purpose, and this employs the use of a so-called charge amplifier. This is essentially an amplifier with a very high gain and a feedback capacitance, and

its (simplified) method of operation is as follows (see FIG.A6.3).

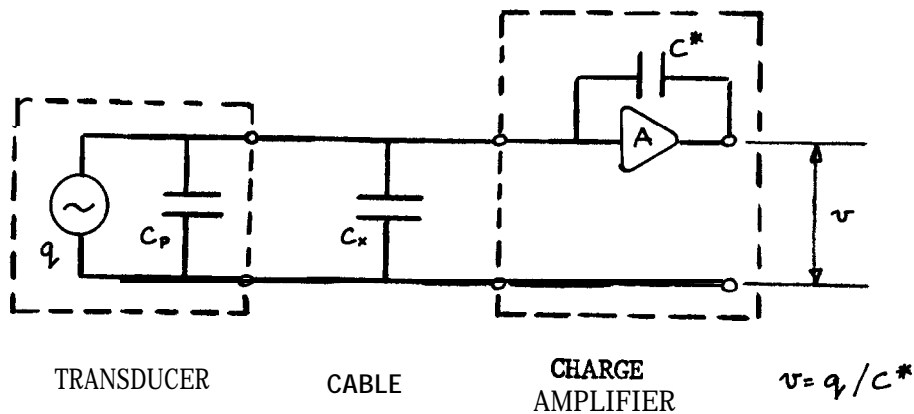


FIG.A6.3 CHARGE AMPLIFIER MEASURING SYSTEM

Suppose the voltage at the output of the amplifier is v , then, since the amplifier gain is extremely high, the voltage across the input of the amplifier is effectively zero. This has two consequences; first that no current flows in the circuit indicating an input impedance of the amplifier of infinite order, and second that the voltage v is thus the voltage across the feedback capacitor, and furthermore, this voltage is numerically equal to the ratio of the generated charge to the feedback capacitance: $v = q / C^*$. The main advantage of this type of amplifier over the voltage amplifier described above, lies in the independence of the overall sensitivity to the externally applied electrical loads in the form of cable capacitance: a value of 15,000 pF for the external capacitance C_x (equivalent to one mile of cable) decreases the sensitivity by a mere 1 per cent, whereas the same value in the previous system would make readings impossible. One refinement which is often found on commercial models is the addition, to the amplifier just described, of a voltage amplifier with a gain of about 50. A fraction of the

charge amplifier output is fed into this second amplifier and the output from that is measured. An accurately calibrated potentiometer is used to determine the fraction taken, and this fraction may be chosen so that the resulting voltmeter readings are scaled directly in lb. or g , this refinement being in the nature of a luxury rather than a necessity.

Finally, another important aspect, as yet unmentioned, is that concerning the relative phase of the measured signal to that of the original physical quantity. In the voltage amplifier system, the signal is subject to phase changes of varying magnitudes, depending upon the frequency and more evident at the lower frequencies. In this case, it is imperative that both the force and the acceleration signals undergo identical electronic transformations if their relative phase is to be meaningful. The charge amplifier system, with its independence of external loading (which is the chief cause of these changes), is less prone to such difficulties.

APPENDIX 7COMPUTATION OF VIBRATION DATA FOR TEE EXPERIMENTAL MODELS

In order to deduce natural frequencies for the models used in the experimental study from the dimensionless quantities computed by the receptance method, it is necessary to establish a value for the constant K in the equation

$$\omega = (K b^2) \text{ cps} \quad ; \quad K = \frac{1}{2\pi} \sqrt{\frac{2 E h}{3 \rho a^4 (1 - \sigma^2)}}$$

The dimensions of the models are known accurately, but the elastic constants of the material from which they are made may not be determined with the same precision. The steel from which the five bladed disc was machined had been hot rolled, and a metallurgical examination of a specimen indicated that it contained a large amount of impurities and was highly anisotropic. As a result, the value of Young's modulus (and probably the density) would vary throughout the model. Thus it was decided that rather than attempt to measure these properties, typical values would be assumed and tolerances accepted on the resulting value of K . Results in Chapter 8 indicate that this is a convenient approach, and that a more accurate value may be deduced from the experimental observations.

The dimensions of the models are as follows:

disc diameter	= 24"
disc thickness	= 1/2"
blade width	= 1"
blade thickness	= 1/2"
blade length	= 6-8"

and the elastic properties are assumed to be:

$$\begin{aligned}\text{Young's modulus} &= 30 \times 10^6 \text{ psi } +3\% \\ \text{density} &= 0,283 \text{ lb/in}^3 \pm 3\% \\ \text{Poisson's ratio} &= 0.287^* \pm 1\%\end{aligned}$$

These figures provide upper and lower limits on K which are:

$$\begin{aligned}K_{\text{MIN}} &= 32.1 \\ K_{\text{MAX}} &= 35.4 \text{ (cps/unit of } b^2\text{)}\end{aligned}$$

*In conformity with Armstrong.

APPENDIX 8REFERENCES AND BIBLIOGRAPHY

- AITKEN A.C. 1949 Determinants and matrices
Oliver and Boyd
- ARMSTRONG E.K. 1955 An investigation into the coupling between
turbine disc and blade vibrations
Ph.D. Thesis Cambridge
- ARMSTRONG E.K., 1966 Natural frequencies of bladed discs
CHRISTIE P.I. &
HAGUE W.M. **App.Mech.Gp.Conf. I.M.E. Cambridge**
- BISHOP R.E.D. & 1960 The mechanics of vibration
JOHNSON D.C. **C.U.P.**
- CARNEGIE W. 1959 Vibrations of pretwisted cantilever blading
Proc.I.Mech.Eng. Vol.173
- CARNEGIE W. 1964 Vibrations of pretwisted cantilever blading
allowing for rotary inertia and shear
deflection
J.Mech.Eng.Sci. Vol.6 No,2
- CARNEGIE W., 1966 Vibration characteristics of cantilever blading
DAWSON B. &
THOMAS J. **App.Mech.Gp. I.Mech.E. Cambridge**
- McLACHLAN 1934 Bessel functions for engineers
O.U.P.
- McLEOD A.J. & 1965 The forced vibration of circular flat plates
BISHOP R.E.D. **Mech.Eng.Sci. Monograph No.1**
- PRESCOTT J. 1924 Applied elasticity
Dover books
- SCHLOSS F. 1965 Recent advances in mechanical impedance
instrumentation and applications
D.T.M.B. Report No.1960
- SHANNON J.F. 1945 Vibration problems in gas turbines, centrifugal
and axial flow compressors
R & M No.2226
- SMITH D.M. 1966 Vibrations in turbomachinery
App.Mech.Gp. I.Mech.E. Cambridge
- STRATFORD B.S. 1966 Rogue blades
Unpublished Rolls Royce internal report **MCR90011**